Molecular-beam studies of Penning ionization

P. E. Siska

Department of Chemistry, University of Pittsburgh, Pittsburgh, Pennsylvania 15260

Molecular-beam experiments have exposed a new wealth of detail on the general reaction $A^*+B\rightarrow A+B^+ +e^-$ first suggested by Penning in 1927. The new capabilities not available to traditional swarm techniques include mass and electron spectroscopy on the reaction products and angle-resolved measurements of the scattering of both reagents and products. These new results have stimulated the recent development of both the electronic structure and the dynamical theories necessary for a first-principles description of at least the simplest of these reactions, those involving small atomic and diatomic species B. Recent progress in both experiment and interpretation is critically reviewed, and the prospects for attaining a global understanding of Penning ionization in larger systems are assessed.

CONTENTS

I. INTRODUCTION

The process now known as Penning ionization (PI) is simply represented by the reaction

$$A^*+B\rightarrow A+B^+ +e^- , \tag{1.1}$$

where the asterisk denotes electronic excitation of species A, usually an atom but perhaps a molecule, and B can vary in complexity from a ground-state atom to a macroscopic metal crystal with adsorbed molecules on its surface. Reaction (1.1) was first suggested by Frans Penning in 1927, in a note, remarkable for its brevity, describing his systematic study of premature breakdown in neon and argon gas discharges upon the addition of small amounts of impurity gases, and implicating the lowest-lying excited, metastable states of Ne and Ar as the A^* of (1.1). This discovery, which coincidentally occurred in the same decade that saw the development of quantum mechanics, as well as the first flowering of the molecular-beam method in the measurement of atomic moments by Otto Stern and his group at Hamburg, grew into a series of experiments that were reviewed by Druyvesteyn and Penning for *Reviews of Modern Physics* in 1940. Later, reaction (1.1) also became implicated in the so-called Jesse effect (Jesse and Sadauskis, 1952), in which pure and mixed noble gases subjected to ionizing α radiation show anomalously low mean energy required per ion formed in the presence of minute impurities.

Though today a quantum-mechanical description of PI that is both rigorous and workable still awaits further development, a situation to be discussed here, great strides have been made in the microscopic theory of reaction (1.1), stimulated in part by the early molecular-beam experiments of the 1960s. Since then the molecular-beam

method, employed in beam-scattering cell or crossed-beam configurations, has played a central role in bringing the study of PI to a new level of detail, exposing the systematic features of the process as well as defining the successes and shortcomings of the quantum and semiclassical theories currently used to describe it. These experiments have revealed connections between the measurable attributes of reaction (1.1) and the electronic structural properties of the reagents and products of an intimacy beyond that found in conventional energy transfer or reactive processes, providing a continuing stimulus for the small band of workers in the field, as well as for this review of recent progress.

Both Penning's and Jesse's studies were carried out at relatively high pressure, precluding an absolute confirmation that reaction (1.1) was responsible for the observed effects. The earliest molecular-beam experiments, by Sholette and Muschiltz (1962) and by Čermák (1966), left no doubt as to the occurrence of PI and the feasibility of studying it in beams. Through the exploitation of the "single-collision conditions" that enable molecular-beam studies to isolate elementary steps in kinetic processes, these pioneering efforts set the stage for most of the experimental advances that have occurred since. In nearly all studies reported to the present time, the species A^* has been one of the lowest-lying metastable excited states of the noble gases $He^*(1s2s\ ^{2,3}S)$, $Ne^*(2p^5 3s\ ^3P_{2,0}), \ldots,$ $Xe^*(5p^5 6s\ ^3P_{2,0})$, with the major focus on He^* and Ne^* owing to the wide range of ionizable collision partners that can be studied. Table I collects characteristics of the noble-gas metastable atoms. Their reactivities are inverted from the ground states, due mainly to the decline of the excitation energy E_* with increasing principal quantum number n, while their lifetimes are all great enough that they survive flight through all but the largest vacuum chambers with negligible radiative decay at thermal velocity. Molecular beams also afford the use of initial-state preparation and selection, allowing the reactivities of the pairs of metastable states to be compared, a point of great current interest and some puzzlement, to be discussed here.

A number of reviews that include molecular-beam studies of PI have appeared relatively recently (Hotop, 1980; Neynaber, 1980; Haberland *et al.*, 1981; Niehaus, 1981, 1982, 1990; Morgner, 1982, 1984, 1988; Siska, 1984; Yencha, 1984, 1985; Beijerinck, 1987, 1990; Brunetti and Vecchiocattivi, 1989, 1992; Harada, 1990; Ohno and Harada, 1991); in addition, an entire issue of *Chemical Physics* [**145**, No. 2 (1990)] has been devoted to recent advances in excited-atom collision processes.

TABLE I. Characteristics of the metastable noble-gas atoms.[a]

Atom	Electron configuration	State	Excitation energy E_* (eV)	Ionization energy (eV)	Lifetime (s)	Dipole polarizability (Å^3)
He	$1s2s$	$2\,^1S_0$	20.6158[b]	3.9716[b]	0.0197[c],0.0195[d]	11.8.9[e]
		$2\,^3S_1$	19.8196[b]	4.7678[b]	9000[f],7900[g]	46.9[e]
Ne	$2p^5 3s$	$^3P_0$	16.7154[h]	4.8491[b]	430[i]	
		$^3P_2$	16.6191[h]	4.9454[h]	>0.8[c],24.4[i]	27.8[i]
Ar	$3p^5 4s$	$^3P_0$	11.7232[k]	4.0364[k]	44.9[i]	
		$^3P_2$	11.5484[k]	4.2112[k]	>1.3[c],55.9[i]	47.9[j]
Kr	$4p^5 5s$	$^3P_0$	10.5624[l]	3.4372[l]	0.49[i]	
		$^3P_2$	9.9152[l]	4.0844[l]	>1[c],85.1[i]	50.7[j]
Xe	$5p^5 6s$	$^3P_0$	9.4472[m]	2.6826[m]	0.078[i]	
		$^3P_2$	8.3153[m]	3.8145[m]	150.0[i]	63.6[j]

[a]All unit conversions for this table (and elsewhere in this article) are based on the 1986 adjustment of the physical constants given by Cohen and Taylor (1987); in particular, 1 eV = 8065.541 cm^{-1}. Sources for energy data all draw on the tables given by Moore (1970, 1971).
[b]Martin (1973).
[c]Van Dyck *et al.* (1970, 1971, 1972).
[d]Drake *et al.* (1969).
[e]Victor *et al.* (1968).
[f]Woodworth and Moos (1975).
[g]Drake (1971).
[h]Kaufman and Minnhagen (1972).
[i]Small-Warren and Chiu (1975).
[j]Molof *et al.* (1974).
[k]Minnhagen (1973).
[l]Yoshino and Tanaka (1979).
[m]Yoshino and Freeman (1985).

Many other articles, most notably those stemming from invited papers at the biennial ICPEAC meetings, have reviewed progress in a particular type of experiment or in a certain laboratory; these will be cited in turn as the need arises. The most extensive modern review is that of Yencha (1984), which includes both beam and "swarm" or bulb experiments and a comprehensive reference list; the present review, which is restricted to gas-phase molecular-beam and theoretical work, may be regarded in some ways as an update. The literature survey has been cut off, somewhat unevenly, in mid 1991 and includes an attempt at a thorough collection of relevant citations back to 1980, providing a comfortable overlap with Yencha's review as well as the majority of papers containing salient results for the present purpose. Tables II–IV sort the recent experimental papers by excited atom and partner molecule; they are cited here for the convenience of those readers needing merely an update on recent work, and are slightly more up to date than the text.

After delving into molecular-beam experimental methods (Sec. II) and features of PI theory (Sec. III) in enough depth to allow a perception of the capabilities and limitations of each, we discuss in detail four fundamental sets of systems (Secs. IV.A–IV.D), each bringing unique features to bear on the PI process. This discussion is followed by a survey of other recent work (Secs. IV.E and IV.F), a summary of the lessons learned (Sec. V), and peering into the crystal ball (Sec. VI). The approach to the selection of results for discussion has been eclectic rather than comprehensive; the author apologizes in advance to those of his colleagues whose work may have been slighted. In addition, experiments with large gas-phase molecular targets are only mentioned in passing (Harada, 1990; Ohno and Harada, 1991), and the entire subfield known as metastable quenching spectroscopy (MQS) on solid surfaces, which stands in dire need of its own review (see, however, Dunning, 1990), has not been covered. Similarly, work on liquid surfaces (Keller *et al.*, 1986a, 1986b, 1986c; Morgner *et al.*, 1991a,

TABLE II. Penning ionization of atoms and small molecules by metastable helium $He^*(1s2s\ ^{1,3}S)$ in molecular beams, 1980—present.[a]

State[b]	Ionized molecule	Experiment type[c]	Reference
1	H,D	PIAED	Khan *et al.* (1991a, 1981)
3	H	PIES	Merz *et al.* (1990)
3		PIES,PIED	Waibel *et al.* (1988)
1,3	$He^*(2\ ^3S)$	PIES	Müller *et al.* (1991, 1987)
3	Li	PIESA	Merz *et al.* (1990, 1989)
1,3		PIES	Ruf *et al.* (1987)
mix		PICSE	Wang *et al.* (1987)
mix	$Ne^*(^3P)$	PICSE	Neynaber and Tang (1980a)
1,3	Na	PIES	Merz *et al.* (1990)
1,3		PIES	Ruf *et al.* (1987)
3	Ar	PICSES	Mitsuke, Takami, and Ohno (1989)
3		PEAD	Mitsuke, Kusafuka, and Ohno (1989)
mix		PIED,PIES	Le Nadan, Sinou, and Tuffin (1989)
3		PIAD	Gillen *et al.* (1986)
1,3		PICSE	Kroon *et al.* (1986)
3		PICSE	Jerram and Smith (1985)
1,3		PICSE	Siddiqui *et al.* (1984)
3		TCSE	Sheldon and Hardy (1983)
1,3		PICSE	Parr *et al.* (1982)
1,3		PEAD	Le Nadan *et al.* (1982)
1,3		NAD	Brutschy *et al.* (1982)
1,3		TICSE	Burdenski *et al.* (1981)
1,3	K	PIES	Ruf *et al.* (1987)
3	Zn	PICS	Fahey *et al.* (1980b)
1,3		PIES	Inaba *et al.* (1982a)
3	Kr	PICS	Jerram and Smith (1985)
3		TCSE	Hardy and Sheldon (1984)
1,3		PICSE	Parr *et al.* (1982)
3		PEAD	Le Nadan *et al.* (1982)
1,3	Cd	PIES	Inaba *et al.* (1982b)
1,3	Rb	PIES	Ruf *et al.* (1987)
3	Cd	PICS	Fahey *et al.* (1980b)
1,3	Xe	TCSE,PICSE	Büermann *et al.* (1987)
3		TCSE	Hardy and Sheldon (1984)

TABLE II. (*Continued*).

State[b]	Ionized molecule	Experiment type[c]	Reference
1,3	Cs	PIES	Ruf *et al.* (1987)
1,3	H_2,D_2,HD	PICSEM	Martin *et al.* (1989, 1984)
1,3	H_2	PIES	Bregel *et al.* (1989)
1,3	H_2,D_2	NAD	Martin and Siska (1988, 1985)
mix		PIED	Tuffin *et al.* (1987, 1984)
3		PICS	Jerram and Smith (1985)
3	H_2	PIECES	Münzer and Niehaus (1981)
1,3	HCl	PIES	Yencha *et al.* (1989)
1,3		PIOS	Simon *et al.* (1988)
1		PIOS	de Vries *et al.* (1984)
1	HBr	PIES	Yencha *et al.* (1991)
1		PIOS	Tyndall *et al.* (1984)
3	N_2	PICSES	Ohno *et al.* (1991)
1		PIESE	Dunlavy *et al.* (1990)
3		PICS	Jerram and Smith (1985)
mix		PEAD	Tuffin, Le Nadan, and Peresse (1985)
3		PIOS	Leisin and Morgner (1984)
3		PIES	Ohno, Mutoh, and Harada (1983)
1,3		PICSE	Parr *et al.* (1982)
mix		PIES	Tuffin, Le Coz, and Peresse (1980a)
mix	CO	PIED	Le Nadan *et al.* (1989a)
3		PICS	Jerram and Smith (1985)
1,3		PIES	Harada *et al.* (1983)
3		PIES	Ohno, Mutoh, and Harada (1983)
1,3		PICSE	Parr *et al.* (1982)
mix		PIES	Tuffin *et al.* (1980b)
	NO		
3	O_2	PICSES,PEAD	Mitsuke, Takami, and Ohno (1989)
3		PICS	Jerram and Smith (1985)
1,3		PIES	Leisin *et al.* (1982)
1,3		PICSE	Parr *et al.* (1982)
1,3	Cl_2	PIECES	Benz and Morgner (1986a)
		PIES,PIOS	Leisin, Morgner, and Seiberle (1985)
1,3		PIECES	Kischlat and Morgner (1983)
1,3	Br_2	PIES,PIOS	Beckmann *et al.* (1986)
1,3		PIECES	Benz and Morgner (1986b)
1,3	I_2	PIECES	Benz and Morgner (1986b)
1,3		PIES,PIOS	Beckmann *et al.* (1986)
1,3	ICI	PIES,PIOS	Beckmann *et al.* (1986)
1,3	IBr	PIES,PIOS	Beckmann *et al.* (1986)
1,3	Ar_2	PICS	Kraft *et al.* (1988)
1,3		PICSE	Siddiqui *et al.* (1984)
3	H_2O	PICSES,PEAD	Mitsuke, Takami, and Ohno (1989)
3		PIES	Haug *et al.* (1985)
3		PIES	Ohno, Mutoh, and Harada (1983)
1,3		PICSE	Allison *et al.* (1981)
3	H_2S	PICSES	Mitsuke, Takami, and Ohno (1989)
3		PEAD	Mitsuke, Kusafuka, and Ohno (1989)
3		PIES	Ohno, Mutoh, and Harada (1983)
3	HCN	PIES	Ohno, Matsumoto, Imai, and Harada (1984)
3	CO_2	PICSES	Ohno, Takami, and Mitsuke (1991)
mix		PIED,PIES	Le Nadan, Le Coz, and Tuffin (1989a)
3		PIES	Ohno, Takano, and Mase (1986)
mix		PIES	Tuffin, Le Coz, and Peresse (1981)
	N_2O		
1,3	NO_2	PIES,PIOS	Leisin *et al.* (1985a)
3		PIECES,PICSE	Goy, Kohls, and Morgner (1981)
	O_3		
1,3	SO_2	PIES,PIOS	Leisin *et al.* (1985b)

TABLE II. (*Continued*).

State[b]	Ionized molecule	Experiment type[c]	Reference
1,3		PIECES	Goy, Morgner, and Yencha (1981)
1,3	CS_2	PIECES,PIOS	Benz *et al.* (1985)
3	NH_3	PICS	Jerram and Smith (1985)
3		PIES	Ohno, Mutoh, and Harada (1983)
3	CH_2O	PIES	Ohno, Takano, and Mase (1986)
3	C_2H_2	PIES	Ohno, Matsumoto, and Harada (1984b)
3		PIES	Ohno, Mutoh, and Harada (1983)
3	CH_4	PICS	Jerram and Smith (1985)
mix	CH_nX_{4-n}	PIES	Brion *et al.* (1981)
3	CF_2Cl_{4-n}	PIECES	Kischlat and Morgner (1985)
3	CF_3Cl	PIECES	Baus *et al.* (1985)

[a]Works on a given system are cited antichronologically.

[b]1 and 3 refer to singlet and triplet helium, respectively, in state-selected experiments, while mix denotes a mixed beam with unresolved contributions from each state.

[c]Abbreviations, in order of their appearance in this table, are as follows: PIAED—Penning ion angle-energy distribution; PIES—Penning ionization electron spectroscopy; PIED—Penning ion energy distribution; PIESA—Penning ionization electron spectrum angle-resolved; PICS—Penning ionization cross section, including all types of ionic products; PICSE—Penning ionization cross-section collision energy E dependence; PICSES—Penning ionization cross-section collision energy dependence with resolved product electronic state; PEAD—Penning electron angular distribution; NAD—nonreactive scattering angular distribution; PICSEM—Penning ionization cross-section collision energy dependence with mass analysis of ionic products; TCSE—total scattering cross section, collision energy (or velocity) dependence; PIECES—Penning ion/electron coincidence electron spectrum; PIOS—Penning ionization optical (luminescence) spectrum; PIESE—Penning ionization electron spectrum collision energy dependence. The more detailed techniques may include their less detailed counterparts; PIAED includes PIED, PIESE, PIESA, and PIECES include PIES; PICSE includes PICS unless the measurements are relative; and PIECES, PICSES, and PICSEM may include PICSE, depending on experimental details.

TABLE III. Penning ionization of atoms and small molecules by metastable neon $Ne^*(2p^5 3s\ ^3P_{2,0})$ in molecular beams, 1980—present.[a]

State[b]	Ionized molecule	Experiment type[c]	Reference
2	H,D	PIAED	Khan *et al.* (1991b)
2,0		PIES,PIED	Lorenzen *et al.* (1983)
mix	$He^*(2s)$	PICSE	Neynaber and Tang (1980a)
2		PIES	Lorenzen *et al.* (1980)
2,0	Li	PIES	Lorenzen *et al.* (1986)
2,0	Na	PIES	Schohl *et al.* (1990)
2,0		PIES	Lorenzen *et al.* (1986)
mix	Ar	NAD	Baudon *et al.* (1991)
mix		PICS	Aguilar, Bianco *et al.* (1990)
2,0		PICSEP	Driessen, Megens, *et al.* (1990)
mix		TCSE	Kerstel *et al.* (1988)
2,0		PICSE	van den Berg *et al.* (1987)
2,0		PICSE	Verheijen and Beijerinck (1986)
2,0		PICSEM	Weiser and Siska (1986)
2,0		PIESP	Bregel *et al.* (1986)
mix		PICSEM	Aguilar-Navarro *et al.* (1985)
mix		PEAD	Le Nadan *et al.* (1982)
2,0		PIES	Hotop, Lorenzen, and Zastrow (1981)
mix		PIAD	Haberland *et al.* (1981)
mix		NAD	Gregor and Siska (1981)

TABLE III. (*Continued*).

State[b]	Ionized molecule	Experiment type[c]	Reference
mix	$Ar^*(^3P)$	PICSE	Neynaber and Tang (1980b)
2,0	K	PIES	Lorenzen *et al.* (1986)
mix	Kr	PICS	Aguilar, Bianco, *et al.* (1990)
mix		TCSE	Kerstel *et al.* (1988)
2,0		TICSE	Verheijen and Beijerinck (1986)
mix		PICSEM	Brunetti *et al.* (1986)
mix		PEAD	Le Nadan *et al.* (1982)
2,0		PIES	Hotop, Lorenzen, and Zastrow (1981)
mix		NAD	Gregor and Siska (1981)
mix	Xe	PICS	Aguilar, Bianco, *et al.* (1990)
mix		TCSE	Kerstel *et al.* (1988)
2,0		PICSE	Verheijen and Beijerinck (1986)
mix		PEAD	Le Nadan *et al.* (1982)
2,0		PIES	Hotop, Lorenzen, and Zastrow (1981)
mix		NAD	Gregor and Siska (1981)
2,0	Cs	PIES	Lorenzen *et al.* (1986)
mix	Hg	PICSEM	Appolloni *et al.* (1987)
2,0		PIES	Hotop, Lorenzen, and Zastrow (1981)
2,0	H_2	PICSE	van den Berg *et al.* (1987)
mix		NAD,PIAD	Robert *et al.* (1987)
mix		PIED	Tuffin, Le Coz, and Le Nadan (1987)
2,0		PIES	Bussert *et al.* (1983)
mix	HCl	PICSEM	Aguilar-Navarro *et al.* (1992)
mix		PICS	Aguilar, Bianco, *et al.* (1990)
mix		PICSEM	Aguilar, Brunetti, *et al.* (1990)
2,0		PIES	Yencha *et al.* (1989)
mix		PIOS	Snyder *et al.* (1983)
mix	HBr	PIES	Yencha *et al.* (1991)
mix		PICS	Aguilar, Bianco, *et al.* (1990)
mix		PICSEM	Aguilar, Brunetti, *et al.* (1990)
mix		PIOS	Tyndall *et al.* (1984)
mix	N_2	NAD	Baudon *et al.* (1991)
mix		PICS	Aguilar, Bianco, *et al.* (1990)
mix		PICSEM	Aguilar, Brunetti, *et al.* (1990)
mix		TCSE	Kerstel *et al.* (1988)
mix		PICSEM	Appolloni *et al.* (1988)
2		PILF	Sonnenfroh and Leone (1987a, 1987b)
2,0		PICSE	van den Berg *et al.* (1987)
2,0		PICSE	Verheijen and Beijerinck (1986)
mix	CO	PICSEM	Aguilar, Brunetti, *et al.* (1990)
mix		PIED	Le Nadan *et al.* (1989a)
mix		PICSEM	Appolloni *et al.* (1988)
mix		PIOS	BelBruno and Krenos (1983)
mix		PIES	Tuffin, Le Coz, and Peresse (1980b)
mix	NO	PICS	Aguilar, Bianco, *et al.* (1990)
mix		PICSEM	Aguilar, Brunetti, *et al.* (1990)
mix		PICSEM	Appolloni *et al.* (1988)
2,0		PICSE	van den Berg *et al.* (1987)
mix	O_2	PICS	Aguilar, Bianco, *et al.* (1990)
mix		PICSEM	Aguilar, Brunetti, *et al.* (1990)
mix		TCSE	Kerstel *et al.* (1988)
mix		PICSEM	Appolloni *et al.* (1988)
2,0		PICSE	van den Berg *et al.* (1987)
mix		PICSEM	Alvarino *et al.* (1984)
mix	Cl_2	PICS	Aguilar, Bianco, *et al.* (1990)
mix		PICSEM	Aguilar, Brunetti, *et al.* (1990)
mix		PICSEM	Alvarino *et al.* (1984)
2,0	Ar_2	PICS	Kraft *et al.* (1988)

TABLE III. (*Continued*).

State[b]	Ionized molecule	Experiment type[c]	Reference
mix		PICS	Birkhofer *et al.* (1984)
mix	CO_2	PICS	Aguilar, Bianco, *et al.* (1990)
mix		PICSEM	Aguilar, Brunetti, *et al.* (1990)
mix		PIED,PIES	Le Nadan *et al.* (1989a, 1989b)
mix		TCSE	Kerstel *et al.* (1988)
2,0		PICSE	van den Berg *et al.* (1987)
mix		PIES	Tuffin, Le Coz, and Peresse (1981)
mix	N_2O	PICS	Aguilar, Bianco, *et al.* (1990)
mix		PICSEM	Aguilar, Brunetti, *et al.* (1990)
2,0		PICSE	van den Berg *et al.* (1987)
mix	C_2H_2	PICS	Aguilar, Bianco, *et al.* (1990)
mix		PICSEM	Aguilar, Brunetti, *et al.* (1990)
mix	CH_4	PICS	Aguilar, Bianco, *et al.* (1990)
mix		PICSEM	Aguilar, Brunetti, *et al.* (1990)
mix		TCSE	Kerstel *et al.* (1988)
2,0		PICSE	van den Berg *et al.* (1987)
mix	CH_3Cl	PICS	Aguilar, Bianco, *et al.* (1990)
mix		PICSEM	Aguilar, Brunetti, *et al.* (1990)
mix	CH_3Br	PICS	Aguilar, Bianco, *et al.* (1990)
mix		PICSEM	Aguilar, Brunetti, *et al.* (1990)
mix	C_2H_4	PICS	Aguilar, Bianco, *et al.* (1990)
mix		PICSEM	Aguilar, Brunetti, *et al.* (1990)
mix	C_2H_6	PICS	Aguilar, Bianco, *et al.* (1990)
mix		PICSEM	Aguilar, Brunetti, *et al.* (1990)

[a]Works are cited antichronologically.
[b]2 and 0 refer to $j=2$ and $j=0$ neon, respectively, in state-selected experiments, while mix denotes a mixed beam with unresolved contributions from each state.
[c]Abbreviations not defined in Table II are as follows: PICSEP—Penning ionization cross-section collision energy dependence and polarization dependence; PIESP—Penning ionization electron spectrum with polarization dependence; PILF—Penning ionization laser-induced fluorescence of product ion; PIAD—Penning ion angular distribution.

1991b, 1991c), as well as continuing work in flowing afterglow spectroscopy (Tsuji, 1990), related studies on nonionizing energy transfer in the metastable noble gases (Beijerinck, 1987, 1990), and the study of Rydberg atoms (Stebbings and Dunning, 1983) are omitted, in order to focus on advances in understanding the basic process. Progress in understanding the closely related associative ionization reaction has recently been reviewed by Weiner *et al.* (1989); while this reaction often competes with reaction (1.1), systems where this is the only open channel are not included here.

II. EVOLUTION OF MOLECULAR-BEAM METHODS FOR PENNING STUDIES

Prior to 1960, the main technical developments in molecular beams had occurred in the laboratories of Stern, Rabi, and Ramsey (Ramsey, 1956), with a focus on the properties of isolated molecules. Thus the earliest Penning beam experiments cited in Sec. I utilized a single metastable noble-gas (He^*) beam with a gas cell containing the partner molecule of interest; the gas cell could be used in place of or in addition to one of the analyzing fields. But an extensive development of the crossed-molecular-beam method for study of the collisions and reactions of alkali atoms pioneered by Greene, Moursund, and Ross (1966) and Herschbach (1966) was quickly reflected in Penning experiments, particularly in the work of Niehaus, an early senior collaborator in Herschbach's laboratory (Fuchs and Niehaus, 1968; Hotop and Niehaus, 1968, 1969a, 1969b, 1970a, 1970b, 1971; Hotop, Niehaus, and Schmeltekopf, 1969). A large and increasing fraction of the PI work over the last 25 years has comprised crossed-beam studies; early single-beam work has been reviewed by Muschlitz (1966, 1968, 1973). Much of the lore of the more recently developed molecular-beam techniques, shared by workers in Penning ionization, has now been collected in *Atomic and Molecular Beam Methods*, edited by Scoles (1988); the reader in search of more details on general beam techniques and characteristics is referred to this volume. In particular, the chapters therein by Pauly (1988) and Bergmann (1988) contain further information and references on excited-beam production and state selection, respectively.

A. Production of excited-atom beams

The finding that excited, metastable noble-gas atoms are present in discharges is naturally applied in using a dc discharge with an aperture as a metastable atom beam source (Rothe *et al.*, 1965; Illenberger and Niehaus, 1975; Hotop *et al.*, 1979). The low pressures necessary to sustain the discharge correspond well to effusive or near-effusive beam characteristics. Electrons and ions are swept off the beam axis by a transverse electric field, leaving a relatively clean near-Maxwellian beam containing up to 10^{-4} atom fraction of the lowest-lying metastable excited states of the noble gas. Both cold and hot cathode sources have been successfully employed (see, for example, Hotop *et al.*, 1979), and, in more recent work, higher discharge pressures have resulted in a mildly supersonic metastable beam [~30–45 % full width at half maximum (FWHM) velocity spread; see Fahey *et al.*, 1980a; Verheijen and Beijerinck, 1984; Verheijen, Beijerinck, Van Moll, *et al.*, 1984; Bussert, Bregel, Allan, *et al.*, 1985; Ohno *et al.*, 1991].

Metastable atoms are presumably excited by energetic electron impact within the discharge, suggesting a second method for excited-beam production, direct electron impact on a preexpanded atomic beam in a separate excitation region (Smith and Muschlitz, 1960; Čermák, 1966; Hotop and Niehaus, 1968, 1969b; Rundel *et al.*, 1974; Martin *et al.*, 1976, 1978; Brutschy and Haberland, 1977; Foreman *et al.*, 1977). In addition to facilitating pulsed, time-resolved experiments through manipulation of the exciting electron beam, separate excitation also allows the use of a supersonic ground-state feeder beam, thus increasing intensity, narrowing the velocity distribution of metastables, and allowing independent control of beam energy (Martin *et al.*, 1976, 1978; Brutschy and Haberland, 1977). As compared to a discharge source, however, the efficiency of excitation followed by retention of metastables within the beam is typically lower by a factor of 10–100 in this method, and thus the discharge is still commonly used.

Charge-transfer neutralization of a keV He^+ beam by Cs vapor has been used by Neynaber *et al.* (1972; Neynaber and Magnuson, 1976) to produce He* for merged-beam PI studies. The lower intensity of this type of source, limited by space-charge dispersion of the parent ion beam, is partially offset by the kinematic advantages in product collection associated with high laboratory-system beam energies. The merged-beam technique has

TABLE IV. Miscellaneous recent beam studies relating to Penning ionization in small systems.

System[a]	Experiment[b]	Reference
$H^*(2\,^2S)+H_2$	TCSE,NAD	Vassilev *et al.* (1990)
$He^*(2\,^1S)$+He,Ar,Kr,Xe	RD	Dehnbostel *et al.* (1990)
$He^{**}(5\,^3P)$+He	PICSEM	Pesnelle *et al.* (1983)
$He^{**}(3\,^1P)$+Ne	PICSEM	Pesnelle *et al.* (1981), Pesnelle and Runge (1984a, 1984b)
$Ne^{**}(3p\,^3D_3)$+Ar	PICSEP	Driessen, Megens, *et al.* (1990)
		Driessen, van de Weijer, *et al.* (1990)
		Driessen, van de Weijer, *et al.* (1989)
	PIESP,PICSP	Bregel *et al.* (1986)
		Bussert, Bregel, Allan, *et al.* (1985)
		Bussert, Bregel, Ganz, *et al.* (1985)
$Ne^{**}(3p,\ J=1,2)$+Ar	PIES,PICS	Bussert, Bregel, Ganz, *et al.* (1985)
$Ne^{**}(3p\,^3D_3)$+Kr, Xe	PICSEP	Driessen, van de Weijer, *et al.* (1990)
$Ne^{**}(3p\,^3D_3)$ +H_2,N_2,CO,O_2,CO_2,N_2O,CH_4	PICSEP	Driessen, Manders, *et al.* (1991)
$Ne^{**}(3p\,^3D_3)+H_2$	PIES	Bussert, Ganz, *et al.* (1983)
$Ne^{**}(3p\,^3D_3)+N_2$	PIES	Hotop (1980)
$Ar^*(^3P)+Ne^*(^3P)$	PICSE	Neynaber and Tang (1980b)
$Ar^*(^3P_{2,0})$+Na	PIES	Schohl *et al.* (1990)
$Ar^*(^3P)$+Hg	PICSEM	Appolloni *et al.* (1987)
$Ar^*(^3P)+O_2$	IPF	Schall *et al.* (1981)
$Ar^*(^3P)+CS_2$	PICSPA	de Vries *et al.* (1987)
$Kr^*(^3P_{2,0})$+Na	PIES	Schohl *et al.* (1990)
$Kr^*(^3P)$+Hg	PICSEM	Appolloni *et al.* (1986, 1987)
$Xe^*(^3P_{2,0})$+Na	PIES	Schohl *et al.* (1990)
$Ba^{**}(17d\,^1D_2)$+Na	PICS	Burkhardt *et al.* (1990)

[a]See Tables II and III for He* and Ne* metastable atom studies, respectively. Lack of subscripts on the state designation indicates an unresolved mixture of fine-structure states. A double asterisk indicates a state formed by laser excitation out of the metastable state, except for Ba**.

[b]Abbreviations: RD—radiative deexcitation; IPF—ion-pair formation; PICSPA—Penning ionization cross section with photodissociation-aligned reagent molecule; see Tables II and III for other acronym definitions.

had the longstanding advantage of allowing a continuously variable center-of-mass collision energy over a wide range (typically 0.01–10 eV).

Among the more recently developed sources is a low-voltage, high-current plasma arc struck between a hollow-cathode beam orifice and first collimator (skimmer) (Theuws, Beijerinck, Verster, and Schram, 1982). Though this source yields a broad range of metastable speeds, it affords much higher laboratory-system energies than available from other sources because of the high plasma temperatures attainable, and lends itself to time-of-flight selection (see Sec. II.C). Another recent development is a high-voltage cold-cathode discharge on a supersonic feeder beam (Snyder *et al.*, 1983; Tyndall *et al.*, 1984).

Table V compares intensities and state populations of the popular sources. In addition to metastable states, all sources except charge transfer produce a small fraction of uv photons and Rydberg states and an inevitable small flux of noble-gas ions, which pass through the fields designed to quench or contain them.

1. Beam composition and state selection

All the beam production methods described create a mixture of the two allowed metastable states for each noble gas, whose populations must in general be determined. Measurement of absolute intensities, populations, and state-specific detection efficiencies has been a recur-

TABLE V. Metastable atom beam sources.

Species	Source type[a]	Intensity[b] (10^{14} s^{-1} sr^{-1})	Energy range[c] (eV)	Population ratio[d]	Reference
He*($2^{1,3}S$)	dca	30	0.2–5	1:3	Ferkel *et al.* (1991)
	ccdn	20	0.06–0.4	1:9	Ohno, Takami, and Mitsuke (1991)
	nei	3	0.03–0.4	7:1	Brutschy and Haberland (1977)
	ccdn	3	0.07	(1:10)	Fahey *et al.* (1980a)
	eei	2	0.05	1:1.2	Riddle *et al.* (1981)
	hca	1	1–6	1:25	Kroon *et al.* (1986)
	ccdn	0.4	0.05–0.25	1:10	Kroon *et al.* (1986)
	ccde	0.4	0.07	1:10	Hotop, Kolb, and Lorenzen (1979)
	nei	0.2	0.02–0.25	9:1	Martin, Gregor, *et al.* (1978)
	nccd	0.1	0.05	9:1	Tyndall *et al.* (1984)
	hcde	0.08	0.2	1:10	Hotop, Kolb, and Lorenzen (1979)
Ne*($3s\ ^3P_{0,2}$)	ccdn	4	0.07	1:5.1	Schohl *et al.* (1991)
	hca	2	0.5–8	1:5	Verheijen and Beijerinck (1986)
	nei	0.4	0.06–0.25	1:3.4	Weiser and Siska (1987)
	nccd	0.3	0.05–0.15	(1:5)	Snyder *et al.* (1983)
	ccdn	0.2	0.05–0.10	(1:5)	Verheijen and Beijerinck (1986)
Ar*($4s\ ^3P_{0,2}$)	ccdn	3	0.07	1:6,3	Schohl *et al.* (1991)
	hca	2	0.05–0.2	1:5	Vredenbregt *et al.* (1990)
	nei	0.6	0.06–0.25	1:3.0	Weiser and Siska (1987)
	ccdn	0.3	0.05–0.2	(1:5)	Vredenbregt *et al.* (1990)
Kr*($5s\ ^3P_{0,2}$)	ccdn	2	0.07	1:10.4	Schohl *et al.* (1991)
	hca	0.8	1–6	(1:5)	Vredenbregt *et al.* (1990)
	nei	0.7	0.06–0.25	1:6.1	Weiser and Siska (1987)
Xe*($6s\ ^3P_{0,2}$)	ccdn	~1	0.07	(1:13)	Schohl *et al.* (1990)
	nei	~1	0.06–0.25	1:2.7	Weiser and Siska (1987)
	hca	0.01	1–6	(1:5)	Vredenbregt *et al.* (1990)

[a]Abbreviations: dca—double-cathode arc; ccdn—cold-cathode-discharge nozzle expansion; nei—nozzle expansion followed by electron impact; eei—effusive expansion follows by electron impact; hca—hollow-cathode arc expansion; ccde—cold-cathode-discharge effusive expansion; nccd—nozzle expansion followed by cold-cathode discharge; hcde—hot-cathode-discharge effusive expansion.

[b]Intensities are uncertain within a factor of 2–3 due to poorly known detection efficiencies (see Table VI).

[c]Beam energy is tunable for the nozzle sources with external excitation, both when nozzle expansion is followed by electron impact and when it is followed by cold-cathode discharge; other ranges given correspond to a broad distribution, for which time-of-flight energy selection has been employed.

[d]Ratios correspond to the order of the states in the left-hand column; those in parentheses are estimated.

ring problem, affecting the intensity estimates in Table V as well as the populations given there. Though detection of excited atoms with a Faraday cup, which operates by surface Penning ionization from a central metal-plate electrode, is straightforward and inexpensive, its sensitivity can be highly variable and its efficiency is difficult to measure. Stainless steel, with or without a colloidal graphite (Aquadag) coating, has become the standard material for the detection electrode. Several methods have been used to estimate the secondary-electron ejection coefficient (Borst, 1971, 1974; Dunning and Smith, 1971; Dunning *et al.*, 1971; Rundel *et al.*, 1974; Dunning, Rundel, and Stebbings, 1975; Woodard *et al.*, 1978; Schohl *et al.*, 1991), but as these experiments have been carried out in simple high vacuum, implying a gas-covered metal surface, the results probably depend on its history. In this connection, warming the detector surface, which removes adsorbates, is found to improve the stability and decrease the sensitivity to surface material and preparation method and can increase the efficiency of the detector (Schohl *et al.*, 1991). Table VI summarizes the highly variable efficiency measurements. Based on gas-phase ionization cross sections for the likely adsorbates N_2, O_2, or CO, it seems likely that the efficiencies would differ somewhat between the $2\,^1S$ and $2\,^3S$ states of He, but less so between the $J=0$ and $J=2$ states of the heavier metastables. Hyperthermal metastable beams might also yield higher efficiencies (Theuws, Beijerinck, Verster, and Schram, 1982).

Recently Schohl *et al.* (1991) have demonstrated a two-cw-laser method for the determination of absolute beam intensities and state populations for Ne*, Ar*, and Kr* as well as secondary ejection coefficients, through intracavity ion-laser photoionization after dye-laser excitation of a metastable atom beam. This method, while more difficult to implement in a general scattering apparatus, should allow the estimation of state-selection efficiencies as well.

State selection of metastable atoms has successfully been done using both magnetic deflection and depletion by optical absorption. Magnetic deflection was employed in the early beam/gas-cell total-collision cross-section measurements of Rothe *et al.* (1965), in which a mixed beam was passed through an inhomogeneous magnetic field after scattering, thereby separating $He^*(2\,^3S)$ from $2\,^1S$, which has no net magnetic moment, and allowing pure ^3S (but not ^1S) cross sections to be obtained. Since the demonstration by Fry and Williams (1969) and by Hotop, Niehaus, and Schmeltekopf (1969) of optical depletion of the $2\,^1S$ state from a mixed beam, however, optical state selection has been the dominant method. For He*, a flowing He resonance lamp, running at 1–5 Torr and ~1 kV, either spiraled around or with arms parallel to the mixed beam, provides infrared photons that pump the $2s \rightarrow 2p$ transitions in both ^1S and ^3S. Only the singlets then radiatively decay to the ground state, yielding a

TABLE VI. Metastable atom detection efficiencies (secondary ejection coefficients γ).

Detector surface	$He^*(2\,^1S)$	$He^*(2\,^3S)$	$Ne^*(^3P)$	$Ar^*(^3P)$	$Kr^*(^3P)$	$Xe^*(^3P)$
Stainless steel	0.95(10)[a] 0.53(8)[d]	0.95(10)[a] 0.69(9)[d]	0.91(11)[a] 0.61(8)[d] 0.30(5)[b]	0.97(15)[a] 0.13(9)[b,c]	0.03(2)[b,c]	
Stainless steel, graphite coated			0.35(5)[b]	0.16(6)[b] 0.21(6)[c]	0.09(2)[b] 0.10(2)[c]	
CuBe	0.51[d]	0.63[d]	0.44[d] 0.40(5)[b,c]	0.15(9)[b] 0.25(9)[c]	~0[b] ~0.06[c]	
CuBeO		0.15(3)[e]	0.12[e]	0.035[e]	0.020[e]	0.005[e]
Au (plated)	0.46(9)[a] 0.45(2)[f]	0.63(7)[a] 0.55(2)[f]	0.52(6)[a] 0.48(2)[f]	0.66(10)[a] 0.03(2)[b] 0.24(5)[c]	0.005(3)[b] 0.06(2)[c]	
Molybdenum				~0.02[b] 0.14(5)[c]	~0.006[b] 0.06(2)[c]	

[a]Dunning and Smith (1971). The He* results for stainless steel refer to a mixture of ^1S and ^3S.
[b]Schohl *et al.* (1991), 300-K surface. The error in each determination is ~1%, but large variations are found between different apparently identically prepared detector plates, giving a large systematic error. In earlier work Weissmann *et al.* (1984) reported efficiency ratios for the fine-structure states of Ne*, Ar*, and Xe* on stainless steel, finding $\gamma_2/\gamma_0 = 1.00(4)$, 0.96(6), and 0.58(3), respectively.
[c]Schohl *et al.* (1991), 360-K surface. The increase in efficiency was found to be greatest for surfaces with low efficiencies at 300 K.
[d]Rundel, Dunning, and Stebbings (1974).
[e]Borst (1971). Surface is the first dynode of a Johnston *MM*-1 multiplier.
[f]Woodard *et al.* (1978).

nearly pure ^3S beam with the lamp on. Subtraction of product signals with the lamp off and on then yields the ^1S component as well. These lamps have been successfully employed with irradiation lengths as small as 2 cm, affording a great advantage over magnetic deflection, which requires an order-of-magnitude longer path to achieve the necessary spatial separation of m_s states, with only $\frac{1}{3}$ of the beam employable for collisions.

To state-select the heavier metastable noble gases requires wavelength selection, as both the $^3P_0$ and $^3P_2$ states can absorb resonance radiation and return to the ground state. Following the demonstration by Dunning, Cook *et al.* (1975) of state selection of Ne* by cw dye-laser absorption in the $3s \rightarrow 3p$ manifold, Hotop *et al.* (1981) successfully employed the method in a Penning ionization electron spectroscopy (PIES) experiment. For the excited noble gases, changes in the $ns \rightarrow np$ transition wavelengths correspond to those in the nearest alkali atom, but are modified strongly by the core spin-orbit interaction in Kr* and Xe*, making new laser dyes and perhaps new pump lasers necessary to cover the family (Schohl *et al.*, 1991). Weissmann *et al.* (1984) have demonstrated state selection for Ar* and Kr* using an intracavity cw dye-laser arrangement. Dye lasers operating in both broadband and single-frequency mode have been used successfully for Ne*; the former allows simultaneous pumping of both ^{20}Ne and ^{22}Ne isotopes but requires high power, while the latter is isotope selective, necessitating correction of the data for the unpumped isotopes. Table VII summarizes conditions employed in state selection of the heavier noble-gas metastables.

If the chosen pumping transition involves a $J=1$ state in the np manifold, fluorescence can occur to both the $J=0$ and $J=2$ metastable levels as well as the radiating $J=1$ state. Repeated pumping cycles then convert a fraction of the flux of the pumped metastable level into its mate. In a PIES experiment the two metastable states produce distinct spectra and thus allow the relative populations of the two states to be determined through monitoring of the fractional increase in signal from the unpumped state (Weissmann *et al.*, 1984), provided the Einstein A coefficient for the decay of the np state is known.

TABLE VII. Representative transitions for laser fine-structure state selection.[a]

Atom	Upper state	Wavelength (nm)	Fractional conversion
Ne*($3s\ ^3P_2$)	$3p\ ^3D_1$	621.7	0.24
	$3p\ ^1D_2$	614.3	0
	$3p'\ ^1P_1$	597.6	0.52
	$3p'\ ^3P_2$	594.5	0
	$3p'\ ^3P_1$	588.2	0.34
Ne*($3s\ ^3P_0$)	$3p'\ ^1P_1$	626.7	0.14
	$3p'\ ^3P_1$	616.4	0.29
Ar*($4s\ ^3P_2$)	$4p\ ^1D_2$	763.5	0
	$4p'\ ^3P_1$	696.5	0.40
Kr*($5s\ ^3P_2$)	$5p\ ^1D_2$	760.2	0
	$5p'\ ^3P_1$	557.0	0.58

[a]For Ne* see Dunning, Cook, *et al.* (1975), Hotop, Lorenzen, and Zastrow (1981), Weissmann, *et al.* (1984), Verheijen and Beijerick (1986), and van den Berg, *et al.* (1987); for Ar* see Chang and Setser (1978) and Weissmann, *et al.* (1984); for Kr* see Weissmann, *et al.* (1984).

Strictly for the purpose of population determination, magnetic deflection is somewhat more direct and does not require a knowledge of the radiative properties of an upper state. Using electron-impact-excited metastable beams and a translatable detector, Weiser and Siska (1987, 1988) derived fine-structure populations (assuming equal detection efficiency of the two states) from fully M_J-resolved deflection patterns for all the heavier metastable noble gases. From the resulting populations (given in Table V) it is evident that, for Ar*, Kr*, and Xe*, discharge sources tend to produce a greater preponderance of the lower-energy $^3P_2$ state, while high-energy electron-impact excitation of a preexpanded beam results in a more nearly statistical (5:1) $J=2/J=0$ ratio. Magnetic deflection has also been used to monitor the production of nonuniform M-state populations in optical pumping experiments with a polarized cw laser (Giberson *et al.*, 1984).

The study of polarization effects in Penning ionization, a more recent development, has centered on Ne*($3s\ ^3P_2$) and the nonmetastable Ne**($3p\ ^3D_3$) state readily excited from $^3P_2$ (Bussert, Bregel, Allan, *et al.*, 1985; Bussert, Bregel, Ganz, *et al.*, 1985; Bregel *et al.*, 1986; Bussert, 1986; Driessen *et al.*, 1989; Driessen, Megens, *et al.*, 1990; Driessen, van de Weijer, *et al.*, 1990). Optical pumping techniques and beam characteristics have been explored by Kroon *et al.* (1981, 1984, 1985) and Verheijen *et al.* (1985). Of the several possible transitions where optical pumping is possible (Hertel and Stoll, 1978; Bussert, Bregel, Ganz, *et al.*, 1985; Bussert, 1986; Bergmann, 1988), the most popular have been from $^3P_2$ to $^3D_2$ at 633.4 nm and $^3D_3$ at 640.2 nm in the $3p$ manifold. The former has the advantage of permitting a high degree of polarization with linearly polarized light (Bussert, 1986), while the latter forms a quasi-two-state system with $^3P_2$, resulting in polarization of $^3P_2$ without loss of flux through decay to other states.

From a collision-dynamics point of view, polarization must be defined with respect to the relative velocity $\mathbf{v}$, and a particular $|M|$-state population, created with respect to the direction of laser polarization [for linear (π) polarization] or propagation [for circular (σ) polarization], must be rotated according to

$$s_M^J(\beta)=\sum_{M'=-J}^{J}[d_{MM'}^J(\beta)]^2 s_{M'}^J(0)\ , \tag{2.1}$$

where s_M^J is the population, β is the angle between the relevant laser axis and $\mathbf{v}$, and d is the Wigner rotation matrix. Equation (2.1) also covers the case of left- or right-handed circular polarization, which can produce orientation (unequal populations in $+|M|$ and $-|M|$

states), but for the present purpose only alignment need be considered. For a beam/gas-cell arrangement, as in Bregel *et al.* (1986), **v** coincides on the average with the excited-beam axis, and β becomes simply the angle between the beam axis and the appropriate laser direction. In crossed beams, however, as in Driessen, van de Weijer, *et al.* (1990), the relative velocity **v** is cocked at an angle Θ_v with respect to the excited-beam direction, an angle which changes with changing collision energy E, and β must be augmented appropriately. In the beam/gas-cell experiment, the spread in the direction of **v** decreases with increasing beam velocity and hence energy; at thermal energy, depending on the mass of the partner and the temperature of the cell, this spread could all but wash away observable polarization effects, and thus crossed beams are to be preferred for this type of measurement despite the variation of the populations with E.

Only two basic types of polarization, σ and π, and therefore only two basic population distributions, are possible for a given pair of states being pumped, with $\beta=0$ being achievable physically by shining the laser along (σ) or perpendicular (π) to **v**. Bussert (1986) has analyzed all combinations of J states arising from Ne* $3s \rightarrow 3p$ transitions by integrating the optical rate equations in the limit of many pumping cycles to obtain asymptotic M-state populations. In $J=2 \leftrightarrow J=2$ pumping with π polarization, the $\Delta M=0$ selection rule, combined with quenching to $J=1$ in the $3s$ manifold, produces 100% $M=0$ in both the upper and lower states. For $\beta=\pi/2$, achieved by rotating the plane of polarization perpendicular to the plane of collision, Eq. (2.1) yields 25% $M=0$, 75% $|M|=2$. In the quasi-two-state $J=2 \leftrightarrow J=3$ excitation, no quenching can take place, and using σ polarization yields pure $|M|=3$ in the upper state and $|M|=2$ in the lower, while π polarization yields identical 47.6, 47.6, 4.8 % $|M|=0,1,2$ populations in both states. Again Eq. (2.1) allows populations for other laser axis orientations to be predicted from these basic populations. The $2 \leftrightarrow 3$ system allows a polarized $3s\ ^3P_2$ population to be prepared prior to the collision zone, owing to the lack of quenching and the ΔM selection rules. When preparation of pure $|M|$ states with respect to **v** is not practical, polarized cross sections may still be obtained by choosing different β's and solving simultaneous linear equations (Driessen, van de Weijer, *et al.*, 1990).

Normally the use of the Zeeman effect for isolating M states in wavelength-selective pumping is not possible in PI studies, due to the effect of the magnetic field on the product ions and electrons. However Driessen, Megens, *et al.* (1990) have recently shown that polarized cross-section measurements are feasible with Zeeman pumping, by using the magnetic field to parallelize the Penning electrons, thereby making possible 2π solid-angle collection.

Of great promise for PI beam studies in new intensity and energy regimes is the recent demonstration of laser manipulation of the speeds and directions of He*($2\ ^3S_1$) and Ne*($3s\ ^3P_2$) beams (Aspect *et al.*, 1990; Shimizu *et al.*, 1990), comprising both transverse and longitudinal cooling and trapping of the metastables.

2. Beam speed distributions

Much of the earlier molecular-beam PI work, especially Penning ionization electron spectroscopy, was carried out with one or two effusive beams, for which Maxwellian speed distributions were assumed. In a few "medieval" experiments (Rundel *et al.*, 1974; Illenberger and Niehaus, 1975; Pesnelle *et al.*, 1975) the metastable He* beam-velocity distribution was measured and found to deviate significantly from the Maxwellian form, whether from a discharge or an electron-impact-excited ground-state beam. Accounting for such deviations can be of importance in the comparison of experiment with theory in PIES studies (Waibel *et al.*, 1988). In experiments with electron-impact-excited supersonic beams (Brutschy and Haberland, 1977; Martin *et al.*, 1978), it was again found that deviations from the expected peak position and width of a supersonic ground-state beam distribution (Anderson, 1974; Beijerinck and Verster, 1981) are the rule in He* and, moreover, than the ^1S and ^3S distributions differ significantly (Brutschy and Haberland, 1977; Jordan *et al.*, 1986), the ^3S distribution being considerably broader, with bimodality appearing for low parent beam speeds. For supersonic Ne* beams produced in this way (Gregor and Siska, 1981), a slight reduction in the apparent Mach number or speed ratio is observed. Verheijen *et al.* (1984), however, find their measured distributions from a nozzle discharge source to be in good agreement with that expected from a mildly supersonic expansion, although at a somewhat elevated temperature; a similar situation obtains for the external cold-cathode discharge source (Snyder *et al.*, 1983). The cathode arc source (Theuws, Beijerinck, Verster, and Schram, 1982) yields a distribution neither thermal nor supersonic.

Velocity distortions in the impact-excited sources are attributed in part to the kinematics of the excitation process; for the most favorable electron-beam directions, collinear isodirectional with or opposed to the ground-state beam, the He* peak velocity is shifted from He due to momentum transfer during excitation, and a convolution of the transverse momentum transfer with the two-dimensional ground-state velocity profile produces a broadening effect. The ^1S-^3S differences appear to arise from the stronger collisions required to flip the spin, which result in greater transverse scattering in producing the excited triplet. Preferential scattering of low-velocity excited atoms out of the beam, and/or resonant energy transfer between slow and fast atoms (see also Sec. II.D) can also distort the distribution, the latter being the present explanation for bimodality (Brutschy and Haberland, 1977). Despite these complications, the distributions are now routinely measured by time-of-flight methods and can be used as readily as the ideal distributions in the interpretation of experimental data; and the

advantage of the narrow supersonic distribution is substantially preserved for supersonic feeder beams.

B. Ground-state reagents: cells and crossed beams

In the pioneering work of Muschlitz and co-workers (Muschlitz, 1966), the traditional scattering cell, filled with 10^{-4}–10^{-3} Torr of reagent gas, was used to monitor total ion production as a function of metastable beam velocity. In this method the cell itself could serve as an ion/electron collector, by being equipped with floatable walls. Replacement of the cell with a "crinkly foil" effusive crossed beam placed about 1 cm from the excited-beam axis was pioneered by Hotop and Niehaus (1968); this allowed better definition of both the collision volume and the relative velocity vector, while retaining the ability to "tune" the attenuation of the metastable beam to maximize product signal while minimizing secondary scattering. Currently, reaction partners are still provided by cell or effusion because of this tunability.

The progression toward supersonic crossed beams has resulted in a sacrifice of scattered intensity on the altar of resolution, for despite the widely advertised high forward intensities inherent in supersonic expansions, the pumping stages and skimming required to prevent the flooding of collision and detector chambers with ambient crossed-beam gas force withdrawal of the nozzle to some distance from the collision region (generally 5 cm or more). But the greatly increased spatial and kinematic resolution has made such experiments worthwhile when feasible. Supersonic ground-state reagent beams have been employed to advantage in angle-resolved measurements of Penning ions (Leu and Siska, 1974a, 1974b), angle-resolved nonreactive scattering in Penning systems (Gregor and Siska, 1981; Haberland *et al.*, 1981; Martin and Siska, 1985; Baudon *et al.*, 1991), total ionization cross-section energy dependence both with supersonic, temperature-programmed metastable beams (Martin *et al.*, 1984, 1989; Weiser and Siska, 1986) and with time-of-flight-selected beams (Verheijen, Beijerinck, Renes, and Verster, 1984; Kroon *et al.*, 1986; Verheijen and Beijerinck, 1986; van den Berg *et al.*, 1987; Driessen *et al.*, 1989), total scattering cross-section velocity dependence in Penning systems (Kerstel *et al.*, 1988), and most recently in Penning ionization electron spectroscopy (Dunlavy *et al.*, 1990).

C. Detectors

In general only a highly excited atom or molecule can engage in Penning ionization; as a consequence, detectors can be tuned to ignore the collision outcomes of the overwhelmingly prevalent ground-state population in the excited beam. This feature, along with the rapid quenching of excited species on the walls and surfaces of the vacuum chamber, greatly reduces the possible sources of background signals in PI beam experiments, with the consequence that the lower bound on measurability of cross sections is often comparable to, and in many cases considerably smaller than, that for the most sensitive ground-state reaction studies in beams (Lee, 1988).

1. Excited states: electron multipliers

As described in Sec. II.A, Faraday cups are commonly used in detection of primary metastable beams; however, they lack the sensitivity for detecting scattered metastables, or even primary beams in long-path-length arrangements. Electron multipliers are also readily actuated by metastable impact, and because of their inherently high gain and short time constant they allow the use of pulse-counting methods (fast amplifier, discriminator, and single-channel or multichannel scaling). Combined with typically very low dark counting rates and the low background level cited above, multipliers enable ready detection of signal counting rates less than 1 Hz. Channel-type multipliers (Channeltron or Spiraltron), air-stable with gains approaching 10^8, have proven ideal in this application and have made possible a host of nonreactive scattering experiments in PI systems (Haberland *et al.*, 1981), to be described further below, as well as time-of-flight collision energy selection and product analysis. Higher quantum efficiencies can be achieved by using a separate metal cathode, i.e., a Faraday cup whose secondary electrons are collected by the multiplier (Theuws, Beijerinck, and Verster, 1982).

2. Ions: charge collection and mass spectrometry

Because of their manipulability by electric and magnetic fields, thermal-energy ions formed in Penning reactions have been collected and detected with efficiencies approaching 100%. Early ion detectors were charge-collection plates or Faraday cups, but these have given way in more recent times to particle multipliers or Daly-type scintillation counters (Daly, 1960). The scintillation counter, with its enclosed photomultiplier tube, is more sensitive to stray light, but less susceptible to poisoning by oxygen- or halogen-containing species. The use of such high-gain detectors has been especially crucial in crossed-beam experiments, where total ion currents are generally 10^{-13} A or less. With no need for an ion-production step, an inefficient process that also typically generates a large number of background ions, mass spectrometry using either a magnetic sector or an electric quadrupole mass analyzer is nearly background free and relatively easy to implement in pulse-counting mode. Mass analysis not only enables a useful discrimination against ionization of ambient gases in the experimental chamber, but provides useful mechanistic information. In every Penning system the possibility exists for forming associative ions, AB^+, and often ionic rearrangement or fragmentation channels are open as well, both of which may be revealed in the product mass spectrum. Ionic

branching in Penning ionization will be discussed further in Secs. III–V.

Most PI experiments employing mass spectral product analysis have used a quadrupole analyzer with total ion extraction from the collision region with an electric field (see, for example, Martin *et al.*, 1984). The required field is determined by the force needed to overwhelm the natural product ion momentum arising from the kinematics and reaction dynamics; fields ranging from 60 to 1000 V/cm have been employed successfully. The extraction field is generally supplied by parallel plates, which may be floated to adjust the ion energy for transmission through the mass analysis and detection train. Time-of-flight mass analysis can also be employed, but this requires pulsing either one of the beams or the product ion stream, implying a low duty cycle.

For recoil angle/energy-resolved measurements of product ions (Leu and Siska, 1974a, 1974b; Kahn *et al.*, 1981, 1991a, 1991b), the extraction plates are replaced by a small Faraday cage to allow field-free flight of product ions into the acceptance aperture of a rotatable quadrupole mass analyzer/ion counter. Owing to the distorting effects of stray fields of only a few mV/cm on the laboratory trajectories of thermal-energy ions, short free-flight paths and small apertures are preferred. Angle-resolved product laboratory recoil energy spectra are conveniently obtained using electrostatic retarding-field analysis; while either electronic or numerical differentiation of the raw spectra is required, this method allows the use of a straight-through detector train, permitting unambiguous total flux measurements at each scattering angle. Angle/energy resolution of 1°/0.5 kcal/mol has been achieved (Longley *et al.*, 1992); energy resolution might be improved by using time-of-flight product analysis, for reactions with sufficient yield to overcome the low duty factor.

Crossed-beam product angle-energy distributions present a kinematic problem in the transformation of velocity-space coordinates and intensities from the laboratory to the center-of-mass frame that has been thoroughly analyzed for ground-state reactive scattering (Herschbach, 1966; Warnock and Bernstein, 1968; Siska, 1973). The assumption of a continuous recoil energy distribution ordinarily made in kinematic analysis of reactive scattering is rigorously true in Penning ionization (see Sec. III).

3. Electrons: electrostatic energy analysis

Electrostatic energy analysis of electrons emitted from energetic systems is a widely used and useful technique; an extensive discussion of different types of analyzers is given in Moore *et al.* (1989). In Penning ionization, collection of electrons and measurement of their energy spectra, known as PIES, occupies a position of unique importance for reasons to be discussed in the remaining sections. Most PIES experiments have employed either cylindrical or spherical sector analyzers singly or in tandem, while more recently a cylindrical-mirror analyzer has been adopted for angle-resolved measurements (Merz *et al.*, 1989, 1990). As for ions, time-of-flight methods might also be feasible if the low duty factor can be tolerated.

Materials for construction of electrostatic analyzers must be nonmagnetic and resistant to the development of insulating oxides or other films; oxygen-free high-conductivity (OFHC) copper or molybdenum have filled this role most often. Copper coated with a vacuum-baked graphite film has proven to be an especially stable surface in the author's laboratory. Analyzers are commonly operated in constant-pass-energy mode, with lower pass energies typically yielding better resolution at the expense of counting rate. Careful shielding of electrical leads to the analyzer from ac induction is essential for operation at or near the limiting performance determined by analyzer geometry. Stray magnetic fields are commonly eliminated by degaussed magnetic shielding material, Helmholtz coils, or a combination of the two (Moore *et al.*, 1989). Detection is normally by a channel or microchannel plate multiplier; it is anticipated that position-sensitive detection will be used increasingly in the future (see, for example, Pollard *et al.*, 1981; Baus *et al.*, 1985).

Calibration of the analyzer as to energy scale and transmission has generally been accomplished through the use of He I or Ne I uv photons (photoelectron spectroscopy, or PES) either as contaminants of the metastable beam itself or from a separate uv light source, for the same reaction partner. Alternatively a gas mixture is employed, one of whose components has a well-established spectrum, for those cases where the PIES and PES are badly overlapped or where significant changes in detection characteristics (due, for example, to gradual contamination of analyzer surfaces) occur within the measurement period. Standard photoelectron spectra measured by Gardner and Samson (1976; see also Lorenzen *et al.*, 1983) are used as primary standards for transmission correction.

While the highest energy resolution thus far demonstrated in PIES is ~18 meV FWHM (Lorenzen *et al.*, 1983), peak positions and widths of spectral features are readily measured to a few meV (0.1 kcal/mol) or better with proper calibration; moreover, much higher resolution than this is not essential, as the "natural" linewidth of PI electron spectral lines is generally larger than 30 meV (see Sec. III).

4. Ion-electron coincidence

The use of coincidence methods in Penning ionization, in which a Penning electron of a given kinetic energy is detected in delayed coincidence with its Penning (or other) ion (PIECES) has been pioneered by Münzer and Niehaus (1981) and by Goy, Kohls, and Morgner (1981). The method provides unique information on the correlation between various product ion channels and the vib-

ronic state of the newborn Penning ion (see Secs. IV.B and IV.E). In the original experiments a retarding-field analyzer was used to measure the electron spectrum, with each electron counted triggering a short ion draw-out pulse, accelerating the coincident ion, which has not yet had time to depart the collision volume, into a time-of-flight drift region; the coincident ion is added to the spectrum only if it falls in a preset time interval determined by the ion mass, drift length, and drift velocity. Improved resolution with no loss of sensitivity has been demonstrated by Baus, Benz, and Morgner (1985) using a dispersive analyzer with a position-sensitive detector. Background in coincidence experiments arises from accidental coincidences; in the PI studies these were accounted for through the use of "blank" draw-out pulses. Once a correction for accidentals is made, the spectra are free of background; this presents a major advantage over noncoincident PIES.

D. A crossed-beams apparatus for Penning ionization

Figure 1 schematically illustrates an idealized crossed-beams apparatus that would have many of the capabilities discussed earlier in this section. Here the metastable beam Ng* is formed by electron impact on a ground-state supersonic beam and optically state-selected before crossing a second supersonic beam B. The possibilities of detection of angle-resolved nonreactive and reactive scattering, the electron-energy spectrum, and ion-electron coincidence are depicted. The secondary beam is modulated by a chopper, permitting phase-sensitive pulse-counting signal collection. Two or more differentially pumped chambers are common in molecular-beam systems; the illustrated apparatus would have five, with each nozzle-skimmer assembly nested in a double chamber, separated from the collision/detection chamber. Typical vacua with experiment in progress are 10^{-3}–10^{-4} Torr in the nozzle-exhaust chambers, 10^{-5}–10^{-6} Torr in the buffer chambers, and 10^{-6}–10^{-8} Torr in the collision/detector chamber. Although an additional stage of pumping has been employed for the detector, it is generally not essential, owing to the efficient deactivation of stray excited atoms on the walls of the apparatus, provided the pumping of the collision/detection region is strong enough to remove beam molecules without excessive buildup of ambient pressure.

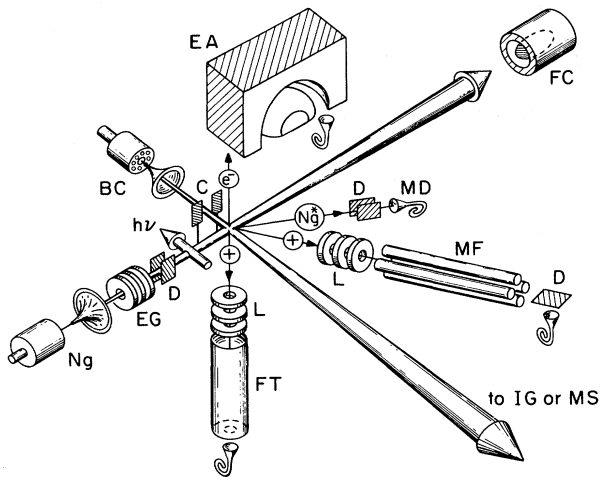

FIG. 1. Schematic illustration of a crossed-beam apparatus for the study of Penning ionization. Ng and BC—nozzle-skimmer assemblies for the excited atom and partner molecule beams, respectively; EG—electron gun used to excite Ng to Ng*; D—electrostatic deflector; $h\nu$—photons for state selection; C—chopper for modulation of BC beam; EA—electrostatic energy analyzer for Penning electrons; FC—Faraday cup metastable beam monitor; MD—metastable detector (electron multipler); L—electrostatic lens/retarding field assembly; MF—quadrupole mass filter; IG or MS—molecular-beam monitor, either ion gauge or mass spectrometer; FT—ion flight tube for coincidence measurements. The curly objects are channel electron multipliers. Not indicated are various collimators and plates surrounding the intersection region for total ion collection experiments.

Insertion of a mechanical pulse-type chopper or fast electrical modulation of the exciting electron beam allows time-of-flight studies as well. In most of the total and total ionization cross-section studies listed in Tables II–IV, the collision energy or velocity was selected by time-resolving a pulsed excited beam with a fast-response detector. The deviations observed from standard velocity distributions cited in Sec. II.B raise a flag of caution concerning this technique, which relies for its valid use on the correlation between detector arrival time and velocity for a known flight path length.

Unlike a ground-state beam, an excited beam can alter its own speed distribution during a time-of-flight pulse through resonant energy transfer between excited atoms and the much larger population of ground-state atoms. The mechanism for this occurrence is the overtaking of slow ground-state atoms nearer the leading edge of the time-of-flight pulse by faster, excited atoms emerging nearer the trailing edge. For a broad (Maxwellian) velocity distribution, where the spread in velocities is comparable to the most probable velocity, the fraction f of the beam that undergoes such energy transfer is given by a simple Beer's law expression, $f=1-\exp(-nLQ)$, where n is the *ground-state* number density, L the flight path length, and Q the resonant energy transfer cross section. Cohen and Schneider (1975) have calculated transfer cross sections theoretically for Ne* + Ne; these are limited to ~ 5 Å^2 at low energy due to the presence of small barriers in the relevant *ab initio* potentials, but rise to 20 Å^2 at 0.2 eV (4.6 kcal). It is likely that the calculated barriers are too high, making these cross sections lower bounds, perhaps weak lower bounds. For typical n and the substantial L's needed for good time resolution, f could easily reach 0.1. Energy transfer causes a fraction f of the shorter arrival times to correspond to a range of velocities, depending upon the point along the length L at which it has occurred, and thus partially blurs the

$v = t/L$ association. This effect is potentially detectable by changing the temperature of the excited-beam source so as to produce an overlapping range of energies in total cross-section measurements; lack of a slope match where the cross-section data overlap indicates energy transfer distortion.

III. THEORY OF PENNING IONIZATION

A. Kinetic overview

Penning ionization can be viewed as passing through not one, but two collision intermediates or "transition states,"

$$A^*+B \underset{a'}{\overset{a}{\rightleftarrows}} [AB]^* \xrightarrow[b]{} \begin{matrix}[AB]^+ + e^- \\ \hookrightarrow \text{ionic products} \\ c\end{matrix} \tag{3.1}$$

and thus the theory of Penning ionization can be broken up into parcels designed to treat each of the steps a, b, and c.

Owing to the nature of the earliest beam measurements of Penning ionization (especially PIES), step a, the formation of the excited complex $[AB]^*$, has generally been treated realistically, utilizing a potential-energy function $V_0(\mathbf{r})$ with appropriate behavior on occasion at long range ($\sim -C_6 r^{-6} - \cdots$) and always at short range (exponential repulsion or a chemical bonding function, as needed). For molecular B, it has even been possible to go beyond the spherical-potential approximation, exploiting the sophisticated modern developments in small-molecule collision theory and calculations (Bernstein, 1979). Underlying this approach (Miller, 1970b) is the usual Born-Oppenheimer separation of electronic and nuclear motion.

As discussed further in the next section, however, this assumed separation must serve as merely a zeroth-order basis for a description of Penning ionization, since $[AB]^*$ can in principle decompose at any time in step b to yield a free electron, a drastic change in the electronic arrangement that signals Born-Oppenheimer breakdown. This step is generally assumed to be irreversible, allowing a formulation of the decay of $[AB]^*$ in terms of an imaginary component of the potential energy $\Gamma(\mathbf{r})$, yielding an optical potential $V_0(\mathbf{r}) - i\Gamma(\mathbf{r})/2$. When $\Gamma(\mathbf{r})$ is defined in this way, it is a resonance width for decay into the ionization continuum and, for fixed nuclei, is rigorously definable in terms of the static (electronic) properties of the system. The use of a local optical potential unites steps a and b and enables collision dynamics and cross sections for Penning ionization to be evaluated independently of the final step c, i.e., regardless of the details or the fate of the $[AB]^+$ ionic complex. This dynamic separability, however, presumes that Γ is independent of the energy and angular momentum of the collision, i.e., of the nuclear motion, a presumption to be discussed later in this section. The reverse step a' is included to indicate that $[AB]^*$ may and often does return to the incoming channel, or to one in which B has perhaps undergone an internal inelastic transition under the "normal" influence of V_0.

While accounting for steps a and b may suffice to describe the overall rate of Penning ionization, knowledge of the final species and state distribution of the ionic products formed in step c can also be of great interest, particularly if these products are produced primarily in excited states. In the usual approach, a potential $V_+(\mathbf{r})$ determines the fate of $[AB]^+$; Figure 2 illustrates the forms of V_0, Γ, and V_+ frequently found in the case when B is a closed-shell atom or molecule with no low-lying empty orbitals. If the Penning electron escapes with sufficient energy, $[AB]^+$ may be unable to undergo step c at all, remaining trapped in the well of V_+ to form an associative ion. When B is molecular, breakup of $[AB]^+$ may involve inelastic or bond-breaking dynamics.

This potential curve model for Penning ionization grows more complicated when a spatial degeneracy is lifted by the approach of A^* and B, as in $Ne^*(^3P)$ reactions, giving rise to two or more V_0's and Γ's on which Penning ionization may occur, or when a similar degeneracy lifting occurs in $[AB]^+$, as in Penning ionization of noble-gas atoms, or when B is molecular, turning the curves into surfaces. These complexities have so far prevented a completely rigorous description of the molecular dynamics of Penning ionization in such cases. Nonetheless there has been tangible progress in modeling and understanding complex PI systems, both as to their dynamics and with regard to the underlying electronic factors, which will be described briefly here.

Though perhaps unnecessary, it is nevertheless fitting

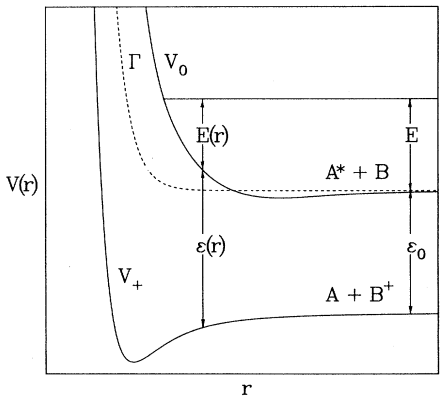

FIG. 2. Two-potential-curve model for Penning ionization. E is the center-of-mass kinetic energy of collision; ε_0 is the separation of the reagent and product potential asymptotes, $\varepsilon_0 = E_*(A^*) - IE(B)$; $E(r)$ is the (classical) local heavy-particle kinetic energy, including centrifugal energy; and $\varepsilon(r)$ is the kinetic energy of the Penning electron when Penning ionization takes place at separation r.

to underscore the importance of the electronic structure factors that determine the potentials; it is only through a sound (i.e., experimentally based) grasp of the most significant of these factors that even a modicum of predictive power in the field can be achieved. As of the present time it is an open question whether such a grasp is yet at hand. It is thus appropriate to plunge first into structural considerations, followed by an overview of the present status of PI collision theory. The aim throughout will be conceptual understanding, with enough of the formalism and formulas included to convey a sense of how to get numbers for experimental comparison.

B. Electronic structure aspects

1. Discrete/continuum coupling

The production of a free electron in the Penning reaction implies a continuum of final electronic states and therefore exact resonance with the initial excited state. Thus, while a nearly exact electronic eigenfunction Φ_0 may in principle be constructed for large separations r between A^* and B, the additional Coulombic terms in the electrostatic Hamiltonian H_{el} that arise when A^* and B are brought together cause this asymptotically defined wave function to mix with the continuum of final-state wave functions $\{\Phi_\varepsilon\}$, and thereby to cease to be an eigenfunction of the full Hamiltonian. Even in the absence of the continuum states, other changes in Φ_0 occur at small R that may be categorized as overlap (Pauli) repulsion, covalent chemical bonding, or charge transfer. It must be noted at this point that such "chemical" influences on Φ_0 are frequently ignored in discussing the discrete/continuum coupling, particularly in the simpler atomic-orbital models for constructing it.

Analysis of the discrete/continuum coupling problem in the form now widely used or assumed in Penning ionization may be traced to a paper by Rice (1933) treating rotational predissociation induced by curve crossing, and applied with extensions by Fano (1935, 1961) to atomic autoionization phenomena. The theory in general describes any situation of this sort, including all types of predissociation, radiationless transitions in large molecules, and autodetachment of negative ions. Within the clamped-nuclei approximation, Penning ionization is simply molecular autoionization, and with the aid of the usual atomic or molecular-orbital basis sets, finding Φ_0 and Φ_ε is a matter of selecting appropriate orbital configurations (Miller and Schaefer, 1970; Miller *et al.*, 1972; Hickman *et al.*, 1977a; Hazi, 1978) that reflect the properties of the reagents and products of Penning ionization. This is now done formally using Feshbach projection operators (Feshbach, 1958, 1962), but, as Morgner (1990) points out, the procedures used to obtain numerical results, relying as they must on a finite basis set, are as a rule somewhat arbitrary regarding selection of configurations and may be inconsistent with the complementarity, disjointness, or idempotency of the projection operators. (The arbitrary selection of configurations is a continuing difficulty in other areas of quantum chemistry as well.)

Morgner (1990) has recently summarized and evaluated the discrete/continuum theory that leads to the treatment of steps *a* and *b* above by a local complex potential. To establish notation and provide a basis for discussion, the electronic part of the theory will be outlined following Fano (1961). The matrix elements of H_{el} are assigned as

$$\begin{aligned} H_{00} &= \langle \Phi_0 | H_{el} | \Phi_0 \rangle = E_0 , \\ H_{0\varepsilon} &= \langle \Phi_0 | H_{el} | \Phi_\varepsilon \rangle = V_{0\varepsilon} , \\ H_{\varepsilon\varepsilon'} &= \langle \Phi_\varepsilon | H_{el} | \Phi_{\varepsilon'} \rangle = (E_+ + \varepsilon)\delta(\varepsilon - \varepsilon') , \end{aligned} \tag{3.2}$$

where Φ_0 and E_0 are the electronic wave function and energy of the A^*+B reagents and Φ_ε and $E_+ + \varepsilon$ are those for the products, with E_+ the energy of $A+B^+$ and ε the kinetic energy of the free electron. All quantities in Eq. (3.2) refer to fixed values of the nuclear coordinates $\mathbf{r}$. (E_0 and E_+ will later become the potential curves or surfaces V_0 and V_+ mentioned previously.) It is assumed that the continuum part of the H_{el} matrix has already been diagonalized; further, Φ_0, in a full treatment of the discrete states, is a result of diagonalizing the discrete part. It is also required that

$$\begin{aligned} \langle \Phi_0 | \Phi_0 \rangle &= 1 , \\ \langle \Phi_\varepsilon | \Phi_0 \rangle &= 0 , \\ \langle \Phi_{\varepsilon'} | \Phi_\varepsilon \rangle &= \delta(\varepsilon - \varepsilon') . \end{aligned} \tag{3.3}$$

The first and third of these conditions are readily maintained, while the second is occasionally violated in actual calculations, for example, when an unmodified Coulomb wave function is selected to represent the free electron (see Sec. III.B.4, however).

In the Feshbach projection-operator formalism, this partitioning of the Hamiltonian matrix corresponds to choosing the discrete projector $Q = |\Phi_0\rangle\langle\Phi_0|$ (see also Miller, 1966, 1970a) and the continuum $P = 1 - Q$. This "one-dimensional projector" choice is certainly the most physically appealing one to use, though it might not be the most convenient or accurate for PI systems. The choice of P and Q will be discussed further in the next section.

The ansatz for diagonalizing the full H_{el} matrix superposes the discrete and continuum solutions,

$$|\Psi_\varepsilon\rangle = u_0 |\Phi_0\rangle + \int d\varepsilon' u_{\varepsilon'} |\Phi_{\varepsilon'}\rangle , \tag{3.4}$$

where Ψ_ε is the mixed state and u_0, u_ε are the mixing coefficients. Substituting Eq. (3.4) into $H_{el}|\Psi\rangle = E_{el}|\Psi\rangle$, where E_{el} is the total electronic energy, leads to secular equations that are analytically soluble (Fano, 1961) with due attention to the behavior of $u_{\varepsilon'}$ at zeroth-order reso-

nance, $E_+ + \varepsilon' = E_0$. Imposing energy normalization on Ψ_ε, $\langle \Psi_\varepsilon | \Psi_{\varepsilon'} \rangle = \delta(\varepsilon - \varepsilon')$, then leads to the discrete-state amplitude

$$|u_0(\varepsilon)|^2 = |V_{0\varepsilon}|^2 / [(E_{\rm el} - E_0 - \Delta)^2 + \pi^2 |V_{0\varepsilon}|^4] , \tag{3.5}$$

where $\varepsilon = E_{\rm el} - E_+$ and

$$\Delta = \text{P.V.} \int d\varepsilon' |V_{0\varepsilon'}|^2 / (E_{\rm el} - E_+ - \varepsilon') , \tag{3.6}$$

where P.V. denotes principal value, is an energy shift. Equation (3.5) is of Lorentzian form, with a width

$$\Gamma = 2\pi |V_{0\varepsilon}|^2 \tag{3.7}$$

and centered on the shifted resonance energy $E_0 + \Delta$. The discrete state Φ_0 is thus transformed by coupling to the continuum into a band of states of width Γ.

If $V_{0\varepsilon}$ is of small magnitude, Γ will be small and $V_{0\varepsilon}$ will likely vary slowly over the width of the resonance, causing the resonance line shape to approach a true Lorentzian. In that case the resonance level can be represented by a complex eigenvalue

$$E_{\rm res} = E_0 + \Delta - i\Gamma/2 , \tag{3.8}$$

and the initially prepared state will decay exponentially in time with a decay constant $k_a = \Gamma/\hbar$. Normally a much more stringent condition is imposed or assumed, namely,

$$V_{0\varepsilon} = \text{const} \ \forall \varepsilon . \tag{3.9}$$

Then, provided the range of ε may be extended to $0 < \varepsilon < 2(E_{\rm el} - E_+)$, the energy shift Δ of Eq. (3.6) vanishes and the real part of the resonance energy, Eq. (3.8), is just E_0, the energy of the discrete state. While the experimentally estimated resonance widths Γ for Penning ionization are quite small, indicating the validity of Eq. (3.8), it is unlikely that Δ is ever strictly zero except in the asymptotic region, A^* and B far apart. Even though both Δ and Γ go as $|V_{0\varepsilon}|^2$ and the condition $\Gamma \ll E_0$ also insures $\Delta \ll E_0$, the PI collision dynamics discussed in Sec. III.C are determined by the potential curve obtained by subtracting out the asymptotic discrete energy, and the effect of Δ, generally ignored in *ab initio* calculations of resonance energies for Penning ionization, may be appreciable.

A more fundamental difficulty with the theory presented here is the occurrence of associative ionization (AI),

$$A^* + B \rightarrow AB^+ + e^- , \tag{3.10}$$

accompanying Penning ionization in nearly every small system thus far observed. It is normally assumed that the phenomenology of Eq. (3.8) with $\Delta = 0$ applies regardless of PI/AI branching. However, as discussed briefly by Siska (1984), the vibration-rotation bound states of AB^+ are of course quantized, implying that ε, the Penning electron's energy, is no longer continuously varying, but can only take on the discrete values

$$\varepsilon_{v'l'} = \mathcal{E} - E_+(\infty) - E'_{v'l'} , \tag{3.11}$$

where $\mathcal{E}$ is the total energy, including that of nuclear motion, and $\{E'_{v'l'}\}$ are the bound-state eigenvalues of AB^+, measured with respect to the asymptotic energy $E_+(\infty)$ of $A + B^+$. Thus Eq. (3.4) needs to be modified to read

$$|\Psi_\varepsilon\rangle = u_0 |\Phi_0\rangle + \int_0^{\varepsilon_{\max}} d\varepsilon' u_{\varepsilon'} |\Phi_{\varepsilon'}\rangle + \sum_{v'l'} u_{\varepsilon'_{v'l'}} |\Phi_{\varepsilon'_{v'l'}}\rangle , \tag{3.12}$$

where $\varepsilon_{\max}$ is the largest electron kinetic energy, which depends on $\mathcal{E}$ and the final angular momentum of the atoms l', for which A and B^+ can remain unbound. The analysis just given shows that only a certain domain of ε' surrounding the resonance can contribute to the decay of the discrete state, and if this domain lies beyond $\varepsilon_{\max}$ within the discrete sum, it appears that the density of states will be lower, perhaps greatly so, leading to substantial reduction of the width for these energies. It seems that Eq. (3.4) when applied to PI presumes the existence of *two* continua, for both the electronic and the nuclear degrees of freedom. In *atomic* autoionization, for which the theory was originally developed, no such presumption is needed. This difficulty should be most noticeable in low reduced-mass systems that possess deep minima in E_+, for example, in noble-gas hydride ions, or for which only a small range of ε can contribute to PI/AI, for example, when mainly repulsion exists between A^* and B. The problem will be discussed more fully in Sec. III.C, where nuclear motion is treated.

2. Orbital models for excited-state forces

Neglecting the energy shift Δ in Eq. (3.8), we find that the real part of the resonance energy is just E_0, the energy of the unperturbed discrete state. This state is intuitively described by some dominant square-integrable orbital configuration that is well known asymptotically, without any calculation, from elementary atomic physics. When A^* and B are closer by, we have an $(AB)^*$ molecule whose orbital configuration must in general be determined by approximately solving the discrete-space Schrödinger equation

$$H_{\rm el} |\Phi_0\rangle = E_0 |\Phi_0\rangle . \tag{3.13}$$

Doing this over a range of nuclear configurations $\mathbf{r}$ generates a (potential) energy surface $E_0(\mathbf{r})$ $[\rightarrow V_0(\mathbf{r})]$ that in the Born-Oppenheimer approximation governs the nuclear motion.

Of course Eq. (3.13) is also satisfied by the exact wave function Ψ_ε, which includes the continuum. Thus some care must be exercised in solving Eq. (3.13) so as to avoid confusing the desired solution Φ_0 with continuumlike solutions. This is readily done in ordinary quantum-chemical calculations, where one chooses a necessarily finite square-integrable atomic/molecular-orbital basis and employs the self-consistent-field/configuration-

interaction (SCF-CI) method to construct the appropriate Φ_0 (see, for example, Szabo and Ostlund, 1982). In its most primitive form, this is known as the "stabilization method" (Hazi and Taylor, 1970; Miller and Schaefer, 1970) and consists in a "business-as-usual" approach to the problem. To better approximate Φ_0, one of course wants a larger basis as well as more configurations; this inevitably produces a predominantly continuum character in many of the eigensolutions of the configuration-interaction matrix. However, those solutions corresponding to true resonances are relatively stable in energy as the size of the calculation is increased, while the continuumlike solutions show strong basis-set dependence. In addition, the discrete-state wave functions are found to be relatively compact, as indicated, for example, by small expectation values for the electron-nucleus distance. Nonetheless, the results of such calculations are considerably less reliable than ordinary quantum-molecular results for truly bound states, as the variation and interleaving theorems do not apply owing to the presence of the continuum.

Hickman *et al.* (1977a) have shown how to take advantage of the fact that the products of Penning ionization include a truly bound *electronic* state of AB^+, in order to disentangle the discrete/continuum mixing that occurs in the configuration-interaction procedure. In their approach, which in its overall framework follows that of Miller and Schaefer (1970) and Miller *et al.* (1972), the $AB^+ + e^-$ states are projected out of a single molecular-orbital basis that describes both the discrete and the continuum solutions, but does not itself contain any continuum orbitals, a major computational advantage. That is, if Φ_+ is the AB^+ wave function, all configurations of the form $|\Phi_\varepsilon\rangle = |\Phi_+ \phi_i\rangle$ are used to construct the continuum projector $P = \sum_i |\Phi_+ \phi_i\rangle\langle\phi_i \Phi_+|$, where ϕ_i is an individual molecular orbital (MO) that is not occupied in AB^+; $Q = 1 - P$ then includes only the resonance states. Hazi (1978) has advocated a similar method of constructing the projectors; his scheme is described more fully in the next section.

Hickman *et al.* (1977a) applied the method to $He^*(2\,^3S) + H$, H_2 using a single determinant for the HeH^+ or $HeH_2{}^+$ Φ_+, but diagonalizing the full Hamiltonian matrix arranged in subblock form. This method should account for the energy shift Δ rigorously within the basis, Δ being given by the difference between the full-matrix "discrete" eigenvalues and those obtained by diagonalizing only the discrete subblock. Unfortunately no eigenvalue differences were given by Hickman *et al.* In addition, if Φ_+ were also a configuration-interaction wave function, it would contain a charge-transfer $(A^+ + B)$ component, whose configuration would coincide with that of the $A^* + B$ core ion. This would vitiate the clean separation of discrete and continuum subspaces; it also raises the question of the quality of the treatment of AB^+ needed to insure reliable results for AB^*.

The most recent advance in *ab initio* methods was made by Isaacson *et al.* (1978) and Isaacson and Miller (1979), who eschewed Feshbach projectors in favor of direct introduction of continuum functions—Siegert-type orbitals (Siegert, 1939)—into the configuration-interaction expansion and extraction of the complex resonance energy Eq. (3.8) more or less directly as an eigenvalue of the now non-Hermitian Hamiltonian matrix. Numerical problems with integral evaluation over the Siegert orbitals have prevented the extension of this method to systems beyond $He^*(2\,^{1,3}S) + H$, for which Isaacson and Miller (1979) presented results for both $V_0(r)$ and $\Gamma(r)$. It is noted that, similar to the work of Hickman *et al.*, the selection of continuum configurations was limited to the use of a single determinant describing HeH^+. Again, the effects of using more sophisticated AB^+ wave functions were not investigated.

The reader aware of general developments in quantum chemistry (Szabo and Ostlund, 1982; Schaefer, 1984; Hinchcliffe, 1988) may note that the work cited predates or is contemporary with the development of more general computer codes (the GAUSSIAN series of Pople and coworkers) for electronic structure calculations. Many of the available studies have utilized Slater-type orbitals rather than Gaussian types, and to this date have not been extended beyond rather simple systems. Table VIII summarizes the *ab initio* work up to the present; the great disparity in the size and chemical scope of this table compared to Tables II–IV is noteworthy. Comparison of some results of these studies with experiment will be made in Sec. IV.

Given the limited scope and uncertain accuracy of the *ab initio* methods, experimentalists have had to rely for the most part on rough-and-ready models and analogies to guide the analysis of molecular-beam data. These have nearly universally exploited the similarity of the excited noble gas to its adjacent alkali-metal atom: $He^*(1s2s\,^{1,3}S)$ and $Li(1s^2 2s\,^2S)$; $Ne^*(2p^5 3s\,^3P_{2,0})$ and $Na(2p^6 3s\,^2S)$; etc. Some of these ideas will be briefly described, working downward toward more qualitative guidelines; details on particular systems are reserved for Sec. IV.

The clean separation of discrete and continuum solutions of the electronic problem still being a thorny if not absolutely insoluble problem in *ab initio* theory, the desirability of a semiempirical method that accomplishes this is clear. In the pseudopotential and model potential methods (Bardsley, 1974, has reviewed early work; Kucal *et al.*, 1990, and Spiegelmann *et al.*, 1990, present recent work on excited noble-gas systems), the core electrons of A^* and B are replaced by potential functions derived from self-consistent-field atomic core wave functions or empirical forms found by fitting atomic energy levels, electron-scattering data, or other empirical atomic properties; and only the valence electrons are explicitly treated. In its most rigorous form (see, for example, Spiegelmann *et al.*, 1990), which we refer to as a pseudopotential theory, results comparable to the best all-electron

TABLE VIII. *ab initio* studies of He* interactions in Penning systems.

He* state	Ionized species	Quantity calculated	Reference
3	H	V_0, Γ, V_+	Merz *et al.* (1990)
3		V_0, Γ	Waibel *et al.* (1988)
1,3		V_0, Γ	Isaacson and Miller (1979)
1,3		Γ	Hickman and Morgner (1977)
1		V_0	Isaacson, Hickman, and Miller (1977)
3		V_0, Γ	Hickman, Isaacson, and Miller (1977a)
3		Γ	Miller, Slocomb, and Schaefer (1972)
1,3		V_0, V_+	Miller and Schaefer (1970)
1,3		V_0, Γ	Fujii *et al.* (1970)
3		V_0, Γ	Bell (1970)
1,3	$He^*(2\,^3S)$	V_0, Γ, V_+	Müller *et al.* (1987, 1991)
3		V_0, Γ, V_+	Garrison, Miller, and Schaefer (1973)
1,3	Li	V_0, Γ, V_+	Kimura and Lane (1990)
1,3		V_0, Γ, V_+	Merz *et al.* (1989)
1,3	Na	V_0, Γ, V_+	Merz *et al.* (1990)
1,3		V_0, Γ, V_+	Padial, Cohen *et al.* (1989)
1,3		V_0, Γ	Cohen, Martin, and Lane (1985)
1,3	K	V_0	Padial, Martin, *et al.* (1989)
1,3		V_0, Γ	Scheibner *et al.* (1987)
1	H_2	V_0	Isaacson, Hickman, and Miller (1977)
3		V_0, Γ	Hickman, Isaacson, and Miller (1977a)
1,3		V_0, Γ	Cohen and Lane (1977)
3	HCl	V_0	Someda *et al.* (1989)
3	H_2O	V_0	Haug, Morgner, and Staemmler (1985)
$Ne^*(^3P)$		V_0	Bentley (1980)

calculations for truly bound states of smaller systems are obtained. This method is of course considerably easier to extend to large systems, the major part of the calculation being the construction of the pseudopotentials themselves, and is widely regarded as a reliable tool of the quantum chemist. The assumption behind the method is that the core wave functions and energies are independent of nuclear configuration **r**.

In Penning ionization A^*+B and $A+B^+$ have distinct core configurations, at least at the self-consistent-field level; hence a pseudopotential or model potential that represents the A^* and B cores can be uniquely constructed, and a configuration-interaction expansion of valence pseudo-orbitals can be carried out without concern for variational collapse or mixing in continuum solutions. In particular, when B is closed shell, as with Ar or H_2, its electron density may be represented entirely by a model potential function, reducing the A^*+B calculation to a one-orbital-center/one-electron problem. In such cases, the exclusion of the continuum is particularly explicit.

If semiempirical methods are used to build the core potentials (Kucal *et al.*, 1990; see also Siska, 1979b; Gregor and Siska, 1981; Martin and Siska, 1985), some rigor is sacrificed, but asymptotically correct polarization behavior can be built in, allowing the recovery of part or all of the van der Waals attraction, a quantity very difficult to obtain even in the most extensive configuration-interaction all-electron treatments. In addition, charge/permanent-moment interactions among the valence electron(s) A^+ and the core of B, when B is molecular, can be explicitly included and their effects investigated (Martin and Siska, 1985). As one cannot turn moments on and off in a full *ab initio* calculation, unique insights into structure-reactivity relations can be gained by such studies. We shall return to this idea in Secs. IV and V.

The pseudopotential outlook also provides a qualitative guide to the general form of $V_0(\mathbf{r})$ for open-shell partners B. In the simple cases B=H or M, an alkali atom (^2S), and A^*=He*($2\,^3S$), we expect $^2\Sigma^+$ and $^4\Sigma^+$ molecular states of HeB^* to form; the $^2\Sigma^+$ component corresponds to singlet pairing of the valence electrons, and hence an attractive state with a potential curve close to that of LiB($^1\Sigma^+$), while the $^4\Sigma^+$ state is a triplet valence state analogous to LiB($^3\Sigma^+$), possessing an antibonding, repulsive potential. In addition, the PI products $He+B^++e^-$ can form only a doublet state, making Penning ionization spin forbidden out of the $^4\Sigma^+$ state. For He*($2\,^1S$)+H, M, only a second $^2\Sigma^+$ state may form; since the $2\,^1S$ asymptote is higher in energy than $2\,^3S$ (by 0.80 eV), this second state, by virtue of its repulsion from the ^3S $^2\Sigma^+$ state beneath it, will have a shallower well. These features will also be quantitatively described in Sec. IV, along with further applications of these ideas.

3. Orbital models for Penning decay

Aside from the Siegert eigenvalue calculations of Isaacson and Miller (1979), all calculations of the PI resonance width Γ to date have employed Eq. (3.7), here expanded as

$$\Gamma = 2\pi |\langle \Phi_\varepsilon | H_{\rm el} | \Phi_0 \rangle|^2 . \tag{3.7'}$$

The units of Eq. (3.7') are indeed consistent, as the energy-normalization requirement Eq. (3.3) causes Φ_ε to have units of (energy)$^{-1/2}$. For other normalizations of Φ_ε, a density-of-states factor ρ_ε would be inserted in Eq. (3.7'). Miller (1966, 1970a) has pointed out the analogy between Eq. (3.7') and Fermi's "golden rule," a result of first-order time-dependent perturbation theory, but the reader is reminded that Eq. (3.7) is *exact* within the Born-Oppenheimer approximation, and it is only the use of $\Gamma/\hbar$ as a decay rate in semiclassical theories of PI dynamics (Sec. III.C) that *might* require the matrix element to be "small." (Here we restrict our discussion to Penning ionization only, disregarding for the moment the presence of associative ionization.)

Miller (1970a) has given a slightly different version of Eq. (3.7'),

$$\Gamma = 2\pi |\langle \Phi_\varepsilon | H_{\rm el} - E_{\rm el} | \Phi_0 \rangle|^2 . \tag{3.14}$$

Equations (3.14) and (3.7') are in fact equivalent, owing to the orthogonality of Φ_0 and Φ_ε, Eq. (3.3), but it may easily be shown that Eq. (3.14) does not require orthogonality for its validity (Miller, 1970a; Miller *et al.*, 1972); i.e., it makes amends for possible mixing of the discrete and continuum subspaces. Hickman *et al.* (1977a), however, found significant differences in the Γ's computed from these two formulas, employed with different but appropriate definitions of the projectors P and Q, for reasons that are as yet unclear. The question of the effect of the level of treatment of AB^+ on the width was assessed, however, with Γ changing by 20% in passing from a single determinant wave function to a full configuration-interaction treatment of the molecular-ion product as carried out by Miller *et al.* (1972).

The Siegert calculation of Isaacson and Miller (1979) agreed more closely with that of Hickman *et al.* (1977a) than with Miller *et al.* (1972) for He*($2\,^3S$)+H; for He*($2\,^1S$)+H the Siegert width was a factor of 2–3 larger than Hickman and Morgner's (1977) "golden rule" calculation, in the direction of improved agreement with experiment (Isaacson, 1979; see Sec. IV.A).

A flexible two-stage method for obtaining Γ has been suggested by Hazi (1978) and has been used in more recent work (Cohen *et al.*, 1985; Merz *et al.*, 1989, 1990; Padial, Cohen, *et al.*, 1989; Padial, Martin, *et al.* 1989; Kimura and Lane, 1990; Müller *et al.*, 1991). The method again avoids the use of continuum functions, employs separately defined projectors to compute the discrete state Φ_0 and the background continuum states Φ_ε, and exploits advances in the application of Stieltjes moment theory (Langhoff and Corcoran, 1974) to derive the width function from the necessarily discrete set of background eigenvalues and off-diagonal matrix elements. In obtaining Φ_0 one projects out all continuum solutions in any reasonable way [all $A\cdots B^+$ core configurations in P, or all $A^+\cdots B$ core configurations in Q, as in the method of Hickman *et al.* (1977a); this excludes the possibility of a charge-transfer component in a configuration-interaction expansion of either Φ_0 or Φ_ε]. Then a *subset* of the original discrete solutions (say, all states of a given symmetry, or perhaps just the single state of interest Φ_0) is projected out, and the remaining states lumped with the continuum. This allows more correlation effects to be built into Φ_ε; however, the finite set $\{\Phi_{\varepsilon i}\}$ is defined only at the discrete energies ε_i, none of which is precisely at the resonance energy. The matrix elements $\gamma_i = 2\pi |\langle \Phi_0 | H_{\rm el} | \Phi_{\varepsilon i} \rangle|^2$ are computed and Stieltjes moments used to construct a smooth $\Gamma(\varepsilon)$ function that may be interpolated to find Γ at the resonance energy $\varepsilon \approx E_0 - E_+$. Hazi (1978) points out that the shift Δ, Eq. (3.6), is then readily found from $\Gamma(\varepsilon)$; all later applications have ignored Δ, however.

For reference in Sec. III.C, we note that a partial-wave decomposition of the continuum function is useful (Nakamura, 1971; Miller *et al.*, 1972):

$$\Phi_\varepsilon = \sum_{\lambda m} Y_{\lambda m}(\hat{\varepsilon}\cdot\hat{r}) i^{-\lambda} \exp(i\sigma_\lambda) \hat{A} \Phi_+ f_{\lambda\varepsilon}(r_\varepsilon) Y_{\lambda m}(\hat{r}_\varepsilon \cdot \hat{r}) , \tag{3.15}$$

where $\hat{\varepsilon}\cdot\hat{r}$ refers to angles of the ejection direction and $r_\varepsilon, \hat{r}_\varepsilon\cdot\hat{r}$ to the position of the Penning electron with respect to the intermolecular vector $\mathbf{r}$, σ_λ is a phase shift, $\hat{A}$ is the antisymmetrizer, $f_{\lambda\varepsilon}(r_\varepsilon)$ is the radial wave function, and λm are the partial-wave indices, the angular momentum of the free electron and its projection on $\mathbf{r}$. In the Born-Oppenheimer approximation, only one value of m contributes, $m = \Lambda_0 - \Lambda_+$, where the Λ's are projections of the electronic angular momentum on $\mathbf{r}$ for the initial and final molecular states. The number of λ terms needed in Eq. (3.15) depends on where the origin of $\mathbf{r}_\varepsilon$ is placed; in calculations of Γ it is usually centered on one of the atoms, but for dynamical purposes it should refer to the center of mass (c.m.). $f_{\lambda\varepsilon}(r_\varepsilon)$ is often assumed to be a Coulomb wave, but in the methods of Hickman *et al.* (1977a) and Hazi (1978) it is a square-integrable linear combination. Because Φ_0 decays exponentially with distance from AB^*, the integrand of Eq. (3.7') must also do so, making the matrix element insensitive to the "free-wave" part of Φ_ε.

Two other innovative approaches to the calculation of Γ are noteworthy. For the He*+H_2 system, Cohen and Lane (1977) have used the instability of the discrete-state eigenvalue to estimate Γ, with some reliability, while Vojtik and Paidarova (1986) have presented a non-Hermitian diatomics-in-molecules perturbation expression for Γ. The latter yields a considerably larger Γ than any of the *ab initio* results.

Physical insight is generally inversely proportional to

the complexity of the treatment of a problem; thus the intuitively guided analysis of molecular-beam data has relied for the most part on empirical or semiempirical models for Γ. The PI process can be thought of as an intermolecular Auger transition, in which the liberation of the Penning electron is accompanied by the filling of the hole in the A^* core. Thus a minimum of two electrons must relocate during the reaction, and they communicate their momenta via the $1/r_{12}$ term in H_{el}. This suggests that when the matrix element of Eq. (3.7′) is expanded two important terms will emerge (Hotop and Niehaus, 1969b; Miller and Morgner, 1977),

$$V_{0\varepsilon} \approx \langle \phi_\varepsilon(2)\phi_{A^+}(1)|H'_{el}|\phi_{A^*}(1)\phi_B(2)\rangle - \langle \phi_\varepsilon(1)\phi_{A^*}(2)|H'_{el}|\phi_{A^*}(1)\phi_B(2)\rangle , \quad (3.16)$$

where ϕ_ε is the continuum orbital, ϕ_{A^+} the A^+ core ion orbital, ϕ_{A^*} the excited A^* orbital, ϕ_B a (valence) orbital on B, H'_{el} includes $1/r_{12}$, and the numbers in parentheses refer to electron coordinates. The first term corresponds to a "radiative" process in which A^* emits a virtual photon that ionizes B, while the second requires the "exchange" of an electron between B and the A^+ core, which frees the excited electron. Physical arguments, as well as experimental evidence (much the better indicator), suggest that for metastable A^* the exchange term is by far the more important. When A^* is metastable the collision must convert a long-lived state into a short-lived one; even if the AB^* intermediate were the most powerful radiator, $\tau_{rad} \approx 10^{-9}$ s, the collision times are $\tau_{col} \lesssim 10^{-13}$ s even for moderately heavy atoms and an attractive V_0; the radiative pathway is therefore too improbable to be compatible with the typically large PI cross sections.

Miller and Morgner (1977) further assume that the second term in Eq. (3.16) factors as

$$V_{0\varepsilon} \approx -\langle \phi_{A^+}|H'|\phi_B\rangle\langle \phi_\varepsilon|\phi_{A^*}\rangle , \quad (3.17)$$

where the first (transition-moment-like) factor is a charge-transfer matrix element, and the second (Franck-Condon-like) factor measures the overlap of the excited orbital with the continuum at energy ε. It is argued that, owing to the relative compactness of ϕ_{A^+}, the charge-transfer factor dominates the r dependence of $V_{0\varepsilon}$. Olson *et al.* (1971) have given an empirical estimate of the charge-transfer matrix element that fits a wide variety of charge-transfer rate data:

$$\langle \phi_{A^+}|H'|\phi_B\rangle \approx Are^{-\alpha r} ,$$
$$\alpha = (I_A^{1/2} + I_B^{1/2})/2^{1/2} , \quad (3.18)$$
$$A = \alpha(I_A I_B)^{1/2} ,$$

where I_A and I_B are the ionization energies of *neutral, ground-state* A and B. Current indications are that Eq. (3.18) yields a slight overestimate of the falloff parameter α, by comparison with both more rigorous theory and experiment. The formula (3.18) is in essence an overlap between two asymptotic one-electron wave functions (Rapp and Francis, 1962), suggesting that orbital symmetry plays an important role in PI selection rules, to be briefly discussed later in this section. Morgner (1988) cites the apparent existence of such rules as evidence for the validity of Eq. (3.17).

Two observations are pertinent to the meaning of Eq. (3.17). The orbitals ϕ_i are taken to be atomic in character, so that (3.16) may break down when A^* and B approach closely, particularly for highly attractive, short-range V_0's. In that case the distinction between the radiative and exchange terms in Eq. (3.16) is lost, and the ϕ_i's become molecular orbitals. Secondly, it is found (Siska, 1979b) that, even for nonbonded A^*+B interactions, the orbital ϕ_{A^*} depends strongly on intermolecular distance, which modulates the Franck-Condon-like factor in Eq. (3.17). However, in view of the role of approximations like (3.17) as guides for the experimentalist, these are factors to be borne in mind rather than serious drawbacks.

Recently, Driessen, Op de Beek, *et al.* (1991) have compared the exchange approximations generated from the two-electron exchange term of Eq. (3.16), using $H'_{el} = 1/r_{12}$, and an overlap approximation to the charge-transfer factor of Eq. (3.17), for $Ne^*(2p^5 3s, 3p) + Ar$. In these calculations unperturbed atomic orbitals were employed, and the energy dependence of the continuum orbital was neglected. As expected, omitting consideration of the second factor of Eq. (3.17) in the overlap approximation caused predictions based on the two approaches to differ appreciably. Neither method was compared to the charge-transfer approximation of Eq. (3.18), nor does either allow for distortion of the excited orbital.

Morgner (1982, 1985, 1988) has advanced the view that, because the electron leaves on a time scale short not only with respect to nuclear motion but also with respect to the inverse of typical spin-orbit splittings, step *b* of Eq. (3.1) occurs with conservation of *both* electron spin and the projection Λ of the electronic orbital angular momentum L on the intermolecular axis. Of course, steps *a* and *c* involve evolution of initially prepared and finally produced states under the influence of spin-orbit effects, but proper account of the admixture of $|LS\Lambda\rangle$ states present at the point of ionization allows a compact and consistent interpretation of most state-resolved experiments to date, in particular in PIES experiments where both the initial spin-orbit state of A^* and the final spin-orbit state of B^+ are known (Hoffman and Morgner, 1979; Morgner, 1985). A more detailed description is reserved for Sec. IV.C.

The orbital propensity rule that has evolved from Morgner's analysis is analogous to the symmetry rule that governs the combination of atomic orbitals to form molecular orbitals: an electron can be exchanged only between orbitals of the same symmetry—σ-σ, π-π, etc. Thus He^* with a 1*s* core hole can create only σ holes in atomic B, while Ne^*, with a 2*p* hole, can create σ or π.

For molecular B, restricted collision geometries also show such propensities; for lower-symmetry nuclear configurations all the orbitals of B may be ionized, although not with equal probability. In the absence of large permanent electric moments (dipole, quadrupole, . . .) on B, those orbitals with the "longest tails" will ionize more readily, as their overlap with the A^+ core hole will be larger at a given intermolecular distance r (Harada, 1990). Particularly in the case of He*, the compact core hole probes the orbitals of B over a small range of distances centered on r. The manifestation of these rules for particular systems will be discussed in Sec. IV.

C. Molecular dynamics of Penning ionization

1. Classical theory

Autoionization is by definition a unimolecular process obeying first-order kinetics according to

$$-dn = k_a n\, dt, \quad n = n_0 \exp\left[-\int^t k_a dt'\right], \tag{3.19}$$

where n (n_0) is the (initial) number or density of autoionizing species AB^*, k_a is the autoionization rate constant, and t is the time. To apply Eq. (3.19) to molecular-level Penning ionization requires the adoption of a classical trajectory for A^*+B over which time passes. While classical mechanics is known to fail in describing molecular collisions accurately, it provides the logical and conceptual underpinning for the quantum-mechanical description to be outlined later in this section. The Born-Oppenheimer approximation provides a potential surface $V_0(\mathbf{r}) = E_0(\mathbf{r}) - E_0(\infty)$ from which forces may be derived that govern the A^*+B collision. For the conceptual purposes of this section, a spherical approximation $V_0(r)$ will be employed for the most part, with indications where appropriate of the modifications necessary to describe the case of a molecular B. At the outset of this classical discussion, it is noted that if B has even the complexity of a diatomic molecule, the exact classical trajectory cannot be written down in closed form, and one must resort to numerical solution of, say, Hamilton's equations of motion.

Defining the probability of ionization at time t by $P(t)dt = -dn(t)/n_0$, we find that the rate equations (3.19) yield

$$P(t)dt = [k_a(t)dt] \exp\left[-\int^t k_a(t')dt'\right]. \tag{3.20}$$

In Eq. (3.20) the prefactor may be identified as the present probability of ionization, and the exponential as the "survival factor," attenuating the present ionization rate by accounting for the historic loss of population. The autoionization rate constant k_a depends on time, as passing time brings changes in the $A^* \cdots B$ distance r, according to

$$\frac{dr}{dt} = \pm v_0 [1 - V_0/E - b^2/r^2]^{1/2}, \quad v_{b,0}(r) \equiv \left|\frac{dr}{dt}\right|, \tag{3.21}$$

where v_0 is the asymptotic relative velocity of the A^*+B collision, E is the kinetic energy of collision $E = \frac{1}{2}\mu_r v_0^2$, μ_r is the reduced mass, b is the impact parameter, and $v_{b,0}(r)$ is the magnitude of the local radial velocity. The $\pm$ corresponds to the two equal halves, incoming and outgoing, of the two-body collision trajectory, separated by the turning point of the collision r_c, for which the radicand in Eq. (3.21) is zero. Now identifying $k_a = \Gamma/\hbar$ and using the definition of $v_{b,0}(r)$ of Eq. (3.21), we see that Eq. (3.20) becomes (Miller, 1970b)

$$P_b^{\text{in}}(r)dr = [\Gamma(r)dr/\hbar v_{b,0}(r)] \exp\left[-\int_r^\infty \Gamma(r')dr'/\hbar v_{b,0}(r')\right], \tag{3.22}$$

$$P_b^{\text{out}}(r)dr = [\Gamma(r)dr/\hbar v_{b,0}(r)] \exp\left[-\left(\int_{r_c}^\infty + \int_{r_c}^r\right)\Gamma(r')dr'/\hbar v_{b,0}(r')\right], \tag{3.23}$$

where $P_b(r)$ is an ionization probability per unit length and the incoming and outgoing survival factors differ only because of the two-branch structure of the trajectory. The in-out distinction is more than academic, however, as the amplitudes will interfere with each other in a quantum picture.

The classical total PI probability at r is

$$P_b(r)dr = [P_b^{\text{in}}(r) + P_b^{\text{out}}(r)]dr, \tag{3.24}$$

and the total ionization probability—the opacity function for PI—is given by

$$P(b) = \int_{r_c}^\infty P_b(r)dr = 1 - \exp\left[-2\int_{r_c}^\infty \Gamma(r)dr/\hbar v_{b,0}(r)\right], \tag{3.25}$$

where the integration over r has been done analytically. The classical total PI cross section is then

$$Q_I = 2\pi \int_0^\infty P(b) b\, db. \tag{3.26}$$

Because of its orbital-overlap dependence [Eqs. (3.17) and (3.18)], $\Gamma(r)$ falls to zero quickly at large r, well inside the uncertainty distance where at thermal collision energy

the quantum shadow looms; hence Q_I calculated from Eq. (3.26) agrees well with its quantum counterpart.

Less useful but still informative are the classical formulas for the angle-resolved and total *nonreactive* scattering. The c.m. differential cross section (nonreactive scattering angular distribution) is given by

$$I_N(\theta)=\sum_{i=1}^{3} b_i[1-P(b_i)]/\sin\theta|\partial\chi/\partial b|_i \ , \tag{3.27}$$

where χ is the classical deflection function,

$$\chi(b)=\pi-2bv_0\int_{r_c}^{\infty} dr/r^2 v_{b,0}(r) \ , \tag{3.28}$$

$P(b)$ is the opacity function, θ is the c.m. scattering angle, $\theta=|\chi|_{\mathrm{mod}\pi}$, and the sum runs over the three branches of χ that produce the angle θ for the usual V_0 (see Fig. 2). The $1-P(b)$ factor in Eq. (3.27) accounts for attenuation of the incoming flux due to ionization. The total nonreactive scattering cross section is

$$Q_N=2\pi\int_0^{\pi} I_N(\theta)\sin\theta\, d\theta=2\pi\int_0^{\infty}[1-P(b)]b\, db \ . \tag{3.29}$$

Q_N given by Eq. (3.29) is infinite for realistic V_0, and Eq. (3.27) is plagued by all the usual classical infinities: rainbow, $\partial\chi/\partial b\to 0$; glory, $\theta\to 0$; and long-range, $\theta\partial\chi/\partial b\to 0$. Although these are all replaced by finite peaks in the quantum treatment, the peaks serve as their signatures, and the classical results thus remain conceptually useful. It is noteworthy that in classical mechanics the force that produces tangible deflections is given entirely by V_0, while the only role of Γ is to dictate the ionization rate.

Equations (3.21)–(3.28) are relatively easy to generalize when B is a linear, rigid molecule (Cohen and Lane, 1977; Martin and Siska, 1985) by using the infinite-order sudden approximation (IOSA) (Pack, 1974; Parker and Pack, 1978). Let γ be the angle between $\mathbf{r}$ and the molecular axis ρ, i.e., $\cos\gamma=\hat{r}\cdot\hat{\rho}$; then $V_0=V_0(r,\gamma)$ and $\Gamma=\Gamma(r,\gamma)$. In the IOSA, γ is held fixed and radial quantities are computed, followed by an average over γ. Thus, for example, the total ionization cross section is

$$Q_I=\pi\int_0^{\pi}\sin\gamma\, d\gamma\int_0^{\infty} P(b,\gamma)b\, db \ , \tag{3.30}$$

where

$$P(b,\gamma)=1-\exp\left[-\frac{2}{\hbar v_0}\int_{r_c}^{\infty}\frac{\Gamma(r,\gamma)dr}{[1-V_0(r,\gamma)/E-b^2/r^2]^{1/2}}\right] ; \tag{3.31}$$

one could reverse the order of integration in Eq. (3.30) and define an angle-averaged $P(b)$. An analogous definition of $\chi(b,\gamma)$, Eq. (3.28), leads to a similar treatment of $I_N(\theta)$, Eq. (3.27), very well known in its semiclassical version, as discussed later in this section. The IOSA works well when one or more of the following frequently fulfilled conditions hold: weak anisotropy, dominance of repulsion, heavy rotor, high collision energy, and small Γ.

The classical theory of Penning ionization presented up to this point, especially Eqs. (3.25)–(3.28), is actually a classical optical model, discussed at some length for molecular collisions by Greene *et al.* (1966), Harris and Wilson (1971), and Micha (1976). To examine differential product properties we must go beyond the optical model, requiring that $V_+(\mathbf{r})$ be specified. The most telling of these properties is the energy distribution of the Penning electron (the PI electron spectrum), denoted by $P(\varepsilon)$.

In the Born-Oppenheimer approximation, the Penning electron's kinetic energy is

$$\varepsilon=E_0(\mathbf{r})-E_+(\mathbf{r})=\varepsilon_0+V_0(\mathbf{r})-V_+(\mathbf{r}) \ , \tag{3.32}$$

where the potential surfaces V_0, V_+ are taken to be zero as $r\to\infty$, and ε_0 is the energy difference $E_0(\infty)-E_+(\infty)=E_*(A^*)-IE(B)$ between the excitation energy of A^* and the ionization energy of B into a particular state of B^+. B^+ may be formed in a variety of (n',v') states, n' the electronic state and v' vibrational, each with its own ionization energy and characteristic $V_+(\mathbf{r})$; it is assumed one of these states is being probed, and therefore the $P(\varepsilon)$ line shape for that ion state is considered. Equation (3.32) implies that the probability for ionizing at a particular configuration $\mathbf{r}$ is related to that for producing a given ε; more specifically, for spherical potentials, we have

$$P_b(\varepsilon)=\sum_{\nu} P_b(r_\nu)/|d\varepsilon/dr|_\nu \ , \tag{3.33}$$

where $P_b(r)$ is given by Eqs. (3.22)–(3.24), $d\varepsilon/dr=V_0'(r)-V_+'(r)$ from Eq. (3.32), and the sum is over those r_ν (usually no more than two) that satisfy Eq. (3.32). The classical PI electron spectrum for a particular state of B^+ is then

$$P(\varepsilon)=2\pi\int_0^{\infty} P_b(\varepsilon)b\, db \ . \tag{3.34}$$

The complete electron spectrum is a sum of terms, each given by Eq. (3.34), for the allowed states of B^+. The resemblance of Eq. (3.33) to Eq. (3.27) is notable; in particular one expects two analogous infinities in $P_b(\varepsilon)$: a "rainbow," $d\varepsilon/dr\to 0$, and a "glory," $v_b(r)\to 0$ at $r=r_c$. The glory is a turning-point singularity that is washed out by the impact-parameter average, but the "rainbow" position depends only on the location of an extremum in $d\varepsilon/dr$, independent of b, and survives in quantum mechanics as a maximum in $P(\varepsilon)$. Normally $d\varepsilon/dr=0$ occurs just inside the minimum in $V_0(r)$, where $V_+(r)$ is slowly varying in its long-range behavior (see Fig. 2), the effect of the corresponding well in $V_+(r)$ on $\varepsilon(r)$ being overwhelmed by the steeply rising repulsive wall of V_0.

When B is a closed-shell atom or nonpolar molecule, the well in V_0 is typically at such a large distance that Γ is too small to make the rainbow visible in $P(\varepsilon)$. However, cases of "repulsive rainbows" are known (Martin *et al.* 1978; Hotop, 1980).

Anisotropy in V_0 is expected to damp the rainbow, just as it is known to do in angular distributions, although to this date no model calculations have been carried out. The IOSA version of Eq. (3.33) may be formulated in a straightforward way by defining $P_b(r,\gamma)$ and $\varepsilon(r,\gamma)$ in an obvious generalization of Eqs. (3.22)–(3.24) and (3.32).

The classical heavy-particle angle-energy distribution $I(E',\theta)$ also becomes calculable once $V_+(r)$ is specified; except for a missing Jacobian factor and garbled formulas the results have been spelled out by Haberland *et al.* (1981) and follow directly from Miller's (1970b) exposition. We have

$$I(E',\theta)=\sum_{ijv} b_i P_{bi}^j(r_v)/\sin\theta\left|\partial(\chi_j,E')/\partial(b,r)\right|_{jv} , \tag{3.35}$$

where the sum over i is analogous to that in Eq. (3.27), that over $j=$in,out to Eq. (3.22), and that over v to Eq. (3.33). Equation (3.32) implies that the r dependence of the recoil energy E' is given by

$$\begin{aligned} E'&=E-V_0(r)+V_+(r) ,\\ \frac{dE'}{dr}&=\frac{-d\varepsilon}{dr}=-V_0'(r)+V_+'(r) , \end{aligned} \tag{3.36}$$

while $|\chi_j|_{\mathrm{mod}\pi}=\theta$ as in the nonreactive case, but with the product-scattering deflection functions given by

$$\chi_{\mathrm{in}}=\pi-bv_0\int_{r_v}^{\infty}\frac{dr}{r^2v_{b,0}(r)} -b'v_+\left[\int_{r_c'}^{r_v}+\int_{r_c'}^{\infty}\right]\frac{dr}{r^2v_{b',+}(r)} , \tag{3.37}$$

$$\chi_{\mathrm{out}}=\pi-bv_0\left[\int_{r_c}^{\infty}+\int_{r_c}^{r_v}\right]\frac{dr}{r^2v_{b,0}(r)} -b'v_+\int_{r_v}^{\infty}\frac{dr}{r^2v_{b',+}(r)} . \tag{3.38}$$

Here the final impact parameter is $b'=b(E/E')^{1/2}$, the final asymptotic velocity is $v_+=v_0(E'/E)^{1/2}=(2E'/\mu_r)^{1/2}$, r_c' is the classical turning point on V_+, and

$$v_{b',+}(r)=v_+[1-V_+(r)/E'-(b')^2/r^2]^{1/2} \tag{3.39}$$

is the local radial velocity of the products. Equation (3.36) implies that

$$v_{b',+}(r_v)=v_{b,0}(r_v) , \tag{3.40}$$

i.e., the local radial velocity is conserved, and leads to the reduction of the Jacobian determinant appearing in Eq. (3.35) to

$$\left|\frac{\partial(\chi_j,E')}{\partial(b,r)}\right|=\left|\frac{\partial\chi_j}{\partial b}\right|\left|\frac{\partial E'}{\partial r}\right| , \tag{3.41}$$

since $\partial E'/\partial b=0$. As many as twelve terms may contribute to the multiple sum in Eq. (3.35), and Eq. (3.41) implies that all the different types of singularities already discussed will remain. For reference in Sec. IV, we note the implied presence of the angular glory and energy rainbow effects. When integrated over solid angle, the recoil energy distribution $P(E')$ is found, as expected from Eq. (3.36), to be the complement of $P(\varepsilon)$ of Eq. (3.34). In addition, all quantities involved in Eq. (3.35) can be defined for a fixed orientation angle γ, enabling a ready IOSA generalization. For Penning ionization, Eq. (3.35) is a rigorous classical formula, but analogous treatments also make valuable models for "direct" chemical reactions (Herschbach, 1966; Riley *et al.*, 1979).

In experiments employing a mass spectrometer (the PICSEM types of Tables II and III) the branching fraction Q_{AI}/Q_I is a commonly measured quantity. In associative ionization a bound rovibrational state of AB^+ is formed; classically the bound-state spectrum is, of course, just as continuous as the translational, and Q_{AI} is easily defined within the same framework as the total ionization cross section, using the criterion that the final translational E' energy of $A+B^+$ must be negative,

$$E'=\mathscr{E}-\varepsilon=E-V_0(\mathbf{r})+V_+(\mathbf{r})<0 . \tag{3.42}$$

This excludes all rotationally predissociated states—all fully bound classically (Miller, 1970b)—but due to the typically short predissociation lifetimes relative to detection time scales, such exclusion is usually valid within a few percent and leads to the tidy formulas

$$P_{\mathrm{AI}}(b)=2\exp\left[-\int_{r_c}^{\infty}\frac{\Gamma(r)dr}{\hbar v_{b,0}(r)}\right] \times\sinh\left[\int_{r_c}^{r_{\mathrm{AI}}}\frac{\Gamma(r)dr}{\hbar v_{b,0}(r)}\right] \tag{3.43}$$

and

$$Q_{\mathrm{AI}}=2\pi\int_0^{\infty}P_{\mathrm{AI}}(b)b\,db , \tag{3.44}$$

where $P_{\mathrm{AI}}(b)$ is the opacity function for associative ionization and r_{AI} is the (unique) root of $E-V_0(r)+V_+(r)=0$. The IOSA generalizations of Eqs. (3.42)–(3.44) are again easy to formulate.

For a nonbonded A^*+B interaction, the PI cross sections, while still "large" by chemical kinetic standards, are typically a factor of 5–10 smaller than for open-shell B, and a factor of 50 or more smaller than the total collision cross section. This suggests that a perturbative approach might be a fruitful source of insight as well as approximate but rapid data reduction. A set of small-Γ perturbation formulas are easily derived for all of the classical quantities discussed here. For example, Eqs. (3.25)–(3.26) and (3.33)–(3.34) yield (Miller *et al.*, 1972)

$$Q_I=\frac{4\pi}{\hbar v_0}\int_{r_0}^{\infty} r^2\Gamma(r)[1-V_0(r)/E]^{1/2}dr \tag{3.45}$$

and

$$P(\varepsilon)=\frac{4\pi}{\hbar v_0}\sum_{\nu} r_\nu^2\Gamma(r_\nu)[1-V_0(r_\nu)/E]^{1/2}/|d\varepsilon/dr|_\nu\ , \tag{3.46}$$

where the integral over b has been carried out analytically and r_0 is the turning point for $b=0$. For most accessible ε's the sum in Eq. (3.46) collapses to one term for a predominantly repulsive V_0. Combining the small-Γ and IOSA limits is also an attractive possibility. These formulas are expected to be considerably more accurate than, say, the classical analog of the first Born approximation, as rigorous classical trajectories are retained, but such formulas have not been widely used (Münzer and Niehaus, 1981; Mitsuke, Takami, and Ohno, 1989). Equation (3.45) is in essence the product of a local transition rate and a line-of-centers cross section (see, for example, Levine and Bernstein, 1987), while Eq. (3.46) explicitly displays the retention of the structure in $P(\varepsilon)$ due to $d\varepsilon/dr$, as well as its differential relationship to Q_I. A realistic assumption for this case is the "double-exponential" model, where $V_0=Ae^{-\beta r}$ and $\Gamma=\Gamma_0 e^{-\alpha r}$. The integral in Eq. (3.45) may then be evaluated analytically; although the full result is a sum of terms, the dominant one is

$$Q_I=(4\pi\Gamma_0/\hbar\beta^3)(\mu_r/2A)^{1/2}\mathrm{B}(\alpha/\beta,\tfrac{3}{2})[\ln(E/A)]^2 \times(E/A)^{\alpha/\beta-(1/2)}\ , \tag{3.47}$$

where $\mathrm{B}(a,b)$ is the beta function (Abramowitz and Stegun, 1964). When $E/A\ll 1$, as is typical, the logarithmic term is slowly varying, and the cross section shows a rising energy dependence, provided $\beta<2\alpha$. This model also suggests realistic parametric forms for $P(\varepsilon)$ in the weak-coupling limit.

On the other hand, for a strongly attractive $V_0(r)$, perturbation methods must fail except at very large b, since the reagents will always be pulled to small r where Γ is large. Miller and Schaefer (1970) and Miller *et al.* (1972) have given classical orbiting models for this case. In the simplest of these, one makes a strong-collision assumption for all collisions that surmount the centrifugal barrier in the effective potential $V_0(r)+Eb^2/r^2$, thereby skirting the need to know anything about Γ. For a V_0 of arbitrary form, the PI cross section is

$$Q_I^{\mathrm{orb}}=\pi r_0^2[1-V_0(r_0)/E]\ , \tag{3.48}$$

where r_0 is the larger root of $E-V_0(r)-(r/2)V_0'(r)=0$. For potentials that behave as $-C_s r^{-s}$ at long range, this becomes (see, for example, Levine and Bernstein, 1987)

$$Q_I^{\mathrm{orb}}=\pi(s/2)[(s-2)/2]^{-(s-2)/s}(C_s/E)^{2/s}\ , \tag{3.49}$$

yielding a characteristic decline in Q_I with E. Further, if the ionizing transition is assumed to occur at the turning point, an expression identical to Eq. (3.48) is obtained for the associative ion cross section, but with r_0 replaced by r_{AI}, where r_{AI} is the root of either $E-V_0(r)-(r/2)V_+'(r)=0$ (for inclusion of quasibound AB^+ as the associative ion) or $E-V_0(r)+V_+(r)=0$ (for only truly bound AB^+, as discussed earlier). In the "scaled" orbiting model, a knowledge of Γ is employed to compute the opacity function of Eq. (3.25) at $b=0$, yielding

$$Q_I=P(0)Q_I^{\mathrm{orb}}\ , \tag{3.50}$$

which produces cross sections in excellent agreement with exact classical calculations [Eq. (3.26)], but badly overestimates the amount of associative ionization, due to the turning-point assumption.

2. Quantum and semiclassical theory

As in all other areas of molecular physics and chemistry, a realistic interpretation of the results of molecular-beam Penning ionization experiments for the most part requires a quantum-mechanical description of the nuclear motion. This is especially true of those differential measurements, such as angular distributions or electron energy distributions, that expose classical singularities. However, many of the observed quantum effects in Penning ionization can be emulated by semiclassical approximations (Miller, 1970b), in which amplitudes formed from classical probabilities and actions are added and squared, presenting a direct connection with the classical quantities of the previous subsection. As a practical matter, though, the increasing speed of modern computers has made numerically exact quantum calculations of PI scattering much more prevalent at the present time, rendering the semiclassical ideas more useful as heuristic guides than as computational tools. Most of the modifications to classical theory can be understood by appealing to two simple, related notions: the interference of two classical paths, and our intrinsic inability to localize the nuclei at a particular $\mathbf{r}$ during a collision.

Morgner (1990) has recently recapitulated the Born-Oppenheimer separation and reduction of the full Schrödinger equation

$$\mathcal{H}\Psi_{\mathrm{tot}}=\mathcal{E}\Psi_{\mathrm{tot}} \tag{3.51}$$

to radial equations describing the A^*+B and $A+B^+$ collision dynamics for spherical interactions. (For the original developments, see Mori *et al.*, 1964; Mori and Fujita, 1965; Mori, 1966, 1969; Nakamura, 1968a, 1968b, 1969a, 1969b, 1971; a thorough overview is given by Bieniek, 1978.) Here the full Hamiltonian $\mathcal{H}=T_{\mathrm{r}}+H_{\mathrm{el}}$ contains the nuclear kinetic-energy operator T_{r}, and Ψ_{tot} denotes the exact total wave function. The ansatz Eq. (3.4) now becomes

$$|\Psi_{\mathrm{tot}}(\mathbf{r})\rangle=u_0(\mathbf{r})|\Phi_0\rangle+\int d\varepsilon' u_{\varepsilon'}(\mathbf{r})|\Phi_{\varepsilon'}\rangle\ , \tag{3.52}$$

where the coefficients $u_0, u_{\varepsilon'}$ are now functions of $\mathbf{r}$, the collisional wave functions describing the nuclear motion,

and the dependence on electron coordinates has been suppressed. Substituting in Eq. (3.51), we obtain the infinite set of coupled equations

$$[T_r+E_0(\mathbf{r})-\mathscr{E}]u_0(\mathbf{r})+\int d\varepsilon' V_{0\varepsilon'}(\mathbf{r})u_{\varepsilon'}(\mathbf{r})=0\ ,$$
$$[T_r+E_+(\mathbf{r})+\varepsilon-\mathscr{E}]u_\varepsilon(\mathbf{r})+V_{0\varepsilon}(\mathbf{r})u_\varepsilon(\mathbf{r})=0\ , \tag{3.53}$$

where coupling between the discrete and continuum electronic manifolds induced by T_r has been neglected, as in the Born-Oppenheimer approximation.

Although complicated by the explicit account of nuclear motion, the assumptions leading to the local, complex potential (optical potential)

$$V_{\rm opt}(\mathbf{r})=V_0(\mathbf{r})+\Delta(\mathbf{r})-i\pi|V_{0\varepsilon}(\mathbf{r})|^2 \tag{3.54}$$

governing the excited-state motion and decay are in essence no different from those that have just been stated in the previous subsection (Morgner, 1990; see also Lam and George, 1983, 1984). Ordinarily the shift Δ is neglected, and the imaginary term is identified as in Eq. (3.7) with $-i\Gamma(\mathbf{r})/2$. Model calculations using a discretized version of Eqs. (3.53) (Bellum and Micha, 1977, 1978; Micha and Piacentini, 1982) yield results in good accord with those based on $V_{\rm opt}$. In the often-encountered case that several states of B^+ may be formed, Δ, $V_{0\varepsilon}$, and hence Γ become product-state specific (to be discussed in Sec. IV). Steps *a* and *b* of Eq. (3.1) are then governed by the single-channel Schrödinger equation

$$[T_r+V_{\rm opt}(\mathbf{r})-E]u_0(\mathbf{r})=0\ , \tag{3.55}$$

and all the features of optical-model analysis (Micha, 1976) then apply. If $V_{\rm opt}$ is spherical, the usual separation of variables and partial-wave analysis may be carried out. For anisotropic $V_{\rm opt}$, Hickman *et al.* (1977b) have shown how to formulate and solve the complex potential rigid-rotor coupled radial equations (see also Martin and Siska, 1985, 1988), and Cohen and Lane (1977) have given an IOSA formulation. If bond-switching reactions are possible on the excited surface, as when B contains a halogen atom, the process becomes quantum-reactive scattering in the presence of discrete/continuum coupling, which is probably a formulatable but not solvable problem at present.

For spherical $V_{\rm opt}$ and V_+, partial-wave analysis yields the radial equations

$$\left[\frac{d^2}{dr^2}+k_0^2\left[1-\frac{V_0-i\Gamma/2}{E}-\frac{l(l+1)}{(k_0r)^2}\right]\right]\psi_l^0(r)=0\ , \tag{3.56}$$

$$\left[\frac{d^2}{dr^2}+k_+^2\left[1-\frac{V_+}{E'}-\frac{l'(l'+1)}{(k_+r)^2}\right]\right]\psi_{l'}^+(r)=0\ , \tag{3.57}$$

where $k_0(k_+)$ is the asymptotic wave number for heavy-particle motion, $k^2=2\mu_r E/\hbar^2$, before (after) ionization; $l(l')$, the partial-wave index, is the angular momentum quantum number for $A^*+B(A+B^+)$, and ψ_l^0 ($\psi_{l'}^+$) is the corresponding radial wave function. For Penning ionization these wave functions take on the asymptotic form

$$\psi_l(r)\underset{r\to\infty}{\sim}k^{-1/2}\sin(kr-l\pi/2+\eta_l)\ , \tag{3.58}$$

where η_l is the phase shift. Normally $l'=l$ is assumed, although recent evidence suggests this is not strictly true (Merz *et al.*, 1989; Khan *et al.*, 1991b). For the entrance channel, η_l^0 is complex,

$$\eta_l^0=\delta_l+i\xi_l,\quad \xi_l\geq 0\ , \tag{3.59}$$

causing a decrease in the amplitude of ψ_l^0, the quantum indicator of a loss of flux due to ionization. The PI opacity function is then

$$P(l)=1-\exp(-4\xi_l) \tag{3.60}$$

and the total ionization cross section

$$Q_I=(\pi/k_0^2)\sum_{l=0}^{\infty}(2l+1)P(l)\ , \tag{3.61}$$

easily recognized as the quantum analogs of Eqs. (3.25) and (3.26), and standard in the optical model. As in the classical case, IOSA extensions are straightforward.

Equation (3.56) suggests we define a complex local radial wave number for A^*+B by

$$\tilde{k}_{l,0}(r)=k_0\{1-[V_0(r)-i\Gamma(r)/2]/E-l(l+1)/(k_0r)^2\}^{1/2}\ . \tag{3.62}$$

The classical implication of this definition is that the local radial velocity $v_b(r)$ is complex due to Γ, and that even in the limit $\hbar\to 0$ the equivalent classical trajectories can be affected by Γ. This phenomenon is thought to account for calculated differences in wide-angle nonreactive scattering between the exact solution of Eq. (3.56) and small-Γ approximations (Martin *et al.*, 1978).

At this point the quantum formulation has simplified sufficiently that the implications of using Eq. (3.12) instead of (3.4) for the exact total wave function may be more clearly perceived. Because the partitioning of the PI and AI branches is energy dependent and angular momentum dependent through $\varepsilon_{\rm max}$ [using $l'=l$ and $E'=E-(\varepsilon-\varepsilon_0)$], the resonance width must also be so, $\Gamma=\Gamma(r;E,l)$. In the simplifying approximation that associative ionization results when $E'<0$, we have $\varepsilon_{\rm max}=E+\varepsilon_0$. For fixed E, the monotone increase of $\varepsilon(r)$ at small r (see Fig. 2) will cause a sharp change in $\Gamma(r)$ at a radius $r_{\rm AI}$ satisfying $\varepsilon_{\rm max}(r_{\rm AI})=E+\varepsilon_0$. As E increases, $r_{\rm AI}$ will shrink, causing the sharp break in Γ to move inward as well. As suggested in the preceding section, Γ is expected to be substantially smaller inside $r_{\rm AI}$ due to the low density of AB^+ states. As typical AB^+ potential curves show a finite number of bound states, the change in Γ at $r_{\rm AI}$ might even be observably abrupt. This situation may obtain in the $He^*(2\,^3S)+H$ system (Waibel

et al., 1988; Merz *et al.*, 1990), as discussed in Sec. IV.A. The observability of the energy dependence of Γ depends both on the steepness of $V_0(r)$ at short range and on the ratio E/ε_0, being less the steeper V_0, and greater the larger E/ε_0. In his model calculations Morgner (1990) sidestepped this problem by taking $E_+(r)$=const, thus excluding the second sum in Eq. (3.12).

The apparent dependence of Γ on the rovibrational spectrum of AB^+ implies that quantities such as Q_I, Eq. (3.61), are not rigorously independent of final state, as has been claimed or assumed quite generally in the PI literature. This is not to say that a $\Gamma(r)$ cannot be constructed that will represent the entrance-channel scattering correctly at a given E, only that it will not correspond in general to the results of *ab initio* calculations using, say, Eq. (3.7'), in which only electronic structure factors are considered.

Nonreactive angular scattering in PI systems is handled simply by inserting the complex phase shift Eq. (3.59) into the standard two-body scattering amplitude, while extensions to molecular systems by the IOSA or close-coupling methods have proven to be only slightly more difficult than the equivalent nonreactive scattering problem. The quantum treatment of product distributions, in particular, PIES and $Q_{\rm AI}$, however, requires $V_{0\varepsilon}$ itself, rather than just its absolute square. The theory is conveniently formulated in terms of the partial-wave S matrix (Miller, 1970b; Khan *et al.*, 1991b); in PI form it is given by

$$S^l_{l'\lambda}(\varepsilon)= -2i(2\mu_r/\hbar^2)\exp[i(\eta^0_l+\eta^+_{l'})] \times\int_0^\infty dr\,\psi^+_{l'}(r)V_{\varepsilon\lambda}(r)\psi^0_l(r)\ , \tag{3.63}$$

where $V_{\varepsilon\lambda}$ is the matrix element arising from the partial-wave expansion of Φ_ε, Eq. (3.15), now taken with respect to the initial relative velocity and the center of mass, and is related to Γ by

$$\Gamma(r)=2\pi\sum_\lambda |V_{\varepsilon\lambda}|^2\ . \tag{3.64}$$

When partial-wave expansions for u_0, u_ε, and $V_{0\varepsilon}$ are inserted into the fully differential scattering amplitude $f(\hat{k}_+,\varepsilon,\hat{\varepsilon})$ (Miller *et al.*, 1972), a Σ-state partial-wave formula for f is obtained (Morgner, 1978, 1979):

$$f(\hat{k}_+,\varepsilon,\hat{\varepsilon})=(\pi^{1/2}/ik_0)\sum_{\lambda=0}^{\infty}\sum_{\mu=-\lambda}^{\lambda}\sum_{l=0}^{\infty}\sum_{l'=|l-\lambda|}^{l+\lambda}[l][l']^{1/2}\begin{pmatrix}l' & \lambda & l\\ 0 & 0 & 0\end{pmatrix}\begin{pmatrix}l' & \lambda & l\\ -\mu & \mu & 0\end{pmatrix}i^{l'-l}S^l_{l'\lambda}(\varepsilon)Y_{l'\mu}(\hat{k}_+)Y_{\lambda-\mu}(\hat{\varepsilon})\ . \tag{3.65}$$

Here $\hat{k}_+$ and $\hat{\varepsilon}$ represent c.m. polar angles for product heavy-particle and electron scattering, respectively, μ is a space-fixed projection of λ, $[x]$ denotes $2x+1$, and $\begin{pmatrix}\cdots\end{pmatrix}$ is a 3-j symbol (Zare, 1988). A variety of cross-section expressions may be obtained by taking the absolute square of Eq. (3.65) and integrating over unobserved variables. Among the more recently available differential measurements are the energy-angle distribution of the Penning electron [equivalent formulas have been given by Morgner (1978) and Bieniek (1978)],

$$P(\varepsilon,\hat{\varepsilon})=(\pi/k_0^2)\sum_{l'\mu}[l']\left|\sum_{\lambda l}[l]\begin{pmatrix}l' & \lambda & l\\ 0 & 0 & 0\end{pmatrix}\begin{pmatrix}l' & \lambda & l\\ -\mu & \mu & 0\end{pmatrix}i^{l'-l}S^l_{l'\lambda}(\varepsilon)Y_{\lambda-\mu}(\hat{\varepsilon})\right|^2\ , \tag{3.66}$$

and the closely similar energy-angle distribution of the heavy particles (Khan *et al.*, 1991b),

$$I(E',\hat{k}_+)=(\pi/k_0^2)\sum_{\lambda\mu}\left|\sum_{ll'}[l][l']^{1/2}\begin{pmatrix}l' & \lambda & l\\ 0 & 0 & 0\end{pmatrix}\begin{pmatrix}l' & \lambda & l\\ -\mu & \mu & 0\end{pmatrix}i^{l'-l}S^l_{l'\lambda}(\varepsilon)Y_{l'\mu}(\hat{k}_+)\right|^2\ . \tag{3.67}$$

Morgner (1978) and Hoffmann and Morgner (1979) have analyzed the electron distribution further by expanding the absolute square to show that

$$P(\varepsilon,\hat{\varepsilon})=(4\pi)^{-1}\sum_{\lambda'}p_{\lambda'}(\varepsilon)P_{\lambda'}(\cos\theta_\varepsilon)\ , \tag{3.68}$$

where

$$p_{\lambda'}(\varepsilon)=([\lambda']/4k_0^2)\sum_{l'l_1l_2\lambda_1\lambda_2}[l'][l_1][l_2]([\lambda_1][\lambda_2])^{1/2}\begin{pmatrix}l' & \lambda_1 & l_1\\ 0 & 0 & 0\end{pmatrix}\begin{pmatrix}l' & \lambda_2 & l_2\\ 0 & 0 & 0\end{pmatrix}\begin{pmatrix}\lambda_1 & \lambda_2 & \lambda'\\ 0 & 0 & 0\end{pmatrix}\begin{pmatrix}l_1 & l_2 & \lambda'\\ 0 & 0 & 0\end{pmatrix}\begin{Bmatrix}\lambda' & \lambda_1 & \lambda_2\\ l' & l_1 & l_2\end{Bmatrix} \times i^{l_2-l_1}S^{l_1^*}_{l'\lambda_1}(\varepsilon)S^{l_2}_{l'\lambda_2}(\varepsilon) \tag{3.69}$$

and $\{\cdots\}$ is a 6-j symbol (Zare, 1988). The angle-averaged electron energy distribution $P(\varepsilon)$ is given by $p_0(\varepsilon)$; for $\lambda'=0$, Eq. (3.69) collapses to

$$P(\varepsilon)\equiv p_0(\varepsilon)=(\pi/k_0^2)\sum_{\lambda ll'}[l][l']\begin{Bmatrix} l' & \lambda & l \\ 0 & 0 & 0 \end{Bmatrix}|S^l_{l'\lambda}(\varepsilon)|^2 . \tag{3.70}$$

Results similar to Eqs. (3.68) and (3.69) may be obtained for the heavy-particle distribution Eq. (3.67), establishing that both $I(E',\hat{k}_+)$ and $P(\varepsilon,\hat{\varepsilon})$ are cylindrically symmetric about the initial relative velocity. This symmetry is lost in a coincidence PIECES measurement (Penning ion-electron coincidence electron spectrum), represented by the absolute square of the full amplitude Eq. (3.65). Hoffmann and Morgner (1979) have also shown how to generalize these formulas in Hund's case (b) for nonzero electronic angular momentum molecular-axis projections Λ.

Until very recently, the angular momentum of the electron has been neglected when treating heavy-particle distributions or PI electron spectra; for $\lambda\equiv 0$, we have $l'=l$, and Eqs. (3.67) and (3.70) simplify to

$$I(E',\theta)=(4k_0^2)^{-1}\left|\sum_{l=0}^{\infty}(2l+1)S^l_{l0}(\varepsilon)P_l(\cos\theta)\right|^2 \tag{3.71}$$

and

$$P(\varepsilon)=(\pi/k_0^2)\sum_{l=0}^{\infty}(2l+1)|S^l_{l0}(\varepsilon)|^2 . \tag{3.72}$$

The assumption $\lambda\equiv 0$ (s waves only) of course cannot be used for $P(\varepsilon,\hat{\varepsilon})$, as it results in an isotropic distribution in θ_ε according to Eq. (3.66); as discussed in Sec. IV, measured electron angular distributions have shown at least some angle dependence in the majority of systems studied to date. However, many of the experimental $P(\varepsilon,\hat{\varepsilon})$ data have been analyzed in a way that preserves the two-body dynamics and neglects any possible correlation between ε and $\hat{\varepsilon}$, using the so-called *internal* angular distribution (Ebding and Niehaus, 1974; Micha and Nakamura, 1975; Morgner, 1978),

$$P_{\rm int}(\varepsilon,\gamma_\varepsilon)=\left|\sum_\lambda V_{\varepsilon\lambda}(r_\varepsilon)Y_{\lambda 0}(\gamma_\varepsilon,0)\right|^2 , \tag{3.73}$$

where r_ε is the interatomic distance corresponding to electron energy ε in the Born-Oppenheimer approximation, and $\cos\gamma_\varepsilon=\hat{\varepsilon}\cdot\hat{r}$ represents the *body-fixed* electron-scattering angle. This distribution is intrinsically unmeasurable, as the space-fixed heavy-particle angular coordinates $\hat{r}=(\theta_r,\phi_r)$ cannot be precisely defined for a fixed collisional angular momentum l, owing to the uncertainty principle, and therefore do not appear in the scattering amplitude Eq. (3.65). In addition, locating r_ε requires simultaneously sharply defined radial position and momentum, again in conflict with the uncertainty relation; this is reflected in the appearance of the radial matrix element $\langle l'|V_{\varepsilon\lambda}|l\rangle$ in the S matrix, Eq. (3.63), rather than $V_{\varepsilon\lambda}(r_\varepsilon)$ itself. r_ε actually results from making a stationary-phase approximation to this matrix element, as discussed later in this section. At that point the semiclassical model employed in the interpretation of $P(\varepsilon,\hat{\varepsilon})$ will also be described.

To date no *ab initio* studies have yielded the $V_{\varepsilon\lambda}(r)$, defined with respect to the c.m., needed to produce numerical results from the S-matrix formalism just given. Hickman and Morgner (1976) have therefore introduced the approximation

$$V_{\varepsilon\lambda}(r)\approx\alpha_\lambda[\Gamma(r)/2\pi]^{1/2},\quad \sum_\lambda|\alpha_\lambda|^2=1 ; \tag{3.74}$$

α_λ is typically assumed to be constant and, as defined by Morgner (1978), includes the $i^{-\lambda}\exp(i\sigma_\lambda)$ phase factor in the partial-wave expansion (3.15). The Hickman-Morgner approximation neglects any ε dependence of the electronic coupling and forces all angular momentum terms to conform to a single radial behavior. While these assumptions are certainly questionable (Bieniek, 1978), they allow numerical results to be obtained with a minimal number of free parameters beyond those in $\Gamma(r)$ itself.

In addition, Morgner (1978) and Hoffmann and Morgner (1979) have shown that, within the Hickman-Morgner approximation and the stationary-phase approximation as embodied in the internal distribution Eq. (3.73), $P_{\rm int}$ and P may both be written as Legendre expansions in the form of Eq. (3.68), with the coefficients proportional to each other. This makes it possible to analyze experimental $P(\varepsilon,\hat{\varepsilon})$ directly in terms of the α_λ within a fully quantum framework, aside from the stationary-phase limitation; such an analysis for He*+Ar has been carried out by Hoffmann and Morgner (1979) and will be discussed further in Sec. IV.C.

For associative ionization, $I(E',\theta)$ is of course not defined, while the S-matrix expression for use in $P(\varepsilon,\hat{\varepsilon})$ and $P(\varepsilon)$ changes to

$$S^l_{l'\lambda}(\varepsilon)=-2i(2\mu_r\pi/\hbar^2)^{1/2}\exp(i\eta^0_l)\times\int_0^\infty dr\,\psi^+_{v'l'}V_{\varepsilon\lambda}\psi^0_l , \tag{3.75}$$

owing to the bound-state character of $\psi^+_{v'l'}$, where v' is the vibrational quantum number. The electron energy is limited to the discrete values $\varepsilon=\varepsilon_{v'l'}=E+\varepsilon_0-E'_{v'l'}$, as discussed in Sec. III.A, and $\psi^+_{v'l'}$ is normalized to unity. The total AI cross section is then readily computed by summing $P(\varepsilon)$ of Eqs. (3.70) or (3.72) over these states. The total electron spectrum is the sum of PI and AI contributions, generally unresolved except in He*, Ne*+H as described in Sec. IV.A.

A complication in AI calculations is the so-called quasiassociative ionization qAI that occurs when AB^+ is formed with $E'>0$ but is trapped behind the product centrifugal barrier. All such AB^+ will eventually dissociate, but perhaps some fraction will do so on a time scale long compared to typical detection times τ_d ($\sim 1-10$ μs

in an ion-extraction experiment); that fraction is then counted as associative ionization. Hickman and Morgner (1976) have calculated the qAI fraction for $He^*(2\,^3S)+Ar$, finding that $<10\%$ of $HeAr^+$ formed is qAI for $\tau_d=10\ \mu s$, representing $\sim 2\%$ of the total ionization cross section. Waibel *et al.* (1988) have found only slightly larger fractions in $He^*(2\,^3S)+H$.

With regard to possible influence on Γ, it thus does not appear that qAI will have a great effect, although the nuclear translational continuum becomes "lumpy" when predissociation resonances are present, thereby introducing l dependence in Γ. qAI might reduce the abruptness of the changeover from PI to AI final-state densities, making any alteration in the r dependence of Γ more gradual.

A situation similar to qAI occurs for ionization of molecular B. In most cases thus far studied (Hotop, 1974) the $B\rightarrow B^+ + e^-$ transition is a near-Franck-Condon process, which often results in vibrational excitation of B^+. Then, even though the translational energy criterion is met for formation of AB^+, the vibrational energy of B^+ will predissociate the erstwhile AI product; for example,

$$A\cdots B^+(v')\rightarrow A+B^+(v'-1)+\Delta E' \ . \tag{3.76}$$

This will greatly reduce Q_{AI} for molecular B as compared to atomic, as found experimentally. Vibrational predissociation of AB^+ should also reduce the effect of associative ionization on the resonance width, as the left-hand-side species of Eq. (3.76) is no longer a discrete state for $v'>0$, but is coupled to the PI translational continuum. This converts part of the sum of Eq. (3.12) to an integral that can be combined with the pure PI integral, thus returning the PI problem more nearly to that of atomic autoionization.

Miller (1970b) has shown how the quantum formulas reduce to their classical counterparts as $\hbar\rightarrow 0$ through the use of the stationary-phase approximation (see also Lam, George, and Bhattacharyya, 1983). This proceeds in two stages, beginning with the matrix-element integral in the S matrix, Eq. (3.63), assuming $l'=l$. When WKB radial wave functions are substituted, a stationary-phase point is found for r such that $k_l^0(r)=k_l^+(r)$; this is the Condon radius, at which the local radial velocity and kinetic energy are conserved during the transition, as in the classical case already considered. The standard "primitive" semiclassical result is then recovered,

$$S_{l0}^l(\varepsilon)=\sum_{j\nu}[P_l^j(r_\nu)/|d\varepsilon/dr|_\nu]^{1/2}\exp[i\phi_l^j(r_\nu)] \ , \tag{3.77}$$

where the $P_l^j(r)$ are the classical probabilities Eqs. (3.22) and (3.23), with $l+\frac{1}{2}=k_0 b=k_+ b'$, the $\phi_l^j(r)$ are cumulative JWKB phases (classical actions in units of $\hbar$) along the incoming and outgoing classical trajectories, and r_ν satisfies Eq. (3.32), $\varepsilon=\varepsilon_0+V_0(r)-V_+(r)$. Semiclassical equivalence relates the phases to the deflection functions χ^j of Eqs. (3.37) and (3.38) through $2\partial\phi_l^j/\partial l=\chi^j$. When the phase difference $\phi_l^{\rm out}-\phi_l^{\rm in}$ is large and rapidly varying with r, the interference term that arises on taking the absolute square of S becomes impossible to resolve, and the classical probability, Eq. (3.24), is obtained. For differential product scattering, a second stationary-phase evaluation is carried out for the partial-wave sum, yielding many types of energy- and angle-dependent interference patterns (Miller, 1970b) that have their origin in the classical paths of Eq. (3.35).

Since the classical probability appears in Eq. (3.77), its singularities at the turning point and at $d\varepsilon(r)/dr=0$ are not yet removed; both of these may be regarded as arising when two stationary-phase points coalesce. The latter "rainbow" singularity is readily treated by Airy-function analysis (Miller, 1970b) and by its uniformized extension (Bieniek, 1974, 1976; Bieniek *et al.*, 1990). Bieniek *et al.* (1990) also give an approximate prescription for treating the turning-point problem by the use of uniform WKB wave functions and have produced the first comparisons between uniform semiclassical and exact quantum calculations for $He^*(2\,^3S)+He^*(2\,^3S)$ PI electron spectra. The computed spectra show close agreement except in regions where tunneling inside the classical turning point dominates the intensity. In addition, computed fine structure superimposed on the rainbow oscillations is with little ambiguity attributed to in-out interference.

The Airy approximation has been frequently used to determine the well depth of V_0 directly from PI electron spectra. This improved stationary-phase method amounts to replacing the singular energy-distance Jacobian according to

$$\begin{aligned}
&\left|\frac{d\varepsilon}{dr}\right|^{-1}\rightarrow 2\pi(2\varepsilon_*'')^{-1/2}a_*^{-1/6}\mathrm{Ai}^2(-z) \ , \\
&\varepsilon_*''\equiv\left|\frac{\partial^2\varepsilon}{\partial r^2}\right|_*=|V_0''(r)-V_+''(r)|_{r=r_*} \ , \\
&a_*=\tfrac{1}{2}[\hbar v_{b,0}(r_*)]^2\varepsilon_*'' \ , \\
&z=(\varepsilon-\varepsilon_*)/a_*^{1/3} \ ,
\end{aligned} \tag{3.78}$$

and (ε_*,r_*) corresponds to the extremum in $\varepsilon(r)$. The corresponding classical result, assuming a quadratic expansion of ε about $r=r_*$, is $|d\varepsilon/dr|^{-1}=[2\varepsilon_*''(\varepsilon-\varepsilon_*)]^{-1/2}$, and Eq. (3.78) is readily shown to reduce to this expression, averaged over the oscillations in Ai^2, for $\varepsilon\gg\varepsilon_*$. The point $\varepsilon=\varepsilon_*$ occurs at 43.93% of the peak intensity, dictated by the principal maximum of $\mathrm{Ai}^2(-z)$ at $z=1.0188$, allowing in principle both ε_* and ε_*'' to be determined by simple calculation from two points on an experimental PI electron spectrum. Approximations that improve on the behavior of Eq. (3.78) away from the point $\varepsilon=\varepsilon_*$ are also available (Niehaus, 1981).

In the semiclassical limit, both the magnitude r and the orientation angles $\hat{r}=(\theta_r,\phi_r)$ of the intermolecular distance vector in space become well defined, enabling the internal electron angular distribution $P_{\rm int}$ of Eq. (3.73) to be transformed into $P(\varepsilon,\hat{\varepsilon})$ through integration over clas-

sical trajectories. The body-fixed angle γ_ε, $\cos\gamma_\varepsilon=\hat{\varepsilon}\cdot\hat{r}$, is obtained from the standard dihedral angle formula $\cos\gamma_\varepsilon=\cos\theta_r\cos\theta_\varepsilon+\sin\theta_r\sin\theta_\varepsilon\cos\phi_r$, and Eq. (3.73) is integrated over t or r, b, and ϕ to yield the electron angular distribution $P(\theta_\varepsilon)$. This procedure has been used by Ebding and Niehaus (1974) and more recently by Mitsuke, Kusafuka, and Ohno (1990) to extract the relative magnitude and phase of α_1 of the Hickman-Morgner model, Eq. (3.74), for a number of He* systems by assuming only s and p waves are present. Further discussion is reserved for Sec. IV.

Despite early misgivings (Morgner and Niehaus, 1979; Siska, 1984), the collision theory description of the PI entrance channel appears to be well in hand if taken by itself. To make the theory more useful in extracting electronic structure information from experiment, two new developments are desirable. Further theoretical insight into the behavior of the center-of-mass partial-wave matrix elements $V_{\varepsilon\lambda}$ and their relation to configuration mixing in the discrete state would enable more realistic models than Eq. (3.74) to be employed. Perhaps more important, a method is needed for feeding back information on AI bound states, obtained routinely in quantum calculations of $Q_{\rm AI}$, into a procedure that corrects $V_{0\varepsilon}$ and Γ for the decreased density of states in the range of r that produces associative ionization. In this way a self-consistent theory could be built that would allow a description of Penning ionization based on a strictly electronic interpretation of Γ.

3. Postionization dynamics

After the Penning electron has departed, the nascent $[AB]^+$ species finds itself with a peculiar distribution of energy (through the potential difference) and angular momentum (through the opacity function), which form the initial conditions for step c of Eq. (3.1). The ensuing dynamics depends on the particular state of AB^+ formed; the entire potential surface changes when, as is often found, two or more electronic states of B^+ are populated, while if vibrational excitation of a molecular B^+ is present, $V\leftrightarrow T$ energy transfer, and possibly reaction, may occur. For a given state of an atomic B^+ product, Eqs. (3.34) and (3.58) completely describe the dynamics, but the more general case of a molecular B^+, henceforward in this subsection denoted BC^+, demands a treatment of inelasticity and reaction that may still be regarded as state-of-the-art collision theory in itself.

A unified approach suggested some time ago by Preston and Cohen (1976), known as the trajectory-surface-leaking (TSL) model, employs numerically computed rigorous classical trajectories for the entire reaction, with transitions determined at random but subject to Γ; this method was applied to $He^*(2\,^3S)+H_2$ on *ab initio* surfaces. While we continue to believe this approach can be of great value (Siska, 1984), a disadvantage is the requirement of complete energy surfaces for both the excited and the ionic states. A more approximate model has been employed by Martin *et al.* (1984, 1989), in which easily estimated spherical potentials like those of Fig. 2 are used to construct the distribution of energy and angular momentum of $[AB]^+$ and, by assuming ionic complex formation, the branching among product channels.

The model of Martin *et al.* (1989) employs exactly calculated opacity functions $P(J)$, where $\mathbf{J}$ is the total heavy-particle angular momentum $\mathbf{J}=\boldsymbol{l}+\mathbf{j}=\boldsymbol{l}'_\alpha+\mathbf{j}'_\alpha$, $\boldsymbol{l}$ and $\mathbf{j}$ now being the collisional and rotational angular momenta of A^*+BC, and $\boldsymbol{l}'_\alpha,\mathbf{j}'_\alpha$ the same for some ionic product arrangement channel $\alpha(A+BC^+$, AB^++C, or $AC^++B)$. $P(J)$ is used together with a near-turning-point (line-of-centers) assumption for ionization out of A^*+BC, and the Langevin (orbiting) criterion for formation of a strongly coupled $[ABC]^+$ complex, to predict through the use of phase-space theory (Light, 1967) the cross sections for the various arrangements. The model was applied to $He^*(2\,^{1,3}S)+H_2,D_2,HD$ Penning ionization with some success; a more detailed discussion is reserved for Sec. IV.B.

The turning-point assumption works well for repulsive interactions, but, as was discussed in the preceding section, is not trustworthy when penetration to configurations where Γ is large can occur. In addition, for systems such as He^*+Cl_2, where bond-switching can occur prior to ionization, the entire notion of an intact Penning ion's forming and undergoing further reactions may have to be discarded. Kischlat and Morgner (1983) and Benz and Morgner (1986a) have developed a model for such reactions that explicitly includes covalent-ionic interactions and bond-stretching effects that are well known in the corresponding alkali reactions. It consists of running two-body classical trajectories that slowly decay in "weight" as dictated by the local ionization probability $k_a(t)dt$ of Eq. (3.20), decomposed into its branches for the various Cl_2^+ final states, but does not include the possibility of autoionization of the saltlike He^+Cl^- bond-switching product (see Miller and Morgner, 1977, for a treatment of He^+F^-), which would yield Cl^+.

IV. PENNING IONIZATION WITH THE NOBLE-GAS METASTABLE ATOMS: EXPERIMENT AND THEORY

Here are examined in detail four reagents in Penning ionization with metastable helium and neon atoms, chosen either because of their close connection with available theoretical work (H and H_2) or because of the vast amount and wide variety of experimental data available (Ar and N_2). Figure 3 illustrates the energetics for these systems. Each of these PI partners also brings unique features to the process that will be emphasized. Other studies of interest to the pursuit of a global understanding of Penning ionization will be briefly surveyed; an attempt at a complete bibliography of recent molecular-beam and theoretical work is made in Tables II–IV and VIII.

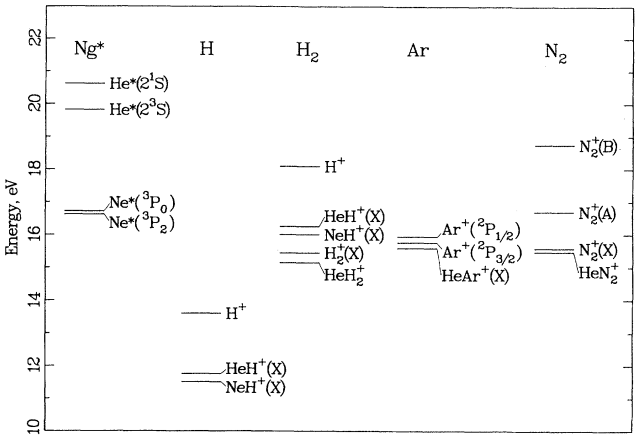

FIG. 3. Energetics of Penning ionization for the four reagents discussed in detail. For molecular-ion products, only the energies of the ground vibrational states are shown. The associative ions for the Ne* reactions with H_2, Ar, and N_2 are not shown, but are expected to lie close to the corresponding He* products. For the Penning ions, these levels form the asymptotes for the two-potential-curve model illustrated in Fig. 2. 1 eV = 23.060 54 kcal/mol = 8065.541 cm^{-1}.

A. He^*, Ne^* + H

1. Overview of experimental results

The total ionization cross section and Q_{AI}/Q_I branching for $He^*(2\,^{1,3}S)+H$ were first reported by Howard *et al.* (1973) in a resonance-lamp state-selected crossed-thermal-beam experiment ($E \approx 8.5$ kcal/mol) employing an electron-impact-excited He* beam, a thermal dissociation H atom source, total ion extraction, and quadrupole mass analysis. Incomplete dissociation of H_2 is a source of error in all the H atom measurements, even when mass analysis is employed, as both H_2 and H produce HeH^+; this requires that a correction be applied to the associative ion component of Q_I. Magnuson and Neynaber (1974) performed the earliest merged-beam experiments on $He^*(2\,^3S)+H$, D, obtaining Q_{AI} over an extended energy range, 0.2–25 kcal. This was followed by a $He^*(2\,^3S)+D$ Q_I study (Neynaber and Magnuson, 1975a) and most recently a complete Q_I, Q_{AI} study, using the ^3He isotope (Neynaber and Tang, 1978). Fort *et al.* (1976, 1978, reviewed by Manus *et al.*, 1978), have also obtained $Q_I(E)$ and $Q_{AI}(E)$ for both ^1S and ^3S + H, D using crossed beams; for ^1S + H (1976) they employed mechanical velocity selection of a thermal He* beam with a low-temperature H atom discharge source and quadrupole mass analysis; for ^3S + H (1978) the He* selection was done by time of flight. The resulting nominal energy range was $E = 0.4$–2.3 kcal. Waibel *et al.* (1988) have thoroughly reviewed and summarized the more recent results for $He^*(2\,^3S)+H$. For both ^1S and ^3S, the total PI cross section declines linearly with E on a log-log scale, up to an energy of 7 kcal/mol, where it begins to fall more steeply. The low-energy behavior is readily understood, in view of the open-shell interaction—similar to LiH—and consequent deep well in V_0, in terms of the orbiting theory of the previous section, but carries little information on the form of $V_0(r)$ or $\Gamma(r)$ at short range. Furthermore, the magnitude of the ^3S Q_I at 8.5 kcal, 9 Å^2±30%, determined by Neynaber and Tang (1978), is more than a factor of 2 smaller than that of Howard *et al.* (21 Å^2±15%). The only direct measurement of Q_I for $He^*(2\,^1S)+H$ is that of Howard *et al.*, 30.3 Å^2±15% at 8.5 kcal.

PIES studies of He^*+H were pioneered by Hotop *et al.* (1971) and refined by Morgner and Niehaus (1979) for both spin states of He* with a Maxwellian crossed-beam arrangement (He* hot-cathode discharge, H radio-frequency discharge). More recently Waibel *et al.* (1988), using a mildly supersonic "pure" $He^*(2\,^3S)$ discharge source in conjunction with a higher-resolution analyzer, have produced what may be the best-resolved PI electron spectrum reported to date, in which many vibration-rotation lines of HeH^+, as well as two supernumerary rainbows, are clearly resolved. As discussed in the previous section, an Airy analysis of even the earliest ^3S spectrum provided quick and in retrospect quite accurate estimates of the well depths of the $^2\Sigma^+$ states produced by $He^*(2\,^{1,3}S)+H(^2S)$, as well as a fair estimate of the curvature of V_0 for ^3S. (Features of the potentials will be summarized in the next subsection.) Employing *ab initio* calculations of the $He^*(2\,^3S)+H$ $^2\Sigma^+$ potential curve $V_0(r)$ and a variable $\Gamma(r)$, along with the wave number accuracy $V_+(r)$ for HeH^+ $X\,^1\Sigma^+$ computed by Kołos and Peek (1976), Waibel *et al.* (1988) and later Merz *et al.* (1990) were able to model the PI electron spectrum nearly to within experimental error using the exact quantum formulas (save for the assumption $l = l'$) of Sec. III.C. The $\Gamma(r)$ function thus determined displays a strong "saturation" effect at small distance, passing from steeply exponential at large r to nearly constant over a narrow range of r, ~1.7–1.5 Å. This is necessary to represent the highly damped supernumerary rainbow structure as well as the AI/PI intensity ratio in the spectrum. The $Q_I(E)$ predicted from this potential agreed well in magnitude with that of Howard *et al.* (1973) at 8.5 kcal, while $Q_{AI}(E)$ agreed closely with the most recent merged-beam results (Neynaber and Tang, 1978) in both magnitude and energy dependence over a wide range. The principal discrepancy was for Q_I at low E between the predictions from PI electron spectroscopy and merged-beam measurements, with the former yielding an $E^{-0.2}$ dependence, the latter $E^{-0.34}$.

Khan *et al.* (1991a) have recently reported a fully quantum analysis of the $He^*(2\,^1S)+H$ Penning ionization electron spectra of Morgner and Niehaus (1979) as well. As these data did not display extensive rainbow or associative ionization structure, Khan *et al.* found it adequate to base the fitting on perturbations to V_0 and energy scaling of Γ from the *ab initio* Siegert calculations of Isaacson and Miller (1979), while again employing the

Kołos-Peek $V_+(r)$. Again, a fit nearly within experimental uncertainties was obtained. The $\Gamma(r)$ of Isaacson and Miller shows a maximum at $r=1.6$ Å, and is well fit by a Gaussian function rather than a simple exponential.

Owing to the use of a thermal-dissociation H atom source instead of a discharge, the Penning ion angle-energy distributions (PIAED) for the $He^*(2\,^1S)+H$ measured by Khan *et al.* (1981, 1991a) referred to a much higher mean collision energy than the electron spectra measurements (9.2 vs 1.2 kcal/mol). They found that the V_0,Γ optimized to fit the low-energy PI electron spectra failed to emulate either the recoil angle or the energy distributions of H^+ or D^+ at the higher energy. Both theory and experiment showed strongly forward scattering, but the prediction was more sharply peaked at 0° c.m. The experimental recoil energy distribution $P(E')$ peaked at a considerably lower energy (by ~ 5 kcal/mol) than the prediction. Khan *et al.* interpreted the energy discrepancy in terms of discrete nonadiabatic coupling with the $^2\Sigma^+$ state arising from $He^*(2\,^3P)+H$, as suggested earlier by Miller and Schaefer (1970). Diabatic states were constructed by "deperturbing" the *ab initio* potential curves of Miller and Schaefer (1970) (which clearly undergo an avoided crossing), thereby allowing the $He^*(2\,^1S)+H$ collision to follow either an adiabatic (normal, attractive) curve or a diabatic curve that turns out to be completely repulsive. Penning transitions on this curve result in lower recoil energy, thus shifting the entire distribution to lower energy, in improved agreement with the measured recoil spectrum. The computed angular distribution, however, appeared to be impervious to nonadiabatic coupling, at least at scattering angles in the forward hemisphere. More recent work on $Ne^*(^3P_{2,0})+H$, D, to be described next, has now clarified the angular distribution discrepancy.

Experimental PI studies on Ne^*+H are few; no direct total-cross-section measurements have been reported. An early PIES effort of Morgner (1979) has been supplanted by the high-resolution study of Lorenzen *et al.* (1983) employing a laser-state-selected cold-cathode discharge-excited Ne^* beam and an effusive discharge H atom source. Ne^* state selection produced the surprising result that nearly all the ionization is due to the $^3P_2$ state: $Q_I^{(0)}/Q_I^{(2)}=0.017$, the superscripts referring to the J states. The $Ne^*(^3P_2)+H$ spectrum of Lorenzen *et al.* is presented in Fig. 4. A recently reported supersonic crossed-beam measurement of the H^+ angle-energy distribution by Khan *et al.* (1991b), resulting in the velocity-space contour map shown in Fig. 5, rounds out the available data. Khan *et al.* (1991b) have also carried out a fully quantum-mechanical analysis, including electron-ion angular momentum coupling using the theory outlined in Sec. III.C, based on a single complex potential for $Ne^*(^3P_2)+H$, which reconciles the $P(\varepsilon)$ and the $I(\theta,E')$ data. From this they have determined characteristics of V_0 and Γ, illustrated in Fig. 6, as well as an estimate of the upper limit to the angular momentum sharing with the Penning electron. The latter esti-

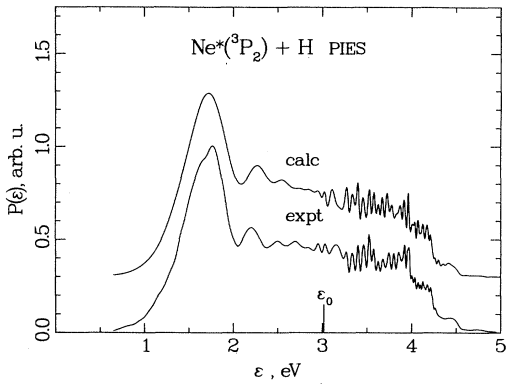

FIG. 4. Electron spectrum from the Penning ionization of H atoms by Ne*, experimental data of Lorenzen *et al.* (1983) compared to calculations of Khan *et al.* (1991b). The smooth structure to the left of ε_0 is assigned to the rainbow effect, while the fine structure to the right reflects the rovibrational states of the NeH^+ associative ion. The calculated curve has been shifted upward by 0.3 units for presentation.

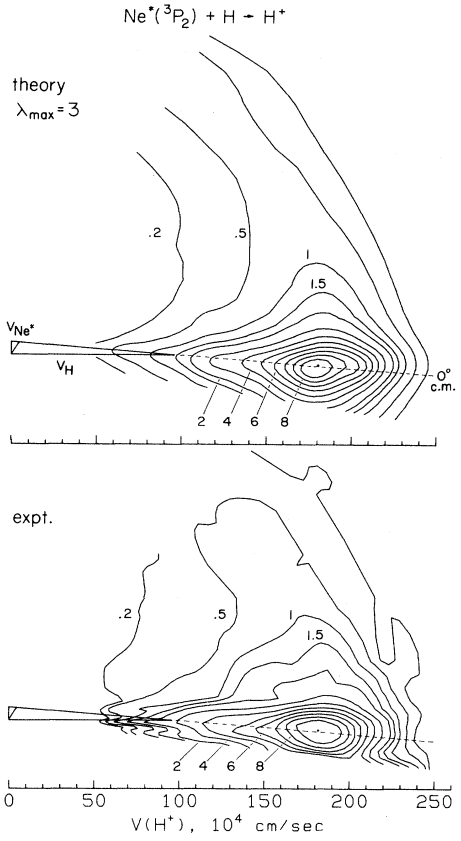

FIG. 5. Velocity-space center-of-mass intensity contour maps of scattered H^+ from Ne^*+H Penning ionization, at $E=10.4$ kcal/mol, from Khan *et al.* (1991b). Both the experimental and the calculated maps are normalized to 10 at the peak. The maps reflect strong forward scattering with substantial translational energy release. The calculations include angular momentum sharing between the Penning electron and the atoms to a maximum of $3\hbar$ ($\lambda_{max}=3$).

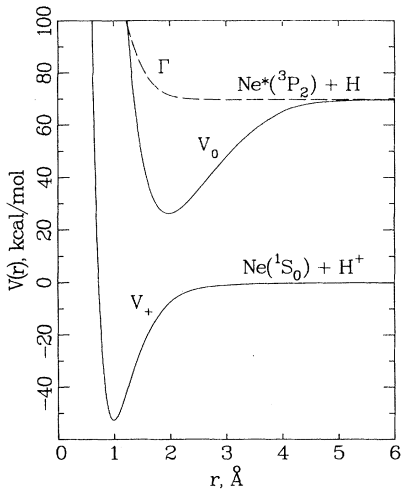

FIG. 6. Potential curves for Ne* + H used in the calculations of Figs. 4 and 5. V_0 and Γ are determined by fitting the PIES and PI angle-energy distribution data, while V_+ was taken from the *ab initio* study of Rosmus and Reinsch (1980).

mate was derived by fitting the angular distribution $\langle I(\theta)\rangle_{E'}$ given in Fig. 7. Such sharing has also been shown, in unpublished calculations, to account for much of the difference between theory and experiment for He*(2 ^1S)+H as well. The optical potential predicts a cross section $Q_I = 22.3$ Å^2 at $E = 1.0$ kcal/mol, $Q_{AI}/Q_I = 0.282$ at this energy, and a 300-K rate constant of 5.9×10^{-10} cm^3 s^{-1}, all targets for future experiments; Fig. 8 shows the predicted energy dependence of Q_I and Q_{AI}.

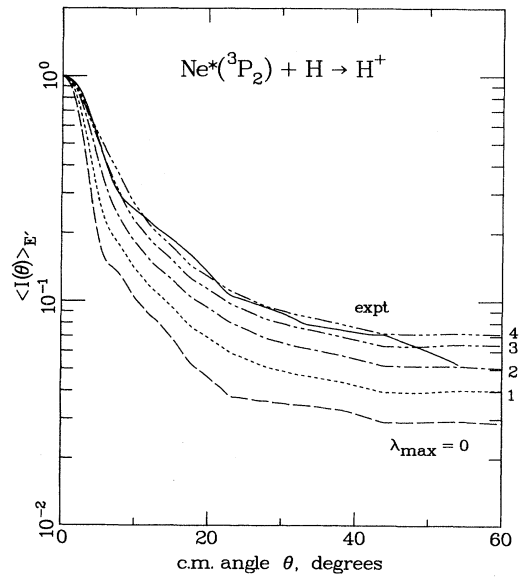

FIG. 7. Variation of the c.m. heavy-particle product angular distribution from Ne* + H with the maximum angular momentum λ_{max} shared with the Penning electron, at $E = 10.4$ kcal/mol. The calculated curves have been fully averaged over experimental spreads in velocity and scattering angle, causing the loss of quantum fine structure present under monochromatic conditions. The experimental curve (solid line) is taken from Khan *et al.* (1991b).

As detailed in Table II, a number of PIES studies of the familial alkali atom partners have been carried out recently. Because of their low ionization energies, the alkalis are readily ionized by all the metastable noble gases. Accurate estimates of V_0 well depths and cross-section ratios for 2 ^1S/2 ^3S He* and $J = 2/J = 0$ heavier metastables have been obtained, owing to the relatively strong bonding forces present, as again suggested by the Ng*-M analogy. In an especially illuminating study, Schohl *et al.* (1990) compared spectra for Ng* + Na, with Ng* = Ne* through Xe*, finding a strong similarity between Ne* + Na and Ne* + H in terms of line strength and shape in the PI segment, but a gradually increasing $^3P_0$ cross section and interaction strength for the heavier Ng*, until for Xe* + Na the $J = 0$ and $J = 2$ well depths and cross sections were found to be comparable. The alkali analogy also carries through to He*(2 $^{1,3}S$) + He*(2 ^3S); recent PIES experiments at ultralow energy from ionization within the metastable beam (Müller *et al.*, 1987, 1991) have also revealed hints of in-out interference not previously observed. (This corresponds to a fine structure superimposed on the "rainbow" pattern, reminiscent of a similar structure found in molecular scattering angular distributions.)

In a recent PIES study of He*(2 $^{1,3}S$) + Li, Merz *et al.* (1989, 1990) have observed an appreciable dependence of $P(\varepsilon)$ on the range of electron-scattering angles detected. A cylindrical-mirror analyzer equipped with a rotatable, slotted inner cylinder and located above the scattering center was employed. The rainbow pattern in $P(\varepsilon)$ showed systematic shifts and damping with angle, being sharper and of higher energy (by 0.05–0.10 eV) at small angles than at large. The findings have also been inter-

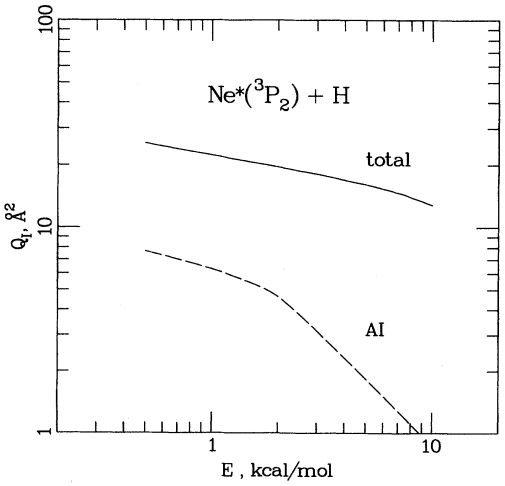

FIG. 8. Predicted total and associative ionization cross sections for Ne* + H using the potentials of Fig. 6. The AI cross sections include qAI products with predissociation lifetimes greater than 10 μs.

preted in terms of angular momentum transfer between the electron and the Penning products. These new features are discussed further in the next section.

2. Theory and interpretation

It is of course impossible to discuss the experimental results just summarized without some recourse to theoretical notions, just as Sec. III drew on specific examples, with natural favorites being the H atom systems. Thanks to the early work of Miller, Schaefer, and coworkers (see Table VIII), theoretical approaches to Penning ionization followed along in the 1970s with more limited scope but at only a slightly slower pace than experiment. If we examine $He^*(2\,^{1,3}S)+H$, we find that characteristics of V_0 have evolved, due to refined experimental and fitting procedures, to a point only 10–20% removed from the early results of Miller and Schaefer (1970). The most recent *ab initio* V_0 (see Müller *et al.*, 1991, for a description of the method) of Merz *et al.* (1990) required no adjustment at all in providing a close fit to highly structured PIES data for $He(2\,^3S)+H$. The situation is not quite so favorable for $He^*(2\,^1S)+H$, a higher root of the "stabilized" set, and, while theory has made progress (as briefly described by Merz *et al.*, 1990) for He* with the "one-electron" alkali targets, results for Ne^*+H, M are so far unsupported by any rigorous electronic structure theory.

The most glaring difficulty, however, is the lack of reliable theoretical results for $\Gamma(r)$ even for $He^*(2\,^3S)+H$; experimentalists have often been content with choosing an alkali-inspired V_0 and determining $\Gamma(r)$ completely empirically by fitting experimental cross sections. Even theoreticians (see for example, Cohen *et al.*, 1985) have been known to eschew their own *ab initio* data in favor of empiricism. The H atom target is of course the most favorable case for theory from several points of view; we shall see later that the common closed-shell heavy-atom or molecular reagents remain virtually untouched by *ab initio* theory. This situation presents us with a welcome opportunity to speculate.

To build a firm foundation for such speculation, it is important to select a realistic analytic potential function for the system under study, a theme that recurs throughout small-molecule chemical physics and is perhaps even more important in Penning ionization, due to the interplay between V_0 and Γ in determining the cross sections and other scattering attributes. An ideal potential function should have a small number of parameters to be determined by fitting experimental data, while maintaining a realistic shape as these parameters are varied over some physically acceptable range. For the hydride and alkali systems, representing V_0 by a modified Morse function (Hulburt and Hirschfelder, 1941) has been found to work well, having been used by Khan *et al.* (1991b) for Ne^*+H (see Fig. 6) and by Schohl *et al.* (1990) for Ng^*+Na. When high-quality *ab initio* data are available, spline interpolation on the *ab initio* points is generally acceptable.

It is important to note that interpretation of $P(\varepsilon)$ or $I(\theta,E')$ measurements in Ng^*+H is more meaningful, owing to the accurate potential curves available for $NgH^+(X\,^1\Sigma^+)$ from *ab initio* studies of Kołos and Peek (1976) for HeH^+ and of Rosmus and Reinsch (1980) for NeH^+; moreover, the $^1\Sigma^+$ state is the only one available to the products. This allows more confidence to be placed in the excited-state potentials obtained and in the speculations based on them.

Modeling the resonance with $\Gamma(r)$ was once thought to be straightforward, a simple decaying exponential, but molecular-beam results now seem to require, as discussed both previously and in the coming sections, small-r saturation, for which everything, from a discontinuous cutaway to a constant value (to be referred to here as a "clipped" Γ) to various damping functions and piecewise forms, has been employed. Figure 9 compares widths for He* and Ne^*+H obtained from experiment with the most recent theoretical results.

It is inviting to interpret the abrupt saturation of the $He^*(^3S)+H$ $\Gamma(r)$ shown in Fig. 9 in terms of the effect of the AI channel, as discussed in Sec. III.B, Eqs. (3.11) and (3.12). Waibel *et al.* (1988) emphasize that the PIES data cannot be fit by a more gradual change in Γ. The criterion that AI correspond only to truly bound HeH^+ yields $\varepsilon_{max}(r)\approx E+\varepsilon_0$. From V_0, V_+ and the mean collision energy of the PIES experiment, $E=1.0$ kcal/mol, we obtain $r_{AI}\approx 1.26$ Å, where r_{AI} is the PI/AI switchover radius. The Γ "saturation radius" r_{sat} is 1.6 Å from experiment. Considering that r_{AI} is a lower bound due to quasi-associative ionization, which will also reduce the density of nuclear states, one might conclude that $r_{sat}\approx r_{AI}$, i.e., that this is a case of AI-induced saturation.

For $Ne^*(^3P_2)+H$, however, Γ does not saturate abruptly (Khan *et al.*, 1991b). Under the conditions of

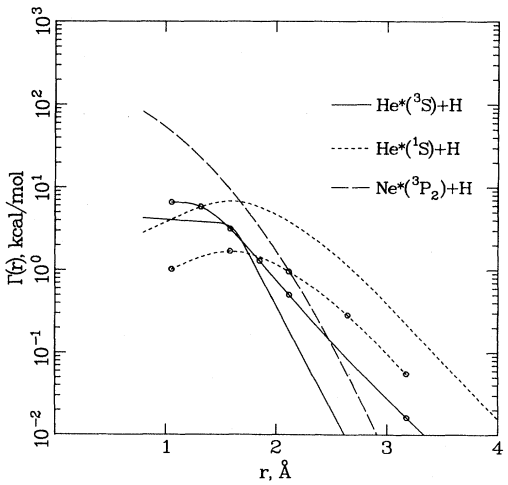

FIG. 9. Comparison of resonance widths for H atom Penning ionization. The curves without points are experimental, while the points represent *ab initio* calculations, for ^1S from Isaacson and Miller (1979) and for ^3S from Hickman *et al.* (1977a).

the PIES experiment of Lorenzen *et al.* (1983), r_{AI} is 1.52 Å, a distance at which Γ is found to be smoothly varying (see Fig. 9). The *ab initio* Γ for $He^*(2\,^1S)+H$ of Isaacson and Miller (1979), on the other hand, shows strong, though again not abrupt, saturation, without any influence of the nuclear degree of freedom. These results cast doubt on the above interpretation, though an effect of AI on Γ cannot be ruled out completely.

Khan *et al.* (1991b) have suggested an alternative saturation mechanism: pre-ionization charge transfer, producing Ng^+H^-. It is well known from *ab initio* studies that the corresponding hydrides LiH and NaH are highly ionic (Docken and Hinze, 1972; Sachs *et al.*, 1975; Zemke *et al.*, 1984), approaching unit fractional ionic character [defined as $\mu(r)/er$ (cgs), with μ the electric dipole moment] at $r=r_e$, the minimum in V_0. LiH in particular comes within 0.1% of fully ionic bonding. As other characteristics of $MH(^1\Sigma^+)$ and $Ng^*+H(^2\Sigma^+)$ are quite similar, we expect similar ionic character as well. If for any reason ionization from the ionic configuration were much slower than from the "covalent" one, Γ would be strongly affected, especially for nearly complete electron transfer. As Khan *et al.* show, this charge-transfer-saturation picture predicts different Γ behavior for He^* and Ne^*+H, in agreement with that derived from experiments. Unfortunately, dipole moments were not evaluated in the available stabilization calculations.

Despite their continuum embedment, the real interactions in the H and alkali atom systems seem to conform to ordinary quantum-chemical rules of behavior, such as atoms-to-molecule state correlations, spin conservation, the noncrossing rule, and the associated repulsion between states of like symmetry. Much insight into the observed magnitude of the V_0 well parameters can be gained by invoking these rules. Table IX gathers V_0 characteristics (largely experimental, mainly derived from PIES) for Ng^*+H, M.

Consider, for example, He^*+H: both ^3S and ^1S He^* can form $^2\Sigma^+$ states with $H(^2S)$, but ^1S arises from an asymptote higher by 0.8 eV, close enough to mix its $^2\Sigma^+$ state strongly with that from ^3S, causing a shallower well at a larger r. The $^4\Sigma^+$ state from ^3S is spin forbidden to ionize, as the products $HeH^+(^1\Sigma^+)+e^-$ form a doublet; experiment indeed shows no evidence of a second ionizing state.

This repulsive effect is even more pronounced in $Ne^*(^3P_{2,0})+H$, M as indicated in Table IX, because the $^3P_2$-$^3P_0$ spin-orbit splitting is only 0.1 eV. For the heavier metastables, a transition from Hund's case (c), $|J\Omega\rangle$, to case (a) or (b), $|\Lambda\Sigma\rangle$, occurs as the atoms are brought together (Herzberg, 1950). Nonetheless, the electronic Hamiltonian remains diagonal in Ω, and states of the same Ω ($\frac{1}{2},\frac{3}{2},\frac{5}{2}$ for $^3P_2+H$, $\frac{1}{2}$ for $^3P_0+H$) will interact. Lorenzen *et al.* (1983) have argued that, as $\Omega=\frac{1}{2},\frac{3}{2}$ states can correlate with "valence singlet" $^2\Sigma^+_{1/2}$ and $^2\Pi_{1/2,3/2}$ states at short range, these attractive states are taken up by the lower-energy $^3P_2,^3P_1$ asymptotes in accord with the noncrossing rule, leaving only antibonding "valence triplet" $^4\Sigma^+,^4\Pi$ states for $^3P_0,^1P_1$. This accounts for the dramatic difference between the $^3P_0$ and $^3P_2$ cross sections and PI electron spectra. According to the spin-conserving exchange model, Penning ionization can occur only out of the $^2\Sigma^+$ state; hence a single optical potential may be used to describe the $^3P_2$ reaction.

As the spin-orbit splitting in Ng* grows, the transition to case (a) or (b) occurs at smaller distance, and the asymptotes pair according to the core ion Ng^+ spin-orbit state. These two factors combine to reduce the repulsion between $\Omega=\frac{1}{2}$ states correlating with the metastable atomic states, as they are associated with different Ng^+ core ion states, and to vitiate more completely the total spin as a good quantum number. Doublets and quartets are then strongly mixed, and "valence singlet" character now permeates the $^3P_0$ PI state as well. The Ng^*+Na potential characteristics in Table IX lend support to this rationale.

As pointed out in the previous subsection, the behavior of the total ionization cross sections with collision energy suggests the domination of the collision dynamics by spiraling and orbiting collisions. Under these conditions the scaled orbiting model, Eqs. (3.48)–(3.50), is quite accurate, with the slope of $\log Q_I$ vs $\log E$ being $-2/s$, where s is the leading inverse power of the long-range attraction. While the merged-beam results of Neynaber and Tang (1978) suggested $s=6$, i.e., the occurrence of the critical centrifugal barrier in the van der Waals region, calculations by Waibel *et al.* (1988), based on the *ab initio* V_0 with Γ fitted to PIES data just described, require an r^{-10} behavior. This anomalous result probably arises because of the influence of the ionic He^+H^- configuration on the form of the potential at longer range, producing a rapid change in slope over a comparatively small segment of r values. [The covalent-ionic crossing radius estimated from $r_c=e^2/[IE(He^*)-EA(H)]$ (cgs) is 3.6 Å, compared to $r_e=1.8$ Å.] This rapid change in the attractive limb of V_0 causes the centrifugal barriers to occur in that range of r over a wide range of b (Anderson and Herschbach, 1975).

Near-orbiting collisions are almost certainly responsible for the sharply forward scattering of H^+ observed by Khan *et al.* (1991a, 1991b) (see Figs. 5 and 7). This is a forward glory effect, enhanced by the "repeats" from collisions that undergo an integral number of orbits, and, for a two-body system, limited in its angular width only by the uncertainty principle governing motion transverse to the forward direction. The observed broadening of the forward peak compared to the prediction of the quantum two-body PI theory, Eq. (3.71), which appears to be well outside the uncertainties in accounting for experimental broadening effects, seems to be a sensitive indicator of the degree of angular momentum coupling between the Penning electron and the product ionic complex. In estimating the maximum angular momentum λ_{max} the Penning electron may carry, it is often assumed (see, for example, Waibel *et al.*, 1988) that the electron originates from Ng*, in line with the exchange mechanism. λ is maxim-

ized when the electron is emitted perpendicular to the molecular axis, according to the classical formula

$$|\lambda| = [m_B/(m_{A^*}+m_B)]k_\varepsilon r \sin\gamma_\varepsilon , \quad (4.1)$$

where k_ε is the Penning electron's wave number, r is the internuclear distance at the instant of ionization, and γ_ε is the electron-scattering angle in the body-fixed frame. However, the existence of a substantial effect in $Ne^*(^3P_2)+H$, where $\lambda_{max}\approx 3-4$ is found empirically, is not accounted for by Eq. (4.1) because of the small lever arm. This suggests that the electron does not originate from Ne*; the likely sizable ionic Ne^+H^- contribution to the electronic wave function implies that the electron is emitted with significant probability from the H nucleus. This increases the lever arm by a factor of 20, by replacing m_B in the numerator of the mass factor in Eq. (4.1) with m_{A^*}, bringing Eq. (4.1) into closer agreement with the experimental result for typical $k_\varepsilon r$. The form of the electronic wave function should also play a role in $He^*(2\,^3S)+Li$, where the promoted electron becomes delocalized in a bonding σ molecular orbital prior to ionization, thereby making the lever arm ambiguous. (Most of the evidence that the electron is emitted from the noble gas comes from studies on closed-shell, nonbonding partners, where the promoted electron remains localized on Ng* prior to ionization; see Morgner, 1988.)

As discussed in Sec. III.C, the form and behavior of the matrix elements $V_{\varepsilon\lambda}$ needed for a rigorous calculation of these angular momentum effects is at present completely unknown, and the quantum scattering calculations must therefore employ simple models for these

TABLE IX. Well depths (kcal/mol) and equilibrium bond lengths (Å) of lowest-lying states for metastable noble gases interacting with atomic hydrogen and alkali metals.[a]

Metastable noble gas	H	Li	Na	K	Rb	Cs
$He^*(2\,^1S)$	10.2(8)[b] 2.9(3)	7.6(4)[c] 3.6(4)	6.4(6)[c] 3.9(4)	4.7(5)[c] 4.3(4)	5.0(4)[c] 4.4(4)	6.4(4)[c] 4.6(4)
$He^*(2\,^3S)$	52.7(5)[d] 1.80(5)	20.0(5)[c] 2.9(4)	17.1(5)[c] 3.1(4)	13.6(5)[c] 3.5(4)	12.6(4)[c] 3.6(4)	12.3(4)[c] 3.8(4)
$Ne^*(^3P_0)$	<1.5[e] 4(1)	<1.5[f]	1.2(4)[g] 5.0(5)	<1.5[f]		
$Ne^*(^3P_2)$	43.5(5)[h] 1.98(5)	18.4(7)[d] 3.0(10)	15.5(5)[f] 3.2(10)	12.9(5)[f] 3.6(10)		
$Ar^*(^3P_0)$			2.5(6)[g] 4.8(5)			
$Ar^*(^3P_2)$			13.9(5)[g] 3.6(2)			
$Kr^*(^3P_0)$			10.0(8)[g] 4.1(3)			
$Kr^*(^3P_2)$			13.0(6)[g] 3.8(2)			
$Xe^*(^3P_0)$			12.2(12)[g] 4.0(2)			
$Xe^*(^3P_2)$			12.8(7)[g] 4.0(2)			

[a]In each case the top entry is the well depth and the bottom the bond length. Numbers in parentheses are uncertainties in the least significant digit(s).
[b]Khan *et al.* (1991a).
[c]Ruf *et al.* (1987).
[d]Merz *et al.* (1990).
[e]Lorenzen, Morgner *et al.* (1983).
[f]Lorenzen, Hotop, and Ruf (1986).
[g]Schohl *et al.* (1990).
[h]Khan *et al.* (1991b).

quantities. In the He^*+Li calculations certain λ, $0 \le \lambda \le 4$, were assumed to dominate in different ranges of total angular momentum, based on classical-trajectory estimates of the average molecular-axis orientation in the c.m. frame, in order to emulate the shifting and damping of the PIES rainbow structure with electron-scattering angle. Merz *et al.* (1989, 1990) were forced to assume a definite *sign* of the rotational energy transfer in certain angular momentum ranges; otherwise the PIES shifts could not be represented. The simplified form of $P(\varepsilon)$, Eq. (3.72), appears to have been used in the PIES modeling, but with the equivalent of the full form of S, Eq. (3.63), using a fixed value or range for $l'-l$.

In modeling their angular distributions Khan *et al.* (1991b) used the full form, Eq. (3.67), but employed the approximation (3.74) for $V_{\varepsilon\lambda}$. The corresponding form for $P(\varepsilon)$, Eq. (3.70), yielded spectra nearly completely insensitive to λ, as expected because of the equal and opposite contributions from $l'<l$ and $l'>l$ when integrated over body-fixed electron angle, combined with extensive molecular-axis averaging due to the spiraling dynamics.

In comparing the resulting λ_{max} values obtained from these studies with Eq. (4.1), it becomes apparent that the Penning electron tends to carry away as much angular momentum as is kinematically possible, and other systems, especially involving He^* with a nonbonding partner, may also show significant effects of the coupling. Modulus and phase behavior of the individual $V_{\varepsilon\lambda}$ cannot yet be determined by the available experimental data, but of course such information, obtained through a theoretical investigation, could be readily and sensitively tested. It appears that electron-angle-resolved ion-electron coincidence measurements would be required for an experimental determination in an atom-atom system.

B. $He^*, Ne^* + H_2$

1. Overview of experimental results

Owing to the ease of use of H_2 in a beam or a scattering cell, the experimental results available for Penning ionization of H_2 are quite extensive and more varied than for H, while a solid base of theoretical studies is also at hand, especially for He^*+H_2. The chemistry is also as varied as it can be in a Penning process; for the HD isotope we have the six ion channels

$$He^*(2\,^{1,3}S)+HD \longrightarrow He+HD^+ + e^- \quad (PI) \qquad (4.2a)$$
$$\longrightarrow HeHD^+ + e^- \quad (AI) \qquad (4.2b)$$
$$\longrightarrow HeH^+ + D + e^- \quad (RI) \qquad (4.2c)$$
$$\longrightarrow HeD^+ + H + e^- \quad (RI) \qquad (4.2d)$$
$$\longrightarrow He+H^+ + D + e^- \quad (DI) \qquad (4.2e)$$
$$\longrightarrow He+D^+ + H + e^- \quad (DI)\,. \qquad (4.2f)$$

For $Ne^*(^3P_{0,2})+HD$, channels [(4.2e) and (4.2f)] are energetically closed.

The many beam studies of the He^*+H_2 systems, dating back to the beam/gas-cell measurements of Sholette and Muschlitz (1962), have been amply reviewed by Yencha (1984). Therefore only a few comments will be made on these studies, with the main focus being on the more recent work cited in Tables II and III. The several measurements of Q_I at thermal energy cluster in the range 1–3 Å^2, with the ^1S cross section ~50% larger than ^3S. This is an order of magnitude smaller than He^*+H, reflecting a complete change in the character of V_0 from strongly bonding to weakly repulsive.

Perhaps the most important experiments from the point of view of describing reactions (4.2) by means of a $V_0(\mathbf{r})-i\Gamma(\mathbf{r})/2$ complex potential surface have been *nonreactive* angular distribution measurements (Martin and Siska, 1985, 1988) that do not examine the reaction products at all, but only the decomposition of HeH_2^* back to reagents. These measurements, for kinematic reasons, have been carried out mainly on He^*+D_2 in a collision energy range of 1.0–2.4 kcal/mol, using the same supersonic He^* source as in Khan *et al.* (1991a), a source described more fully in Martin *et al.* (1978), crossed by a supersonic D_2 beam. Figures 10 and 11 display these data. Notable features included the detection of substantial intensity at 180° c.m. for both ^1S and

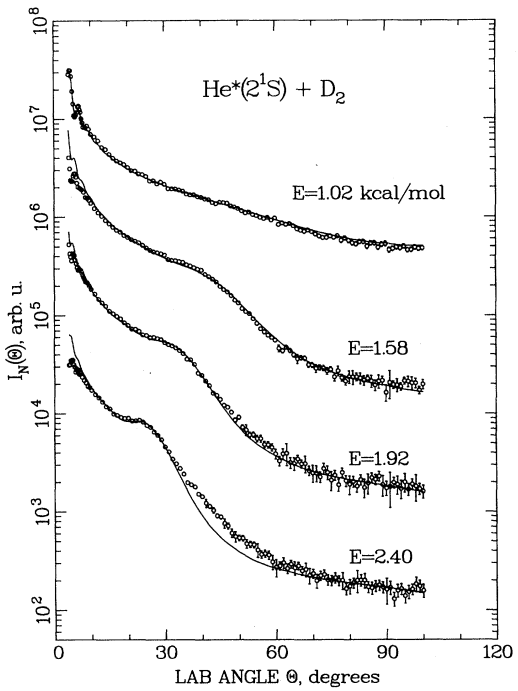

FIG. 10. Nonreactive laboratory angular distributions for the scattering of $He^*(2\,^1S)$ by D_2, experimental data (points) from Martin and Siska (1985), and calculated curves from complex anisotropic potential rigid-rotor close-coupling calculations of Martin and Siska (1988). The intensity units at the highest E reflect total scattered counts at each angle, while the lower energies have been adjusted upward by factors of 10, 50, and 1000 for clarity of presentation. $\Theta=90°$ lab corresponds to $\theta=180°$ c.m.

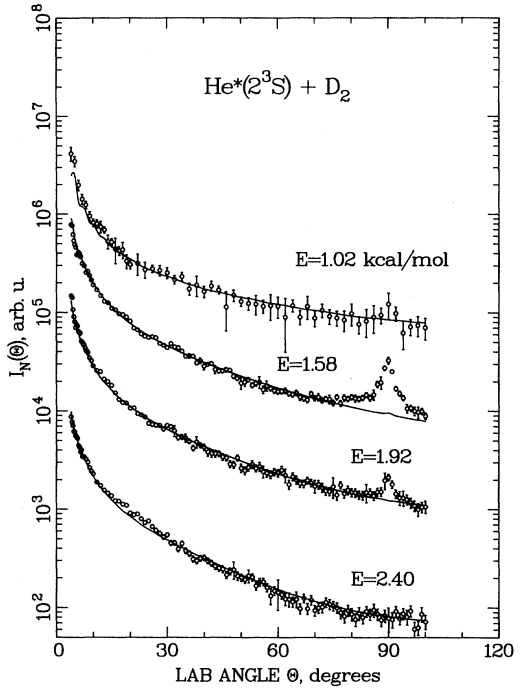

FIG. 11. Nonreactive laboratory angular distributions for the scattering of $He^*(2\,^3S)$ by D_2. The intensity adjustments are identical to those in Fig. 10, except for an additional factor-of-2 increase for the lowest energy.

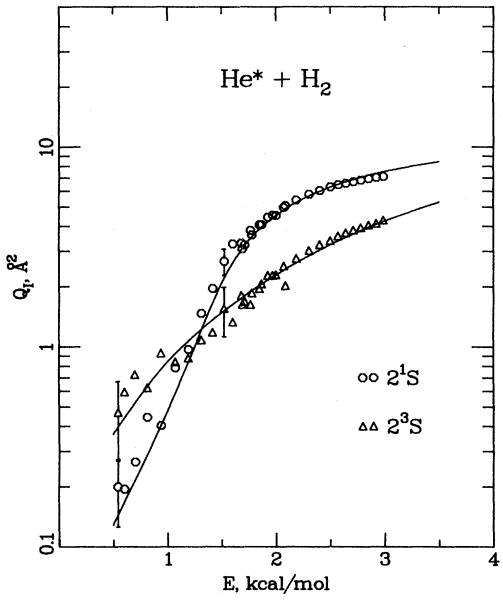

FIG. 12. Total ionization cross sections for $He^* + H_2$, experimental data (points) from Martin *et al.* (1984, 1989), and calculated curves from Martin and Siska (1985, 1988). The experimental measurements are relative, the absolute units being derived from the theoretical curves, which, when integrated over a Maxwellian energy distribution, match the measured total quenching rates at 300 K (Schmeltekopf and Fehsenfeld, 1970).

^3S, with ^3S showing an energy-dependent peak there, and a broad shoulder in the ^1S scattering that shifts to smaller angles with increasing energy in a manner expected for molecular rainbow scattering. Combining these data with quenching rate constants k_Q and using the IOSA followed by an exact close-coupling treatment on a physically motivated complex potential surface model, Martin and Siska (1985, 1988) were able to obtain realistic estimates of $V_0(\mathbf{r})-i\Gamma(\mathbf{r})/2$ for both ^1S and ^3S with H_2. To date these represent the only *molecular* PI potential surfaces determined from experiment, though the situation appears ripe for improvement in the near future, as described in Sec. IV.D. Interpretation of the H_2 data and comparison with theoretical work will be given in the next subsection.

Without any further adjustment, these surfaces were found to fit the total ionization cross-section energy dependence $Q_I(E)$ as measured by Martin *et al.* (1984, 1989) within experimental error, as illustrated in Fig. 12. The ^1S and ^3S $Q_I(E)$ show quite distinct shapes, ^1S rising very rapidly from less than 0.2 Å^2 for $E<0.5$ kcal/mol to 5 Å^2 at $E=1.5$ kcal, and less rapidly thereafter, while ^3S rises more slowly and smoothly from 0.04 Å^2 to 1.6 Å^2 over this same range and continues to rise without much change in slope at higher E. A significant feature of the measurements was the use of crossed supersonic beams with temperature programming, which yielded energy resolution sharp enough to make energy-averaging effects on $Q_I(E)$ negligibly small. The steeply rising $Q_I(E)$ found for ^1S implies that all previous work, which was done with at least one Maxwellian beam or a scattering cell, suffers from substantial distortion due to energy averaging. As an illustration of the effect, at very low energy the energy-resolved ^3S cross section is larger than ^1S, the opposite of the thermally averaged result.

Energy-averaging effects, however, are not generally severe enough to prevent the resolving of product states in PIES. Bregel *et al.* (1989) have recently presented PI electron spectra for pure $He^*(2\,^3S)+H_2$ using a cold-cathode, mildly supersonic He* discharge source and an H_2 gas cell, as well as a mixed $^{1,3}S$ electron spectrum using an effusive H_2 crossed-beam arrangement. The mean collision energy was 1.2 kcal/mol, and great care was taken to reduce the background to very low levels. The spectrum for each spin state, as is well known from earlier work cited in Bregel *et al.* (1989), consists of a progression of H_2^+ vibrational (v') peaks very similar in appearance to that obtained in the He I photoelectron spectrum of H_2. As discussed in Sec. III, each Penning ion internal state may be treated as defining a new reference energy $\varepsilon_0=E_*(\mathrm{Ng}^*)-IE[B(n',v')]$, where n' is the electronic quantum number. The fact that the H_2^+ v' states are cleanly resolved is a result of the narrow PIES lines characteristic of a predominantly repulsive interaction between He* and H_2, consistent with the potential surface results just described. While the widths of the

observed lines are dominated by the effects of analyzer resolution (40 meV here) and averaging over the spread in collision energy, they are all blueshifted ($\varepsilon-\varepsilon_0>0$) by an amount $\varepsilon-\varepsilon_0$ independent of v' but dependent on the spin state of He*, $\varepsilon-\varepsilon_0=74\pm4$ meV (1.71 kcal/mol) for ^1S and 40 ± 4 meV (0.92 kcal) for ^3S. Using single-orientation semiclassical calculations [Eqs. (3.22)–(3.24) and (3.33)–(3.34)] with the classical integration over b replaced by a partial-wave sum, and performing full resolution and energy averaging, Bregel *et al.* (1989) showed that these shifts as well as the slight differences in line shape are predictable from the potentials of Martin and Siska (1985). Line-shape differences between ^1S and ^3S tend to be more marked in Penning ionization of noble gases and will be discussed more thoroughly in Sec. IV.C.

As is usual in many types of spectroscopy, determination of relative *intensities* of spectral features is more difficult than measuring their positions. Nonetheless Bregel *et al.* (1989), through a minor transmission correction of their spectra from photoelectron spectrum calibrations compared with theoretical H_2 photoionization cross sections $Q_{h\nu}(v')$ (O'Neil and Reinhardt, 1978), have given relative vibrational populations $P_1(v')$ and $P_3(v')$ for both ^1S and ^3S PI of H_2. The PIES $P(v')$, the theoretical $Q_{h\nu}(v')$, and the Franck-Condon factors $f_{0v'}$ for $H_2(v=0)\rightarrow H_2^+(v')$ all show a peak at $v'=2$ (due to the increase in bond length, $r_e=0.74$ Å$\rightarrow r_e=1.06$ Å, in ionizing H_2) but differ in detail, particularly in the high-v' limb. The ratio $Q_{h\nu}(v')/f_{0v'}$ is found to increase monotonically from 0.83 to 1.44 for $v'=0-15$, while $P_3(v')/f_{0v'}$ decreases from 1.05 to 0.64 in the same range, where each ratio is normalized to unity at $v'=2$. Surprisingly, Bregel *et al.* (1989) found that $P_1(v')/f_{0v'}$ is nearly constant for $v'=0-10$. However, they did not measure a state-selected ^1S spectrum, and the populations for $v'>2$ were inferred from spectral simulations of strongly overlapped mixed-beam spectra, where ^3S dominated the intensity (a characteristic of the discharge source; see Sec. II.A.1). In recent work in the author's laboratory (Bevsek *et al.*, 1992) state-selected ^1S populations for $v'=0-11$ have been obtained that are similar to the ^3S results of Bregel *et al.* (1989). These experiments, carried out with crossed supersonic beams and rigorous background correction, are described further in Sec. IV.D; see also Dunlavy *et al.* (1990). The general conclusion is that He^*+H_2 Penning ionization produces appreciably less vibrational excitation in H_2^+ than uv photoionization, or even than predicted by the Franck-Condon factors. This result will be discussed further in the next subsection; now we turn to product ion measurements that reflect the overall dynamics of the reaction.

One of the most convincing proofs available for the two-complex mechanism, Eq. (3.1), was given by Münzer and Niehaus (1981) in an ion-electron coincidence (PIECES) experiment on $He^*(2\,^3S)+H_2$. The AI and RI (rearrangement ionization) channels were found to coincide exclusively with electrons that leave H_2^+ in $v'=0$ and $v'\geq4$, respectively. The former is readily interpreted in terms of vibrational predissociation or reaction of nascent associative ions formed from H_2^+ ($v'>0$), and the latter in terms of the energy requirements for the endothermic ion-molecule reaction $He+H_2^+\rightarrow HeH^++H$, $\Delta E=18.58$ kcal/mol.

The coincidence results have been combined with the experimental excited-state optical potentials for $He^*(2\,^{1,3}S)+H_2$ to develop a model for the product branching by Martin *et al.* (1984, 1989), who measured relative cross sections for PI, RI, AI, and DI (dissociative ionization) in state-selected crossed supersonic beams with quadrupole mass analysis of the products, over an energy range of 0.5–4.0 kcal/mol. These data, given in Fig. 13, demonstrated that PI remains the dominant product channel even at very low E, that RI and AI become progressively less important for increasing E, that DI is significantly lower than that from uv photoionization of H_2, and that in the HD reaction deuteron abstraction in RI (HeD^+) is favored over proton abstraction by 1.9:1. The branching fractions Q_{RI}/Q_I, etc., remain remarkably constant for $E\lesssim2.5$ kcal/mol, and the measurements of Martin *et al.* (1989) of these quantities were in good to excellent agreement with earlier measurements where prior data existed. The model (see Sec. III.B.3 and the following subsection) combines line-of-centers, Langevin orbiting, and phase-space theory.

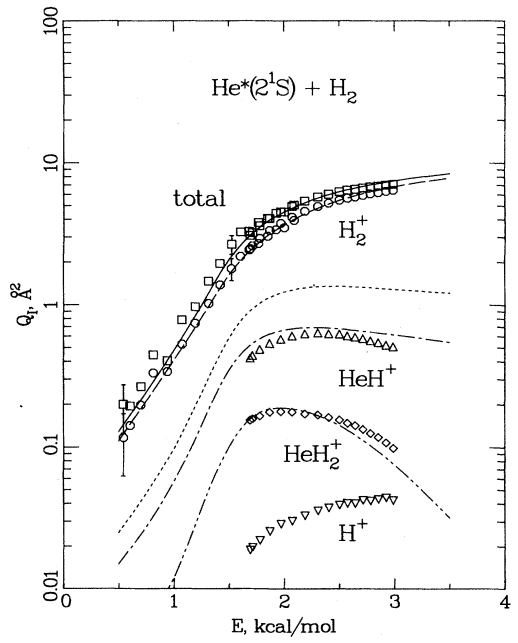

FIG. 13. Energy dependence of product branching for $He^*(2\,^1S)+H_2$ PI, experimental data from Martin *et al.* (1984, 1989), and calculated branching patterns from the modified phase-space model of Martin *et al.* (1989). The short-dashed curve represents the maximum cross section for HeH^+ allowed by the Langevin capture criterion, while the other curves correspond with the experimental data they lie closest to.

Some time ago Leu and Siska (1974b) reported an angular distribution measurement of H_2^+ from $He^*(2\,^1S)+H_2$ in crossed supersonic beams at $E=2.4$ kcal/mol that showed sharply forward scattering. Though no energy analysis of H_2^+ was performed, an approximate transformation to the center-of-mass system yielded an $I(\theta)$ that fall to half-intensity by $\theta=25°$, with very little scattering beyond 90°. The width of the laboratory angular distribution was used to infer a peak c.m. product recoil energy E' of 1.3 kcal. The implied translational energy loss is consistent with the PIES blueshift given above. The merged-beam results of Neynaber *et al.* (1972) on the RI channel of He^*+H_2 (He* a mixed beam containing $\sim 85\%$ ^3S) also showed, as inferred from the shift of the HeH^+ laboratory recoil distribution with respect to the centroid, forward scattering for RI as well, at collision energies above ~ 2 kcal/mol. The strongly forward scattering is somewhat surprising in view of the repulsive excited-state forces; this is also discussed further in Sec. IV.B.3.

As is the case for Ne^*+H, there is much less experimental information available for $Ne^*(^3P_{2,0})+H_2$. Van den Berg *et al.* (1987) have reported J-state-selected total ionization cross sections $Q_I^{(J)}(E)$ using both discharge and hollow-cathode arc Ne* sources to cover a wider energy range (see Table V). This range is substantially smaller for H_2 than for the other, heavier reagents studied, since the lab velocity of H_2 dominates the relative velocity and hence the energy. The experiments spanned the nonoverlapping ranges 1.7–2.0 kcal/mol and 4.6–19 kcal/mol. An absolute calibration of the H_2 beam density-length product yielded Q_I magnitudes that, when extrapolated to lower energy to overlap with earlier measurements, agreed well with them. In the actual range of E covered, the cross sections are quite similar in shape for $J=0$ and 2, increasing by $\sim 30\%$ in the narrow lower-energy range and leveling out in the higher (despite the fitted curves given, which show cross-section maxima); this behavior is similar to $He^*(2\,^1S)+H_2$. The calibration cross sections given at $E=2.3$ kcal are actually interpolated in the H_2 case, with the values of $Q_I^{(0)}=11.8$ Å^2 and $Q_I^{(2)}=7.9$ Å^2, yielding a ratio $R_{02}\equiv Q_I^{(0)}/Q_I^{(2)}$ of 1.48. This ratio appears to approach 1.0 at low energy and to level out at 1.9 at higher energy. Unpublished work on $Q_I(E)$ in the author's laboratory (Pazun *et al.*, 1992), which bridges the gap in energy between the two intervals of van den Berg *et al.*, seems to indicate that the relative normalization of each interval is accurate, though R_{02} is found to be somewhat larger, 2.6(5), at the high-energy limit. Although both experiments employ laser J-state selection, the details of the methods diverge greatly (see Sec. II.A.1).

The similarity between $Ne^*(^3P)$ and $He^*(^3S)$ is also apparent in the earlier H_2 gas-cell PIES study of Bussert *et al.* (1983). Owing to the energetic limitation, $^3P_0$ may populate only H_2^+ ($v'\leq 5$) and $^3P_2$, $v'\leq 4$. As in He^*+H_2, the H_2^+ vibrational peaks are well resolved and blueshifted, indicating a repulsive potential surface, although a substantial background correction had to be applied owing to the confinement of the spectrum to near-zero electron energies ε. The high-efficiency laser state selection employed allowed clean $^3P_0$ and $^3P_2$ spectra to be obtained. Line shapes were skewed toward high ε, due to domination by the Maxwellian spread in E, while vibrational populations were similar to the Franck-Condon factors, but somewhat lower in the higher vibrational states ($v'\geq 3$, close to those in $He^*(2\,^3S)+H_2$. The cross-section ratio obtained was $R_{02}=1.20(12)$ at a mean energy $E=40$ meV, 0.9 kcal/mol, in good agreement for this energy with the work cited above. Aside from R_{02}, little difference was observed between the $J=0$ and $J=2$ electron spectra, in particular in the magnitude of the line shifts (both 50 meV, 1.2 kcal). Quite different results were obtained, as reported in the same work, with laser-excited $Ne^{**}(2p^5 3p\,^3D_3)+H_2$; these will be touched on in Sec. IV.F.

2. Theory and interpretation: the entrance channel

In the minimal molecular-orbital description, H_2 has a closed-shell σ_g^2 configuration, which, by analogy with $M+H_2$, should produce predominantly nonbonded repulsion with He* and Ne*. Rearrangement on the excited surface (to make HeH* or NeH*) is energetically closed by at least 50 kcal/mol. Thus a slightly anisotropic van der Waals potential surface is expected to provide a realistic model for V_0 in Ng^*+H_2; this is in accord with most of the experimental results just cited. Figure 14 presents the experimentally derived potentials of Martin and Siska (1985, 1988). The general properties of these surfaces will be more thoroughly examined in Secs.

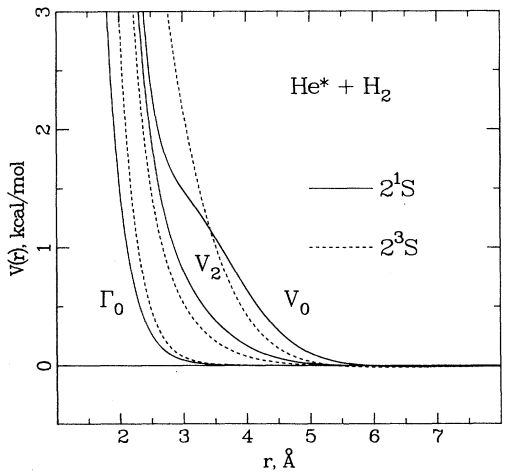

FIG. 14. Comparison of anisotropic optical potentials for $He^*(2\,^{1,3}S)+H_2$ derived from experimental scattering data (Martin and Siska, 1988). The subscripts on V and Γ here refer to radial coefficients in a Legendre expansion of the potential surface.

IV.C and IV.D; for the present discussion, comparisons with *ab initio* results will be highlighted.

Martin and Siska (1985, 1988) give detailed comparisons of their experimental optical potentials for $He^*(2\,^{1,3}S)+H_2$ to the *ab initio* calculations of Cohen and Lane (1977), Hickman *et al.* (1977a), and Isaacson *et al.* (1977). The 1985 comparisons were based on complex-potential infinite-order sudden (CIOS) analysis of the scattering data, but the 1988 complex-potential rotational close-coupling (CPCC) calculations in essence have confirmed and rendered more quantitative the differences between theory and experiment; the more recent comparisons are illustrated in Fig. 15.

None of the theoretical potentials possesses any van der Waals attraction. Among the experimental data cited above (including all those obtained prior to 1980) only the low-energy scattering data of Martin and Siska (1985) for ^1S with D_2 appears to require an attractive van der Waals potential minimum. However, such minima are expected on rather general theoretical grounds, and more substantial evidence of their existence for other closed-shell PI partners is readily available. It is therefore reasonably certain that the lack of long-range minima in the *ab initio* work is a reflection of orbital bases and configuration-interaction expansions insufficiently large to "pick up" the attraction. To be sure, the attractive interaction is quite weak and long range; the well parameters ϵ, r_m given by Martin and Siska (1985, 1988) are 0.0104 kcal, 6.73 Å for ^1S with D_2, and 0.0135 kcal, 6.2 Å for ^3S.

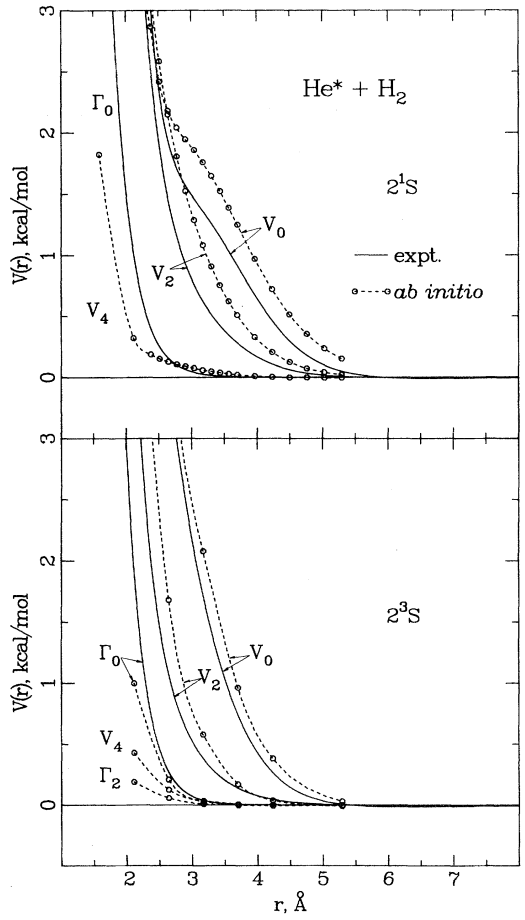

FIG. 15. Comparison of experimental and theoretical potentials for He^*+H_2. As in Fig. 14, the subscripts on V and Γ refer to Legendre coefficients. For ^1S the *ab initio* results are those of Isaacson *et al.* (1977), and for ^3S those of Hickman *et al.* (1977a).

The major deficiency of the *ab initio* potentials, which may be related to their lack of attraction, is that their low-energy repulsions are of too great a radial extent compared to experiment, by amounts ranging from 0.2 Å for the calculations of Hickman *et al.* (1977a) and Isaacson *et al.* (1977) to 0.4 Å for the results of Cohen and Lane (1977). This is a sensible sign and magnitude for the discrepancy, given that there is no competition from dispersion attraction to countervail the more accurately computed overlap (Pauli-principle) repulsion. There is still a potentially sizable uncertainty in the range of the $^3S+H_2$ surface, but reducing this is likely to increase the distance from theory (see Sec. IV.B.3).

Despite these shortcomings, the *ab initio* results are remarkable in their general resemblance to the experimental V_0 for both ^1S and ^3S. The rainbowlike scattering found in ^1S required a local slope maximum in the repulsive wall of the spherical part of $V_0(\mathbf{r})$. Such structure appears in both of the 1977 *ab initio* studies of this system, with that of Isaacson *et al.* being of nearly the same form as required by experiment, but lying at a slightly higher energy (2.0 vs 1.5 kcal). Blame for the discrepancy in energy can again be assigned to the poor theoretical account of dispersion. The form of the ^1S "repulsive rainbows" was found to be quite sensitive to the short-range anisotropy in $V_0(\mathbf{r})$; the anisotropic components of the *ab initio* potentials are nearly the same proportion of the total as given by experiment. No rainbows were observed for ^3S. Correspondingly, the theory yields only a hint of repulsive-wall structure. These areas of agreement suggest that *ab initio* theory, for V_0 at least, has done reasonably well and is, moreover, unlikely to do much better without a massive increase in the scale of the already extensive computations.

Unless the interaction is such as to yield a broad range of r for which ionization is highly probable, experimental constraints on the width are much weaker than on V_0. Martin and Siska (1985) employed a spherical exponential model $\Gamma=\Gamma_0\exp(-\alpha r)$, with the α parameters taken from the calculations of Cohen and Lane (1977) and only Γ_0 determined from experiment. Unlike the situation for V_0, the widths obtained for ^1S and ^3S were nearly identical, indicating little or no role for the radiative mechanism in ^1S Penning ionization. Saturation at small r was not required to fit any of the measurements. The total cross sections do not show a "droop" at high energy that would indicate saturation, and the associative ionization cross sections form a small part of the total

($Q_{AI}/Q_I \approx 0.01-0.04$). Repulsion sets in at such a large r that low-energy collisions cannot easily reach separations where strong attraction between the products $He+H_2^+$ occurs, thereby reducing access to the discrete part of the electron spectrum. Moreover, vibrational predissociation of nascent associative ions, owing to the long H_2^+ vibrational progression and consequent large fraction of vibrationally excited H_2^+ ($>87\%$), converts most of the potentially discrete AI spectrum into a "lumpy" continuum. It may also be that ionization radii are simply too large at thermal energy to probe possible overlap saturation.

Extracting realistic potential estimates from experiment requires, as discussed for Ng*+H, realistic parametric forms for both V_0 and Γ. Such forms, if successful in emulating experiment, can also yield insight into the electronic structure factors critical in determining the details of the interaction. A favorite of the author (Martin *et al.*, 1978) is one that exploits the Rydberg-like "peel-core" structure of the metastable atom, viz.,

$$V_0(\mathbf{r})=[1-f(\mathbf{r})]V_c(\mathbf{r})+f(\mathbf{r})V_*(\mathbf{r}) . \quad (4.3)$$

$V_c(\mathbf{r})$ is the interaction of the core ion with the partner ($He^+ + H_2$), $V_*(\mathbf{r})$ is the long-range interaction, dominated by dispersion and overlap repulsion involving the promoted electron, and $f(\mathbf{r})$ is a switchover function, approaching unity at large r and zero at small. As one ascends the Rydberg ladder from the metastable noble gas to its core ion, $V_c(\mathbf{r})$ remains relatively unperturbed, and only $f(\mathbf{r})$ and $V_*(\mathbf{r})$ change, becoming longer range and weaker.

What is known about alkali interactions might lead one to expect that for our systems $f(\mathbf{r})$ does not differ appreciably from unity in the interesting domain of r (>2.5 Å); however, this appears not to be the case, especially for He*. One-electron calculations (Siska, 1979b), supported by *ab initio* results (Guberman and Goddard, 1975), show that the He* $2s$ orbital hybridizes, forming roughly an $sp^{0.5}$ antibonding hybrid when brought near a closed-shell reagent. This occurs to a greater extent for He* than for Li owing to the substantially smaller $2s$-$2p$ splitting in He* (0.6 eV in ^1S, 1.1 eV in ^3S, compared to 1.8 eV in Li). The antibonding hybridization causes exposure of the core ion and a consequently appreciable influence of V_c on the low-energy repulsion in V_0, as reflected in a decline in $f(\mathbf{r})$ at small r and a concomitant softening of the repulsion.

In He*($2\,^1S$) systems, where hybridization is most complete, V_c leaves its imprint on V_0 in the form of a "shelf" or "kink" in the repulsive wall, which occurs at a distance $r \sim 3$ Å corresponding closely in known cases to the inflection point on the outer attractive limb of V_c. There is solid experimental evidence for the kinky ^1S potentials, some of which has already been introduced in the previous subsection and more of which will be discussed in Secs. IV.C and IV.D. The phenomenon can be regarded as an early onset of Rydberg behavior, where V_c dominates the short-range interaction, and is a more plausible explanation, in the author's view, for the peculiar V_0's than curve-crossing or ion-pair postulates.

As described further below, Martin and Siska (1985, 1988) dealt with the anisotropy of the He^*+H_2 interaction by concentrating it in V_c and V_*, allowing $f(r)$ to remain a radial function, and employing the known long-range forms of the dispersion (V_*) and induction (V_c) potentials, along with the ion-quadrupole interaction, which enters only in the anisotropic part of V_c. H_2 has a positive quadrupole moment, meaning that the negative charge is concentrated in the bond region. One-electron calculations (Martin and Siska, 1985) show that the negative charge causes increased hybridization and consequent ion-core attraction for T-shaped (C_{2v}) geometry. This attraction is already maximized for a positive quadrupole in this geometry. This produces a kink near $\gamma=90°$ in $V_0(r,\gamma)$ and, apparently, nearly an order-of-magnitude greater reactivity for $He^*(2\,^1S)+H_2$ in this geometry at collision energies near and above the energy of the kink (>1.6 kcal/mol), relative to end-on approach. Because $\gamma=90°$ is the most likely collision geometry due to the $\sin\gamma$ solid-angle weighting factor, a repulsive rainbow survives angle averaging to appear in the differential nonreactive scattering distributions (Martin and Siska, 1985), as described in the previous subsection (see Fig. 10). He*($2\,^3S$), hybridizing less, shows only a slight undulation in the slope of its repulsion from H_2 for $\gamma=90°$, and consequently only a slight preference for broadside ionization. Although the wide-angle scattering for ^3S is not completely smooth in its falloff with increasing angle (Fig. 11), nothing resembling the ^1S rainbow is apparent. As discussed at greater length in Secs. IV.C and IV.D, these differences in the repulsive behavior of the two spin states of He* appear to be characteristic of their interactions with all closed-shell reaction partners.

This disparity in the repulsion between ^1S and ^3S produces a readily identifiable signature in $Q_I(E)$. The ^1S kink at 1.5 kcal/mol implies that at energies just above this value the reagents can now penetrate to considerably smaller r (for $b=0$, $r_0=3.5$ Å at $E=1.0$ kcal, shrinking to $r_0=2.6$ Å for $E=2.0$). Provided the width is smoothly increasing as r decreases, deeper penetration will likely produce PI saturation, $P_I(b)\rightarrow 1$, as E increases further, causing $Q_I(E)$ to level out. Calculations for H_2 as well as noble-gas partners show that the bendover energy is very close to the potential energy of the repulsive structure. The smooth, unstructured rise in $Q_I(E)$ as E increases for ^3S betrays the lack of structure in V_0 in this case. Saturation still occurs at sufficiently high E, but sets in much more gradually. For modeling purposes, the behavior of V_0 in particular must be precisely tunable to emulate the observed cross-section behavior.

Piecewise potentials, constrained by the form of their components to behave properly at both short and long range, have been widely used in modeling nonbonded interactions as a means of replacing the ubiquitous Lennard-Jones potential. Martin and Siska (1988), how-

ever, introduced single analytic functions for V_* and V_c based on a modification (Siska, 1986) of the model of Tang and Toennies (1984), in which damping functions are used to turn off the long-range r^{-6} etc. dispersion interaction in favor of short-range exponentials. For H_2, V_*, and V_c were approximated by two-term Legendre expansions, $v_0(r)+v_2(r)P_2(\cos\gamma)$. These include all the leading terms in the long-range interaction. Because the Tang-Toennies model is a sum of attractive and repulsive terms, separate anisotropies could be assigned to each, and theoretical values used for the attraction. Among several free parameters in V_0 only the short-range anisotropy and the switchover function had a substantial influence over the shape of the computed scattering angle distributions.

As mentioned earlier, a spherical, simple exponential width function proved to be adequate for the purpose of modeling the scattering and quenching of He* by H_2. Selection of a spherical function was based on trial calculations using both *ab initio* and empirical V_0's, together with *ab initio* estimates of the width anisotropy (see Fig. 15), which yielded $\Gamma_2 < 0.15\Gamma_0$ (subscripts denoting Legendre expansion coefficients). These calculations showed $<1\%$ effect of Γ_2 on the wide-angle nonreactive scattering, and less than that on the ionization cross section and rate constant.

Close-coupling calculations (Martin and Siska, 1988), on the other hand, revealed an appreciable effect of the initial rotational state j of H_2 on the magnitude of Q_I that correlates with the anisotropy in V_0. The ^1S Q_I declines by $>20\%$ as j goes from 0 to 3 at energies above that of the kink in V_0, while for ^3S the change is less than 5% at any E. This phenomenon may provide a nontunneling scenario for the apparent 20% isotope effect in the total quenching rate (Schmeltekopf and Fehsenfeld, 1970) favoring H_2 over D_2: D_2 has a larger probability at a given temperature of possessing nonzero j, for which the cross section is lower. The rate measurements, however, show an isotope effect independent of the spin state of He*, while the calculations predict an isotopic rate ratio for ^3S (1.03) too small to be reliably measured. The calculated result must arise from anisotropy averaging due to rotational motion; the strong 90° preference of ^1S is averaged away, while the more isotropic ^3S surface is relatively unaffected.

A feature of the differential cross section for ^3S not yet clarified by calculation is the appearance of an energy-dependent backscattering maximum (see Fig. 11). In this case the estimated van der Waals well depth, 0.0135 kcal/mol, is too small to allow trapping of the HeH_2* complex in a rotational resonance, and the imputed opacity function is too slowly varying with b to yield edge effects in the scattering. The close-coupling calculations do show slight structure near $\theta = 180°$ for $j=0$, but this does not survive energy averaging.

Owing mainly to the lack of angle-resolved nonreactive scattering data, there is as yet no experimentally derived estimate of the optical potential for $Ne^*(^3P_{0,2})+H_2$. The most detailed analysis to date has been that given by van den Berg *et al.* (1987), who modeled their total ionization cross-section energy dependence measurements with spherical optical potentials. V_0 was taken from the C_{2v} geometry of an *ab initio* calculation of the $Na+H_2$ ground-state potential surface by Botschwina *et al.* (1981), while Γ was given a "clipped" exponential form, being set equal to a constant inside $r=2.8$ Å. Separate exponential Γ parameters were assigned for $^3P_0$ and $^3P_2$, with the $J=0$ width being three times larger at $r=2.8$ Å and more steeply falling with increasing r, consistent with the observed differences in $Q_I^{(J)}(E)$. The clipping (abrupt saturation) was found necessary to reproduce the flattening of the cross section at higher energy, for the given, smoothly repulsive V_0. Were V_0 to possess structure similar to that in $He^*(2\,^1S)+H_2$, however, a similar $Q_I(E)$ would result without the need to clip Γ. Within the peel-core model Eq. (4.3), this would require a dramatic difference between $Na^+ + H_2$ and $Ne^+ + H_2$ ion-molecule interactions, as the valence properties of Ne* and Na are more nearly alike than are He* and Li, and the extent of hybridization of the Ne* 3*s* orbital is therefore substantially less.

Whether or not V_0 has a peculiar shape, this sort of modeling does not address the *origins* of the differences in cross-section magnitude and energy dependence between the $J=0$ and 2 states of Ne*. This problem will be discussed more fully in Sec. IV.C.2; for now we state only that these fine-structure reactivity differences, which occur quite generally, remain anomalous.

It seems reasonably certain that the purely repulsive $Ne^* + H_2$ potential of van den Berg *et al.* (1987) would also give a good account of the narrow, blueshifted PIES vibronic lines of Bussert *et al.* (1983).

3. Postionization dynamics and product branching

A major factor determining branching into the PI, AI, RI,and DI channels of Eq. (4.2), particularly as shown by coincidence experiments, is the $P(v')$ distribution in H_2^+. The fact that in $He^* + H_2$ $P(v')$ is skewed toward lower vibrational states for both ^3S and ^1S Penning ionization compared to either Franck-Condon factors $f_{0v'}$ or photoionization cross sections $Q_{h\nu}(v')$ may be a result of the H_2 bond-length dependence of the complex potential-energy surface. In a semiclassical picture $v'<2$ results from stretched H_2 and $v'>2$ from compressed H_2. Based on the constancy of the PI electron spectral line shift ε-ε_0 over the vibrational manifold, it might be concluded that the bond-length dependence of Γ is the deciding factor, with Γ increasing as the H_2 bond is stretched.

As described in Sec. III.C.3, Martin *et al.* (1984, 1989) have employed a spherical-potential model based on the two-step mechanism (3.1) that shows encouraging agreement for the most part with their energy-dependent branching data, as illustrated in Fig. 13 for

$He^*(2\,^1S)+H_2$. The model combines an assumption of ionization at the maximum in the product $\Gamma(r)|\psi_i^0(r)|^2$ (just outside the classical turning point) for motion on V_0, the Langevin criterion for forming a long-lived molecular-ion HeH_2^+ complex, and phase-space theory for partitioning decay of the complex into the PI or RI channels. Within the model, associative ionization results only when the internal energy of the complex lies below all channel asymptotes. Exact quantum counting of product states, proper consideration of product centrifugal barriers (neglecting tunneling), and parity conservation in the homonuclear PI channels (H_2^+ or D_2^+, but not HD^+) were incorporated into the calculation of branching fractions. Necessary input included $P(v')$, which in this case was taken from Münzer and Niehaus (1981), whose populations agree well with the more recent work of Bregel *et al.* (1989). The recent measurements of Bevsek *et al.* (1992) confirm an assumption made in the modeling that the $P(v')$ are similar for ^1S and ^3S.

The model did require one modification before RI branching was well represented, the difficulty stemming from a mysteriously low estimate of the $He+H_2^+$ ion-molecule reaction cross section by phase-space theory (Light, 1967). When the total energy is high (in our case due to vibrational excitation), conservation of angular momentum places very little constraint on product rotation, with the majority of states in the PI channel having j' antiparallel to l'. Normally such coupling occurs only when the potential surface is highly repulsive for the complex dissociation channel considered (Hijazi and Polanyi, 1975). The HeH_2^+ surface, however, is highly attractive (McLaughlin and Thompson, 1979), implying that such angular momentum combinations are unphysical. Eliminating these combinations for the PI channel, i.e., choosing only those states in which j' and l' both point in the "northern" hemisphere with **J** as north pole, brought rearrangement ionization into greatly improved agreement with experiment. (This limitation on angular momentum phase space was dubbed the "slingshot model" and might apply in other cases with a purely attractive channel, e.g., $Ar^+ + N_2$ charge transfer.)

While representing the entire set of ^1S branching data, including the isotope effect favoring HeD^+ over HeH^+ by 1.9:1, the model still underestimated the amount of rearrangement ionization for ^3S by 20–25 %, and associative ionization by 60–90 %. These discrepancies may indicate that the experimental ^3S complex potential, whose major uncertainty is in its range, might need to be shifted toward smaller r, in a direction away from current theory. Unpublished work in the author's laboratory (Falcetta and Siska, 1992) confirms this expectation. This would allow a greater fraction of ionizing transitions to occur in a more strongly attractive region of the $He+H_2^+$ potential.

In view of the almost purely repulsive V_0's that obtain for He^*+H_2, the strongly forward scattering observed for H_2^+—representing >90% of the reaction flux at all E—might seem enigmatic. However, model calculations the author has carried out on atom-atom systems with potentials similar to the spherical parts of those for He^*+H_2 and $He+H_2^+$ show that peaked forward scattering, arising from a forward glory effect in these two-body-like systems, is found for a substantial range of repulsive V_0's, provided the product interaction V_c has a shorter range than V_0 along with the appropriate long-range inductive attraction. V_0 holds the reagents apart during the ionizing transition, and the transition itself bursts the He^* "balloon" to reveal a much smaller ground-state He, interacting attractively with the Penning ion. The attractive V_c then swings the products past each other, yielding the usual geometric $(\sin\theta)^{-1}$ enhancement for those products that undergo zero net deflection. The lack of appreciable backscattering may be understood in terms of the small impact-parameter flux's being captured into the ionic complex, with much of it converted to other channels.

C. He^*, Ne^* + Ar

1. Experimental results

As might be expected based on considerations of feasibility and simplicity, the $He^*(2\,^{1,3}S)+Ar$ systems have been bellwethers for both experimental and theoretical studies of Penning ionization. The era of molecular-beam studies on these systems was ushered in by Sholette and Muschlitz (1962) with Q_I measurements, as well as by the total scattering cross-section experiments of Rothe *et al.* (1965), and has been thoroughly reviewed by Haberland *et al.* (1981) and by Yencha (1984). Again we shall focus on more recent developments referred to in Table II, with only an eclectic overview of earlier work.

A remarkable consensus has emerged with respect to the magnitude of Q_I, the values being 25 Å^2 for ^1S and 8 Å^2 for ^3S at a reference energy $E=1.75$ kcal/mol; the factor-of-three favoring ^1S is also reflected in the total quenching rate constants at 300 K. A definitive, high-resolution spin-state-selected measurement of $Q_I(E)$ and $Q(v)$ for both ^1S and ^3S in the E range 0.05–5.0 kcal/mol by Burdenski *et al.* (1981) shows, in agreement with less complete earlier work, differences in $Q_I(E)$ between ^1S and ^3S similar to those found for H_2: for ^1S, steeply rising with increasing E followed by flattening out beyond $E=2$ kcal, while for ^3S, a more gradual, unbroken rise. In addition, Burdenski *et al.* find cross-section minima at very low E (0.16 kcal for ^1S, 0.21 for ^3S).

As in the H_2 systems, the major impact on the excited-state optical potentials for He^*+Ar is due to nonreactive angular distribution measurements. Yencha (1984) gives a complete bibliography, while experimental details are discussed by Haberland *et al.* (1981). "Final" results for $V_0(r)$ and $\Gamma(r)$ are given for ^1S by Martin *et al.* (1978), for ^3S by Siska (1979a), and for a revised ^1S by Brutschy *et al.* (1982). The potentials were deter-

mined mainly by closely fitting highly resolved nonreactive scattering angular distributions extending to wide angles over a wide range of E, measured in crossed supersonic beams. Figure 16 shows a comparison of ^1S and ^3S scattering at a single energy, while Fig. 17 illustrates the strong energy dependence of the scattering for ^1S (Martin *et al.*, 1978; Siska, 1979a). Unlike the data for H_2, the angular data show entire series of regularly spaced "quantum" oscillations at small angles, followed for ^1S by a broad but well-resolved intensity maximum and very low wide-angle scattering, but for ^3S by a smoothly declining intensity at wide angles, substantially higher relative to the small-angle scattering than for ^1S (Fig. 16). The ^1S maximum, almost certainly a "repulsive rainbow," shows a threshold at $E=0.6$ kcal/mol, below which energy the scattering at wide angles is smooth and similar to that for ^3S.

The resulting ^1S and ^3S V_0's for Ar show differences similar to those in the (spherical parts of the) H_2 potentials, but more pronounced, as shown in Fig. 18. The ^1S V_0 has a sharp kink, which may even be a small barrier-well oscillation, in its repulsive wall at $r=3.2$ Å, $V_0=0.60$ kcal/mol, while ^3S possesses a much smoother overlap repulsion. The van der Waals wells were found to be considerably deeper and shorter range for Ar than for H_2, 0.098 kcal/mol at 5.67 Å for ^1S and 0.118 kcal at 5.17 Å for ^3S, as required by the extensive small-angle structure. In these cases, the close fitting of the quantum oscillation frequency yielded accurate estimates of the range of V_0 for both spin states. As with the results for H_2, Γ for ^1S and ^3S was found to have nearly identical r dependence.

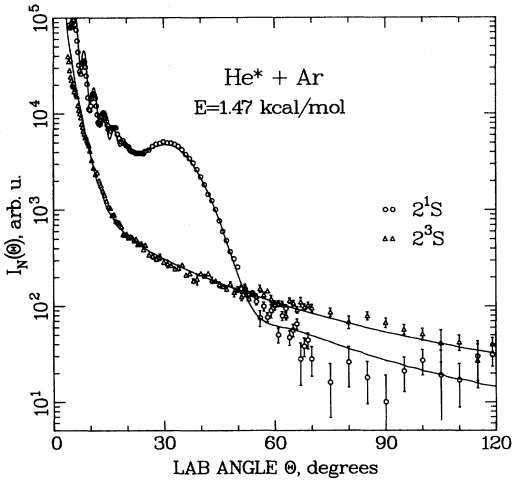

FIG. 16. Comparison of nonreactive laboratory scattering angular distributions of spin-state-selected He* by Ar (Martin *et al.*, 1978; Siska, 1979a), experimental points, and calculated optical-model fits. The intensity units are total scattered counts observed in a given scan, and the relative intensities are as measured, reflecting beam populations and relative cross sections. Under any conditions, extraction of reliable ^1S data at wide angles is difficult.

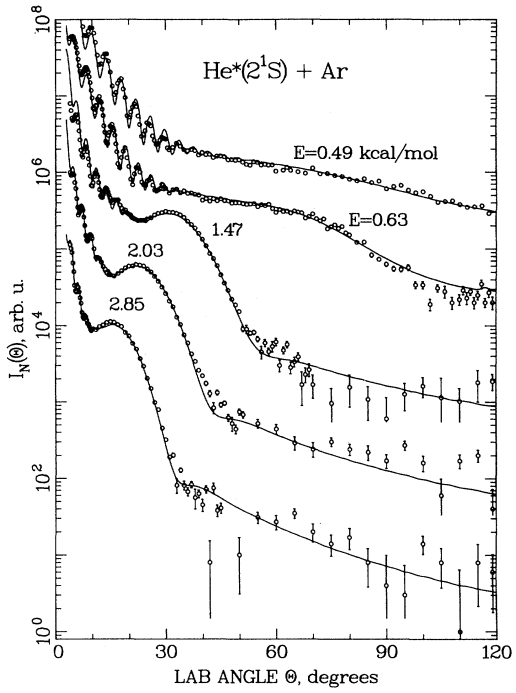

FIG. 17. Energy dependence of the nonreactive laboratory-system scattering of He*($2\,^1S$) by Ar (Martin *et al.*, 1978). As in Fig. 10, the intensities are adjusted for clarity of presentation. The curves are calculated from an optical potential.

It was for these systems that the peel-core model, Eq. (4.3), was first formulated, while the width was assumed to be purely exponential. The uniqueness of the derived potentials was improved by using the same V_c for both ^1S and ^3S. The author believes, however, that the last chapter on the determination of these potentials, particu-

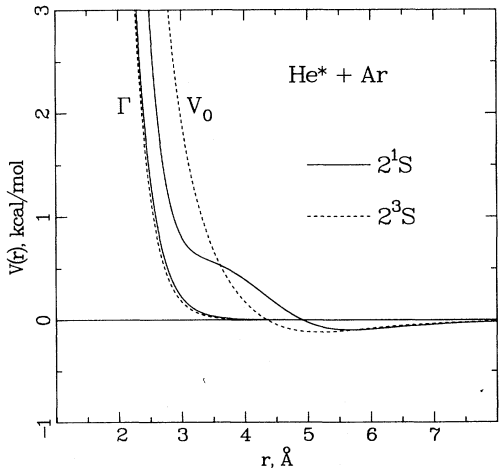

FIG. 18. Comparison of He*($2\,^{1,3}S$)+Ar optical potentials derived from fitting scattering data (Martin *et al.*, 1978; Siska, 1979a). The similarity to the He*+H_2 potentials of Fig. 14 is noteworthy. Brutschy *et al.* (1982) have derived a ^1S V_0 with sharper repulsive structure.

larly that for ^1S, is yet to be written, as insufficient attention has been given to incorporating other properties into the fitting procedure. For example, Burdenski *et al.* (1981) have modified the ^1S potential of Martin *et al.* (1978) by clipping the width at $r=3.14$ Å, $\Gamma=0.23$ kcal to accommodate a slight droop in $Q_I(E)$ beyond $E=2$ kcal/mol. This modification, however, is probably not consistent with the observed wide-angle scattering. In addition, the ^1S Q_I and quenching rate constants calculated from the optical potential of Martin *et al.* (1978), while within experimental error bounds, are each 20–25 % lower than the experimental results. For ^3S, Burdenski *et al.* also modified Γ by introducing a weak, diffuse exponential tail to improve the fit to their $Q_I(E)$ at low E.

The more recent experiments cited in Table II have not altered the situation with respect to the potentials in the thermal energy range, although superthermal experiments on $Q_I(E)$ by Kroon *et al.* (1986) and PI neutral-ion coincidence measurements by Gillen *et al.* (1986) have suggested that the ^3S resonance width must also saturate at small r. Kroon *et al.* employed a clipped Γ, as Burdenski *et al.* (1981) did for ^1S, but with a considerably smaller clipping radius of 2.27 Å, where $\Gamma=1.6$ kcal/mol; they also used a V_0 with a somewhat more steeply rising repulsion above 2 kcal, corresponding to $r\leq 2.9$ Å. These modifications are a response to the flat $Q_I(E)$ found for the superthermal He* source. However, as in Ne^*+H_2, the two energy ranges probed (1.0–5.5 kcal and 14–110 kcal) are nonoverlapping, and require separate normalization. The ^3S potential of Siska (1979a) also shows leveling followed by a decline at high energy, though with a magnitude 15% higher than the normalized experimental data. The results of Gillen *et al.* (1986) (in the energy range 100–1000 eV) have not yet been analyzed quantitatively. At these high energies, well above the threshold for exciting He* to higher states, which may also undergo Penning ionization, one may question the use of a single complex potential to interpret the scattering and hence any conclusions drawn concerning width saturation.

PIES experiments on He^*+Ar were among the first to be reported. The most recent published work is that of Hotop (1980), who also reviewed earlier work. The PI electron spectrum for each spin state consists of only two peaks, corresponding to formation of Ar^+ ($3p^5\,^2P_{3/2},^2P_{1/2}$). The fine-structure states are split by 1432 cm^{-1} (177 meV, 4.1 kcal) and are easily resolved. In addition, since the ^1S-^3S splitting is 0.796 eV, the two sets of peaks from a mixed He* beam are well separated and no state selection is necessary. Taken with a Maxwellian He* discharge source, an Ar scattering gas cell, and a 127° cylindrical electron energy analyzer of 18 meV resolution, Hotop's spectra show significant differences between ^3S and ^1S in both the width of the peaks and their shifts ε-ε_0, in agreement with earlier lower-resolution studies. At $E=1.4$ kcal (59 meV) for ^3S, a positive 0.9-kcal (40-meV) shift and 2.1-kcal (90-meV) linewidth were found for each fine-structure state, while ^1S under similar conditions yielded a 1.0-kcal (45-meV) shift and 0.9-kcal (40-meV) width. Measurements of the energy dependence of the ^3S spectrum by velocity-selecting the He* beam showed monotonically increasing shift and linewidth, to 2.0 kcal and 3.1 kcal, respectively, at $E=3.9$ kcal, while a similar increase in the (mean) energy of ^1S produced an increase in the shift of only 0.03 kcal and in the linewidth of only 0.2 kcal. The spin-state differences in linewidth are considerably greater than those for H_2, while at low energy the shifts are more nearly equal, although the energy dependence of these quantities has not yet been reported for H_2. Full quantum modeling is needed for a quantitative evaluation of these data, but the observations appear consistent with the spin-state differences in V_0 for Ar from nonreactive scattering. In recent supersonic beam experiments in the author's laboratory (Bevsek *et al.*, 1992), given in Fig. 19, comparably narrow ^1S PIES features have been measured, despite somewhat poorer analyzer resolution, underscoring the importance of the velocity spread in determining linewidths for these nonbonded systems.

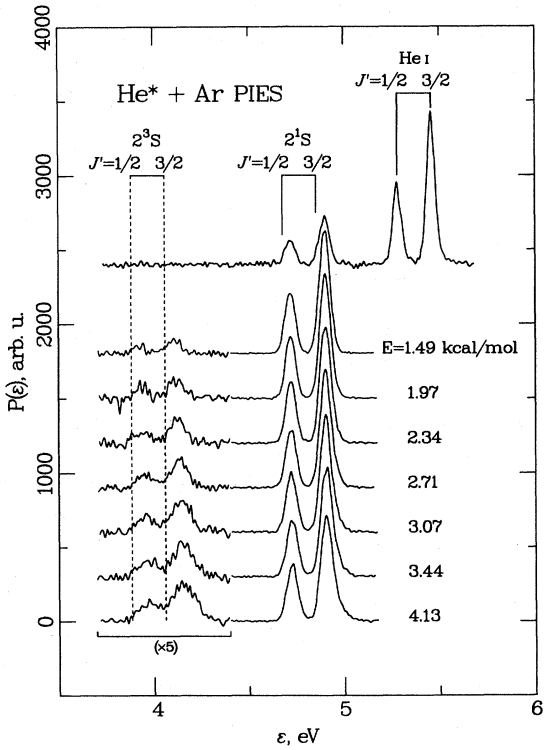

FIG. 19. Energy dependence of electron spectra from He^*+Ar PI (Bevsek *et al.*, 1992). The uppermost spectrum is a simultaneous PI electron/photoelectron measurement used for calibration of the energy scale; the J' values refer to the final Ar^+ fine-structure state. The remaining PI electron spectra are normalized to the same area under the $J'=\frac{3}{2}$ peak; base lines are shifted for clarity of viewing. The variations in intensity and line position with energy for ^3S are noteworthy; the fine structure in these data is noise, due to a low counting rate.

As indicated in Table II, several measurements of Penning electron angular distributions $P(\theta_\varepsilon)$ for He^*+Ar have been reported recently, following the earlier work of Ebding and Niehaus (1974), with which the newer results are in good agreement. Again there is a pronounced difference between ^3S and ^1S, with $P(\theta_\varepsilon)$ peaking more strongly backward for ^3S, $P(150°)/P(30°)\approx 3$, than for ^1S, where this ratio is <1.5. Both results are unlike photoionization, for which symmetry about 90° is rigorously expected, and is observed in the same apparatus.

The PI electron spectra also yield the Ar^+ fine-structure branching ratio $R'_{3/2,1,2}\equiv Q_I(J'=\frac{3}{2})/Q_I(J'=\frac{1}{2})$. In agreement with earlier work, Hotop (1980) finds this ratio for both ^1S and ^3S to be slightly greater than 2, 2.10(2) at $E=1.4$ kcal, and slowly rising with E. An interpretation of this ratio will be given in the next subsection, but it leads naturally to a discussion of results for AI branching, owing to the more attractive potential correlating with the $\frac{3}{2}$ ion state, which produces a slightly broader PIES line for $\frac{3}{2}$. The AI/PI partitioning can be estimated from the line-shape areas of the electron energy spectrum lying to the high and low sides of $\varepsilon=\varepsilon_0+\bar{E}$, but can be greatly in error for narrow lines and broad E distributions. Owing to the Maxwellian tailing of the line to high ε, AI is generally overestimated from PIES. AI/PI can vary strongly with E; thus direct mass spectral measurements are more readily interpreted if done under sub-Maxwellian conditions. The supersonic crossed-beam determination of Chen *et al.* (1974) yields $Q_{AI}/Q_I=0.136$ at $E=1.5$ kcal, falling to 0.021 at 5.1 kcal. The author has carried out model calculations showing that at slightly above thermal energy the $^2P_{3/2}$ state begins to dominate the AI channel. Further PIES studies with better-resolved E may be able to test this prediction, while PIECES $HeAr^+/e^-$ experiments may probe the preference directly.

The overall heavy-particle dynamics of the PI channel, as in He^*+H_2, is reflected in forward-hemisphere Ar^+ scattering for ^1S that becomes more sharply forward as E increases, as demonstrated by the angle-resolved experiments of Leu and Siska (1974a). At low E the peak position of the c.m. angular distribution appears to be slightly away from forward, but this conclusion is based on an approximate lab→c.m. transformation. Doubly-differential PI angle-energy distribution (PIAED) measurements are needed to confirm this; if it is correct, rainbow scattering from the kink in V_0 may be its cause. Such measurements are in progress in the author's laboratory (Longley *et al.*, 1992). Using resonance-lamp state selection, Longley *et al.* have also observed forward scattering in ^3S. A preliminary angle-velocity contour map for ^1S at $E=4.1$ kcal/mol is shown in Fig. 20. These measurements are intrinsically unable to distinguish the Ar^+ fine-structure components, but this might be done in ion-angle-resolved PIECES experiments. A translational energy loss is also inferred from these data that agrees well with the observed PIES line shifts.

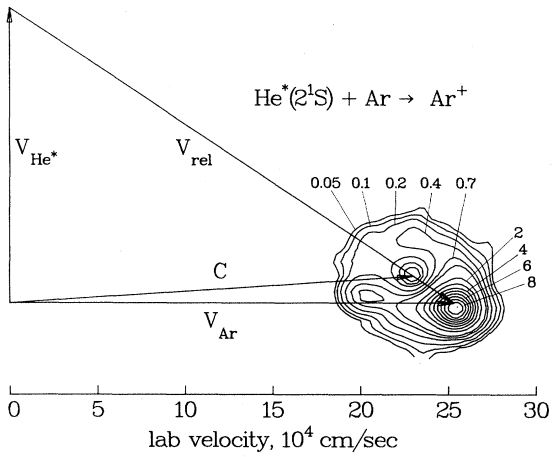

FIG. 20. Velocity-space c.m. Ar^+ intensity contour map for $He^*(2\,^1S)+Ar$ at $E=4.2$ kcal/mol (Longley *et al.*, 1992). The map is arbitrarily normalized to 10 at the peak. Strong forward scattering is indicated, with $E'\approx E$ and moderate coupling between E' and θ.

Studies of the familial He^*+Kr, Xe systems have improved our understanding of the nature of the excited-state forces by showing how they vary with noble-gas reagent and further reinforcing the alkali analogy. Recent state-selected $Q_I(E)$ studies (see Table II) illustrate the effects of the deepening van der Waals well with increasing noble-gas size, showing in the case of ^1S a reversal of slope from positive to negative in the intermediate range of energy and a substantially flatter dependence for ^3S+Kr and Xe Penning ionization. The Penning electron angular distributions of Ebding and Niehaus (1974) correspondingly show a dramatic onset of isotropy in ^1S+Kr, Xe, but a continued backscattering preference for ^3S. The best estimates of potential curves have again come from nonreactive scattering measurements; Table X collects the van der Waals well characteristics for He^* and Ne^* with the noble gases, including He^*+Ne, as well as for the H_2 and N_2 systems discussed in detail here. In addition to the trends displayed there, the ^1S potentials also show a decrease in the energy of the repulsive kink with increasing noble-gas size, until for Xe it appears very close to the zero-crossing radius.

Büermann *et al.* (1987) have carried out extensive cross-section calculations for $He^*(2\,^1S)+Xe$ that indicate, as Burdenski *et al.* (1981) had found for Ar, that the ^1S width saturates at small r. To fit their $Q_I(E)$ above $E\sim 2$ kcal, Büermann *et al.* were obliged to employ a sharply peaked $\Gamma(r)$ (0.21 kcal at 3.5 Å) rather than simply clipping the width, while to fit the higher-energy $Q_I(E)$ of Illenberger and Niehaus (1975) as well required that Γ increase again at still smaller r.

In contrast to He^*+Ar, many of the extant Ne^*+Ar molecular-beam studies are of more recent vintage, as given in Table III. Earlier mixed-beam $Ne^*(^3P_{0,2})$ mea-

TABLE X. van der Waals well depths (cal/mol) and positions (Å) for He* and Ne*.[a]

Metastable noble gas	Ne	Ar	Kr	Xe	H_2	N_2
$He^*(2\,^1S)$	9.6(5)[b]	98(6)[c]	158(10)[c]	252(10)[c]	9.6(4)[d]	48(4)[e]
	6.46(5)	5.67(4)	5.69(4)	5.69(4)	6.73(6)	6.63(4)
$He^*(2\,^3S)$	19.8(10)[f]	118(14)[g]	175[h]	267[i]	13.5(40)[d]	73(8)[e]
	6.01(15)	5.17(12)	5.18	5.33	6.2(2)	6.1(1)
$Ne^*(^3P)$		125(10)[j]	196(10)[j]	294(10)[j]		82[k]
		5.0(1)	5.0(1)	5.0(1)		5.4

[a]In each case the top entry is the well depth and the bottom the position. Numbers in parentheses are uncertainties in the least significant digit(s).
[b]Martin, Fukuyama, and Siska (1990).
[c]Martin, Gregor, *et al.* (1978); Burdenski *et al.* (1981); Brutschy *et al.* (1982).
[d]Martin and Siska (1985, 1988).
[e]Sperlein (1986).
[f]Fukuyama and Siska (1989).
[g]Siska (1979a); Burdenski *et al.* (1981).
[h]Rothe *et al.* (1965); Parr *et al.* (1982).
[i]Büermann *et al.* (1987).
[j]Gregor and Siska (1981); Kerstel *et al.* (1988).
[k]Kerstel *et al.* (1988); Baudon *et al.* (1991).

surements of $Q_I(E)$ have now been supplemented with state-selected and/or mass-analyzed Q_I data; in addition, the experiments of Verheijen and Beijerinck (1986; see also van den Berg *et al.*, 1987) and Weiser and Siska (1986) have employed supersonic Ar beams, instead of effusive beams or scattering cells as still used in other laboratories, thereby preserving a narrow energy spread even at low Ne* velocities. (The configuration of the Ar scatterers is a more important energy-resolution factor for Ne* than for He*, owing to the loss of the 10:1 mass advantage.) Substantial discrepancies in magnitude and appreciable differences in energy dependence of Q_I present in earlier data (Tang *et al.*, 1972; Neynaber and Magnuson, 1975b; a summary and comparison have been made by Gregor and Siska, 1981) have not been reconciled by the newer measurements. Starting from low energy, $E<0.5$ kcal/mol, the early results showed a monotonic decline with increasing E, with a consensus that the decline leveled out near $E=1.5$ kcal, with perhaps a slight minimum there, and a relatively flat behavior for higher energies. The newer data, by contrast, show an appreciable (30%) rise in Q_I from $E=1.5$–4.5 kcal, implying a more pronounced minimum for $E<1.5$ kcal. This sort of difference is what might be expected if the earlier experiments were more distorted by energy smearing (see, for example, Parr *et al.*, 1982, for a discussion of averaging effects). The most recent consensus fine-structure-averaged cross section is 19 Å^2 at $E=2$ kcal.

The state-selected experiments agree that, in the range $E=1.5$–4.5 kcal, the ratio $R_{02}\equiv Q_I^{(0)}/Q_I^{(2)}$ increases monotonically from 1.25 to 1.40; at much higher E (14–130 kcal), Verheijen and Beijerinck (1986) find the ratio to level out at 2.0. Overall the fine-structure effect is very similar to that found in Ne^*+H_2. This implies that the results of mixed-beam experiments are sensitive to the J-state populations, which in many cases are unknown or at least unmeasured. As discussed in Sec. II.A, the populations depend on the beam production method and cannot in general be assumed to be statistical ($^3P_2/^3P_0=5$). At $E=2$ kcal these measurements yield $Q_I^{(0)}=24$ Å^2 and $Q_I^{(2)}=18$ Å^2 (van den Berg *et al.*, 1987).

As before, a substantial contribution to the determination of an optical potential for Ne^*+Ar has come from differential nonreactive scattering measurements. Gregor and Siska (1981) used a simultaneous multiproperty fitting technique employing their own nonreactive scattering data at $E=0.81$ and 1.48 kcal, along with $Q_I(E)$ and k_Q data then available, to yield an optical potential for Ne^*+Ar undifferentiated with respect to fine-structure state. This potential reproduced later absolute $Q(v)$ measurements of Kerstel *et al.* (1988) to within a few percent. Very recently Baudon *et al.* (1991) have employed newer nonreactive data at higher energy (7.3 kcal) in conjunction with the same auxiliary data used by Gregor and Siska to derive a Ne^*+Ar potential differing from the earlier one mainly in having a steeper repulsion for $V_0>2$ kcal and a Γ clipped for $r<2.75$ Å. Unfortunately Baudon *et al.* were unable to find a consistent fit using the newer, and presumably better resolved, $Q_I(E)$ data. Moreover, no progress was made in analyzing the origins of the fine-structure reactivity difference.

The form of the interaction derived in this way is of the nonbonded van der Waals type, similar to that obtained for $He^*(2\,^3S)+Ar$. $V_0(r)$ shows a hint of repul-

sive wall structure associated with the "peel-core" transition, while Γ is exponential, at least at long range. However the exponential decay constant is found to be 1.6–1.9 Å^{-1}, lower by a factor of 2 than the He* result. This difference may be partly due to fitting the earlier $Q_I(E)$ data. The more recent data appear to require a steeper decay with r. The spin-orbit state-selected cross sections might be fit by assuming different Γ's for each J, as van den Berg *et al.* (1987) have done for H_2; however, dynamical factors may also contribute to the fine-structure differences, as discussed in the next subsection.

The directionality of the Ne* $2p^5$ core, along with use of a laser of known polarization for state selection, allows measurement of the polarization ($|M|$) dependence of Q_I, denoted $Q_I^{(JM)}$, where the relative velocity is the quantization axis, as discussed in Sec. II.A. Of most interest is the ratio $R_{20,22} \equiv Q_I^{(20)}/Q_I^{(22)}$, in which the $2p$ hole is pointing as nearly along ($M=0$) and perpendicular ($M=2$) to **v** as possible given the constraint imposed by the spin-orbit interaction. The early thermal-energy measurement of Bregel *et al.* (1986) of $R_{20,22}=1.30(10)$ using an Ar scattering cell has been supplemented by the Zeeman sublevel pumping supersonic Ar beam experiments of Driessen, Megens, *et al.* (1990), who obtained $R_{20,22}=1.55(6)$ at thermal energy and $R_{20,22}=1.05(6)$ at hyperthermal, using the two Ne* sources described in Sec. II.A. The polarization dependence is expected to be closely connected to the overall fine-structure differences; again the next subsection will touch on this further.

Once more a summary of measurements of product properties for Ne*+Ar begins with PIES experiments, which here provide truly striking results. Due to the small Ne* fine-structure splitting (96 meV) and broad PI spectral lines (90 meV), state selection is essential for separating lines and obtaining positions, shapes, and intensities for $J=0$ and 2. In an experiment of both very high signal-to-noise (S/N) ratio and optical quenching efficiency, Hotop *et al.* (1981) have reported fully J-state-resolved spectra for Ne*+Ar, Kr, and Xe. The Ar results are very similar in form to those for He*($2\,^3S$)+Ar, with in addition nearly identical line shifts (+30 meV, 0.7 kcal), widths, and shapes for both fine-structure states of Ne* and both fine-structure states of the Ar^+ product. As the experiment was performed with a near-Maxwellian Ne* beam and an Ar gas cell, the line shapes for these largely repulsive interactions may be dominated by the collision energy distribution. The extraordinary feature of the measurements is a substantial dependence of the Ar^+ fine-structure intensities on the initial Ne* state; Ne*($^3P_2$) yields a ratio $R'_{3/2,1/2} \equiv Q_I(J'=\frac{3}{2})/Q_I(J'=\frac{1}{2})=1.51(7)$, while $^3P_0$ gives $R'_{3/2,1/2}=3.94(24)$. Not only are these remarkably dissimilar, but neither is statistical (2.0) nor close to the He*($2\,^3S$) result (2.1). These same measurements also yielded $R_{02}=1.21(10)$, in good agreement with a mild extrapolation of the more recent results downward to $E=1$ kcal.

As discussed in the next subsection, the anomalous product fine-structure branching is connected with the observation by Weiser and Siska (1986) of a substantially greater preference for associative ionization on the part of $^3P_0$. They find the ratio of AI branching fractions $(Q_{AI}^{(0)}/Q_I^{(0)})/(Q_{AI}^{(2)}/Q_I^{(2)})$ to be 1.33 at $E=1.5$ kcal, increasing to 1.72 at $E=4.5$, in a crossed-supersonic-beam experiment with a temperature-programmed Ne* nozzle. The cross-section ratios R_{02} measured in the same experiment agree closely with the results of van den Berg *et al.* (1987).

An Ar^+ angular distribution measurement reported in Haberland *et al.* (1981) again shows strongly forward scattering with slight energy loss, indicating a range relationship between V_0 and V_c similar to that in He*+Ar and H_2.

Most of the experimental results cited for Ne*+Ar have also included data for Kr and Xe, the only exceptions being the recent Zeeman polarization measurements of Driessen, Megens, *et al.* (1990) and the multiproperty study of Baudon *et al.* (1991). The differential scattering measurements of Gregor and Siska (1981) show the alkali analogy to be useful in understanding the trends in nonbonded interaction strength, the results presented in Table X for Ne* being similar to those for Na (Buck and Pauly, 1968; Düren *et al.*, 1968). It is noted that the van der Waals well characteristics are much better determined for Kr and Xe than for Ar, owing to a larger number of experimentally fully resolved rainbow and glory interferences. Gregor and Siska were able to invert the rainbow scattering pattern for Ne*+Xe directly to yield $V_0(r)$. The resonance widths $\Gamma(r)$ found by Gregor and Siska have similar logarithmic slopes and increasing magnitudes for Ar, Kr, and Xe results reminiscent of those of Martin *et al.* (1978) for He*($2\,^1S$)+Ar, Kr, Xe.

These scattering findings all refer to mixed Ne* beam conditions, but the highly resolved interference patterns for Kr and Xe, as well as the excellent agreement between van der Waals parameters derived from differential and total scattering cross sections measured with different beam sources and fine-structure populations, suggest that there is very little difference between the $V_0^{(J)}$ for a given noble-gas partner, at least in the well and low-energy repulsive regions ($r \geq 3.5$ Å). Despite this similarity, Verheijen and Beijerinck (1986), in agreement with unpublished work from the author's laboratory and with the PIES findings of Hotop *et al.* (1981), have found $R_{02}>1$ for Kr and Xe as well. (The Kr and Xe data of Hotop *et al.* are misrepresented in Fig. 11 of Verheijen and Beijerinck, and the Xe ratio is in better agreement with the latter's result than shown there.) Verheijen and Beijerinck find that, while R_{02} at thermal energy is slightly smaller for Xe than for Ar or Kr, in all three cases it approaches 2.0 at high energy ($E>10$ kcal).

As to product scattering attributes, the PIES experiments of Hotop *et al.* (1981), while displaying only minor changes in line shape and shift with noble-gas partner, continue to show nonstatistical $R'_{3/2,1/2}$ similar to those

for Ar. These ratios appear to decline slightly in the Ar, Kr, Xe sequence. The decline of the $^3P_2$ ratio is a greater fraction of its Ar value, yielding a ratio of ratios that increases in this sequence.

2. Modeling the scattering: the entrance channel

Although a number of theoretical studies have employed He*+Ar as a model system (see, for example, Hickman and Morgner, 1976), interpretation of the results just surveyed has proceeded without a whit of *ab initio* input as to the form of V_0 or Γ. Needless to say, such input would be invaluable as an independent yardstick for gauging the meaning of unusual experimental findings. As discussed in Sec. III.B, for the most part experimentalists have relied on the alkali analogy and on semiempirical electronic structure calculations. The alkali analogy is weakest for the He*($2\,^1S$)+Ng interactions where, as just discussed, strong evidence points to a pronounced structure in the repulsive wall of V_0. Although, when viewed on suitable energy and distance scales, similar but weaker structure appears in the He*($2\,^3S$) and Ne*(^3P) Ng potentials and may indeed be realistic, unambiguous experimental evidence is lacking in these cases. The best-studied alkali-noble-gas potential, NaAr($X^2\Sigma^+$) (Smalley *et al.*, 1977; Tellinghuisen *et al.*, 1979), nonetheless shows a similar repulsive structure.

One-electron model potential calculations of $V_0(r)$ (Siska, 1979b; Gregor and Siska, 1981; see Sec. III.A.2 for the logic of these calculations in terms of projecting out appropriate configurations for the quasidiscrete state) have produced semiquantitative agreement with experimentally derived curves, including the difference between He*($2\,^1S$) and the others, and a major fraction of the dispersion interaction, especially in the Ne* systems. This agreement lends some credence to the delineation of the origins of the repulsive structure implied by the form of the electronic wave functions obtained in the calculations. The antibonding-hybridization descreening mechanism, already discussed in some detail for He*+H_2 in Sec. IV.B.2, is cleanly applied to these closed-shell atomic partners, free of the complications caused by permanent electric moments. This mechanism does not rely for its operation on either a curve crossing (the diagonal terms in the model electronic Hamiltonian do not cross) or charge transfer (a one-center configuration-interaction expansion is used), but only on the reduction of the overlap repulsion arising from orbital mixing involving the promoted electron. The reduced repulsion then allows the sharp changes in curvature of the core-ion atom potential in the outer limb of its well to exert a greater influence on the shape of the overall interaction. [It is likely that such mixing plays a significant role in the entire molecular Rydberg series He**(ns)+Ar, but especially for small n.]

As may be derived in a straightforward way from perturbation theory, the smaller $2s$-$2p$ energy gap in He*($2\,^1S$), already discussed for the H_2 case, leads to stronger mixing, yielding more pronounced structure in V_0. The postulated role of the core potential is supported by a comparison of the one-electron results for ^1S in the Ar, Kr, Xe sequence with the experimental potentials, both showing successively more pronounced structure that occurs at successively lower energies on the repulsive wall. The calculations show that this trend is due largely to the increased strength of the He*+X core attraction, arising from the growing polarizability of the noble-gas partner.

As to the experimentally derived behavior of $\Gamma(r)$, in view of the possible influences of overlap saturation and/or AI state density reduction, it is perhaps not surprising that, as the PI cross-section behavior at high E seem to require, Γ would level out at small r. The saturation radii, however, especially for ^1S+Ar, Xe, seem too large (≥ 3 Å) to be due to overlap saturation, pointing perhaps to the AI effect, as discussed in Sec. III.B. Still enigmatic is the small-r behavior of $\Gamma(r)$ for ^1S+Xe found by Büermann *et al.* (1987). The successive maximum, minimum, and sharp rise as r decreases could conceivably arise from interference between the exchange and radiative terms in Eq. (3.16); it may be that only Xe is attractive enough to allow this behavior to be exposed.

As for H_2, the differences in the repulsion for ^1S and ^3S provide a ready explanation for the differences in $Q_I(E)$; for Ar, the kink energy 0.6 kcal is lower than for H_2, moving the energy of the bendover in Q_I down correspondingly.

Although detailed modeling calculations have yet to be published for He*+Ar PIES, unpublished results from the author's laboratory indicate a good, although perhaps not fully quantitative, account of the spin-state differences outlined earlier, based on potentials derived as described above. In particular, the relatively strong increase in line shift ε-ε_0 and linewidth with E, independent of product fine-structure state, found for ^3S is typical for Penning ionization out of a smoothly repulsive $V_0(r)$, while the near independence of E of these quantities for ^1S is nicely accounted for by the repulsive kink in V_0, which gives rise to a rainbowlike maximum in $P(\varepsilon)$, whose location and width are only weakly energy dependent. Ideally, PIES data, preferably with small spread in E, should be incorporated into a generalized fitting procedure to determine V_0, Γ, and V_c. This requires, however, a careful account of branching between the Ar^+ fine-structure states, a topic to be covered later in this section.

The spin-state differences in V_0 give rise to characteristic differences in the PI opacity functions $P(b)$, providing a qualitative explanation for the different anisotropies observed in $P(\theta_\varepsilon)$, the Penning electron angular distribution (PEAD). $P(\theta_\varepsilon)$ is expected to show strong anisotropy only if the molecular axis has on average a well-defined orientation in space. This typically implies small impact parameters, for which θ_c, the heavy-particle angle of closest approach, varies little from zero. Opacity func-

tions that rise toward $b=0$, as are found for $^3S+$Ar, then may yield angle dependence, i.e., the internal angular distribution $P_{\rm int}(\gamma_\varepsilon)$ is more strongly reflected in $P(\theta_\varepsilon)$, where $\cos\gamma_\varepsilon=\hat{\varepsilon}\cdot\hat{r}$. The structure in V_0 for ^1S gives rise to near saturation, $P(b)\rightarrow 1$, for b smaller than that needed to pass over the kink, and thus to a wider range of axis orientations that effectively smear out $P_{\rm int}$. The correlation between the observation of nearly isotropic $P(\theta_\varepsilon)$ for $^1S+$Kr, Xe and the lower potential energy of the kink in V_0 in these systems, which allows a yet wider range of b for which $P(b)\approx 1$, lends credence to this view. It does not appear that $P(\theta_\varepsilon)$ is sensitive to the precise form of V_0, except to the extent that it allows the critical ionization configurations to have some spatial definition. Ebding and Niehaus (1974) were quite successful in reproducing their experiments with hard-sphere potentials. It is also noted that lack of definition of the relative velocity vector in laboratory coordinates as well as energy averaging can strongly affect $P(\theta_\varepsilon)$.

The above analysis indicates that information on the electron partial-wave coefficients α_λ of Eq. (3.74) is more readily obtained for $^3S+$Ar, and that the lower anisotropy observed for ^1S does not necessarily reflect a less anisotropic $P_{\rm int}$ (Niehaus, 1981). Substituting the Hickman-Morgner approximation, Eq. (3.74), into $P_{\rm int}$ [Eq. (3.73)], yields

$$P_{\rm int}(\varepsilon,\gamma_\varepsilon)\propto\Gamma(r_\varepsilon)\left|\sum_\lambda(\alpha_\lambda/\alpha_0)P_\lambda(\cos\gamma_\varepsilon)\right|^2 . \tag{4.4}$$

Semiclassical analyses by Ebding and Niehaus (1974), Niehaus (1981), and Mitsuke, Kusafuka, and Ohno (1989) have assumed s and p waves only, $\lambda=0,1$ in Eq. (4.4). For ^3S the two latter analyses, which employ realistic V_0's, have determined $|\alpha_1/\alpha_0|\approx 0.6$ and $\arg\alpha_1-\arg\alpha_0\approx\pi/4$. A quantum analysis including d waves by Hoffmann and Morgner (1979), while providing improved fits to the earlier observations and apparently ruling out nonzero μ, the projection of λ in the body frame, led to ambiguous results for the α_λ.

The result for $|\alpha_1/\alpha_0|$ may be related to the sp hybridization of the He* $2s$ orbital that occurs during a collision. In view of the factorization approximation [Eq. (3.17)], $|\alpha_1/\alpha_0|$ may be identified with the ratio $|a_{2p}/a_{2s}|$ of orbital mixing coefficients. Siska (1979b) has shown that the limiting value of this ratio at small r is 0.58, quite close to the experimental α ratio. As the $3d$ orbital of He* cannot mix nearly so strongly, this connection also suggests that d waves contribute negligibly to $P_{\rm int}$.

The state-dependent differences in Ne*($^3P_{0,2}$)+Ar documented above are not nearly so well understood at present, at least in part because they have come to light more recently. On the face of it one might expect more complicated behavior in these systems, as $^3P+{}^1S$ yields $^3\Sigma^+$ and $^3\Pi$ molecular states. However, the p character of Ne* is vested in the Ne^+ core, while the thermal-energy dynamics is dominated by the interaction of Ar with the promoted $3s$ electron. This implies that, at least to a first approximation, a single $V_0(r)$ consisting of degenerate Σ and Π components governs the PI entrance channel; evidence for this comes from the well-resolved interference effects observed for nonreactive scattering, as discussed earlier. Adding the spin-orbit interaction, which is again confined almost exclusively to the core ion (Cohen and Schneider, 1974), causes the $^3P_2$ and $^3P_0$ states to split by the well-known 777 cm^{-1} (96 meV, 2.22 kcal), but has little effect on the atomic wave function. In the approximation that the spin-orbit matrix element remains constant, independent of r, the resulting differences among the Ω potentials $V_0^{(J\Omega)}$ (Ω the absolute value of the projection of $\mathbf{J}$ on $\mathbf{r}$, distinct from $|M|$, the corresponding projection on $\mathbf{v}$) depend directly on the purely electrostatic Σ-Π splitting, and where this splitting is small the $V_0^{(J\Omega)}$ curves will run parallel. Since the Σ-Π splitting is expected to be appreciable only at small r, where the $\langle 2p_{\rm Ne}|3p_{\rm Ar}\rangle$ overlap is important, there is little reason to expect much Ω splitting for $J=2$ nor much difference between the $J=0$ and $J=2$ curves in the van der Waals region (see Gregor and Siska, 1981). Differences in Ne* spin-orbit reactivity apparently do not lie chiefly in V_0 differences, unlike the case for the He* spin states.

The Σ and Π components of the resonance width, Γ_Σ and Γ_Π, on the other hand, are expected to differ substantially (Morgner, 1985; Driessen *et al.*, 1989; Driessen, Op de Beek, *et al.*, 1991). At van der Waals distances it is likely that $\Gamma_\Sigma\gg\Gamma_\Pi$ in view of the approximate factorization Eq. (3.17), as the σ overlap $\langle 2p\sigma_{\rm Ne}|3p\sigma_{\rm Ar}\rangle$ dominates over $\pi\ \langle 2p\pi_{\rm Ne}|3p\pi_{\rm Ar}\rangle$ at large r.

A straightforward vector coupling analysis (Zare, 1988) leads to the asymptotic ($r\rightarrow\infty$) relations among the full optical potentials, with and without spin-orbit coupling,

$$\begin{aligned} V^{(00)}&=\tfrac{1}{3}V_\Sigma+\tfrac{2}{3}V_\Pi ,\\ V^{(20)}&=\tfrac{2}{3}V_\Sigma+\tfrac{1}{3}V_\Pi ,\\ V^{(21)}&=\tfrac{1}{2}V_\Sigma+\tfrac{1}{2}V_\Pi ,\\ V^{(22)}&=V_\Pi , \end{aligned} \tag{4.5}$$

where spin differences among the V_Λ are ignored and the asymptotic spin-orbit energy splitting has been subtracted out. These same relations hold between the $\Gamma^{(J\Omega)}$ and Γ_Λ imaginary parts if the real parts $V_0^{(J\Omega)}$ are equal. In that case, in a collision at finite b, the $J=2$ Ω states will be scrambled by the Coriolis effect, since "locking" of $\mathbf{J}$ onto $\mathbf{r}$ cannot occur in the absence of a real splitting. The Ω-averaged optical potential for $J=2$ reduces to the same Σ-Π admixture as that for $J=0$, for which $\Omega=0$ only, and scrambling thus makes the $J=0$ and $J=2$ cross sections equal despite the width difference. As $b\rightarrow 0$, however, Coriolis coupling disappears, and Ω becomes a good quantum number. Then the increasing Π character with increasing Ω indicated in Eq. (4.5) implies lower $P(b)$ at small b for $\Omega>0$, with the pure Π $V^{(22)}$ showing the largest opacity decrease. Relative to $P(b)$

for $V^{(00)}$, the small-b opacity must be higher for $V^{(20)}$ and $V^{(21)}$ and lower for $V^{(22)}$, but if Γ_Σ is large enough at the small-b turning points to saturate the ionization, the decrease in the $V^{(22)}$ opacity will not be completely offset by the increases in the others. At large b the Coriolis effect reverses the Σ-Π composition of each state near the turning point, but $P(b)$ is small there, and large differences among the Ω states cannot occur. The net effect, as shown by the semiclassical calculations of Driessen, van de Weijer, *et al.* (1990), is to make $Q_I^{(2)}$ slightly smaller than $Q_I^{(0)}$. Driessen, van de Weijer, *et al.* (1990) calculate $R_{02}=1.10$ at $E=1.2$ kcal, assuming a width ratio $\Gamma_\Sigma/\Gamma_\Pi=9$; while this appears encouraging, incomplete dynamic scrambling alone was not able to reproduce the experimental value 1.25(5) at this energy, and an almost negligible increase, much milder than the observed increase in R_{02} with increasing E, was predicted.

Polarization measurements, in which $|M|$ and hence the asymptotic Ω is fixed, should constitute a further test of this scenario. While the measured thermal-energy value $R_{20,22}=1.4(2)$ supports it, the polarization effect disappears at high energy, while the model suggests that $R_{20,22}$ should increase along with R_{02}. It is likely that some locking onto r is occurring at high E, where smaller r is probed and splittings may be appreciable; however, in the limit of perfect locking, a stronger rather than weaker polarization effect is expected.

The J-independent positive PI spectral line shift meshes well with other evidence as to the lack of splitting among the $V^{(J\Omega)}$, although the line shape, which was obscured by thermal averaging, might be a more sensitive gauge of splittings. The Ng independence of the shift also indicates that this situation is more general, in agreement with other evidence. The anomalous population of the Ng^+ fine-structure states, which does depend on Ng, is discussed in the next subsection.

The experimentally determined $\Gamma(r)$ from mixed-beam measurements is at present too uncertain as to its falloff with r, which appears anomalously slow, to permit firm conclusions concerning the exchange mechanism or intersystem comparisons. Nonreactive scattering angular distributions cannot determine the decay exponent [the α in $\Gamma=\Gamma_0\exp(-\alpha r)$] uniquely, owing to the competition between the repulsive branch of V_0 and Γ in fixing the relative intensity and slope of the wide-angle scattering. As noted in the previous subsection, currently available $Q_I(E)$ measurements, whose form is more sensitive to α, are conflicting, but more recent work points to higher α, moving toward better agreement both with $He^*(2\,^3S)+Ar$ and with the exchange model. PIES measurements for nonbonding reagents such as Ar have so far proved to be of little value in constraining Γ.

3. Postionization fine-structure branching and dynamics

Hoffmann and Morgner (1979) have interpreted the measured product fine-structure cross-section ratio $R'_{3/2,1,2}$ for $He^*(2\,^3S)$, which is slightly larger than statistical and slowly increasing with E, in terms of the variable Σ character of the $X^2\Sigma_{1/2}$ and $A_2{}^2\Pi_{1/2}$ $HeAr^+$ product states with r, under the experimentally supported assumption that Penning ionization in this system produces a pure Σ state. For $r\leq 2$ Å, where the Σ-Π splitting far exceeds the spin orbit, the $X(J'=\frac{3}{2})$ state carries nearly all the Σ character, while for $r\geq 3$ Å, Σ divides $\frac{2}{3}$ to $\frac{1}{3}$ between X and $A_2(J'=\frac{1}{2})$, the asymptotic fractions. Thus at any E the proportion of X state will be larger than 2, the statistical value, and branching into X will increase with E as the reagents are able to penetrate to ever smaller r. Hoffmann and Morgner obtained a quantitative fit to the data (Hotop, 1980) for both ^1S and ^3S+Ar, based on a classical calculation, for each E, of the mean radius of ionization (a valid approach for a repulsive V_0) and equating the cross-section ratio to the ratio of fractional Σ characters of the X and A_2 states at that radius (a perturbation approximation). For modeling of other types of product data, such as PIES line shapes and Ar^+ angle-energy distributions, the width Γ would be additively partitioned into its Σ and Π components, and the dynamics on the two product potentials computed separately. Such calculations have not yet been reported, even for these key systems, but are soon to be carried out in the author's laboratory.

As found for H_2, the stripping dynamics observed for both ^1S and ^3S+Ar, remarkable in view of the repulsive V_0's, is readily accounted for by the shorter-range, more attractive character of the product potentials and indicates a dominant role for the product interactions in the overall dynamics. Unpublished model calculations by the author show that the forward scattering persists over an appreciable range of assumed V_0 repulsive ranges and slopes, and that V_0 need not possess a van der Waals well to produce it.

A discussion of the branching into the AI ($HeAr^+$) channel must necessarily bring in the possibility of a "clipped" or saturated Γ, as employed by Burdenski *et al.* (1981) and by Kroon *et al.* (1986). If associative ionization influences the r dependence of Γ, the clipping distance should be slowly decreasing with increasing E, as the AI fraction declines. In the high-E limit, where $Q_{AI}\rightarrow 0$, r_{AI} must approach zero as well. The fact that saturation is needed to fit only the higher-E Q_I data, which are slowly falling with E, may be a reflection of the shortened collision time, for which a saturated Γ might allow $P(b)$ to droop below unity at small b.

The rapid decrease of Q_{AI} with E is readily understood, at least qualitatively, in terms of the expected direct correlation between E and the peak recoil energy E', which yields a smaller fraction of collision products with $E'<0$ as E grows. Q_{AI} is also sensitive to fine-structure branching, as the $HeAr^+$ X state well is deeper than A_2 (0.81 vs 0.53 kcal); as E increases, the stronger attraction of the X state combined with its greater propensity for being formed make it the dominant final state

for associative ionization.

In contrast to the He* case, the existence of both Σ and Π transition amplitudes for $Ne^*(^3P_{0,2})+Ar$ has been shown by Morgner (1985) to be an essential factor in understanding the markedly nonstatistical product fine-structure branching observed. Morgner's analysis is based on the assumption of separate conservation of electron spin and orbital angular momentum during the PI transition, step b of Eq. (3.1); i.e., spin-orbit effects are accounted for purely by the geometry of vector coupling through an $|LS\Lambda\Sigma\rangle$ basis to create the final $|L'S'J'\Omega'\rangle$ states out of the initial $|LSJ\Omega\rangle$. Equations (4.5) illustrate this on the reagents' side when product states are not resolved; as usual, when product states are known, amplitudes rather than merely their squares are needed, as given by

$$\langle\phi_\varepsilon J'\Omega'|H_{\rm el}|J\Omega\rangle\equiv V^{(J\Omega)}_{\varepsilon J'\Omega'}=\sum_{\Lambda'\Lambda m_s\Omega_c}\langle L'\Lambda's'm_s'|J'\Omega'\rangle\langle L\Lambda sm_s|J_c\Omega_c\rangle\langle J_c\Omega_c s_v m_v|J\Omega\rangle\langle\phi_\varepsilon L'\Lambda'|H_{\rm el}|L\Lambda\phi_{3s}\rangle\ , \tag{4.6}$$

where $\langle\cdots\cdot|\cdot\cdot\rangle$ is a Clebsch-Gordan coefficient (Zare, 1988), $L\Lambda$ ($L'\Lambda'$) refers to the Ne^+ (Ng^+) ion, sm_s ($s'm_s'$) to the spin of this ion, $J_c\Omega_c$ to the Ne^+ ion, and $s_v m_v$ to the spin of the $3s$ electron. For the purpose of formal summation, the Λ's and Ω's are allowed to take on negative values; however, the contributions of the negative values are equal to those of the positive values. The angular momenta in the present case take on the particular values $L'=L=1$ and $s'=s=s_v=\frac{1}{2}$, and a fourth Clebsch-Gordan coefficient has been eliminated by assuming that the promoted electron remains in a $3s$ orbital prior to ionization. Abbreviating the coupling matrix elements in the $L\Lambda$ representation by

$$\langle\phi_\varepsilon L'\Lambda'|H_{\rm el}|L\Lambda\phi_{3s}\rangle\equiv u_{\Lambda'\Lambda}\ , \tag{4.7}$$

Morgner (1985) showed that, in addition to the Σ amplitude u_{00}, only the pure Π amplitude u_{11} is required to reproduce the observed product branching, although the other off-diagonal elements are not strongly constrained.

Averaging over Ω (only significant for $J=2$) yields widths whose ratios can be compared directly in the perturbation limit with the PIES experiments,

$$\Gamma^{(J)}_{J'\Omega'}=2\pi(2J+1)^{-1}\sum_{\Omega=-J}^{J}|V^{(J\Omega)}_{\varepsilon J'\Omega'}|^2\ . \tag{4.8}$$

Equation (4.8) is still resolved with respect to the molecular electronic state of $NeNg^+$ ($X\,^2\Sigma_{1/2}$, $A_1\,^2\Pi_{3/2}$, $A_2\,^2\Pi_{1/2}$). Summing over Ω' then yields the fine-structure-specific widths $\Gamma^{(J)}_{J'}$. Under the assumption that only u_{00} and u_{11} are nonzero, Eqs. (4.6)–(4.8) reduce to the simple formulas

$$\begin{aligned}
&\Gamma^{(0)}_X=\tfrac{2}{9}(u_{00}-u_{11})^2,\quad \Gamma^{(0)}_{A_1}=0\ ,\\
&\Gamma^{(0)}_{A_2}=\tfrac{1}{9}(u_{00}+2u_{11})^2\ ,\\
&\Gamma^{(2)}_X=\tfrac{1}{18}(2u_{00}+u_{11})^2,\quad \Gamma^{(2)}_{A_1}=\tfrac{1}{2}u_{11}^2\ ,\\
&\Gamma^{(2)}_{A_2}=\tfrac{1}{9}(u_{00}-u_{11})^2\ ,
\end{aligned} \tag{4.9}$$

where $X=(\frac{3}{2},\frac{1}{2})$, $A_1=(\frac{3}{2},\frac{3}{2})$, and $A_2=(\frac{1}{2},\frac{1}{2})$ are the $J'\Omega'$ final-state labels. The fine-structure ratios, which, as for He*, Morgner takes to be the Q_I ratios (a perturbation approximation), are then

$$\Gamma^{(J)}_{3/2}/\Gamma^{(J)}_{1/2}=[\Gamma^{(J)}_X+\Gamma^{(J)}_{A_1}]/\Gamma^{(J)}_{A_2}\ . \tag{4.10}$$

Only the amplitude ratio u_{11}/u_{00} is now significant, and by choosing $u_{11}/u_{00}=-0.106$ one may simultaneously reproduce both the $J=0$ and $J=2$ branching ratios [3.94(24) and 1.51(7), respectively], as may be readily verified from Eqs. (4.9) and (4.10). Further summing over J' and identifying Γ_Σ and Γ_Π with $|u_{00}|^2$ and $|u_{11}|^2$, respectively, confirms that the Ω-averaged widths are identical for $J=2$ and 0, as would be obtained from Eqs. (4.5), implying that in the perturbation limit the fine-structure cross sections are equal, as was concluded above, in disagreement with experiment.

While there is little doubt that Morgner's analysis has uncovered a key factor governing the nonstatistical $R'_{3/2,1/2}$, several issues remain unresolved. Hotop *et al.* (1981) find that $R'_{3/2,1/2}$ declines for both $^3P_0$ and $^3P_2$ in the Ar, Kr, Xe sequence, inconsistent with Eqs. (4.9) and (4.10), which require a simultaneous approach to or departure from the statistical ratio 2 for each J with changes in the real-valued u_{11}/u_{00} ratio. A single real value of u_{11}/u_{00} is no longer able to reproduce both R's. This calls into question the neglect of dynamical effects—ionization over a range of r and b—and the use of the perturbation limit. Treating the dynamics more rigorously might also require accounting for angular momentum recoupling effects at small ionization radii. It is not yet known whether the $R'_{3/2,1/2}$ are E dependent. Such data could provide evidence of recoupling, as found for He*+Ar. Moreover, as Morgner (1985) has discussed, u_{00} and u_{11} are expected to have different r dependences, a feature that would increase the influence of dynamics on the branching. Finally, the influence of *spd* hybridization of the promoted electron (Gregor and Siska, 1981) is not contained in the model. The extent of hybridization is found to increase in the Ar, Kr, Xe sequence, which would progressively alter the amplitude Eq. (4.6).

It is remarkable that the Π amplitude, which contributes only 2% to the total ionization rate according to Morgner's model, produces such striking deviations from statistical behavior. Equations (4.9) show that this is an interference effect, with the Σ and Π amplitudes added or

substracted before squaring. Consistency with experiment requires $u_{11}/u_{00}<0$ for Ar; in general, a phase difference less than π reduces the effect for a given modulus ratio.

Weiser and Siska (1986) employed Morgner's model in the interpretation of state-selected AI branching in Ne^*+Ar, using exact classical dynamics on molecular-ion potentials from the semiempirical estimation of Hausamann and Morgner (1985) and assuming the r-independent u_{11}/u_{00} ratio found by Morgner (1985). While the observed effect of preferential associative ionization for $J=0$ is qualitatively reproduced by the calculations, the predicted preference is too small by a factor of three or more depending on E. The origin of the preference is clearly the greater tendency for $J=0$ to funnel into $J'=\frac{3}{2}$ due to the Σ-Π interference. According to Eqs. (4.9), all the $\frac{3}{2}$ flux lands in the X state, which, according to Hausamann and Morgner (1985), is more attractive (well depth 1.78 kcal/mol) than A_1 (1.15 kcal) or A_2 (1.33 kcal) and thus has a greater propensity for associative ionization. The small calculated AI enhancement for $^3P_0$ appears to be due to the relatively small difference between the X and A_2 state well depths, although the other factors just mentioned could also contribute to the experimentally observed effect. The latter is likely in view of the continued $J=0$ AI enhancement observed for Kr and Xe, while the apparently decreasing difference between X and A_2 wells for $Ne+Kr^+$, Xe^+ yields almost no predicted effect in these systems. The steep decline in Q_{AI}/Q_I found in all cases is likely to be due to the same $E\rightarrow E'$ correlation as discussed for He^*+Ar.

It is unlikely that the branching and product potential differences play a large role in producing the observed sharply forward scattering of Ar^+; rather, the widely different ranges of the reagent and product forces ($r_m=5.0$ Å for Ne^*+Ar, 2.9 Å for $Ne+Ar^+$) are probably responsible, as was discussed for He^*+H_2, Ar.

D. He^*, Ne^*+N_2

Despite the residual difficulties in the interpretation of the data on the Penning ionization of atoms, it appears that the present stage of development of PI experiments and theory puts the field at the threshold of a detailed description of the Penning ionization of molecules. The features of molecular Penning ionization of greatest current interest are connected with the presence of two or more ionizable orbitals in the molecule. Among readily studied molecules, N_2 seems destined to serve as the archetype for nonpolar multiorbital reaction partners.

1. Experimental results

Owing to the powerful bonding in N_2 and N_2^+, neither rearrangement nor dissociative ionization can take place in either He^* or Ne^*+N_2, and the ionization products are limited to PI (N_2^+) and AI (HeN_2^+). The earliest molecular-beam measurement of Q_I is again due to Sholette and Muschlitz (1962); more recent crossed-beam results (Illenberger and Niehaus, 1975; Parr *et al.*, 1982, Kroon *et al.*, 1986) yield ionization cross sections of 16 Å^2 for $He^*(2\,^1S)$ and 8 Å^2 for $2\,^3S$ at a reference energy $E=1.7$ kcal/mol. Again the larger cross section for ^1S is also reflected in the quenching rate constants, although the cross-section ratio is distinctly less than the factor of three for Ar. The differences in the measured $Q_I(E)$ between ^1S and ^3S (Illenberger and Niehaus, 1975; Parr *et al.*, 1982; Kroon *et al.*, 1986) are qualitatively similar to those found for H_2 and Ar but somewhat less pronounced; for ^3S, $Q_I(E)$ rises roughly linearly with E, while for ^1S there is a more rapid rise at low E followed by a smaller slope at high E.

Currently there are no published He^*+N_2 nonreactive angular distributions; Sperlein (1986), working in the author's laboratory, has fitted both spherical and anisotropic optical potentials to measured state-selected distributions, in which both rapid oscillations at small angles and extensive wide-angle scattering are present with signal-to-noise ratios of 10 or better. van der Waals well depths and positions resulting from this work have been included in Table X. In the fitting procedure the potentials were constrained also to fit the quenching rate constants and, under the assumption that quenching is entirely PI, to fit relative $Q_I(E)$ measurements from the author's laboratory. No unusual features at intermediate angles, such as would arise from repulsive structure in $V_0(r,\gamma)$, are apparent for either ^3S or ^1S, unlike the cases for H_2 and Ar. Sperlein's scattering calculations demonstrate that structure in V_0 is not ruled out, but must be confined to $\gamma\approx 0$ and π; this is discussed further in the next section.

He^*+N_2 PIES studies first demonstrated the resolving of individual electronic (Čermàk, 1966) and vibronic (Hotop and Niehaus, 1970b) states of a molecular PI product. More recent work has focused on $He^*(2\,^3S)+N_2$ (Hotop *et al.*, 1979; Hotop, 1980; Ohno, Imai, *et al.*, 1983) mainly for reasons of superior ^3S intensity and convenient removal of ^1S by resonance quenching. The vibronic peaks in the PI electron spectrum are all assignable by comparison with photoelectron spectra of N_2; the $X\,^2\Sigma_g^+$, $A\,^2\Pi_u$, and $B\,^2\Sigma_u^+$ electronic states of N_2^+ are formed, corresponding to removal of a σ_g bonding, π_u bonding, and σ_u^* antibonding electron, respectively, in the minimal molecular-orbital picture. As the π_u electrons are most strongly bonding, their removal leads to a substantial increase in bond length and a long vibrational progression in the A state. Hotop *et al.* (1979) achieved particularly high resolution and signal-to-noise ratio, resolving $A\,^2\Pi_u$ vibrational states out to $v'=6$. The most immediately striking feature of the PIES is the substantial difference in electronic state populations compared to He I photoelectron spectroscopy. This disparity is now recognized as a general feature of molecular PIES (Ohno, Imai, *et al.*, 1983; Harada, 1990) and, in view of the necessity for orbital overlap to pro-

duce Penning ionization, can be taken to be a measure of the accessibility of the various molecular orbitals to attack by He*. For N_2 the relative photoelectron spectroscopy populations are $X:A:B=1:1.49:0.25$, while for thermal-energy ($E\approx 1.8$ kcal/mol) PIES, from Hotop *et al.* (1979), they are 1:0.83:1.13. Hotop *et al.* also employed a hot-cathode discharge ~1000-K He* beam ($E\approx 5$ kcal), finding the ratios to alter to 1:1.18:1.32, a 40% increase in A/X, 17% in B/X. The He* beams were near-Maxwellian, so that the branching ratios are essentially thermal averages. An N_2 gas cell rather than a crossed beam was employed, contributing further to the kinetic averaging, although affording an excellent signal-to noise ratio.

Recently Dunlavy *et al.* (1990) presented PIES data for He*($2\,^1S$)+N_2 at five energies measured in crossed supersonic beams, for which $\Delta E/E\sim 0.2$. In further, unpublished work, Dunlavy *et al.* (1992) have taken spectra with resonance-lamp state selection at seven kinetic energies in the range $E=1.6$–5 kcal; these data are given in Fig. 21. The signal-to-noise ratio and spectral resolution (70 meV) of these measurements do not approach those of Hotop *et al.* (1979), but the dynamic resolution is greatly improved, and the spectral resolution is adequate

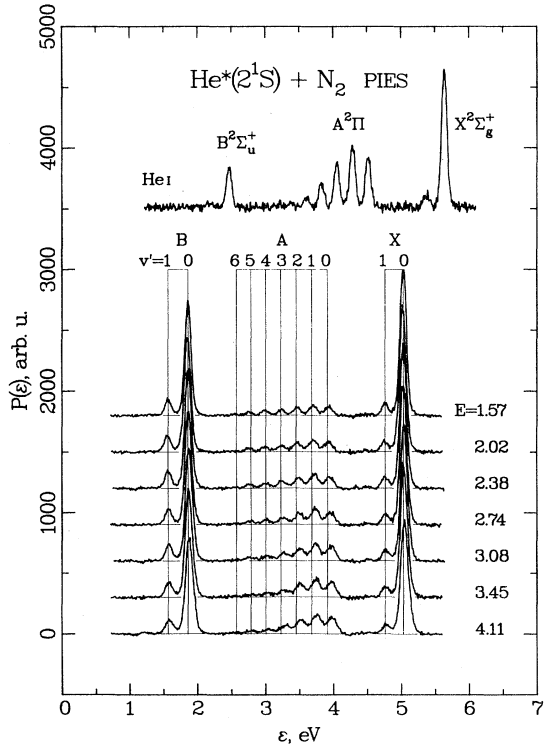

FIG. 21. Energy dependence of electron spectra from state-selected He*($2\,^1S$)+N_2, from Dunlavy *et al.* (1990, 1992). The uppermost spectrum is a photoelectron spectrum for reference, with N_2^+ electronic state assignments indicated. Noteworthy PIES features include the population change in A and B states relative to X compared to photoelectron spectroscopy and vibronic peak intensity and position changes with E (kcal/mol) of the A state.

to resolve vibrational states. Although the low ^3S fraction in the supersonic He* beam (see Table V) produces a minuscule ^3S PIES signal, reliable populations were derived from prolonged experiments, with the results $X:A:B=1.00:0.65:0.99$ at $E=1.6$ kcal and 1.00:1.03:1.14 at $E=4.9$ kcal, and smooth increases in the A and B populations at intermediate energies. These ratios are somewhat lower than those of Hotop *et al.* at comparable energy, and the A state shows a sharper increase (58%), but both differences are consistent with the broad and skewed energy averaging present in the earlier results. The total ionization cross section is increasing moderately over this energy range, and these data demonstrate that most of this increase originates with π-electron ionization. State-selected He*($2\,^1S$)+N_2 PIES has not been available prior to the work of Dunlavy *et al.* (1990, 1992). Despite the more gradual increase in $Q_I(E)$ at moderate to high energies, as compared to ^3S, the ^1S electronic state branching shows a more pronounced disparity with photoelectron spectroscopy and steeper energy dependence, with $X:A:B$ changing from 1:0.33:0.78 to 1:0.70:0.89, a 110% increase in A/X, over the same 1.6–5 kcal range of energy.

Like He*+H_2 and Ar, He*+N_2 is a nonbonded system, and positive line shifts ε-ε_0 are expected; the feature of most interest here is that these are found to depend on the electronic state of the ion. As in the case of relative populations, this is a general characteristic of molecular Penning ionization; the shifts are correlated with the populations, as will be discussed in Sec. IV.D.3. For ^3S, Hotop *et al.* (1979) found virtually identical shifts for (X, A, B) of (1.24,1.31,1.24±0.10 kcal) averaged over v' at $E=1.8$ kcal and increased but unequal shifts (1.61,2.08,1.71 kcal) at $E=4.9$ kcal. Dunlavy *et al.* (1992) find (X, A, B)=(1.11,1.06,1.27±0.2 kcal) at $E=1.6$ kcal and (1.35,1.89,1.48 kcal) at $E=4.9$ kcal, agreeing within the mutual error limits with the thermally averaged results. The tendency for the X and B shifts to show relatively weak energy dependence and to remain similar to one another, while A increases with energy, is magnified for ^1S, where Dunlavy *et al.* (1992) find (X, A, B)=(0.07,0.41,0.08±0.07 kcal) at $E=1.6$ kcal and (0.59,1.87,0.66) at 4.9 kcal. The A-state shifts are averaged over $v'=0$–3 only; $v'=4$–6 show peculiar peak shapes, indicating perhaps the presence of a secondary vibrational progression. Further experiments are in progress that may clarify this situation. The differentially pumped cross-beam experiments afford the advantage of modulation of the N_2 beam for two-channel phase-sensitive electron counting (see Sec. II.D), resulting in unambiguous background subtraction. This makes detection of low-intensity broad features feasible and improves the reliability of population data. While no underlying continua appear to be present for He*+N_2, there is evidence (Bevsek *et al.*, 1992) that He*+CO PIES is not wholly discrete; this is discussed further in Sec. IV.E.

The vibrational populations within a given electronic

state are found to agree well, within 10% or within experimental error, with those from photoelectron spectroscopy or from Franck-Condon factors, in some contrast to the results for H_2. This is perhaps owing to smaller zero-point vibrational excursions in N_2 vs H_2.

Hotop *et al.* (1979) also report a dramatic increase in linewidth for all states when going from low to high energy. The results of Dunlavy *et al.* (1990, 1992), who also note an appreciable increase in linewidth for both ^3S and ^1S despite their poorer spectral resolution, suggest that this is not entirely due to the increased absolute range of energy contributing to the dynamics for the hot He* discharge.

Yencha (1984) has reviewed the closely related Penning ionization optical spectroscopy (PIOS) results for He^*+N_2 (not possible for H, H_2, or Ar), including a mixed-beam study by Sanders *et al.* (1976). A more recent $He^*(2\,^3S)+N_2$ PIOS experiment by Leisin and Morgner (1984) shows $N_2^+(B\,^2\Sigma_u^+)$ vibrational populations in $v'=0,1$ in good agreement with photoelectron and PI electron spectroscopy, indicating little disturbance of the nascent (PIES) distributions by postionization dynamics, at least for this state.

Recently, Ohno, Takami, and Mitsuke (1991) have combined electron energy analysis with time-of-flight velocity dispersion to measure electronic-state-specific ionization cross sections. Aside from the intrinsic problem with intrabeam energy transfer in the time-of-flight pulse, the method employed by Ohno *et al.* (first introduced by Mitsuke, Takami, and Ohno, 1989) also employs a fixed electron energy of analysis during the time-of-flight sweep, leading to possible systematic errors associated with peak shifts as a function of energy. Although quantitative comparisons with results from full PIES scans at a range of fixed energies E have yet to be made, the two experimental approaches are certainly in qualitative accord, with the data of Ohno *et al.* also showing a steeper rise in Q_I with E for the $A\,^2\Pi_u$ state of N_2^+ than either $X\,^2\Sigma_g^+$ or $B\,^2\Sigma_u^+$, which in turn are nearly identical to each other.

The Penning electron angular distribution data for He^*+N_2 obtained by Ebding and Niehaus (1974) are remarkably similar, quantitatively, to those for Ar described above, with ^3S again showing greater anisotropy in favor of the backward hemisphere than ^1S. Equally remarkably, West *et al.* (1975) failed to find any AI branching for either ^3S or ^1S in experiments capable of detecting as little as 1% flux fraction. In unpublished work Sperlein (1986) was able to measure $Q_{AI}/Q_I = 0.0013(3)$ at $E=1.6$ kcal, falling rapidly with increasing energy. The N_2^+ angular distributions (Leu and Siska, 1974b) also resemble those of Ar^+ closely at comparable energies. Again the scattering is overwhelmingly forward for ^1S.

Many of the experimental data for Ne^*+N_2, as for the other Ne* systems, have been acquired only recently, as detailed in Table III, but J-state-selected experiments are still in the minority. In state-selected $Q_I^{(J)}$ crossed-beam measurements, van den Berg *et al.* (1987) have obtained the values 18.0 Å^2 and 13.5 Å^2 for $J=0$ and 2 respectively, quite comparable in magnitude to those for He*, and again, as for H_2 and Ar, showing a substantial preference for $J=0$, the cross-section ratio R_{02} being 1.33. The energy dependences of the J states in this case are closer to each other, in the range $E=1.5$ to 100 kcal, than for H_2 or Ar, with R_{02} increasing mildly to 1.5 at higher energy. The overall energy dependence is very similar to that presented in the same paper for $^3P_0+Ar$, a mild rise at low energy and a shallow decline beyond $E\sim 10$ kcal. As before, the two beam sources employed by the Eindhoven group leave a gap in E, here from about 5 to 15 kcal. Aguilar *et al.* (1985) in mixed-beam measurements have presented $Q_I(E)$ data down to $E=0.7$ kcal that show a decrease in slope at low energy but do not extend beyond $E=5$ kcal on the high end. The agreement between the data from the two groups in the overlapping region is excellent for N_2, unlike the case for Ar.

The total scattering cross-section velocity dependence $Q(v)$ measurements of Kerstel *et al.* (1988) also refer to a mixed Ne* beam; they resolved a single glory maximum and obtained a glory-averaged cross section of 482.5 Å^2. Using the peel-core potential model of Gregor and Siska (1981), they obtained a spherical-potential well depth 0.080 kcal and position 5.43 Å (see Table X). Effects of fine structure, anisotropy, Penning ionization, and quenching were neglected in the analysis. More recently, Baudon *et al.* (1991), in the same paper discussed in Sec. IV.C for Ar, have presented two structureless mixed-beam nonreactive differential cross sections $I_N(\theta)$ at $E=1.63$ and 6.8 kcal. Combining $I_N(\theta)$, fine-structure-averaged $Q_I(E)$ and $Q(v)$ data in a multiproperty analysis, they have obtained a spherical complex potential based on a potential function $V_0(r)$ having six piecewise segments (as for Ar), but capable of emulating peel-core behavior. They do not compare their $V_0(r)$ to that of Kerstel *et al.* (1988), but the van der Waals well characteristics are nearly identical, and the short-range behavior appears to be similar. Baudon *et al.* also employed a biexponential $\Gamma(r)$ clipped at $r=3.3$ Å, $\Gamma=0.25$ kcal. Again all complications arising from fine structure, anisotropy, and inelasticity, other than PI, were ignored.

The only reported PIES study occurs in the early series of Hotop and Niehaus (1970b), using a mixed Ne* beam, effusive N_2, and a retarding-field analyzer. As Fig. 3 illustrates, only the $X\,^2\Sigma_g^+$ state of N_2^+ is energetically open, and Hotop and Niehaus observed broad peaks assignable to $^3P_2$ for $v'=0,1,2$ with populations in good accord with the Ne I photoelectron spectrum. As discussed in Sec. IV.C for Ar, the contribution of the N_2 beam to the kinetic-energy spread is greater for Ne* than He*, and the linewidths are probably dominated by averaging. No line shifts for Ne^*+N_2 were quoted.

Although optical spectroscopy experiments based on product luminescence are energetically impossible for

$Ne^* + N_2$, Sonnenfroh and Leone (1987a, 1987b) have reported laser-induced fluorescence measurements of the vibrational-rotational (v',j') distributions in the X state, utilizing pulsed-laser-induced $B \rightarrow X$ fluorescence at 380–430 nm. This experiment combined an effusive $Ne^*(^3P_2)$ source based on sampling a flowing Ne^* discharge with a synchronously pulsed supersonic N_2 beam, for which the N_2 rotational temperature was ~ 8 K. They observed monotonically decaying vibrational populations out to $v'=4$, in good agreement with photoelectron spectra, with rotational distributions peaking at $j' \approx 4$ but with a long high-j' tail extending to $j' \approx 20$ and beyond. The rotational distributions were fitted to a sum of two Boltzmann distributions with $T_1 \sim 50$ K and $T_2 \sim 200-500$ K. The proportion of hot component increased mildly with increasing v' and was hottest for $v'=1,2$. Normally rotations are unresolvable in PI electron spectra, so that these data provide a new constraint on PI dynamics.

The mass-resolved time-of-flight ionization measurements of Appolloni *et al.* (1988), carried out with a mixed Ne^* beam and an effusive N_2 beam, show, in contrast to $He^* + N_2$, $Q_{AI}/Q_I = 0.052$ at $E = 1.0$ kcal, in good agreement with the earlier thermal crossed-beam measurement of West *et al.* (1975) at a similar mean energy. The energy-resolved measurements show a slow decline in the ratio out to $E = 2.5$ kcal, followed by a more rapid falloff, reaching 0.007 by $E = 7$ kcal. More recently, in as yet unpublished work, Pazun *et al.* (1992) have performed similar measurements, but using J-state-selected crossed supersonic beams, and find much greater ratios at low energy, $Q_{AI}^{(2)}/Q_I^{(2)} = 0.145(8)$ and $Q_{AI}^{(0)}/Q_I^{(0)} = 0.18(2)$ at $E = 1.6$ kcal. The disagreement with earlier work may stem from the lower rotational temperature of the supersonic N_2 beam (< 45 K), while the enhancement of AI for $^3P_0$ is slightly weaker than that for Ar, but still definite.

2. Interpretation: the entrance channel

For $He^* + N_2$, it is expected, both by analogy with H_2 and Ar and by the appearance of the various experimental measurements, especially $Q_I(E)$, that the source of the factor-of-two enhancement in ^1S reactivity over ^3S lies in the form of the real part $V_0(r,\gamma)$ of the optical potential. The quadrupole moment of N_2, which is negative and larger by a factor of three than that of H_2, ought to produce strong anisotropy in the *sp* hybridization of He^*. Combined with the relative ease of hybridization of ^1S, this may cause pronounced radial structure for $\gamma \approx 0°$ in the low-energy repulsion of the $V_0(r,\gamma)$ that diminishes substantially as γ approaches 90°. The structure and anisotropy are expected to be muted in ^3S, owing to the lesser extent of hybridization. One-electron calculations carried out by Sperlein (1986) support this hypothesis. In turn Penning ionization becomes much more probable for near-collinear configurations in ^1S, leading to the enhanced Q_I. The enhancement is not as great as in Ar because a collinear approach is disfavored by the $\sin\gamma$ weighting factor arising from opening out the azimuth. The differences in the form of $Q_I(E)$ for ^1S and ^3S are thus expected to be smaller as well, as is observed.

The lack of structure in the observed $I_N(\theta)$ for ^1S at wide angles, where one might expect a repulsive rainbow, may be due to the domination of the wide-angle scattering by broadside collisions, which are both geometrically more probable and less attenuated by quenching. Another possibility, discussed further below, is that the structure in V_0 occurs at very low energy [as in $He^*(2\,^1S) + Xe$], moving the rainbow to smaller angles, where it is masked by attractive scattering.

It is of interest to note that the He^* hybridization in the case of a negative quadrupole induces changes in the repulsion that are in opposition to the normally expected elliptically shaped angular dependence. If the effects of hybridization are not too pronounced, the net result could be a relatively spherical V_0. Sperlein (1986) in fact had good success in fitting a spherical V_0 to $I_N(\theta)$, $Q_I(E)$, and k_Q. Moreover, by comparison with the H_2 case, where *ab initio* results are available, and on more general grounds, the overall width $\Gamma(r,\gamma)$ is expected to be considerably less anisotropic than V_0. In the exchange model, overlap of the ionizable valence orbital with the Ng* core orbital determines the form of Γ; at any (r,γ) the core orbital tail is more distant, relative to the promoted orbital, from that of the target valence orbital. At large distance from the reactant molecule, all its valence orbitals become more spherical, thereby reducing the γ dependence of the orbital overlap and Γ.

An abnormally spherical optical potential may also lie behind the success Baudon *et al.* (1991) have had in fitting a variety of data for $Ne^* + N_2$ in a spherical approximation and may account for the well-resolved glory oscillation in $Q(v)$ seen by Kerstel *et al.* (1988). As discussed later, there are grounds for believing that serious discrepancies might arise if there were significant anisotropy present. These observations also make it doubtful that the five potential surfaces that correlate with $^3P_2 + N_2$ are anything but degenerate in the relevant range of repulsive energy. The observed 30% greater reactivity for $^3P_0$ apparently requires some difference in the optical potentials, but at present it is difficult to pinpoint the origin of such differences. In addition, the considerably smaller expected extent of hybridization in Ne^* (see the discussion above for $Ne^* + Ar$) makes it unlikely that structure occurs in the repulsion, as proposed by Sonnenfroh and Leone (1987a, 1987b) in interpreting their N_2^+ rotational distributions.

3. Differential behavior of N_2^+ internal states

The striking differences in the N_2^+ electronic state populations as measured in $He^* + N_2$ PIES vs those in photoelectron spectra point to a correlation between the

N_2 orbital being ionized and the behavior of the optical potential $V(r,\gamma)$ for those N_2 orientations most favorable for ionization of that orbital. While collision dynamics determines the probability of ionization of a particular orbital, collisional forces apparently do not greatly perturb the target wave function, as indicated by the similarity in vibrational populations within a given electronic state between PI electron spectra and photoelectron spectra. Ohno, Mutoh, and Harada (1983) and Ohno *et al.* (1984a, 1984b) have proposed a simple model for describing the electronic propensities, the exterior-electron-density (EED) model, in which the integrated fraction of the molecular-orbital density lying outside a "van der Waals surface" constructed from atomic van der Waals radii is taken to be proportional to the relative cross section for that orbital. (See Ishida and Ohno, 1989, for an investigation of the "tails" of molecular-orbital wave functions.) While in light of the above discussion of the experimentally indicated form of $V_0(r,\gamma)$ it is not surprising that N_2 fails to conform to the EED model, the model generally produces fair agreement with observed populations for molecules, such as unsaturated hydrocarbons, without substantial permanent moments. For N_2 the model predicts N_2^+ state ratios $X:A:B=1.00:2.66:0.83$, compared with the $He^*(2\,^3S)+N_2$ ratios of Hotop *et al.* (1979), 1.00:0.83:1.13, similar results from Ohno, Imai, *et al.* (1983), and the $^1S+N_2$ ratios of Dunlavy *et al.* (1990) of 1.00:0.33:0.78. The overestimate of the $A\,^2\Pi$ state is due to the incorrect dumbbell shape of the van der Waals surface obtained from atomic radii, from which the π_u orbital protrudes to a much greater extent than does either σ_g or σ_u. If the exterior electron density were obtained with the more spherical surface suggested above, the agreement would undoubtedly improve, and the author believes the idea behind the model is fundamentally sound. However, the model predicts ratios independent of He^* spin state, not in accord with experiment, and, because it neglects collision dynamics and realistic soft repulsions, cannot account for ratios that change with energy as observed.

Compared with ^3S, the substantially lower relative A-state population for ^1S may be interpreted in terms of the postulated kink in $V_0(r,\gamma)$ that occurs for $\gamma\approx 0°, 180°$, which "opens up" the surface for preferential ionization of the σ orbitals. Thus it is not that the π ionization efficiency is very different between ^1S and ^3S, but that σ ionization is enhanced for ^1S, leading to the observed factor-of-two total ionization cross-section disparity.

On general grounds for predominantly repulsive interactions it is expected that relative state populations will be strongly correlated with their energy dependence, as well as with PIES line shifts and their energy dependence. The observed differences in energy dependence of the electronic state branching ratios, weak dependence for the $B:X$ ratio and strong for $A:X$, particularly for ^1S, reinforces the notion that σ and π orbital electron removal occurs in distinct regions of the potential surface, since both X- and B-state production involve σ ionization and therefore the same near-collinear transition states. When these data are combined with $Q_I(E)$ data for ^1S and ^3S, it becomes clear that the dominant factor in the increase in Q_I with E is π orbital ionization, more so for ^1S than ^3S. The weaker dependence at intermediate to high energy for ^1S arises from the greater likelihood of σ ionization, which, owing to the end-on repulsive structure, is produced by collisions that sample large Γ's, giving near-saturated opacities and weak energy dependence. The fact that differences in $Q_I(E)$ between ^1S and ^3S mirror those for He^*+Ar then allows us to surmise that not only are the spherical-average potentials for N_2 similar to the corresponding Ar potentials, but broadside collisions, yielding π ionization, sample a ^3S+Ar-type potential, regardless of spin state, while the end-on approach, σ ionization, involves a more ^1S+Ar-like interaction, with $^1S+N_2$ being better described by this analogy than $^3S+N_2$.

Within this picture of regiospecific ionization, the observed differences in ^1S PIES line shifts—larger and more strongly increasing with energy for the A state, smaller, nearly identical, weakly increasing for X and B—take on enhanced significance in arising from spatially distinct parts of $V(r,\gamma)$. From a dynamic point of view, a small shift in a repulsive system implies that much of the collision energy is tied up in centrifugal motion, a situation calling for large b and therefore a large cross section. As the shift grows, the required b shrinks, and the cross section declines. Thus the branching fraction and shift for a given state are inversely correlated. The structure in V_0 for $^1S+N_2$ expected for $\gamma=0°$ may contribute in addition an E-independent singularity in the Jacobian $|d\varepsilon/dr|^{-1}$; the line shift in this case may yield a direct estimate of the potential-energy magnitude in the structured region. All these features are muted for ^3S because of the expected smaller anisotropy in V_0 and the probable lack of unusual behavior for $\gamma\approx 0°$, as well as the observed smaller state dependence of the shift.

The correlation between the orbital ionized and collision geometry suggested by experiment can be taken as an indication of the extended validity of the orbital symmetry model of Morgner (1982, 1985, 1988) for molecular partners. Ionization of the π molecular-orbital by He^* apparently does not take place with high probability in the potentially favorable end-on geometry; the $\langle He^*1s|N_2\pi_u\rangle$ overlap is rigorously zero in $C_{\infty v}$ symmetry. Likewise the $\langle He^*1s|N_2\sigma_u\rangle$ overlap is zero in C_{2v}, though the experimental results do not show the effect of this explicitly in view of the similar PI branching fractions and other properties for σ_u and σ_g.

Only $N_2^+(X)$ can be formed in Ne^*+N_2, making any regional specificity difficult to assess experimentally. However, if near-collinear geometries, which produce $\langle Ne^*2p\sigma|N_2\sigma_g\rangle$ overlap, are favored over broadside attack, then appreciable inconsistencies would be expected in attempting to fit both nonreactive and reactive cross-section data to the same (assumed spherical) potential,

were the optical surface $V(r,\gamma)$ appreciably different for $\gamma=0°$ and $\gamma=90°$. Thus if there exists a preferred configuration for reaction, $V(r,\gamma)$ must also be close to spherical. Given the theoretical result that the quadrupole moment of N_2 exerts the major influence on both the angle dependence of and the occurrence of possible structure in V_0, it is again unlikely that either prevails for Ne^*+N_2.

Sonnenfroh and Leone (1987a, 1987b) have interpreted their two-temperature $N_2^+(X)$ rotational distributions in terms of a substantial splitting among the possible Ne^*+N_2 incoming states, with the Σ-like state having substantial repulsive structure. In the light of the evidence just discussed, it appears that an alternative explanation is needed. In view of the substantial AI branching fraction found for rotationally relaxed N_2, as in the supersonic pulsed beam used by Sonnenfroh and Leone, an even larger fraction of the ionizing collisions must sample close configurations, where the collisional angular momentum can be efficiently transferred into N_2 or N_2^+ rotation. The logical place for this to occur is on the product $N_2^+ + Ne$ surface V_c, as a result of ionization "on the way in" on V_0. The incoming and outgoing ionization events, at b sufficiently small that the Langevin criterion on V_c is satisfied, then form two dynamically distinct collision types. The latter may result in very little angular momentum exchange, while the former may result in a NeN_2^+ complex with a lifetime sufficient to randomize the energy. It seems reasonable to suppose that this would yield a two-temperature rotational distribution. Moreover, if a scenario similar to that elucidated by coincidence studies on He^*+H_2 is followed in Ne^*+N_2, only $v'=0$ results in associative ionization, with any vibrational excitation causing predissociation of NeH_2^+ to PI products. Such predissociation inevitably induces rotational excitation through $V\rightarrow R$ transfer; thus the $v'\neq 0$ products should have a larger rotationally hot component, as observed. In addition, the temperature of the hot component should be higher for $v'\neq 0$; this is observed for $v'=1$ and 2, but not for $v'=3$ or 4. The hot component's temperature declines monotonically for $v'=1-4$, perhaps due to the decreasing size of the anharmonic vibrational quanta involved in $V\rightarrow R$.

Another possible mechanism arises owing to the just-barely-closed $N_2^+(A)$ channel: Rydberg states N_2^{**} with an A core may be formed, which then decay into $N_2^+(X,v')$. The vibrational *and* rotational distributions of Rydberg state products are expected to differ from those of the direct PI process. Although this possibility is mentioned and dismissed by Sonnenfroh and Leone, it appears that Rydberg crossings on the way in will lead to close collisions due to the expected attractive potential for $Ne+N_2^{**}$ at short range, again giving rise to a hot component. Some evidence for this possibility appears in the observed N_2^+ vibrational populations, which show $P(v'=2)\approx P(v'=3)$ in an otherwise smooth decline with increasing v'. Hotop (1980) has actually observed strong Rydberg progressions in $Ne^*(3p\,^3D_3)+N_2$ PIES, which are discussed further in Sec. IV.F. A high-resolution J-state-selected $Ne^*(^3P)+N_2$ PIES measurement might resolve these questions.

As for He^*+H_2, the vibrational excitation of N_2^+ for either He* or Ne* Penning ionization is highly likely to reduce the AI branching fraction by the fractional population in $v'\neq 0$. In addition, the $N_2^+ + He$ potential has now been found theoretically to have a rather shallow well (Miller *et al.*, 1988), further reducing the likelihood of associative ionization. Taken together, these factors imply that the shortcomings in the formulation of PI theory discussed in Sec. III are probably of minor importance to the description of these and other molecular PI systems that possess weakly attractive product potentials.

E. Other metastable noble-gas systems

Despite the many features of Penning ionization brought to light by the four sets of systems thus far surveyed, these only begin to reveal the potential complexity of the PI process. In what follows, extensions and possible failures of the ideas developed thus far are touched on in a brief overview of Penning ionization with other small molecular partners. Among the issues to be explored are the generality of the orbital selectivity found for Ar and N_2, the effects of spin multiplicity explored earlier for H and M, the role of dipole moments and orbital asymmetry, and the possible involvement of charge transfer and/or Rydberg states, i.e., the breakdown of the two-potential-curve model of Penning ionization. These themes as well as common structural features form the basis of the groupings of molecular partners discussed here.

1. He^*, Ne^*+CO, O_2, NO, CO_2, N_2O, and C_2H_2

This group of molecular partners, second-row diatomics and linear molecules, shares the ability of N_2 to donate either a σ or a π electron in He* Penning ionization, but introduces the molecular electric dipole (CO, NO, N_2O) and concomitant end-to-end orbital asymmetry, as well as partially filled valence orbitals (NO and O_2, both antibonding π orbitals). Of special significance for Ne* Penning ionization due to the energy limitations, the highest-lying occupied molecular orbital (frontier HOMO) switches from σ in N_2 and CO to π in the others. In addition, CO_2, N_2O, and C_2H_2 are expected to provide a more anisotropic short-range interaction due to the increased molecular length-to-width ratio.

As detailed in Tables II and III, several recent molecular-beam studies have included these molecules or subsets of them. The omissions of course leave an incomplete picture in some cases, but in no instance is there anything more than a crude estimate of the incoming or outgoing potential surfaces, due in large part to the ab-

sence of published nonreactive scattering angular distributions. Nonetheless the work that has been done sheds some light on the roles played by the various structural features just listed.

CO is isoelectronic with N_2 but possesses a small dipole (0.12 Debye, negative end on C) and relatively pronounced molecular-orbital asymmetry. This molecule is also of interest because of its ubiquity in transition-metal complexes and in surface chemistry. The behavior of $Q_I(E)$ for He^*+CO (Parr *et al.*, 1982) is quite similar to that for N_2, except that the ^1S Q_I is twice as large at low energy (<1 kcal) for CO and does not "droop" at high energy ($E>4$ kcal). Overall the thermal-energy PI cross sections (24 Å^2 for ^1S, 7.4 Å^2 for ^3S) show a $^1S/^3S$ ratio (3.1) significantly larger than for N_2, due mainly to the larger ^1S value. For Ne^*+CO the similarity in $Q_I(E)$ with N_2 is stronger (van den Berg *et al.*, 1987), including the nearly identical behavior of fine-structure Q_I with $E(Q_I^{(2)}=13$ Å^2 at 2.3 kcal) and the ratio $R_{02}\equiv Q_I^{(0)}/Q_I^{(2)}$, which is again nearly constant at 1.34. Except for the $He^*(2\,^1S)$ $Q_I(E)$, these results indicate a minor role for the molecular asymmetry. For ^1S, considering the likely repulsive structure in $^1S+N_2$, the higher Q_I at low energy may imply that such structure both is more pronounced and occurs at lower energy on a particular end of the molecule.

PIES studies on He^*+CO (for ^3S, Ohno, Imai, *et al.*, 1983; for ^1S, Harada *et al.*, 1983, and unpublished work of Bevsek *et al.*, 1992) show an even more pronounced preference for σ orbital ionization compared to photoelectron spectroscopy than shown by N_2; on a scale that fully displays the σ ionization peaks, the π progression for ^1S is nearly at base line. This occurs despite the fact that the asymmetry must weaken any orbital-overlap selection rules. As for N_2, the antibonding σ orbital is also enhanced relative to the bonding σ compared to photoelectron spectroscopy. For CO this orbital is dominated by the O atom and uniquely shows a *negative* energy shift for ^1S, implying an attractive interaction on the O end, giving enhanced Penning ionization for $He^*\cdots OC$ near-collinear configurations. Bevsek *et al.* (1992) also find weak continua in the PI electron spectrum for ^1S+CO associated with each of the three electronic states of CO^+; these continua slowly decay with decreasing electron energy. This feature, which accounts for $\geq 10\%$ of Q_I, may arise from an ion-pair state He^+CO^- or from overlapping of several Rydberg progressions; each mechanism has its shortcomings. Regarding the ion-pair mechanism, for a collinear complex, He* cannot "backbond" into the π^* orbitals of CO, the conventional mode of attraction between CO and metal atoms, due to symmetry. However, backbonding into the σ^* is possible. The $B\,^2\Sigma^+$-state vibrational progression extends to $\varepsilon=0$, but the intensity there does not seem adequate to account for the continuum contribution as arising from, e.g., $CO^+(B,v'=4)\cdots e^-$ Rydberg decay. The $C\,^2\Sigma^+$ state of CO^+ is too high lying to be of importance in Rydberg state formation.

For O_2 the possibility of an ion-pair state $Ng^+O_2^-$ is enhanced due to the open π_g shell and the positive electron affinity (0.44 eV) of O_2. However, $Q_I(E)$ measurements on He^*+O_2 (Parr *et al.*, 1982) show evidence only of a somewhat less repulsive interaction: the same characteristic differences between ^1S and ^3S are observed, such as the larger Q_I for ^1S (at $E=2$ kcal, $Q_I=32$ Å^2 for ^1S, 12 Å^2 for ^3S, ratio 2.8), but both $Q_I(E)$ curves display a muted energy dependence, except possibly at very low energy for ^1S, where a sharp increase with energy occurs. For Ne^*+O_2 (van den Berg *et al.*, 1987), each J state displays a similar, nearly flat but slowly decreasing Q_I with increasing energy, with an appreciably larger ratio $R_{02}=1.58$ [$Q_I^{(2)}=25$ Å^2] compared to N_2 or CO. Kerstel *et al.* (1988) report a well-resolved glory oscillation in $Q(v)$ and a derived (spherical) well depth and position for Ne^*+O_2 of 0.098 kcal and 5.17 Å, respectively, a slightly deeper and shorter-range well than that for Ne^*+N_2. In addition, unpublished nonreactive angular distributions for He^*+O_2 (Sperlein, 1986) show well-resolved quantum oscillations at small angles for both ^1S and ^3S, indicating a relatively spherical, intact repulsive wall.

However, the suggested picture of O_2 as a relatively "normal" PI partner is strongly modified by the appearance of the PI electron spectrum for He^*+O_2 (Leisin *et al.*, 1982, and references therein), which shows an extensive continuum underlying resolved discrete vibrational structure for the four (^3S) or five (^1S) electronic states that can be formed, $X\,^2\Pi_g$, $a\,^4\Pi_u$, $A\,^2\Pi_u$, $b\,^4\Sigma_g^-$, and $B\,^2\Sigma_g^-$ (^1S only). These states correspond to the removal of a π_g^*, π_u, π_u, σ_g, and σ_g electron, respectively, i.e., from only three O_2 molecular orbitals. Low-intensity features near $\varepsilon=0$ are assigned to autoionizing O** atoms. The continuum may contribute *more than 80%* of the total PIES intensity, although uncertainties in background correction preclude a more precise estimate. Leisin *et al.* plausibly attribute the continuum to formation of an autoionizing $He^+O_2^-$ ion-pair intermediate, whose Coulomb potential is estimated to cross the incoming triplet state of $^1S+O_2(^3\Sigma_g^-)$ at $r\approx 4$ Å and the singlet, triplet, and quintet states of $^3S+O_2$ at $r\approx 3.3$ Å. Although these radii are well inside the estimated r_m's for these states, the crossings are expected to be strongly avoided and thus accessible at thermal energy. The rapid drop in potential upon crossing onto the ionic surface causes a broad electron energy distribution for any particular O_2^+ vibronic level formed, thus merging the vibrational peaks into a continuum. Further discussion of the ion-pair model is given for He^*+Cl_2 below. If spin is conserved, only the $^3S+O_2$ quintet should be unaffected by the crossing, as the ion pair can only be singlet or triplet and therefore should dominate the "normal" Penning ionization, producing exclusively the quartet ion states. Indeed, the discrete part of the $^3S+O_2$ spectrum shows the predominance of the a and b states. However, smaller but distinct discrete structure is also found for X and

A, and $^1S + O_2$ shows reduced but distinct structure assignable to each of the energetically allowed states, although quartets are no longer preferred.

Leisin *et al.* (1982) argue that, due to symmetry restrictions on the covalent-ionic electron jump into the π_g^* orbital, which in a one-electron approximation is forbidden for $He^* + O_2$ in both C_{2v} and $C_{\infty v}$ geometries, many collisions remain on covalent surfaces, thus accounting for the discrete bands observed in ^1S as well as the doublet states in ^3S. A non-Franck-Condon high-v' tail in the vibrational distribution for $O_2^+(X\,^2\Pi_g)$ in ^3S is attributed to a Rydberg state of O_2, nearly resonant with the incoming energy, that belongs to the $O_2^+ B\,^2\Sigma_g^-(v'=0)$ series. Leisin *et al.* suggest on the same symmetry grounds that the entire X band is due to Rydberg formation; however, a similar X-state distribution tail is observed for ^1S, for which a Rydberg assignment is less certain, unless a double-curve-crossing $^1S \rightarrow$ ion pair $\rightarrow {}^3S$ through either the singlet or triplet manifolds is invoked. Positive PIES energy shifts ($\varepsilon - \varepsilon_0 \approx 1$ kcal) for the discrete bands are consistent with the cross sections and scattering discussed earlier. O_2^+ angular distributions from $^1S + O_2$ (Leu and Siska, 1974b) show a good deal of nonforward scattering and high recoil energy. The latter supports the double-curve-crossing mechanism, which would convert low-E $^1S + O_2$ collisions into high-E $^3S + O_2$ ones. Recently Mitsuke, Takami, and Ohno (1989) have reported final-electronic-state-resolved $Q_I(E)$ data for $He^*(2\,^3S) + O_2$ using the PIES time-of-flight technique discussed above for N_2. They find the doublet O_2^+ states to decline mildly with increasing energy and the quartet states to rise as sharply as the $He^* + Ar$ $Q_I(E)$ does. This correlates with the expected absence of covalent-ionic interaction for the quartet products.

In view of the complexities in the Penning ionization of O_2 by He*, it may not be surprising that this system also quenches through neutral channels to a small extent (Chang and Setser, 1978); however, no beam studies of neutral channels are extant. For a review emphasizing competing quenching channels, see Golde (1977).

All the recent beam studies of Penning ionization of NO have been $Q_I(E)$ measurements for Ne*, as listed in Table III; so far as the author is aware, $He^* + NO$ $Q_I(E)$ data have never been published, although unpublished work exists (e.g., Sperlein, 1986). The differences between ^1S and ^3S in both cross-section magnitude and energy dependence are smaller than for O_2 (300 K thermally averaged $Q_I = 33$ Å^2 for ^1S, 18 Å^2 for ^3S, ratio 1.8; Schmeltekopf and Fehsenfeld, 1970). For Ne*, the differences between $J=0$ and $J=2$ are the smallest yet recorded for a diatomic partner ($R_{02}=1.06$, $Q_I^{(2)}=23$ Å^2 at $E=2.3$ kcal). The energy behavior of all the Q_I is consistent with primarily attractive or at most weakly repulsive interactions.

Ion-pair Ng^+NO^- formation is again expected to be significant owing to NO's open π_g^* shell and slightly positive electron affinity (~ 0.15 eV). This is consistent with $He^*(2\,^3S) + NO$ PIES (Hotop *et al.*, 1979), which appears to contain a considerable continuum component, though not nearly so intense or extensive as for O_2. Similar to O_2, five NO^+ electronic states are open for He* Penning ionization: $X\,^1\Sigma^+$, $a\,^3\Sigma^+$, $b\,^3\Pi$, $w\,^3\Delta$, and $A\,^1\Pi$, which correspond to ionization out of the three highest-lying orbitals π^*, π, σ, π, and σ, respectively. All five states are seen, but $b\,^3\Pi$ is by far the most popular, followed by $A\,^1\Pi$, both corresponding to σ ionization. As for CO, this orbital is dominated by O $2p\sigma$, and as end-on ionization is again expected to be favored, near-linear $He^* \cdots ON$ geometries should be most conducive to reaction. NO's dipole ($\mu = 0.15$ D) is only slightly larger than that for CO, but in this case puts the negative charge on O, further enhancing hybridization of He* and thereby encouraging close approach on the O end. As for O_2, symmetry restrictions, although weakened for perpendicular geometry, simultaneously inhibit ionization out of π^* and electron transfer into this orbital. Because no incoming spin states are excluded from ion-pair formation for ^3S, preferential reduction of particular discrete vibronic features in PIES is not expected on this account for NO. The "covalent" properties just discussed are considered a more likely origin of the observed propensity for forming the b and A states of NO^+. Vibronic energy shifts are much as for O_2, small and positive for all but the X state, which is nearly zero.

$He^*(2\,^1S) + NO$ Penning ionization electron spectra have not been published, though presumably a picture of the interacting ^1S and ^3S covalent-ionic crossings similar to that of Leisin *et al.* (1982) for O_2 may be drawn. In this case the ion-pair states are doublet or quartet, while the incoming $He^* + NO(^2\Pi)$ surface is a doublet for ^1S and doublet or quartet for ^3S. Thus ^1S can feed only into the doublet ion-pair state and conserve spin. Since all ^3S incoming states can form ion pairs, the second crossing is again always feasible.

As for NO, recent published beam studies on N_2O and CO_2 Penning ionization have focused on Ne* $Q_I(E)$; these measurements display very similar negative energy dependence, but again appreciably larger $Q_I^{(0)}$. Unpublished He* results (Sperlein, 1986) still indicate differences between ^1S and ^3S in both magnitude [ratio 2.0(2) for both molecules] and energy dependence, but the latter is less than for N_2. He* PIES data (Hotop *et al.*, 1979) do not include a detectable continuum, indicating negligible direct influence of ion-pair states; the results can thus be discussed entirely in terms of nonbonded interactions. All energetically open ion states for He* Penning ionization ($\tilde{X}\,^2\Pi$, $\tilde{A}\,^2\Sigma^+$, $\tilde{B}\,^2\Pi$ for N_2O^+; $\tilde{X}\,^2\Pi_g$, $\tilde{A}\,^2\Pi_u$, $\tilde{C}\,^2\Sigma_g^+$ for CO_2^+) are found with comparable intensities. The substantial prohibition of π ionization found for N_2 and CO does not generalize. This equalization probably originates from the more attractive potential surfaces in these systems as well as the delocalization of the π molecular orbitals. However, when the integrated band intensities are compared to those from

photoelectron spectroscopy, significant enhancement of the Σ states is found, by a factor of three for the $\tilde{A}$ state of N_2O^+, ten for the $\tilde{C}$ state of CO_2^+, again hinting at a more favorable end-on approach for Penning ionization that preferentially removes σ electrons. In their PIES time-of-flight study of $He^*(2\,^3S)+CO_2$, in which final electronic states were resolved, Ohno, Takami, and Mitsuke (1991) found that the Π-state cross sections increase mildly with energy, while the Σ states remain nearly constant. This correlates well with the mildly enhanced PIES intensities for the Σ states. The PIES line shifts for all states are small and slightly negative ($\varepsilon-\varepsilon_0\approx 0.0$ to -0.5 kcal) for both N_2O and CO_2. As for the other closed-shell partners, PI angular distributions for $He^*(2\,^1S)+CO_2$ (presented in Haberland *et al.*, 1981) show strongly forward scattering, but in this case with $E'\approx E$, consistent with the near-zero PIES shifts.

Penning ionization of C_2H_2 provides an interesting contrast with N_2 and the other molecules of this section, the $He^*(2\,^3S)+C_2H_2$ PIES (Ohno, Mutoh, and Harada, 1983) showing a 2:1 ratio of π_u intensity to either σ_g or σ_u, similar to photoelectron spectroscopy and as might be predicted just from the number of electrons of each type. The return of the π intensity correlates with a reversal of the sign and reduction in magnitude of the quadrupole moment from that of the isoelectronic N_2 due to the somewhat positive H termini. C_2H_2 also shows, among small molecules, the best agreement with the exterior-electron-density model, implying that the "van der Waals surface" obtained from atomic radii is somewhat more realistic in this case; this situation persists for larger hydrocarbon partners (Ohno *et al.*, 1984b). For $Ne^*+C_2H_2$, the magnitude and energy dependence of Q_I (Aguilar, Brunetti, *et al.*, 1990) are closer to those of O_2 and NO than to N_2.

Observation of different $Q_I(E)$ behavior in Ne* ionization, smaller and increasing Q_I for H_2, N_2, and CO on the one hand, and larger and slowly decreasing Q_I for O_2, NO, N_2O, and CO_2 on the other, has elicited different interpretations from van den Berg *et al.* (1987) and Appolloni *et al.* (1988). The former authors invoke σ vs π orbital ionization as the differential factor, while the latter cite ion-pair formation, at least for O_2 and NO. It seems, in light of the other findings discussed in this section, that a combination of ion-pair states for O_2 and NO, whose avoided crossings with entrance-channel surfaces must soften the repulsion for those states affected by them, and overall greater van der Waals and Ne* hybridization-induced attraction for N_2O and CO_2, is responsible. Although the Ne* $2p$ hole is allowed by symmetry to interact with either σ or π partner orbitals in either end-on or broadside attack, the Ne^*+Ng results suggest that $2p\sigma$ exchange will dominate, leading to the same symmetry-determined propensities found in the He* systems, namely, predominantly molecular σ ionization in all cases. For all these partners, σ ionization is near threshold but always open, making the assumption of only π ionization in the latter group of reagents questionable at best. Further Ne* PIES measurements are needed to establish relative σ and π populations.

2. He^*, Ne^*+HCl, HBr

Molecular-beam studies on these systems hearken back to the earliest years of the alkali age, when the K+HBr reaction (Taylor and Datz, 1955) was of abiding interest. However, the focus of recent Ng* beam work, Tables II and III, has naturally been on Penning ionization and related processes. Nonetheless it seems that these modern Ng^*+HX experiments carry information relating to the bellwether M+HX systems beyond that embodied in studies of those reactions themselves. The hydrogen halides present a highly dipolar version of the halogen's noble-gas neighbor ($\mu=1.08$ D for HCl, 0.82 D for HBr), and it might be anticipated that the halogen end is significantly more attractive, especially for $He^*(2\,^1S)$, due to increased hybridization of Ng*. Ion-pair formation may also be of importance, though the question of the electron affinities of the HX family is still unsettled.

Under the perhaps dubious assumption that all of the quenching of He* by HCl and HBr occurs as Penning ionization, the thermal Q_I's are among the largest yet measured, 145 Å^2 for ^1S+HCl, 62 Å^2 for ^3S; and 180 Å^2 for ^1S+HBr, 80 Å^2 for ^3S (300 K k_Q measurement of Bush *et al.*, 1973). As in every other He* system thus far considered, ^1S ionizes more efficiently, here by a factor of 2.3 for both HCl and HBr. Q_I for mixed-beam Ne^*+HX is considerably smaller, 23 Å^2 for HCl and 34 Å^2 for HBr, as measured in crossed beams at $E=1$ kcal by Aguilar, Bianco, *et al.* (1990). Unpublished state-selected results of Pazun *et al.* (1992) yield fine-structure ratios $R_{02}=1.0(1)$ for HCl, 1.2(1) for HBr at $E=1.5$ kcal; the lack of a spin-orbit effect for HCl contrasts with the Ar result. The He^*+HCl Q_I declines steeply with energy (Parr *et al.*, 1979), much faster than expected for an r^{-6} long-range interaction, while that for Ne^*+HCl, HBr shows a slower decline more compatible with van der Waals capture (Aguilar, Brunetti, *et al.*, 1990).

Recently a number of molecular-beam optical as well as electron spectroscopy studies for these systems have appeared. Ionization of the singly bonded HX produces only the two known bound ionic states $X\,^2\Pi$ and $A\,^2\Sigma^+$, corresponding to the removal of a nonbonding π electron from the halogen $np\pi$ lone pairs and a bonding σ electron, respectively. As expected based on Franck-Condon factors, X-state production is accompanied by little apparent vibrational excitation, with $P(v'=1)/P(v'=0)=0.043$ for $He^*(2\,^3S)+HCl$ (Yencha *et al.*, 1989), lower than that from He I photoelectron spectroscopy by a factor of two. However, Yencha *et al.* find a long, low-intensity vibrational progression out to $v'=6$, where the intensity relative to $v'=0$ has fallen to 0.002. The A state, which has been observed in both electron and optical spectroscopy (Simon *et al.*,

1988) with ^3S, has an extensive vibrational band, $v'=0-12$ observed, peaked at $v'=1$, with populations shifted somewhat to lower v' than either photoelectron spectroscopy or the Franck-Condon envelope, behavior analogous to the H_2 system. The He*($2\,^1S$)+HCl electron spectrum, however, is anomalous in appearance, with a broad, almost structureless X-state peak encompassing $v'=0$ and 1, while the A state shows an apparent continuum underlying a set of v' peaks, 0–3 resolved, with intensities substantially shifted toward $v'=0$ compared to ^3S. More detailed information could not be obtained owing to the low ^1S intensity and overlap with ^3S features. Yencha *et al.* also reported J-state-selected Ne*+HCl electron spectra, whose vibrational populations for X and A are more comparable to those for ^3S, save for an energetic limitation to $v'\leq 2$ in the A state.

The PIES experiments were of the beam/gas-cell variety, contributing to the observed 1.4-kcal FWHM linewidths for ^3S+HCl and the asymmetric 2.2-kcal widths for Ne*+HCl. Nonetheless the spin-orbit doublet in HCl^+ $X\,^2\Pi_{3/2,1/2}$, splitting 1.9 kcal, was readily resolved for both He* and Ne* and displayed unequal fine-structure state populations in both systems. For ^3S, the population ratio $R'_{3/2,1/2}$ was 1.8(1) for $v'=0$ and dropped rapidly toward unity in the low-intensity tail to high v', while for Ne*, $^3P_0$ yielded $R'=2.3(1)$ and $^3P_2$ 0.88(5). The difference between Ne* J states is reminiscent of the anomaly found for Ar. The analogy is strengthened when we note that Π state production occurs out of Cl 3p *atomic* orbitals, thus allowing for interference of σ and π amplitudes much as in Ar. A possible scheme for making the analogy more quantitative is suggested by the propensity for σ-like exchange interactions, which would require a roughly L-shaped H-Cl-Ne* complex to allow the efficient extraction of a π electron from HCl. With respect to the Ne*-Cl axis, HCl now appears as an Ar atom with one lopsided $3p\pi$ orbital, the one bonded to H. For Ar, Eqs. (4.9) show that the coupling to $J'=\frac{3}{2}$ gives rise almost exclusively to $\Omega_{Ne^*Ar}=\frac{1}{2}$; when reprojected onto the perpendicular H-Cl axis, this yields $\Omega_{HCl}=\frac{3}{2}$. For the perpendicular geometry we may therefore associate the J' states of Eqs. (4.9) and (4.10) nearly uniquely with the corresponding Ω_{HCl} values. A similar line of reasoning for He*+HCl again suggests that the contribution from $J'=\frac{3}{2}$, $\Omega_{HCl}=\frac{1}{2}$ will be missing; as there is no σ-π interference for He*, the deletion of half the $\Omega=\frac{1}{2}$ products leads to the prediction $R'=2$, in fair agreement with observation.

Yencha *et al.* (1989) also report a weak threshold at $\varepsilon=1.5$ eV followed by a continuum extending to $\varepsilon=0$ for He*($2\,^{1,3}S$)+HCl. Overlying the continuum are a series of sharp features that are assignable to Cl**[$3p^4(^1D_2)nl$] doubly excited, autoionizing Rydberg states. *Ab initio* calculations of Someda *et al.* (1989) for ^3S+HCl show several dissociative doubly excited states of HCl nearly resonant with the incoming state, whose mainly repulsive interactions with He are calculated to result in avoided crossings on the repulsive limb of the incoming potential. One or more of these states are likely candidates for $Cl^{**}\rightarrow Cl^+ + e^-$. Considering the minor ^1S component in the beam, the apparent substantial enhancement of these features in the mixed beam implies higher relative branching into these states for ^1S, as might be expected because of its higher energy and the consequently larger number of HCl** states available. The energy of Ne* on the other hand is well below threshold for accessing these states, and no evidence of a continuum is seen in the spectrum.

Currently the best available probes of the nature of the incoming potential surfaces are the PIES line shifts. For He*($2\,^3S$)+HCl they are found to be identical, −1.8 kcal, for the X and A states; for He*($2\,^1S$)+HCl they are highly uncertain due to the peculiar line shapes; and for Ne*+HCl they are also nearly identical for X and A, but positive, 0.6 kcal for $^3P_0$ and 0.4 kcal for $^3P_2$. The negative shifts for ^3S indicate substantial attraction, larger than expected for a nonbonded interaction or by comparison with ^3S+Ar. In this case the dispersion force is augmented by permanent-dipole/induced-dipole attraction, and a further contribution, mentioned at the start of this subsection, may arise from the expected substantial He* 2s-2p hybridization occurring for collisions on the Cl end due to the dipole moment. It may be—calculations of the sort that revealed the hybridization effect in the Ng and H_2 systems not yet having been performed—that the descreening of the He^+ClH ion-dipole attraction that accompanies hybridization accounts for the major part of the attractive well, implied to be greater than 2 kcal by the observed shifts. Indeed, the rapid falloff of the He*+HCl Q_I with E is more consistent with an ionic interaction than with a neutral one, and the comparatively broad PI electron spectral lines, especially for ^1S, where hybridization is expected to be more extensive, also bespeak an additional attractive contribution. For Ne*+HCl, on the other hand, the positive shifts are somewhat smaller than, but typical for, a normal repulsive wall for a closed-shell reagent. As orbital propensities suggest that, for both He* and Ne*, collinear Ng*ClH should populate $HCl^+(A)$ and, as already mentioned, perpendicular should yield $HCl^+(X)$, the nearly identical shifts for each state suggest that V_0 is nearly spherical, at least for those geometries that readily lead to Penning ionization. While orbital symmetry does not forbid Penning ionization for collinear Ng*HCl, it is expected that an approach on the H end will be considerably less attractive, as the positive end of the dipole will inhibit antibonding hybridization, with the end-to-end anisotropy increasing in the sequence Ne*, He*($2\,^3S$), He*($2\,^1S$). Further, collinear Ng*HCl is optimal for ion-pair Ng^+HCl^- formation, due to maximized overlap of the promoted electron orbital with the lowest unoccupied orbital σ^* of HCl.

In terms of ionization energy and polarizability (see Table I), Ne* is much like its neighboring alkali atom

Na, but He*($2\,^3S$) is more like K than Li, while He*($2\,^1S$) is more like Cs. This implies that the ion-pair channel, which is activated upon reaching the covalent-ionic crossing radius $r_x \approx 14.4$ eV Å/$[IE(\mathrm{Ng}^*) - EA(\mathrm{HCl})]$, should be increasingly important in the Ne*, He*($2\,^3S$), He*($2\,^1S$) sequence. The long, low-intensity tail in the X-state v' distribution for ^3S + HCl is plausibly due to the ion pair, whose formation would stretch the HCl bond prior to Penning ionization, as well as break the connection between incoming geometry and final product state. This extra tail is notably absent in the Ne* + HCl PIES and is thus far unobserved in ^1S + HCl due to low signal, although portions of the anomalously broad X- and A-state vibronic lines from ^1S might be due to Penning ionization from the ion-pair surface.

The Ne* + HBr system currently appears to be a case in which substantially different vibronic populations in the A state of HBr^+ are observed in PI electron and optical spectroscopy (Tyndall *et al.*, 1984); other systems, notably He* + HCl, where such differences were thought to exist, proved to be cases where relaxation in secondary collisions in flowing-afterglow PI optical experiments was important (de Vries *et al.*, 1984). As for HCl, $HBr^+(A\,^2\Sigma^+)$ is expected and observed to be predominantly vibrationally excited in PIES (Čermák, 1976), but is found to be relaxed to mainly $v'=0$ and 1 in crossed-beam optical spectroscopy, with $P(v'=1)/P(v'=0) = 0.75(5)$ (Tyndall *et al.*, 1984). The smaller HBr dipole vs HCl and the less hybridizable Ne* may combine to make A-state ionization via a Ne*HBr collinear complex more likely. Then the greater likelihood of $V \rightarrow T$ or $V \rightarrow R$ transfer, due to the small mass of the central H atom, would enhance relaxation of HBr. If this explanation is realistic, even greater relaxation effects should be observed in HI; unfortunately $HI^+(A)$ is strongly predissociated, and the $A \rightarrow X$ emission spectrum shows no vibrational structure.

Hotop *et al.* (1975) reported product mass spectra for He*($2\,^{1,3}S$) + HCl that showed the ions HCl^+, Cl^+, HeH^+, and H^+ in the proportions 1.00:0.13:0.04:0.02 for ^3S and 1.00:0.40:0.05:0.06 for ^1S. Oddly, the associative ion $HeHCl^+$ was not seen, even though there is appreciable intensity in $v'=0$ for both the X and A states, while production of the rearrangement ion HeH^+, a possible sink for nascent associative ions, is energetically possible only in the A state. Cl^+ production levels correlate well with the relative intensity of the PIES autoionization features.

3. He*, Ne* + Cl_2

These systems present the closest connections to the prototypical alkali-halogen harpooning reactions (Herschbach, 1966). Few published measurements exist; for He* + Cl_2 we have the PIES, ion-electron coincidence, and optical spectroscopy studies of Kischlat and Morgner (1983), Leisin, Morgner, and Seiberle (1985), and Benz and Morgner (1986a), while for Ne* + Cl_2 Aguilar, Bianco, *et al.* (1990) have measured $Q_I = 47$ Å^2 at $E = 1$ kcal, and Aguilar, Brunetti, *et al.* (1990) its energy dependence, which is more rapidly falling than Ne* + HCl.

Morgner and co-workers find a PI electron spectrum dominated by low-energy electrons in a broad continuum with a shallow threshold at $\varepsilon \approx 4$ eV and a second, sharper threshold with superimposed sharp structure for $\varepsilon < 1.45$ eV. The He I photoelectron spectrum of Cl_2 shows three main peaks assigned to the $X\,^2\Pi_g$, $A\,^2\Pi_u$, and $B\,^2\Sigma_g^+$ states of Cl_2^+ in the intensity ratio 1.00:0.55:0.15, corresponding to the removal of a π_g^*, π_u, and σ_g electron, respectively. Relative to the continuum, PIES shows weak intensities at the energies expected for these states with greatly altered ratios, 1.00:1.40:0.24 for ^1S and 1.00:4.43:0.005 for ^3S. The strongly favored π_u ionization contrasts with the results for N_2 and the other σ/π donors, but as Kischlat and Morgner (1983) point out, the expected highly probable ion-pair $He^+Cl_2^-$ production by electron transfer from He* $2s$ to Cl_2 σ_u^* is symmetry forbidden in a one-electron approximation for a broadside C_{2v} approach of He* to Cl_2. The PIES populations should therefore be regarded as showing suppression of σ_g ionization, which would occur most probably in collinear geometry, and π_g^*, which might be restricted to an oblique C_s approach, rather than enhancement of π_u. The electron jump occurs at such large distances ($r \gtrsim 5$ Å) that few collisions survive for the latter approach geometries to distances small enough for "covalent" PI to occur.

As outlined briefly in Sec. III.C, Morgner and coworkers have constructed a classical trajectory model that allows simulation of the smoothly undulating continuous spectrum below $\varepsilon = 4$ eV, by including direct transitions between $He^+Cl_2^-$ and $HeCl_2^+ + e^-$ with realistic Cl_2^+ potentials and adjustable channel-specific widths. The B state of Cl_2^+, along with transitions to Cl_2^{**} states (which correspond to negative ε in the model) were found to contribute to the intense structure for $\varepsilon < 1.45$ eV, nearly all of which results in Cl^+ production; as in HCl PI, the 1.45 eV threshold corresponds to formation of the $Cl^+(3p^4\,^3P_2)$ ground state.

The combination of the intense experimental signals and the success of the modeling assures that the rate of autoionization of $He^+Cl_2^-$ is competitive with the harpooning reaction to form $He^+Cl^- + Cl$. The power of PIES and ion-electron coincidence studies as forms of transition-region spectroscopy is thus particularly well illustrated by this example, in which electron emission from the ion-pair reaction intermediate actually dominates the spectrum. Information about the ionic portion of the corresponding alkali-halogen reaction dynamics still must be inferred from product distributions, and very likely would be difficult to obtain by the emerging optical methods for transition-region spectroscopy (Brooks, 1988), because the system spends so little time in the steeply attractive region of the potential surface.

4. $He^* + H_2O$, H_2S, NH_3

In this section, which represents within the scope of this review the only examination in any detail of nonlinear molecular partners, PIES experiments and their offshoots, the only recent studies performed for H_2O, H_2S, or NH_3, will be highlighted. For $He^*(2\,^3S) + H_2O$ the most recent published PIES spectra (Ohno, Mutoh, and Harada, 1983; Haug *et al.*, 1985) agree closely, while the line intensities, positions, and widths differ substantially from photoelectron spectroscopy. The $\tilde{X}\,^2B_1$, $\tilde{A}\,^2A_1$, and $\tilde{B}\,^2B_2$ states of H_2O^+ are readily assigned, corresponding to removal of b_1 and a_1 nonbonding (lone pair) and b_2 bonding electrons, all arising from H(1*s*) and O(2*p*) AO's in the minimal molecular-orbital picture. The photoelectron spectrum shows $\tilde{X}:\tilde{A}:\tilde{B}$ ratios of 1.00:1.06:0.88, while ^3S PIES yields 1.00:1.63:0.61; the lone pair orbitals are thus enhanced in PI, as expected owing to the more extensive hybridization of the He* 2*s* orbital when approaching the negative end of the large H_2O dipole ($\mu = 1.85$ D). One might anticipate a larger than usual anisotropy and attraction in this case due to the large dipole and short bonds, yielding a relatively high concentration of charge on O ($\sim -0.8e$ in a point-charge model). This expectation is confirmed by the breadth of the vibrational peaks (~ 6 kcal) which are largely unresolvable in the spectrum, and the substantial -10 kcal line shifts observed for the $\tilde{X}$ and $\tilde{A}$ states. In more recent PIES time-of-flight (PICSES) studies, Mitsuke, Takami, and Ohno (1989) have found negative energy dependences for all H_2O^+ product states, but more steeply so for $\tilde{X}$ and $\tilde{A}$, which supports the conclusions drawn from PIES. State-resolved electron angular distributions reported in the same paper are nearly identical for $\tilde{X}$ and $\tilde{A}$, showing weak angle dependence peaking at 90° with approximate forward-backward symmetry, while weak backscattering occurs for $\tilde{B}$. This also indicates attraction for $\tilde{X}$ and $\tilde{A}$, but at least some contribution from repulsive Penning ionization for $\tilde{B}$, which would lessen the decline in $Q_I(E)$ as observed.

These results may be revealingly compared to similar measurements for H_2S (see Table II). First, though the orbital configurations and symmetries are the same as in H_2O, the dipole moment of H_2S is little more than half that of H_2O despite the longer bonds; second, the larger sulfur atom orbitals tend to dominate to a greater extent the MO shapes (Ohno, Mutoh, and Harada, 1983); and third, the overall electron density is considerably less compact. The first and third differences should reduce the extent of He* 2*s* orbital hybridization relative to H_2O, and the second should make it less orientation dependent. Observed PIES populations are very similar to those in photoelectron spectra—partially resolved vibronic lines and relatively small -2-kcal line shifts. State-resolved $Q_I(E)$ shows negligible state differences, though the falloff with energy again suggests an ion-induced dipole interaction, $s \sim 4$. Electron angular distributions are weakly backward biased for all states, again implying some contribution from repulsive Penning ionization. The results all point to a more isotropic V_0 for H_2S.

Haug *et al.* (1985) also present an *ab initio* calculation of the V_0 surface for $He^* + H_2O$, which shows a deep 14-kcal potential well for the approach of He* from the O end (He*-O distance only 2.2 Å), slightly out of plane from a pure C_{2v} symmetry. Further He*-OH_2 out-of-plane bending is only weakly constrained, and the well is still 10-kcal deep for an approach of He* along the axis of the nonbonding O 2*p* orbital perpendicular to the molecular plane. Weak repulsion is found for a C_{2v} approach from the H end, reaching 2 kcal only when the He*-H distance is 2.6 Å. These approach distances are smaller and the attractive energies much larger than those inferred from any sort of van der Waals interaction and are consistent with the broad, shifted lines in PIES. Substantial contributions from ion-pair production seem to be ruled out by the apparent lack of any such influence in the *ab initio* study and the good agreement between H_2O^+ vibrational populations in PIES, obtained by modeling the unresolved envelopes, with those from photoelectron spectroscopy.

Like H_2O, NH_3 has a substantial dipole ($\mu = 1.49$ D) and is also the archetype for organic amine bases. Two states, $\tilde{X}\,^2A_1$ and $\tilde{A}\,^2E$ (in C_{3v} symmetry) of NH_3^+, may be formed, and both photoelectron spectroscopy and $He^*(2\,^3S)$ PIES (Ohno, Mutoh, and Harada, 1983) show broad vibrational bands for each state, the $\tilde{X}$ band consisting largely of the umbrella-mode progression. As for H_2O, individual vibronic peaks are unresolved in PIES, but the width and shape of the envelopes suggests a relatively unperturbed Franck-Condon-like ionization. The a_1 lone pair orbital is enhanced in PIES, as for H_2O, but by a somewhat smaller factor. A substantial -10-kcal attractive line shift in the $\tilde{X}$ state suggests a hybridization-induced attraction similar to that found for H_2O. These results imply comparable donative capacity for the NH_3 a_1 and H_2O b_1 lone pairs, though NH_3 is of course a stronger base than H_2O in aqueous solution.

Owing to the contributions from collisions of lower symmetry in the bent-molecule case, orbital selectivity is expected to decline. For a C_{2v} molecule such as H_2O, the exchange model still forbids ionization in certain cases, for examples b_1 and b_2 orbitals for C_{2v} complex symmetry (He* along the C_{2v} axis); but the general expectation is that the influence of the combination of anisotropy in V_0 and orbital selection rules on the relative populations of the ion states will be weaker, since it is more likely that low-symmetry orbitally allowed ionizing configurations for all orbitals will be sampled by the attractive complexes. Thus the great disparity in state populations found for N_2, for example, does not occur for H_2O, nor for the most part for other larger nonlinear molecules, except in cases where an orbital is well localized. This decline in selectivity is expected to be accompanied by increasing linewidths in PIES, for if symmetry restrictions are weakened or absent, ionization of a particular

orbital may be allowed for a wider range of complex geometries, and the angular as well as radial dependence of V_0 will then be mapped into the linewidth. The $\tilde{B}$ state of H_2O^+, for example, probably is formed in both attractive and repulsive regions of V_0, adding to the vibronic linewidth on both the low- and high-energy side of the nominal line position ε_0.

F. Higher excited states

Table IV includes citations of recent work on nonmetastable atom Penning ionization; the earliest beam studies of laser-excited Ne Penning ionization were reported by Hotop (1980), who presented $Ne^{**}(3p\ ^3D_3)$ PIES data with Kr and N_2 partners. The metastable states of the noble gases provide excellent platforms from which their higher excited states may be formed using infrared-to-visible cw lasers, pumping transitions neighboring those employed in metastable state selection. The $^3D_3$ state of Ne is particularly favorable for such experiments, as it forms a quasi-two-level system with $3s\ ^3P_2$ at a convenient wavelength, 640.2 nm, and because the core $2p$ and valence $3p$ orbitals are aligned with each other, suggesting possibly substantial polarization dependence, as indeed is observed experimentally. This section will therefore focus on $Ne^{**}\ ^3D_3$ PI studies.

In the discharge-beam/gas-cell experiments of Hotop (1980), perpendicular laser excitation with linear polarization perpendicular ($\pi_\perp$) and parallel ($\pi_\parallel$) to the Ne* beam axis, as well as circular polarization (σ_+), was used to vary the M-state populations (see Sec. II.A). The $\pi_\parallel$ and σ_+ Ne*+Kr PI electron spectra were quite similar, despite somewhat different M-state distributions, but the $\pi_\perp$ showed appreciable differences in peak shapes and Kr^+ fine-structure branching. In contrast to the polarized $Ne^*(^3P_2)$ case discussed in Sec. IV.C, here a pronounced difference is expected between the potential curves for the Π-like states, $\Omega=2,3$, excited asymptotically in $\pi_\parallel$ and σ_+ and the Σ-like states, $\Omega=0,1$, excited in $\pi_\perp$. The high-Ω states are more Rydberg-like, reflecting the attractive Ne^++Ng interactions, while the low-Ω are more repulsive. The implied short range of the Π-like states permits ionization into the more strongly attractive regions of the product $Ne+Ng^+(^2P_{3/2,1/2})$ potentials. In more recent work on Ne**+Ar, Bussert, Bregel, Ganz, *et al.* (1985); Bussert, Bregel, Allan, *et al.* (1985); and Bregel *et al.* (1986) have reported PIES data of higher quality over a range of Ne** beam velocities. These experiments included collinear excitation of Ne** with circular polarization and showed resolved fine structure in the peaks that differed substantially between $\pi_\parallel$ and $\pi_\perp$ excitation and between Ar^+ fine-structure states; the same fine structure changed appreciably with collision energy. This structure was undoubtedly connected with the presence of extrema in both $V_0^{(\Omega)}$ and $V_+^{(\Omega')}$ and was qualitatively reproduced in model calculations using straight-line trajectories and semiempirical $V_0^{(\Omega)}$ potentials based on the $Ne^{**}(3p)$-$Na^*(3p)$ analogy.

In recent work Driessen *et al.* (1989), Driessen, Megens, *et al.* (1990), and Driessen, van de Weijer, *et al.* (1990) have studied the polarization dependence of $Q_I(E)$ for Ne**+Ar, Kr, Xe, finding an effect similar to that described for Ne*+Ar in Sec. IV.C. At thermal energy, the low-$|M|$ states ionize more efficiently, with the cross-section ratio $R_{30,33}\equiv Q_I^{(3,01)}/Q_I^{(3,23)}=1.65(6)$; however, at superthermal energy no effect is seen. In $R_{30,33}$ the adjacent $|M|$ states are averaged together to improve statistical reliability; despite this, the effect is larger than that for Ne*+Ar and is well reproduced by an orbital locking model with $V_0^{(\Omega)}$ potentials similar to those of Bregel *et al.* (1986). The total PI cross section $Q_I^{(3)}(E)$ is found to decline steeply with E at low energy, and more slowly at high energy, where it appears to merge with $Q_I^{(2)}(E)$ in both shape and magnitude. These features together suggest the continued dominance of the Γ_Σ width component, coupled with an overall more attractive interaction than Ne*+Ar. The preference for ionization at low $|M|$ appears to be at odds with the less attractive low-Ω potentials; however, the requirement of σ-σ overlap is better met at low Ω, and reaction at large impact parameters b, implied by the large cross sections, tends to reverse the local Ω population from that prepared asymptotically, as discussed in Sec. IV.C.

An even more pronounced enhancement of $Q_I^{(3)}$ relative to $Q_I^{(2)}$ is found in the case of Ne**+H_2, nearly a factor of ten larger at thermal energy, as reported by Bussert *et al.* (1983) in a PIES study. The vibronic H_2^+ lines in the Ne** spectrum are shifted by −4 kcal and broadened to the extent that the higher v' states are barely resolved. In addition, the vibrational populations deviate substantially from Franck-Condon behavior, with enhancement of $v'=0$ and 1. These results were rationalized by the analogy with $Na(3s,3p)+H_2$, where *ab initio* calculations of Botschwina *et al.* (1981) have shown a highly attractive $C_{2v}\ ^2B_2$ potential (well depth 10 kcal) for $Na^*(3p)+H_2$ attributed to the favorable interaction of the Na $3p\ b_2$ (π-like) orbital and σ_u^* on H_2. This interaction leads to H_2 bond stretching as Ne** approaches. Through Franck-Condon factor calculations for stretched H_2, Bussert *et al.* were able to interpret semiquantitatively the enhanced low-v' populations. Part of the attractive energy must also arise from the ion-quadrupole interaction (see the discussion of He^*+H_2 in Sec. IV.B), which is favored both by the perpendicularity of the $3p$ orbital in the $^2B_2$ state, which descreens the Ne^+ core, and by the positive sign of the H_2 quadrupole moment.

For the H_2 system Driessen, Megens, *et al.* (1990) report a weaker but measurable polarization effect, $R_{30,33}=1.22(6)$, at thermal energy. It is remarkable that the effect is seen at all, considering the anisotropy of the presumably analogous Na^*H_2 surfaces. The continued but reduced propensity for low-$|M|$ ionization suggests that the competition between stronger overlap of the a_1

(σ-like) Ne** core with σ_g of H_2 and the more attractive b_2 (π-like) approach may be more balanced than for Ar. As just pointed out, large-b ionization redirects the orbitals in the body frame and might reconcile the bond-stretching effects seen in PIES, expected to occur in a b_2 orientation, with the low-$|M|$ preference, which corresponds asymptotically to a_1. These considerations ignore reaction for other approach geometries.

For $Ne^{**}+N_2$ the B state of N_2^+ lies just 0.196 eV (4.5 kcal) above the incoming electronic energy, a favorable situation for the appearance of autoionizing Rydberg (n^*) states terminating on N_2^+ (B) but decaying into N_2^+ (A and X). Hotop (1980) reported a highly structured PI electron spectrum in the X vibrational band assignable to an $n^*=5-9$ B state Rydberg progression, and speculated that the observed very narrow lines (<0.5 kcal FWHM) arose from $Ne^{**}N_2$-NeN_2^{**} curve crossings in the attractive limb of the incoming potential(s). This would require a $Ne^{**}N_2$ well depth of $\gtrsim 8$ kcal to accommodate the range of Rydberg states assigned.

Due to differential core screening of the nuclear charge, the Ne** $3p$ orbital is far more Rydberg-like than Ne* $3s$; hence all the Ne** interactions discussed here are expected to bear some resemblance to the Ne^+ core ion potentials, unlike those that are known for Ne*. The ion states are not expected to show large splittings between the σ and π orientations of the $2p$ hole, so that splittings among the $V_0^{(\Omega)}$ curves are dominated by the $3p$ orientation. On the other hand, provided the exchange model is still valid for these optical states, the width and its components are expected to depend only on the character of the ion core. This has been exploited in the model calculation of Bussert, Bregel, Ganz, *et al.* (1985) and Driessen, van de Weijer, *et al.* (1990); both studies show that a consistent picture emerges for Ne* and Ne** with Ar using the same Γ_Σ and Γ_Π width components, appropriately mixed, for each system.

V. PARADIGMS FOR PENNING IONIZATION

As the discussion of the previous section was intended to convey, molecular-beam studies have by now provided more than a glimpse into the nature of the Penning process; the powerful and still growing array of reagent preparation and product detection techniques now permits connections to be made among orbital propensities, potential surfaces, and reaction dynamics in ways that are not yet possible in the wider field of chemical dynamics. In this section an attempt will be made to delineate those features, exemplified by the systems chosen for detailed examination in Sec. IV, that appear to cut across a substantial part of the range of small molecular systems discussed there, and that therefore may provide useful paradigms for understanding the Penning ionization of larger molecules.

A. Influence of electronic structure on excited-state forces and dynamics

Save for the open-shell examples of H and M, the bulk of the molecular partners, whose Penning ionization is readily examined in beams, interact with He* and Ne* via nonbonded forces, making the low-energy repulsion important if not dominant in determining Q_I and the dynamics. These forces depend of course on the electronic structures of both the excited atom and the molecular partner. All the evidence currently points to the excited atom as the primary influence, with the parade of partners providing variations on the atomic theme. A negative contribution to the repulsive force is made by the exchange-induced antibonding hybridization of the promoted electron's orbital, whose magnitude increases with decreasing energy gaps among the orbitals mixed by the interaction, in these cases in the order $Ne^*(^3P) < He^*(^3S) < He^*(^1S)$. The decreased repulsion, in addition to allowing deeper penetration and more efficient ionization, inevitably leads to the appearance of some structure, induced by the hybridization-descreened core ion-molecule interaction, whose well typically occurs in the range of r where the repulsion is at thermal-to-intermediate energy. The sharpness of the structure again is inverse to the orbital splitting, with $He^*(^1S)$ yielding notoriously "kinky" potential curves.

The extent of antibonding hybridization is also sensitive to the electron density on the reactant molecule, being greater for larger densities or for those that rise more steeply with decreasing r; on the other hand, charge-depleted regions inhibit hybridization. This variation gives rise to moderate-to-strong anisotropy in the repulsion for diatomic and larger partners. For a given excited atom, this anisotropy is mainly determined by the magnitude and sign of the molecule's lowest-order permanent electric moment.

As shown by the examples given here, repulsive structure in V_0 manifests itself directly in the magnitude and energy dependence of Q_I, as an apparent small activation barrier in the ^1S systems, causing Q_I to rise rapidly from rather small values at low E and level out or crest at an energy corresponding closely to the potential energy of the kink. The rise reflects the rapidly growing fraction of impact parameters b that allow the reagents to approach the structured region of V_0, where the repulsion begins to soften. This is the major factor in the characteristic differences between the Q_I for ^1S and ^3S (and Ne*) already described. Anisotropy is found to mute but not obscure these differences, and local structure in V_0 (r, angles) is readily apparent in the product electronic state selectivity and the energy dependence of line shifts found in PIES.

It seems to hold quite generally that Q_I is dominated by electron-rich regions of the partner, provided the orbitals with significant amplitude in those regions are energetically accessible. It is therefore expected that molecules classified as Lewis bases, typically containing a lo-

calized lone-pair orbital, will show a substantial preference for Penning ionization out of that orbital. It is to be emphasized that this propensity is more likely due to a modification, a softening, of V_0 in the vicinity of the orbital than to the tendency of that orbital to protrude out of some sort of van der Waals contact surface surrounding the lone pair. If the Ng* excited orbital were not able to hybridize, it is quite certain (Siska, 1979b) that electron-rich regions would prove even more repulsive than electron-deficient ones. Thus, instead of a longer orbital "tail," a shorter-range, less repulsive potential surface at particular sites on the molecule seems to govern the final-state preference. That is, V_0 rather than Γ dictates selectivity. This conclusion runs counter to the ideas behind the exterior-electron-density (EED) model (Ohno, Mutoh, and Harada, 1983; Ohno, Matsumoto, and Harada, 1984a, 1984b; Ohno and Ishida, 1986; Ohno, 1988), which assumes that orbitals with the greatest amplitude exterior to the "van der Waals surface," a rigid outline constructed from atomic van der Waals radii, is the major determinant of PI orbital preference. This model may be adequate for unsaturated hydrocarbon partners (Ohno, Matsumoto, and Harada, 1984b), where permanent moments are small or zero, and little variation in the radial dependence of V_0 is expected, but is not expected to be quantitatively realistic in highly dipolar or quadrupolar systems, especially for partners that are strong Lewis bases (Ohno, Imai, *et al.*, 1983; Ohno, Mutoh, and Harada, 1983; Ohno, Takano, and Mase, 1986). More recent cross-section collision energy-dependence measurements of Mitsuke, Takami, and Ohno (1989) may be interpreted as supporting the hybridization model over the EED.

Orbital preferences are also influenced by molecular-orbital nodal properties, as discussed in Secs. IV.D and IV.E. Orbitals with more nodes (such as π^* vs π) appear to ionize less efficiently, owing to destruction of appreciable overlap with the He* $1s$ or Ne* $2p\sigma$ acceptor orbitals. The EED model counts all exterior density regardless of the multilobal nature of the donor molecular orbital. The observed preference for π_s ionization over π_a by He*($2\,^3S$) in the norbornadiene molecule (Ohno, Ishida *et al.*, 1985) may well be traced to the fewer nodes in π_s rather than to a simply greater electron density. The unusually high π density in this molecule may also give rise to hybridization-induced modification of the van der Waals surface, although such effects are not so pronounced for He*($2\,^3S$) as they would be for ^1S.

In the absence of symmetry or nodal effects, whether the interaction is predominantly attractive or repulsive should be reflected in correlations among currently measurable reaction attributes. For example, the negative PIES line shift associated with an attractive V_0 should be accompanied by large Q_I and high relative PI spectral intensity, along with a negative E dependence of both quantities. Moreover this correlation should extend to individual product states in the multiorbital cases, thereby probing the V_0 surface specifically by region. In systems involving potentially structured repulsion, as expected for He*($2\,^1S$), the PI spectral line shift is typically small and nearly E independent, while the spectral intensity and the behavior of Q_I with E will depend sensitively on the energetic location of the structure.

B. Global reaction dynamics

As outlined in Secs. III.B, IV.B, and IV.D, the overall dynamics of the PI event is dominated by the substantial difference in the range of V_0 and V_+, a difference that is anticipated to persist for a large group of closed-shell reaction partners. The only exceptions may be those systems possessing low-energy covalent-ionic surface intersections, or where strongly dipolar or quadrupolar electron distributions greatly reduce the overlap repulsion in V_0. This range disparity neatly divides ionizing collisions into two classes, depending on whether the inward or outward leg of the excited-state trajectory is being traversed when ionization occurs. The inward events, at b sufficiently small as to satisfy the Langevin capture criterion, will almost certainly result in a "strongly coupled collision complex" (Light, 1967), whose fate may be determined only by the conservation laws. The outward transitions, on the other hand, are expected to be describable by simplified two-body-like dynamics even for complex molecular reagents. The strongly forward PI product scattering observed in the systems thus far examined is likely to be dominated by the latter, while the former is probably responsible for the weaker but still appreciable wide-angle product scattering, as well as for flux reaching the RI channel when it is open and possible differences in Penning ion rovibrational state distributions from those expected for a vertical transition.

The pronounced structure in the V_0 repulsion for He*($2\,^1S$) interaction with noble-gas partners, well known owing to the production of a strong repulsive rainbow effect in nonreactive scattering angular distributions, is also expected to make its presence felt in PI product distributions. PIES already provides evidence that such structure is a more general occurrence, yielding vibronic peaks from ^1S ionization that change little in position or width with changing E, a phenomenon interpretable in terms of the energy rainbow effect (see Sec. III.C). PI product angular distributions, as well as recoil energy distributions, are expected to show a repulsive rainbow effect as well, though so far only a hint of this has been observed. Such product rainbows may be prominent in molecular systems even when nonreactive scattering gives little or no indication of their presence, since more pronounced structure in V_0 goes hand in hand with enhanced ionization, which deletes flux from the nonreactive channel and which may occur mainly for a limited range of collision geometries.

C. Electronic angular momentum

The variety of systems discussed in Sec. IV points to an electronic mechanism for Penning ionization that is orbital dominated, yet for several of these, notably Ne* with the heavier noble gases, spin-orbit coupling is significant in both the incoming and outgoing channels. As mentioned in Secs. III.B and IV.C, Morgner (1985) has suggested that, as the Penning electron must depart—in the absence of a core-excited resonance—on a time scale of a few atomic units (10^{-16} s), and the period associated with spin-orbit splittings is at least an order of magnitude longer, the system has no choice but to conserve both orbital and spin angular momentum independently at the instant of transition. In addition, the overlap requirement of the exchange mechanism strongly favors zero projection of both the excited-atom core and the partner valence orbital angular momentum on the intermolecular axis, i.e., σ-like ionization. In this picture, spin-orbit effects govern only the distribution of flux among reagent and product states in accord with the vectorial composition of each. This can give rise to surprising product-state distributions, but these appear readily interpretable by pure orbital transition amplitudes.

As for the promoted electron on the excited atom, even though it typically enters as an s electron, as in the metastable noble gases, it undergoes extensive mixing (hybridization) with other angular momenta during an encounter with a closed-shell molecule. Hybridization must affect the behavior of Γ as well as V_0, by changing the overlap between the excited orbital and the continuum orbital in a distance-dependent way. This "electronic Franck-Condon factor" might be playing a far more important role in the overall picture of the Penning process than has previously been supposed. Orbital mixing involving the promoted electron is also expected to be significant in the production of nonzero Penning electron angular momenta λ, whether the mixing results from a bonding or a nonbonding interaction; in either case, where the electron density is shifted further from the nuclear center of mass, a greater limiting value of λ is anticipated. The occurrence of substantial λ's in Penning ionization is suspected to be a general phenomenon, but one to which the majority of measurements, even in beams, are insensitive, save for angle-resolved product distributions.

VI. PROSPECTS

Predicting the course of scientific endeavor and development in any area is notoriously difficult and likely to be unreliable. But in the field of Penning ionization a number of significant problems remain whose resolution is sure to engender new viewpoints, new capabilities, or new avenues of inquiry, even if it cannot be said with any assurance where these in turn might lead. Quantitative results from quantum chemistry accurate and complete enough to be predictive, the kind of data so useful in other areas of chemical structure and dynamics, are available only in the simplest PI systems, and for these the resonance widths cannot be used for reliable modeling. Proper inclusion of the quantized nuclear motion that occurs in the AI channel may also be needed before even an accurate *ab initio* Γ can be successfully compared with experiment. Recent advances in computing power and algorithmic sophistication make it likely that a new attack on the electronic structure problem would be fruitful; however, marrying the electronic coupling to the nuclear motion will require an analytic reformulation. *Ab initio* treatments that include spin-orbit effects are also sorely needed to aid in understanding the large and growing group of Ne* PI systems that show spin-orbit-dependent cross sections.

The recent increase in the variety and quality of PI experiments documented here suggests that multiproperty analysis to obtain complex potentials will become more common, and the outlook is good for extending such analysis to small molecular partners, where the anisotropy of the interaction is included at least within a sudden approximation. Effective use of product distribution data requires in addition accurate molecular-ion atom potentials as well as the use of the branching formalism discussed in Sec. IV.C. It is hoped that minor extensions of the formalism will also aid in uncovering the origins of the spin-orbit effects in Ne* PI, while the latest electronic structure capabilities may be the best source of reliable product interactions. The experiments that probably have the most to contribute to future developments toward a global model of Penning ionization are those that employ controlled collision energy, preferably scanning a well-defined range of E, and that are differential in two or more variables. Particularly valuable will be coincidence measurements (PIECES) in a wider range of systems and energies, especially when combined with angle-resolved product measurements.

There are several chemical species of great current interest in gas-phase chemical physics that are promising candidates for PI beam studies: cations, anions, van der Waals molecules, and clusters both neutral and ionic. Cations of metal atoms as well as many larger molecules can often be readily ionized further by He*. Polyatomic molecular cations often have structures that are appreciably different from their parent neutrals and are occasionally the subject of some speculation, e.g., "classical" vs "nonclassical" carbocations. Assuming problems with low beam intensities can be overcome (a difficulty molecular beamists have always faced), Penning ionization of cations might provide new information on questions of electronic structure, such as charge delocalization, as well as molecular geometry. The new ionic entrance channel interaction would be expected to increase the cross section as well as alter the dynamics and orbital selectivity. Most of these remarks also apply to the anion case—which may be referred to as a "Penning detachment" reaction, as the molecular products are neutral—save that many more excited atoms are now eligible

reagents due to the generally low (≤ 4 eV) detachment energies, and the cross sections may be even larger than for cation partners. (These larger cross sections should offset to some extent the expected deficit in beam intensity.)

PIES measurements have proven sensitive to the environment of an ionizable orbital, particularly in the lone-pair case, as demonstrated, for example, by the reduction of lone-pair intensity due to intramolecular hydrogen bonding observed by Ohno, Imai, and Harada (1985). Findings such as this signal that such measurements on van der Waals dimers, for example, might reveal direct evidence of orbital involvement in intermolecular bonding, a feature that can generally only be inferred from measured average geometries derived from more conventional spectroscopies. Other PI studies may also provide information on the intermolecular ion-molecule interaction that ensues and that must occur with very low initial energy. The sensitivity to orbital environment should carry over to both homogeneous and heterogeneous molecular clusters, with the hope of delineating "surface" and "interior" orbitals. Of particular interest are solvation studies (Castleman and Keesee, 1986) where a number of characteristics, such as the degree of embedment of the solute molecule in the cluster and the participation of both solvent and solute orbitals in the interactions, may potentially be probed. These studies might be readily extended to charged clusters of either sign, where issues of charge localization and geometry as well as solvation properties could be probed at an orbital level.

Molecular-beam studies of Penning ionization may be said to form a bridge that reaches from the halcyon days of revisiting the Polanyi flame reactions with a powerful new technique to the orbital-specific probing of large molecules and surfaces with beams of excited atoms. Despite the fundamental questions that remain regarding both the basic theory of the process and its implementation, and despite anomalous experimental observations, the extent of current understanding is now sufficient to allow the landscape to be viewed with some perspective and practical applications to be painted in. The remarkably direct connection now established between molecular-beam observations in Penning systems and the electronic properties of the reacting species suggests that, very much as it has in recent years. the field will continue in a tandem development of basic theoretical description and increasingly complex applications, creating excitement at both ends of the spectrum.

ACKNOWLEDGMENTS

The author gratefully acknowledges the inspiration of his mentors, students, and colleagues over the past 22 years, the duration (thus far!) of his involvement in the study of metastable noble-gas interactions, as well as the nearly continuous support of the National Science Foundation and the Petroleum Research Fund, administered by the American Chemical Society, over the last 18 years at the University of Pittsburgh. Special thanks are due to Dr. M. Bower for help with the literature survey and to Computing and Information Services at the University of Pittsburgh for computing and plotting facilities.

REFERENCES

Abramowitz, M., and I. A. Stegun, 1964, Eds., *Handbook of Mathematical Functions,* Natl. Bur. Stand. (U.S.) Appl. Math. Ser. Vol. 55 (U.S. GPO, Washington, D.C.).

Aguilar, A., S. Bianco, B. Brunetti, M. Gonzalez, and F. Vecchiocattivi, 1990, Mol. Phys.**71**, 897.

Aguilar, A., B. Brunetti, M. Gonzalez, and F. Vecchiocattivi, 1990, Chem. Phys. **145**, 211.

Aguilar-Navarro, A., B. Brunetti, S. Falcinelli, M. Gonzalez, and F. Vecchiocattivi, 1992, J. Chem. Phys. **96**, 433.

Aguilar-Navarro, A., B. Brunetti, S. Rosi, F. Vecchiocattivi, and G. G. Volpi, 1985, J. Chem. Phys. **82**, 773.

Allison, W., J. W. Sheldon, and E. E. Muschlitz, Jr., 1981, J. Electron Spectrosc. Relat. Phenom. **23**, 339.

Alvarino, J. M., C. Hepp, M. Kreiensen, B. Staudenmayer, F. Vecchiocattivi, and V. Kempter, 1984, J. Chem. Phys. **80**, 765.

Anderson, J. B., 1974, in *Molecular Beams and Low Density Gas Dynamics,* edited by P. P. Wegener (Marcel Dekker, New York), p. 1.

Anderson, R. W., and D. R. Herschbach, 1975, J. Chem. Phys. **62**, 2666.

Appolloni, L., B. Brunetti, J. Hermanussen, F. Vecchiocattivi, and G. G. Volpi, 1986, Chem. Phys. Lett. **129**, 287.

Appolloni, L., B. Brunetti, J. Hermanussen, F. Vecchiocattivi, and G. G. Volpi, 1987, J. Chem. Phys. **87**, 3804.

Appolloni, L., B. Brunetti, J. Hermanussen, F. Vecchiocattivi, and G. G. Volpi, 1988, J. Phys. Chem. **92**, 918.

Aspect, A., N. Vansteenkiste, R. Kaiser, H. Haberland, and M. Karrais, 1990, Chem. Phys. **145**, 307.

Bardsley, J. N., 1974, Case Stud. At. Phys. **4**, 299.

Baudon, J., P. Feron, C. Miniatura, F. Perales, J. Reinhardt, J. Robert, H. Haberland, B. Brunetti, and F. Vecchiocattivi, 1991, J. Chem. Phys. **95**, 1801.

Baus, J., A. Benz, and H. Morgner, 1985, J. Phys. B **18**, 2271.

Beckmann, K., O. Leisin, and H. Morgner, 1986, Mol. Phys. **59**, 829.

Beijerinck, H. C. W., 1987, Comments At. Mol. Phys. **19**, 227.

Beijerinck, H. C. W., 1990, in *The Physics of Electronic and Atomic Collisions* (XVI International Conference), AIP Conference Proceedings No. 205, edited by A. Dalgarno *et al.* (AIP, New York), p. 317.

Beijerinck, H. C. W., and N. F. Verster, 1981, Physica C **111**, 327.

BelBruno, J., and J. Krenos, 1983, J. Chem. Phys. **78**, 2800.

Bell, K. L., 1970, J. Phys. B **3**, 1308.

Bellum, J. C., and D. A. Micha, 1977, Chem. Phys. **20**, 121.

Bellum, J. C., and D. A. Micha, 1978, Phys. Rev. A **18**, 1435.

Bentley, J., 1980, J. Chem. Phys. **73**, 1805.

Benz, A., O. Leisin, H. Morgner, H. Seiberle, and J. Stegmaier, 1985, Z. Phys. A **320**, 11.

Benz, A., and H. Morgner, 1986a, Mol. Phys. **57**, 319.

Benz, A., and H. Morgner, 1986b, Mol. Phys. **58**, 223.

Bergmann, K., 1988, in *Atomic and Molecular Beam Methods,* edited by G. Scoles (Oxford University Press, New York/Oxford), Vol. I, pp. 193, 293.

Bernstein, R. B., 1979, Ed., *Atom-Molecule Collision Theory: A*

Guide for the Experimentalist (Plenum, New York).
Bevsek, H. M., D. C. Dunlavy, and P. E. Siska, 1992, unpublished.
Bieniek, R. J., 1974, J. Phys. B **7**, L266.
Bieniek, R. J., 1976, Chem. Phys. Lett. **40**, 72.
Bieniek, R. J., 1978, Phys. Rev. A **18**, 392.
Bieniek, R. J., M. W. Müller, and M. Movre, 1990, J. Phys. B **23**, 4521; **24**, 2247(E).
Birkhofer, H. P., H. Haberland, M. Winterer, and D. R. Worsnop, 1984, Ber. Bunsenges. Phys. Chem. **88**, 207.
Borst, W. L., 1971, Rev. Sci. Instrum. **42**, 1543.
Borst, W. L., 1974, Phys. Rev. A **9**, 1195.
Botschwina, P., M. Meijer, I. V. Hertel, and W. Reiland, 1981, J. Chem. Phys. **75**, 5438.
Bregel, T., W. Bussert, J. Ganz, H. Hotop, and M.-W. Ruf, 1986, in *Electronic and Atomic Collisions,* ICPEAC XIV, edited by D. C. Lorents, W. E. Meyerhof, and J. R. Peterson (North-Holland, Amsterdam), p. 577.
Bregel, T., A. J. Yencha, M-W. Ruf, H. Waibel, and H. Hotop, 1989, Z. Phys. D **13**, 51.
Brion, C. E., W. B. Stewart, D. S. C. Yee, and P. Crowley, 1981, J. Electron Spectrosc. Relat. Phenom. **23**, 399.
Brooks, P. R., 1988, Chem. Rev. **88**, 407.
Brunetti, B., and F. Vecchiocattivi, 1989, *Collision Theory for Atoms and Molecules,* Vol. 196 of NATO Advanced Study Institute, Series B: Physics, edited by F. A. Gianturco (Plenum, New York), p. 413.
Brunetti, B., and F. Vecchiocattivi, 1993, in *Current Topics in Ion Chemistry and Physics,* edited by C.-Y. Ng (Wiley, New York), Vol. 1, to be published.
Brunetti, B., F. Vecchiocattivi, and G. G. Volpi, 1986, J. Chem. Phys. **84**, 536.
Brutschy, B., and H. Haberland, 1977, J. Phys. E **10**, 90.
Brutschy, B., H. Haberland, and F. Werner, 1982, J. Phys. B **15**, 731.
Buck, U., and H. Pauly, 1968, Z. Phys. **208**, 390.
Büermann, L., S. Burdenski, R. Feltgen, and G. Hoffmann, 1987, J. Phys. B **20**, 2809.
Burdenski, S., R. Feltgen, F. Lichterfeld, and H. Pauly, 1981, Chem. Phys. Lett. **78**, 296.
Burkhardt, C. E., M. Ciocca, J. J. Leventhal, and J. D. Kelley, 1990, Phys. Rev. Lett. **65**, 2151.
Bush, Y. A., M. McFarland, D. L. Albritton, and A. L. Schmeltekopf, 1973, J. Chem. Phys. **58**, 4020.
Bussert, W., 1986, Z. Phys. D **1**, 321.
Bussert, W., T. Bregel, R. J. Allan, M.-W. Ruf, and H. Hotop, 1985, Z. Phys. A **320**, 105.
Bussert, W., T. Bregel, J. Ganz, K. Harth, A. Seigel, M.-W. Ruf, H. Hotop, and H. Morgner, 1985, J. Phys. (Paris) Colloq. C1 **46**, 199.
Bussert, W., J. Ganz, H. Hotop, M.-W. Ruf, A. Siegel, H. Waibel, P. Botschwina, and J. Lorenzen, 1983, Chem. Phys. Lett. **95**, 277.
Castleman, A. W., Jr., and R. G. Keesee, 1986, Chem. Rev. **86**, 589.
Čermák, V., 1966, J. Chem. Phys. **44**, 3774, 3781.
Čermák, V., 1976a, J. Electron Spectrosc. Relat. Phenom. **8**, 325.
Čermák, V., 1976b, J. Electron Spectrosc. Relat. Phenom. **9**, 419.
Chang, R. S. F., and D. W. Setser, 1978, J. Chem. Phys. **69**, 3885.
Chen, C. H., H. Haberland, Y. T. Lee, 1974, J. Chem. Phys. **61**, 3098.
Cohen, E. R., and B. N. Taylor, 1987, Rev. Mod. Phys. **59**, 1121.
Cohen, J. S., and N. F. Lane, 1977, J. Chem. Phys. **66**, 586.
Cohen, J. S., R. L. Martin, and N. F. Lane, 1985, Phys. Rev. A **31**, 152.
Cohen, J. S., and B. Schneider, 1974, J. Chem. Phys. **61**, 3420.
Cohen, J. S., and B. Schneider, 1975, Phys. Rev. A **11**, 884.
Daly, N. R., 1960, Rev. Sci. Instrum. **31**, 264.
Dehnbostel, C., R. Feltgen, and G. Hoffmann, 1990, Phys. Rev. A **42**, 5389.
de Vries, M. S., G. W. Tyndall, and R. M. Martin, 1984, J. Chem. Phys. **80**, 1366.
de Vries, M. S., G. W. Tyndall, C. L. Cobb, and R. M. Martin, 1987, J. Chem. Phys. **86**, 2653.
Docken, K. K., and J. Hinze, 1972, J. Chem. Phys. **57**, 4936.
Drake, G. W. F., 1971, Phys. Rev. A **3**, 908.
Drake, G. W. F., G. A. Victor, and A. Dalgarno, 1969, Phys. Rev. **180**, 25.
Driessen, J. P. J., M. P. I. Manders, F. J. M. van de Weijer, G. J. Sandker, W. Boom, H. C. W. Beijerinck, and B. J. Verhaar, 1991, Chem. Phys. **155**, 447.
Driessen, J. P. J., H. J. L. Megens, M. J. Zonneveld, H. A. J. Senhorst, H. C. W. Beijerinck, and B. J. Verhaar, 1990, Chem. Phys. **147**, 447.
Driessen, J. P. J., S. S. Op de Beek, L. M. T. Somers, H. C. W. Beijerinck, and B. J. Verhaar, 1991, Phys. Rev. A **44**, 167.
Driessen, J. P. J., F. J. M. van de Weijer, M. J. Zonneveld, L. M. T. Somers, M. F. M. Janssens, H. C. W. Beijerinck, and B. J. Verhaar, 1989, Phys. Rev. Lett. **62**, 2369; **64**, 2106(E).
Driessen, J. P. J., F. J. M. van de Weijer, M. J. Zonneveld, L. M. T. Somers, M. F. M. Janssens, H. C. W. Beijerinck, and B. J. Verhaar, 1990, Phys. Rev. A **42**, 4058.
Druyvesteyn, M. J., and F. M. Penning, 1940, Rev. Mod. Phys. **12**, 87; **13**, 72(E).
Dunlavy, D. C., H. M. Bevsek, and P. E. Siska, 1992, unpublished.
Dunlavy, D. C., D. W. Martin, and P. E. Siska, 1990, J. Chem. Phys. **93**, 5347.
Dunning, F. B., 1990, in *The Physics of Electronic and Atomic Collisions,* AIP Conference Proceedings No. 205, edited by A. Dalgarno *et al.* (AIP, New York), p. 519.
Dunning, F. B., T. B. Cook, W. P. West, and R. F. Stebbings, 1975, Rev. Sci. Instrum. **46**, 1072.
Dunning, F. B., R. D. Rundel, and R. F. Stebbings, 1975, Rev. Sci. Instrum. **46**, 697.
Dunning, F. B., and A. C. H. Smith, 1971, J. Phys. B **4**, 1696.
Dunning, F. B., A. C. H. Smith, and R. F. Stebbings, 1971, J. Phys. B **4**, 1683.
Düren, R., G. P. Raabe, and Ch. Schlier, 1968, Z. Phys. **214**, 410.
Ebding, T., and A. Niehaus, 1974, Z. Phys. **270**, 43.
Fahey, D. W., W. F. Parks, and L. D. Schearer, 1980a, J. Phys. E **13**, 381.
Fahey, D. W., W. F. Parks, and L. D. Schearer, 1980b, J. Chem. Phys. **72**, 2310.
Falcetta, M. F., and P. E. Siska, 1992, unpublished.
Fano, U., 1935, Nuovo Cimento **12**, 156.
Fano, U., 1961, Phys. Rev. **124**, 1866.
Ferkel, H., R. Feltgen, and D. Pikorz, 1991, Rev. Sci. Instrum. **62**, 2626.
Feshbach, H., 1958, Ann. Phys. (N.Y.) **5**, 357.
Feshbach, H., 1962, Ann. Phys. (N.Y.) **19**, 287.
Foreman, P. B., T. P. Parr, and R. M. Martin, 1977, J. Chem. Phys. **67**, 5591.

Fort, J., J. J. Laucagne, A. Pesnelle, and G. Watel, 1976, Phys. Rev. A **14**, 658.
Fort, J., J. J. Laucagne, A. Pesnelle, and G. Watel, 1978, Phys. Rev. A **18**, 2063.
Fry, E. S., and W. L. Williams, 1969, Rev. Sci. Instrum. **40**, 1141.
Fuchs, V., and A. Niehaus, 1968, Phys. Rev. Lett. **21**, 1136.
Fujii, H., H. Nakamura, and M. Mori, 1970, J. Phys. Soc. Jpn. **29**, 1030.
Fukuyama, T., and P. E. Siska, 1989, J. Chem. Phys. **90**, 7118.
Gardner, J. L., and J. A. R. Samson, 1976, J. Electron Spectrosc. Relat. Phenom. **8**, 469.
Garrison, B. J., W. H. Miller, and H. F. Schaefer, 1973, J. Chem. Phys. **59**, 3193.
Giberson, K. W., L. K. Johnson, M. W. Hart, M. S. Hammond, T. H. Jeys, and F. B. Dunning, 1984, Opt. Commun. **52**, 103.
Gillen, K. T., P. R. Jones, and T. Tsuboi, 1986, Phys. Rev. Lett. **56**, 2610.
Golde, M. F., 1977, in *Gas Kinetics and Energy Transfer,* edited by P. G. Ashmore and R. J. Donovan (The Chemical Society, London), Vol. 2, p. 123.
Goy, W., V. Kohls, and H. Morgner, 1981, J. Electron Spectrosc. Relat. Phenom. **23**, 383.
Goy, W., H. Morgner, and A. J. Yencha, 1981, J. Electron Spectrosc. Relat. Phenom. **24**, 77.
Greeene, E. F., A. L. Moursund, and J. Ross, 1966, Adv. Chem. Phys. **10**, 135.
Gregor, R. W., and P. E. Siska, 1981, J. Chem. Phys. **74**, 1078.
Guberman, S. L., and W. A. Goddard, 1975, Phys. Rev. A **12**, 1203.
Haberland, H., Y. T. Lee, and P. E. Siska, 1981, Adv. Chem. Phys. **45**, 487.
Harada, Y., 1990, Pure Appl. Chem. **62**, 457.
Harada, Y., K. Ohno, and H. Mutoh, 1983, J. Chem. Phys. **79**, 3251.
Hardy, K. A., and J. W. Sheldon, 1984, Phys. Rev. A **30**, 2761.
Harris, R. M., and J. F. Wilson, 1971, J. Chem. Phys. **54**, 2088.
Haug, B., H. Morgner, and V. Staemmler, 1985, J. Phys. B **18**, 259.
Hausamann, D., and H. Morgner, 1985, Mol. Phys. **54**, 1085.
Hazi, A. U., 1978, J. Phys. B **11**, L259.
Hazi, A. U., and H. S. Taylor, 1970, Phys. Rev. A **1**, 1109.
Herschbach, D. R., 1966, Adv. Chem. Phys. **10**, 319.
Hertel, I. V., and W. Stoll, 1978, Adv. At. Mol. Phys. **13**, 113.
Herzberg, G., 1950, *Molecular Spectra and Molecular Structure I. Spectra of Diatomic Molecules,* 2nd ed. (Van Nostrand Reinhold, New York), Chap. V.
Hickman, A. P., A. D. Isaacson, and W. H. Miller, 1977a, J. Chem. Phys. **66**, 1483.
Hickman, A. P., A. D. Isaacson, and W. H. Miller, 1977b, J. Chem. Phys. **66**, 1492.
Hickman, A. P., and H. Morgner, 1976, J. Phys. B **9**, 1765.
Hickman, A. P., and H. Morgner, 1977, J. Chem. Phys. **67**, 5484.
Hijazi, N. H., and J. C. Polanyi, 1975, Chem. Phys. **11**, 1.
Hinchcliffe, A., 1988, *Computational Quantum Chemistry* (Wiley, New York).
Hoffmann, V., and H. Morgner, 1979, J. Phys. B **12**, 2857.
Hotop, H., 1974, Radiat. Res. **59**, 379.
Hotop, H., 1980, in *Electronic and Atomic Collisions,* ICPEAC XI, edited by N. Oda and K. Takayanagi (North-Holland, Amsterdam), p. 271.
Hotop, H., G. Hübler, and L. Kaufhold, 1975, Int. J. Mass Spectrom. Ion Phys. **17**, 163.
Hotop, H., E. Illenberger, H. Morgner, and A. Niehaus, 1971, Chem. Phys. Lett. **10**, 493.
Hotop, H., E. Kolb, and J. Lorenzen, 1979, J. Electron Spectrosc. Relat. Phenom. **16**, 213.
Hotop, H., J. Lorenzen, and A. Zastrow, 1981, J. Electron Spectrosc. Relat. Phenom. **23**, 347.
Hotop, H., and A. Niehaus, 1968, Z. Phys. **215**, 395.
Hotop, H., and A. Niehaus, 1969a, Chem. Phys. Lett. **3**, 687.
Hotop, H., and A. Niehaus, 1969b, Z. Phys. **228**, 68.
Hotop, H., and A. Niehaus, 1970a, Z. Phys. **238**, 452.
Hotop, H., and A. Niehaus, 1970b, Int. J. Mass Spectrom. Ion Phys. **5**, 415.
Hotop, H., and A. Niehaus, 1971, Chem. Phys. Lett. **8**, 497.
Hotop, H., A. Niehaus, and A. L. Schmeltekopf, 1969, Z. Phys. **229**, 1.
Howard, J. S., J. P. Riola, R. D. Rundel, and R. F. Stebbings, 1973, J. Phys. B **6**, L109.
Hulburt, H. M., and J. O. Hirschfelder, 1941, J. Chem. Phys. **9**, 61.
Illenberger, E., and A. Niehaus, 1975, Z. Phys. B **20**, 33.
Inaba, S., T. Goto, and S. Hattori, 1982a, J. Phys. Soc. Jpn. **51**, 627.
Inaba, S., T. Goto, and S. Hattori, 1982b, J. Phys. D **15**, 35.
Isaacson, A. D., 1979, J. Chem. Phys. **71**, 180.
Isaacson, A. D., A. P. Hickman, and W. H. Miller, 1977, J. Chem. Phys. **67**, 370.
Isaacson, A. D., C. W. McCurdy, and W. H. Miller, 1978, Chem. Phys. **34**, 311.
Isaacson, A. D., and W. H. Miller, 1979, Chem. Phys. Lett. **62**, 374.
Ishida, T., and K. Ohno, 1989, Int. J. Quantum Chem. **35**, 257.
Jerram, P. A., and A. C. H. Smith, 1985, J. Phys. B **18**, 1747.
Jesse, W. P., and J. Sadauskis, 1952, Phys. Rev. **88**, 417.
Jordan, R. M., H. R. Siddiqui, and P. E. Siska, 1986, J. Chem. Phys. **84**, 6719.
Kamke, B., W. Kamke, R. Herrmann, and I. V. Hertel, 1989, Z. Phys. D **11**, 153.
Kaufman, V., and L. Minnhagen, 1972, J. Opt. Soc. Am. **63**, 1185.
Keller, W., H. Morgner, and W. A. Müller, 1986a, in *Electronic and Atomic Collisions,* ICPEAC XIV, edited by D. C. Lorents, W. E. Meyerhof, and J. R. Peterson (North-Holland, Amsterdam), p. 605.
Keller, W., H. Morgner, and W. A. Müller, 1986b, Mol. Phys. **57**, 623.
Keller, W., H. Morgner, and W. A. Müller, 1986c, Mol. Phys. **58**, 1039.
Kerstel, E. R. T., M. F. M. Janssens, K. A. H. Van Leeuwen, H. C. W. Beijerinck, 1988, Chem. Phys. **119**, 325.
Khan, A., H. R. Siddiqui, D. W. Martin, and P. E. Siska, 1981, Chem. Phys. Lett. **84**, 280.
Khan, A., H. R. Siddiqui, and P. E. Siska, 1991a, J. Chem. Phys. **94**, 2588.
Khan, A., H. R. Siddiqui, and P. E. Siska, 1991b, J. Chem. Phys. **95**, 3371.
Kimura, M., and N. F. Lane, 1990, Phys. Rev. A **41**, 5938.
Kischlat, W., and H. Morgner, 1983, Z. Phys. A **312**, 305.
Kischlat, W., and H. Morgner, 1985, J. Electron Spectrosc. Relat. Phenom. **35**, 273.
Kołos, W., and H. M. Peek, 1976, Chem. Phys. **12**, 381.
Kraft, T., T. Bregel, J. Ganz, K. Harth, M-W. Ruf, and H. Hotop, 1988, Z. Phys. D **10**, 473.
Kroon, J. P. C., H. C. W. Beijerinck, B. J. Verhaar, and N. F. Verster, 1984, Chem. Phys. **90**, 195.

Kroon, J. P. C., H. C. W. Beijerinck, and N. F. Verster, 1981, J. Chem. Phys. **74**, 6528.
Kroon, J. P. C., A. C. Haverkorn, and H. C. W. Beijerinck, 1986, Chem. Phys. **103**, 119.
Kroon, J. P. C., H. A. J. Senhorst, H. C. W. Beijerinck, B. J. Verhaar, and N. F. Verster, 1985, Phys. Rev. A **31**, 3724.
Kucal, H., D. Hennecart, and F. Masnou-Seeuws, 1990, Chem. Phys. **45**, 163.
Lam, K. S., and T. F. George, 1983, J. Phys. Chem. **87**, 2799.
Lam, K. S., and T. F. George, 1984, Phys. Rev. A **29**, 492.
Lam, K. S., T. F. George, and D. K. Bhattacharyya, 1983, Phys. Rev. A **27**, 1353.
Langhoff, P. W., and C. T. Corcoran, 1974, J. Chem. Phys. **61**, 146.
Lee, Y. T., 1988, in *Atomic and Molecular Beam Methods,* edited by G. Scoles (Oxford University Press, New York/Oxford), Vol. I, p. 553.
Leisin, O., and H. Morgner, 1984, Phys. Rev. A **30**, 2791.
Leisin, O., H. Morgner, and W. Müller, 1982, Z. Phys. A **304**, 23.
Leisin, O., H. Morgner, W. A. Müller, H. Seiberle, and J. Stegmaier, 1985a, Mol. Phys. **54**, 1101.
Leisin, O., H. Morgner, W. A. Müller, H. Seiberle, and J. Stegmaier, 1985b, Mol. Phys. **55**, 225.
Le Nadan, A., G. Le Coz, F. Tuffin, and J. Peresse, 1982, J. Phys. (Paris) **43**, 1607.
Le Nadan, A., G. Le Coz, and F. Tuffin, 1989a, J. Phys. (Paris) **50**, 387.
Le Nadan, A., G. Le Coz, and F. Tuffin, 1989b, J. Phys. (Paris) **50**, 1777.
Le Nadan, A., G. Sinou, and F. Tuffin, 1989, Chem. Phys. Lett. **156**, 24.
Leone, S. R., and V. M. Bierbaum, 1987, Faraday Discuss. Chem. Soc. **84**, 253.
Leu, M. T., and P. E. Siska, 1974a, J. Chem. Phys. **60**, 2179.
Leu, M. T., and P. E. Siska, 1974b, J. Chem. Phys. **60**, 4082.
Levine, R. D., and R. B. Bernstein, 1987, *Molecular Reaction Dynamics and Chemical Reactivity* (Oxford University Press, London).
Light, J. C., 1967, Discuss. Faraday Soc. **44**, 14.
Longley, E. J., M. F. Falcetta, and P. E. Siska, 1992, unpublished.
Lorenzen, J., H. Hotop, and M.-W. Ruf, 1986, Z. Phys. D **1**, 261.
Lorenzen, J., H. Hotop, M-W. Ruf, and H. Morgner, 1980, Z. Phys. A **297**, 19.
Lorenzen, J., H. Morgner, W. Bussert, M.-W. Ruf, and H. Hotop, 1983, Z. Phys. A **310**, 141.
Magnuson, G. D., and R. H. Neynaber, 1974, J. Chem. Phys. **60**, 3385.
Manus, C., A. Pesnelle, and G. Watel, 1978, in *Electronic and Atomic Collisions,* ICPEAC X, edited by G. Watel (North-Holland, Amsterdam), p. 525.
Martin, W. C., 1973, J. Phys. Chem. Ref. Data **2**, 257.
Martin, D. W., D. Bernfeld, and P. E. Siska, 1984, Chem. Phys. Lett. **110**, 298.
Martin, D. W., T. Fukuyama, R. W. Gregor, R. M. Jordan, and P. E. Siska, 1976, J. Chem. Phys. **65**, 3720.
Martin, D. W., T. Fukuyama, and P. E. Siska, 1990, J. Chem. Phys. **92**, 5963.
Martin, D. W., R. W. Gregor, R. M. Jordan, and P. E. Siska, 1978, J. Chem. Phys. **69**, 2833.
Martin, D. W., and P. E. Siska, 1985, J. Chem. Phys. **82**, 2630.
Martin, D. W., and P. E. Siska, 1988, J. Chem. Phys. **89**, 240.
Martin, D. W., C. Weiser, R. F. Sperlein, D. L. Bernfeld, and P. E. Siska, 1989, J. Chem. Phys. **90**, 1564.
McLaughlin, D. R., and D. L. Thompson, 1979, J. Chem. Phys. **70**, 2748.
Merz, A., M. W. Müller, M.-W. Ruf, H. Hotop, W. Meyer, and M. Movre, 1989, Chem. Phys. Lett. **160**, 377.
Merz, A., M. W. Müller, M-W. Ruf, H. Hotop, W. Meyer, and M. Movre, 1990, Chem. Phys. **145**, 219.
Micha, D. A., 1976, in *Dynamics of Molecular Collisions,* edited by W. H. Miller (Plenum, New York), Part A, p. 81.
Micha, D. A., and H. Nakamura, 1975, Phys. Rev. A **11**, 1988.
Micha, D. A., and R. D. Piacentini, 1982, Phys. Rev. A **25**, 204.
Miller, S., J. Tennyson, B. Follmeg, P. Rosmus, and H. J. Werner, 1988, J. Chem. Phys. **89**, 2178.
Miller, W. H., 1966, Phys. Rev. **152**, 70.
Miller, W. H., 1970a, Chem. Phys. Lett. **4**, 627.
Miller, W. H., 1970b, J. Chem. Phys. **52**, 3563.
Miller, W. H., and H. Morgner, 1977, J. Chem. Phys. **67**, 4923.
Miller, W. H., and H. F. Schaefer III, 1970, J. Chem. Phys. **53**, 1421.
Miller, W. H., C. A. Slocomb, and H. F. Schaefer III, 1972, J. Chem. Phys. **56**, 1347.
Minnhagen, L., 1973, J. Opt. Soc. Am. **63**, 1185.
Mitsuke, K., K. Kusafuka, and K. Ohno, 1989, J. Phys. Chem. **93**, 3062.
Mitsuke, K., T. Takami, and K. Ohno, 1989, J. Chem. Phys. **91**, 1618.
Molof, R. A., H. L. Schwartz, T. M. Miller, and B. Bederson, 1974, Phys. Rev. A **10**, 1131.
Moore, C. E., 1970, *Ionization Potentials and Ionization Limits,* Natl. Bur. Stand. (U.S.), Natl. Stand. Ref. Data Ser. No. 34 (U.S. GPO, Washington, D.C.).
Moore, C. E., 1971, *Atomic Energy Levels,* Natl. Bur. Stand. (U.S.), Natl. Stand. Ref. Data Ser. No. 35 (U.S. GPO, Washington, D.C.), Vol. I–III.
Moore, J. H., C. C. Davis, and M. A. Coplan, 1989, *Building Scientific Apparatus,* 2nd ed. (Addison-Wesley, New York).
Morgner, H., 1978, J. Phys. B **11**, 269.
Morgner, H., 1979, J. Phys. B **12**, 2171.
Morgner, H., 1982, Comments At. Mol. Phys. **11**, 271.
Morgner, H., 1984, in *Electronic and Atomic Collisions,* ICPEAC XIII, edited by J. Eichler, I. V. Hertel, and N. Stolterfoht (North-Holland, Amsterdam), p. 451.
Morgner, H., 1985, J. Phys. B **18**, 251.
Morgner, H., 1988, Comments At. Mol. Phys. **21**, 195.
Morgner, H., 1990, Chem. Phys. **145**, 239.
Morgner, H., and A. Niehaus, 1979, J. Phys. B **12**, 1805.
Morgner, H., J. Oberbrodhage, K. Richter, and K. Roth, 1991a, J. Phys. Condens. Matter **3**, 5639.
Morgner, H., J. Oberbrodhage, K. Richter, and K. Roth, 1991b, Mol. Phys. **73**, 1011.
Morgner, H., J. Oberbrodhage, K. Richter, and K. Roth, 1991c, J. Electron Spectrosc. Relat. Phenom. **57**, 61.
Mori, M., 1966, J. Phys. Soc. Jpn. **21**, 979.
Mori, M., 1969, J. Phys. Soc. Jpn. **26**, 773.
Mori, M., and H. Fujita, 1965, J. Phys. Soc. Jpn. **20**, 432.
Mori, M., T. Wanatabe, and K. Katsuura, 1964, J. Phys. Soc. Jpn. **19**, 380.
Müller, M. W., W. Bussert, M.-W. Ruf, H. Hotop, and W. Meyer, 1987, Phys. Rev. Lett. **59**, 2279.
Müller, M. W., A. Merz, M.-W. Ruf, H. Hotop, W. Meyer, and M. Movre, 1991, Z. Phys. D **21**, 89.
Münzer, A., and A. Niehaus, 1981, J. Electron Spectrosc. Relat. Phenom. **23**, 367.

Muschlitz, E. E., Jr., 1966, Adv. Chem. Phys. **10**, 171.
Muschlitz, E. E., Jr., 1968, Science **159**, 599.
Muschlitz, E. E., Jr., 1973, Ber. Bunsenges. Phys. Chem. **77**, 628.
Nakamura, H., 1968a, J. Phys. Soc. Jpn. **24**, 1353.
Nakamura, H., 1968b, J. Phys. Soc. Jpn. **25**, 519.
Nakamura, H., 1969a, J. Phys. Soc. Jpn. **26**, 614.
Nakamura, H., 1969b, J. Phys. Soc. Jpn. **26**, 1473.
Nakamura, H., 1971, J. Phys. Soc. Jpn. **31**, 574.
Neynaber, R. H., 1980, in *Electronic and Atomic Collisions,* ICPEAC XI, edited by N. Oda and K. Takayanagi (North-Holland, Amsterdam), p. 287.
Neynaber, R. H., and G. D. Magnuson, 1975a, J. Chem. Phys. **62**, 4953.
Neynaber, R. H., and G. D. Magnuson, 1975b, Phys. Rev. A **11**, 865.
Neynaber, R. H., and G. D. Magnuson, 1976, J. Chem. Phys. **65**, 5239.
Neynaber, R. H., G. D. Magnuson, and J. K. Layton, 1972, J. Chem. Phys. **57**, 5128.
Neynaber, R. H., and S. Y. Tang, 1978, J. Chem. Phys. **69**, 4851.
Neynaber, R. H., and S. Y. Tang, 1980a, J. Chem. Phys. **72**, 5783.
Neynaber, R. H., and S. Y. Tang, 1980b, J. Chem. Phys. **72**, 6176.
Niehaus, A., 1980, Comments At. Mol. Phys. **9**, 153.
Niehaus, A., 1981, Adv. Chem. Phys. **45**, 399.
Niehaus, A., 1982, in *Electronic and Atomic Collisions,* ICPEAC XII, edited by S. Datz (North-Holland, Amsterdam), p. 237.
Niehaus, A., 1990, Phys. Rep. **186**, 149.
Ohno, K., 1988, Theor. Chim. Acta **74**, 239.
Ohno, K., and Y. Harada, 1991, in *Theoretical Models of Chemical Bonding,* edited by Z. B. Maksic (Springer, Berlin), Vol. 3, p. 199.
Ohno, K., K. Imai, and Y. Harada, 1985, J. Am. Chem. Soc. **107**, 8078.
Ohno, K., K. Imai, S. Matsumoto, and Y. Harada, 1983, J. Phys. Chem. **87**, 4346.
Ohno, K., and T. Ishida, 1986, Int. J. Quantum Chem. **29**, 677.
Ohno, K., T. Ishida, Y. Naitoh, and Y. Izumi, 1985, J. Am. Chem. Soc. **107**, 8082.
Ohno, K., S. Matsumoto, and Y. Harada, 1984a, J. Chem. Phys. **81**, 2183.
Ohno, K., S. Matsumoto, and Y. Harada, 1984b, J. Chem. Phys. **81**, 4447.
Ohno, K., S. Matsumoto, K. Imai, and Y. Harada, 1984, J. Phys. Chem. **88**, 206.
Ohno, K., H. Mutoh, and Y. Harada, 1983, J. Am. Chem. Soc. **105**, 4555.
Ohno, K., T. Takami, and K. Mitsuke, 1991, J. Chem. Phys. **94**, 2675.
Ohno, K., S. Takano, and K. Mase, 1986, J. Phys. Chem. **90**, 2015.
Olson, R. E., F. T. Smith, and E. Bauer, 1971, Appl. Opt. **10**, 1848.
O'Neil, S. V., and W. P. Reinhardt, 1978, J. Chem. Phys. **69**, 2126.
Pack, R. T, 1974, J. Chem. Phys. **60**, 633.
Padial, N. T., J. S. Cohen, R. L. Martin, and N. F. Lane, 1989, Phys. Rev. A **40**, 117.
Padial, N. T., R. L. Martin, J. S. Cohen, and N. F. Lane, 1989, Phys. Rev. A **39**, 2715.
Parker, G. A., and R. T Pack, 1978, J. Chem. Phys. **68**, 1585.
Parr, T. P., D. Hanson-Parr, and R. M. Martin, 1979, in *Eleventh International Conference on the Physics of Electronic and Atomic Collisions,* ICPEAC XI, Abstracts of Contributed Papers, edited by K. Takaynagi and N. Oda (The Society for Atomic Collision Research, Japan), p. 878.
Parr, T. P., D. M. Parr, and R. M. Martin, 1982, J. Chem. Phys. **76**, 316.
Pauly, H., 1988, in *Atomic and Molecular Beam Methods,* edited by G. Scoles (Oxford University Press, New York/Oxford), Vol. I, pp. 83, 124.
Pazun, J. L., K. M. Beer, C. Weiser, and P. E. Siska, 1992, unpublished.
Penning, F. M., 1927, Naturwissenschaften **15**, 818.
Pesnelle, A., and S. Runge, 1984a, J. Phys. B **17**, 4689.
Pesnelle, A., and S. Runge, 1984b, in *Electronic and Atomic Collisions,* ICPEAC XIII, edited by J. Eichler, I. V. Hertel, and N. Stolterfoht (North-Holland, Amsterdam), p. 559.
Pesnelle, A., S. Runge, M. Perdrix, D. Sevin, and G. Watel, 1983, J. Phys. B **16**, L193.
Pesnelle, A., S. Runge, D. Sevin, N. Wolffer, and G. Watel, 1981, J. Phys. B **14**, 1827.
Pesnelle, A., G. Watel, and C. Manus, 1975, J. Chem. Phys. **62**, 3590.
Pollard, J. E., D. J. Trevor, Y. T. Lee, and D. A. Shirley, 1981, Rev. Sci. Instrum. **52**, 1837.
Preston, R. K., and J. S. Cohen, 1976, J. Chem. Phys. **65**, 1589.
Ramsey, N. F., 1956, *Molecular Beams* (Oxford University Press, London).
Rapp, D., and W. E. Francis, 1962, J. Chem. Phys. **37**, 2631.
Rice, O. K., 1933, J. Chem. Phys. **1**, 375.
Riddle, T. W., M. Onellian, F. B. Dunning, and G. K. Walters, 1981, Rev. Sci. Instrum. **52**, 797.
Riley, S. J., P. E. Siska, and D. R. Herschbach, 1979, Faraday Disc. Chem. Soc. **67**, 27.
Riola, J. P., J. S. Howard, R. D. Rundel, and R. F. Stebbings, 1974, J. Phys. B **7**, 376.
Robert, J., V. Bocvarski, B. Stern, J. Reinhardt, and J. Baudon, 1987, Z. Phys. D **6**, 279.
Rosmus, P., and E. A. Reinsch, 1980, Z. Naturforsch. Teil A **35**, 1066.
Rothe, E. W., R. H. Neynaber, and S. Trujillo, 1965, J. Chem. Phys. **42**, 3310.
Ruf, M.-W., A. J. Yencha, and H. Hotop, 1987, Z. Phys. D **5**, 9.
Rundel, R. D., F. B. Dunning, and R. F. Stebbings, 1974, Rev. Sci. Instrum. **45**, 116.
Sachs, E. S., J. Hinze, and N. H. Sabelli, 1975, J. Chem. Phys. **62**, 3367.
Sanders, R. A., A. N. Schweid, M. Weiss, and E. E. Muschlitz, Jr., 1976, J. Chem. Phys. **65**, 2700.
Schaefer, H. F., III, 1984, *Quantum Chemistry: The Development of Ab Initio Methods in Molecular Electronic Structure Theory* (Clarendon, Oxford).
Schall, H., T. Beckert, J. M. Alvarino, F. Vecchiocattivi, and V. Kempter, 1981, Nuovo Cimento B **63**, 378.
Scheibner, K. F., J. S. Cohen, R. L. Martin, and N. F. Lane, 1987, Phys. Rev. A **36**, 2633.
Schmeltekopf, A. L., and F. C. Fehsenfeld, 1970, J. Chem. Phys. **53**, 3173.
Schohl, S., D. Klar, T. Kraft, H. A. J. Meijer, M.-W. Ruf, U. Schmitz, S. J. Smith, and H. Hotop, 1991, Z. Phys. D **21**, 25.
Schohl, S., M. W. Müller, H. A. J. Meijer, M.-W. Ruf, H. Hotop, and H. Morgner, 1990, Z. Phys. D **16**, 237.
Scoles, G., 1988, Ed., *Atomic and Molecular Beam Methods* (Oxford University Press, New York/Oxford), Vol. I.

Sheldon, J. W., and K. A. Hardy, 1983, Phys. Lett. A **98**, 332.
Shimizu, F., K. Shimizu, and H. Takama, 1990, Chem. Phys. **145**, 327.
Sholette, W. P., and E. E. Muschlitz, Jr., 1962, J. Chem. Phys. **36**, 3368.
Siddiqui, H. R., D. Bernfeld, and P. E. Siska, 1984, J. Chem. Phys. **80**, 567.
Siegert, A. J. F., 1939, Phys. Rev. **56**, 750.
Simon, W., A. J. Yencha, M.-W. Ruf, and H. Hotop, 1988, Z. Phys. D **8**, 71.
Siska, P. E., 1973, J. Chem. Phys. **59**, 6052.
Siska, P. E., 1979a, Chem. Phys. Lett. **63**, 25.
Siska, P. E., 1979b, J. Chem. Phys. **71**, 3942.
Siska, P. E., 1984, Comments At. Mol. Phys. **15**, 155.
Siska, P. E., 1986, J. Chem. Phys. **85**, 7497.
Smalley, R. E., D. J. Auerbach, P. S. H. Fitch, D. H. Levy, and L. Wharton, 1977, J. Chem. Phys. **66**, 3778.
Small-Warren, N. E., and L.-C. Y. Chiu, 1975, Phys. Rev. A **11**, 1777.
Smith, G. M., and E. E. Muschlitz, Jr., 1960, J. Chem. Phys. **33**, 1819.
Snyder, H. L., B. T. Smith, and R. M. Martin, 1983, Chem. Phys. Lett. **94**, 90.
Someda, K., N. Kosugi, T. Kondow, and K. Kuchitsu, 1989, J. Phys. Chem. **93**, 35.
Sonnenfroh, D. M., and S. R. Leone, 1987a, J. Chem. Phys. **87**, 5041.
Sonnenfroh, D. M., and S. R. Leone, 1987b, Int. J. Mass Spectrom. Ion Processes **80**, 63.
Sperlein, R. F., 1986, Ph.D. thesis (University of Pittsburgh).
Spiegelmann, F., F. X. Gadea, and M. C. Castex, 1990, Chem. Phys. **45**, 173.
Stebbings, R. F., and F. B. Dunning, 1983, Eds., *Rydberg States of Atoms and Molecules* (Cambridge University, Cambridge, UK).
Szabo, A., and N. S. Ostlund, 1982, *Modern Quantum Chemistry: Introduction to Advanced Electronic Structure Theory* (Macmillan, New York).
Tang, K. T., and J. P. Toennies, 1984, J. Chem. Phys. **80**, 3726.
Tang, S. Y., A. B. Marcus, and E. E. Muschlitz, Jr., 1972, J. Chem. Phys. **56**, 566.
Taylor, E. H., and S. Datz, 1955, J. Chem. Phys. **23**, 1711.
Tellinghuisen, J., A. Ragone, M. S. Kim, D. J. Auerbach, R. E. Smalley, L. Wharton, and D. H. Levy, 1979, J. Chem. Phys. **71**, 1283.
Theuws, P. G. A., H. C. W. Beijerinck, and N. F. Verster, 1982, J. Phys. E **15**, 328.
Theuws, P. G. A., H. C. W. Beijerinck, N. F. Verster, and D. C. Schram, 1982, J. Phys. E **15**, 573.
Tsuji, M., 1990, in *The Physics of Electronic and Atomic Collisions* (XVI International Conference), AIP Conference Proceedings No. 205, edited by A. Dalgarno *et al.* (AIP, New York), p. 342.
Tuffin, F., G. Le Coz, and A. Le Nadan, 1987, J. Phys. (Paris) **46**, 1291.
Tuffin, F., G. Le Coz, and J. Peresse, 1980a, J. Phys. Lett. **41**, 109.
Tuffin, F., G. Le Coz, and J. Peresse, 1980b, C. R. Acad. Sci. Ser. B **291**, 141.
Tuffin, F., G. Le Coz, and J. Peresse, 1981, J. Phys. Lett. **42**, 25.
Tuffin, F., A. Le Nadan, and J. Peresse, 1984, Phys. Lett. A **106**, 23.
Tuffin, F., A. Le Nadan, and J. Peresse, 1985, J. Phys. (Paris) **46**, 181.
Tyndall, G. W., M. S. de Vries, and R. M. Martin, 1984, Chem. Phys. Lett. **110**, 400.
van den Berg, F. T. M., J. H. M. Schonenberg, and H. C. W. Beijerinck, 1987, Chem. Phys. **115**, 359.
Van Dyck, R. S., Jr., C. E. Johnson, and H. A. Shugart, 1970, Phys. Rev. Lett. **25**, 1403.
Van Dyck, R. S., Jr., C. E. Johnson, and H. A. Shugart, 1971, Phys. Rev. A **4**, 1327.
Van Dyck, R. S., Jr., C. E. Johnson, and H. A. Shugart, 1972, Phys. Rev. A **5**, 991.
Vassilev, G., F. Perales, C. Miniatura, J. Robert, J. Reinhardt, F. Vecchiocattivi, and J. Baudon, 1990, Z. Phys. D **17**, 101.
Verheijen, M. J., and H. C. W. Beijerinck, 1984, in *Rarefied Gas Dynamics,* Proceedings of the 14th International Symposium, edited by H. Oguchi (University of Tokyo Press, Tokyo), Vol. 2, p. 1001.
Verheijen, M. J., and H. C. W. Beijerinck, 1986, Chem. Phys. **102**, 255.
Verheijen, M. J., H. C. W. Beijerinck, W. A. Renes, and N. F. Verster, 1984, J. Phys. E **17**, 1207.
Verheijen, M. J., H. C. W. Beijerinck, L. H. A. M. Van Moll, J. Driessen, and N. F. Verster, 1984, J. Phys. E **17**, 904.
Verheijen, M. J., H. C. W. Beijerinck, and N. F. Verster, 1985, Rev. Sci. Instrum. **56**, 62.
Victor, G. A., A. Dalgarno, and A. J. Taylor, 1968, J. Phys. B **1**, 13.
Vojtik, J., and I. Paidarova, 1986, Chem. Phys. **108**, 115.
Vredenbregt, E. J. D., W. Boom, R. J. F. van Gerwen, H. C. W. Beijerinck, 1990, Chem. Phys. **145**, 267.
Waibel, H., M.-W. Ruf, and H. Hotop, 1988, Z. Phys. D **9**, 191.
Wang, D. P., S. Y. Tang, and R. H. Neynaber, 1987, J. Phys. B **20**, 1527.
Warnock, T. T., and R. B. Bernstein, 1968, J. Chem. Phys. **49**, 1818.
Weiner, J., F. Masnou-Seeuws, and A. Giusti-Suzor, 1989, Adv. At. Mol. Opt. Phys. **26**, 209.
Weiser, C., and P. E. Siska, 1986, J. Chem. Phys. **85**, 4746.
Weiser, C., and P. E. Siska, 1987, Rev. Sci. Instrum. **58**, 2124.
Weiser, C., and P. E. Siska, 1988, Z. Phys. D **10**, 165.
Weissman, G., J. Ganz, A. Siegel, H. Waibel, and H. Hotop, 1984, Opt. Commun. **49**, 335.
West, W. P., T. B. Cook, F. B. Dunning, R. D. Rundel, and R. F. Stebbings, 1975, J. Chem. Phys. **63**, 1237.
Woodard, M. R., R. C. Sharp, M. Seely, and E. E. Muschlitz, Jr., 1978, J. Chem. Phys. **69**, 2978.
Woodworth, J. R., and H. W. Moos, 1975, Phys. Rev. A **12**, 2455.
Yencha, A. J., 1984, in *Electron Spectroscopy: Theory, Techniques and Applications,* edited by C. R. Brundle and A. D. Baker (Academic, London), Vol. 5, p. 197.
Yencha, A. J., 1985, in *Gas-Phase Chemiluminescence and Chemi-Ionization,* edited by A. Fontijn (North-Holland, Amsterdam), p. 67.
Yencha, A. J., J. Ganz, M.-W. Ruf, and H. Hotop, 1989, Z. Phys. D **14**, 57.
Yencha, A. J., M.-W. Ruf, and H. Hotop, 1991, Z. Phys. D **21**, 113.
Yoshino, K., and D. E. Freeman, 1985, J. Opt. Soc. Am. B **2**, 1268.
Yoshino, K., and Y. Tanaka, 1979, J. Opt. Soc. Am. **69**, 159.
Zare, R. N., 1988, *Angular Momentum: Understanding Spatial Aspects in Chemistry and Physics* (Wiley, New York).
Zemke, W. T., R. E. Olson, K. K. Verma, W. C. Stwalley, and B. Liu, 1984, J. Chem. Phys. **80**, 356.